Synthesis of Layered-Silica/Polymer Nanocomposites

by

Xue Tian

A dissertation submitted to the Graduate Faculty in Chemistry in partial fulfillment of the requirements for the degree of Doctor of Philosophy, The City University of New York

2013

This manuscript has been read and accepted for the
Graduate Faculty in Chemistry in satisfaction of the
dissertation requirement for the degree of Doctor of Philosophy.

Dr. Nan-Loh Yang

Date	Chair of Examining Committee

Dr. Maria Tamargo

Date	Executive Officer

Dr. Yujia Xu

Dr. Shuiqin Zhou

Dr. Michal Kruk

Dr. Nan-Loh Yang

Supervision Committee

THE CITY UNIVERSITY OF NEW YORK

Abstract

Synthesis of Layered-Silica/Polymer Nanocomposites

by

Xue Tian

Advisors: Dr. Nan-Loh Yang, Dr. Michal Kruk

This dissertation includes four chapters. Chapter I is the introduction of nanocomposite materials, the traditional synthesis methods are discussed and the properties of the nanocomposites are reviewed.

Chapter II provides a general introduction of mesoporous silicas, and introduces the synthesis of two lamellar phase silicas template by different surfactant mixtures based on published literature procesures. The preparation was successful, as confirmed by small-angle X-ray scattering (SAXS).

Chapter III describes the synthesis of nanocomposites by surface-initiated atom transfer radical polymerization (ATRP) and Chapter IV introduces the synthesis of nanocomposites by activators regenerated by electron transfer atom transfer radical polymerization (ARGET ATRP). The mechanism and components of the reaction mixtures in the living ATRP are discussed. It is shown that 3-(chlorodimethylsilyl)propyl 2-bromo-2-methylpropanoate is a suitable initiator

grafted on the surface of the layered silicas. It is described that polymerization of methyl methacrylate (MMA), styrene (St) and acrylonitrile (AN) was carried out by using ATRP or ARGET ATRP. The polymer loadings were accessed by thermogravimetric analysis (TGA), morphologies of the nanocomposites were examined by SAXS and transmission electron microscopy (TEM), and their thermal properties were accessed by using differential scanning calorimetry (DSC). Generally, normal ATRP was found to allow for better retention of lamellar (intercalated) morphology. However, ARGET ATRP also worked well and allowed us to lower the copper catalyst content to several ppm, that is, by about two orders of magnatitude.

This is

dedicated to my parents

Zhonglin Tian and Shumei Liu,

(田中林与刘淑梅)

my husband

Zinan Li

(李子男)

Acknowledgments

May I have the pleasure to express my sincere thanks to my mentors, Professor Nan-Loh Yang and Professor Michal Kruk, for their advice, encouragement and mentoring during my graduate study. It has been an honor to work with them.

I also want to express my thanks to my research committee members, Professor Shuiqin Zhou and Professor Yujia Xu for their time, advice and support. I am grateful for the help from faculty members in College of Staten Island, Professor Ralf Peetz, Professor Krishnaswami Raja, Professor Chwen-Yang Shew, Professor Alan Lyons, and Professor Qiao-sheng Hu. I also appreciate the trainings and help from technicians, Mr. Tai Park, Dr. Yalin Wang and Ms. Sara Guariglia.

I especially thank my group members Dr. Xuewu Yan, Liang Cao, Liang Huang, Manik Mandal, Chin Ming Hui, Tiffany Man and Amanpreet Singh Manchenda for the cooperation during my Ph.D study. I would also like to thank lab members Dr. Kai Su and Dr. Iwei Chu and other friends, colleagues in CSI and Graduate Center.

I would like in particular to express my gratitude to my families, my husband, Zinan Li, my father Zhonglin Tian and my mother Shumei Liu. Great thanks for their priceless love, support, understanding and encouragement.

I acknowledge the financial support from College of Staten Island, Graduate Center at the City University of New York and Center for Engineered Polymeric Materials.

Table of Contents

List of Figures

List of Tables

List of Schemes

List of Equations

List of Abbreviations

AGET: activators generated by electron transfer

AN: acrylonitrile

ARGET: activators regenerated by electron transfer

ATRP: atom transfer radical polymerization

BDMCS: n-butyldimethylchlorosilane

CDMSPBMP: 3-(chlorodimethylsilyl)propyl 2-bromo-2-methylpropanoate

CMPETS: chloromethyl phenylethyl trichlorosilane

CRP: controlled/living radical polymerization

CSPETCS: 2-(4-chlorosulfonyl phenyl) ethyl trichlorosilane

CTAB: cetyltrimethylammonium bromide

DMF: dimethyl formamide

DMOCS: dimethyloctylchlorosilane

DMSO: dimethyl sulfoxide

DP: degree of polymerization

DSC: differential scanning calorimeter

HTMABr: hexadecyltrimethylammonium bromide

MMA: methyl methacrylate

PAN: polyacrylonitrile

PDI: polydispersity index

PMDETA: 1, 1, 4, 7, 7-pentamethyl-diethylenetriamine

PMMA: poly(methyl methacrylate)

PS: polystyrene

SAXS: small-angle X-ray scattering

$Sn(EH)_2$: tin (II) 2-ethylhexanoate

St: styrene

TEM: transmission electron microscopy

T_g: glass transition temperature

TGA: thermogravimetric analyzer

TMCS: trimethylchlorosilane

TPMA: tris[(2-pyridyl)methyl]amine

XRD: X-ray diffraction

Chapter I.

Introduction to Nanocomposites

1.1. Definition, Classification and Preparation of Nanoscale Polymer-Inorganic Nanocomposites

Organic-inorganic nanocomposites have generated much interest, [1-4] principally because of the potential they offer for applications in tough, high-temperature-compatible particle reinforced polymers, [3] coatings, [4] electronics, [4] and in the study of polymers in confined environments. [1b] Toyota's pioneering work on polymer-clay nanocomposites two decades ago[3b, 5] has generated great interest in the materials science community. [6, 7] Because of the nanoscale dispersion of the clay layers, this new family of materials exhibits properties that are completely different from those properties of composites with microscale level dispersed inorganic component.

Polymer-inorganic nanocomposites are defined as composites having inorganic particles dispersed in a polymer matrix, differing from traditional composites, in that the dispersed particles have at least one dimension (length or / and width or / and height) on the nanometer lengthscale. [6a] Nanoscale fillers can be classified into three types, depending on how many dimensions of the dispersed particles are in the nanometer range. [6a] The first type includes isodimensional particles, such as spherical silica nanoparticles, [8a, 8b]for which all of the three dimensions are the same and are on the order of nanometers. The second type is illustrated by nanofibers and nanotubes, such as carbon nanotubes in polymer matrix, [9] for which two dimensions are at nanometer scale and the third dimension is larger. The third type is exemplified by polymer-(layered material) nanocomposite, for which only one dimension of the filler particles is in the nanometer range, and the dispersed particles are sheets. These nanocomposites are typically obtained by the intercalation of polymers between the layers of layered host materials. The layred host materials can be synthetic or of natural origin.

There are three main types of architecture of the composites that could be achieved with a layered nanoscale inorganic material (such as a clay) and a polymer (Scheme 1.1).[6a] A phase-separated composite (Scheme 1.1.(a)) is the first type, for which the polymer chains cannot be intercalated between nanoscale sheets, and the sheets keep their original aggregation state. The properties of such a type of composites remain the same as those of microcomposites, which usually are not as good as the properties of nanocomposite. For instance the epoxy/montmorillonite nanocomposites shows better anticorrosion and physical properties comparing with epoxy/barium sulfate microcomposites in coating applications.[10] The other two types belong to the nanocomposites family. When the polymer chains are intercalated between the inorganic layers, but a well ordered arrangement of the layers is maintained, the resulting structure is called an intercalated structure (Scheme 1.1.(b)). An exfoliated or delaminated structure (Scheme 1.1.(c)) is obtained when the inorganic layers are completely dispersed inside the polymer matrix and the ordering between the layers is not maintained. Small-angle X-ray scattering (SAXS) and transmission electron microscopy (TEM) are the techniques to identify those structures. The well ordered morphology of the intercalated structure can be recognized by SAXS, for which the interlayer spacing usually will be increased by the polymer chains intercalated between the silicate sheets when compared to the interplanar spacing of the original inorganic layers. The exfoliated structure is difficult to be recognized in SAXS, because either the spacing might be too large or the ordered structure is lost. In such cases, TEM is helpful to identify the morphology. [6a]

Scheme 1.1. (a) Phase-separated Microcomposite; (b) Intercalated Nanocomposite and (c) Exfoliated Nanocomposite. [6a]

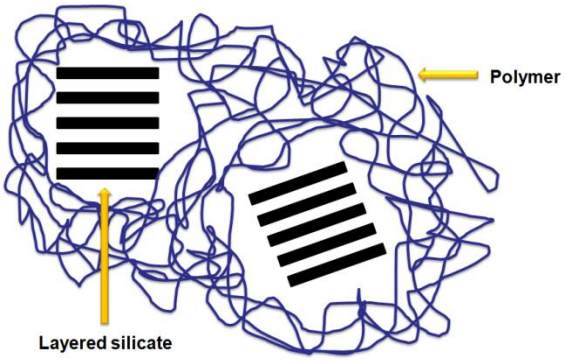

(a)Phase separated microcomposite

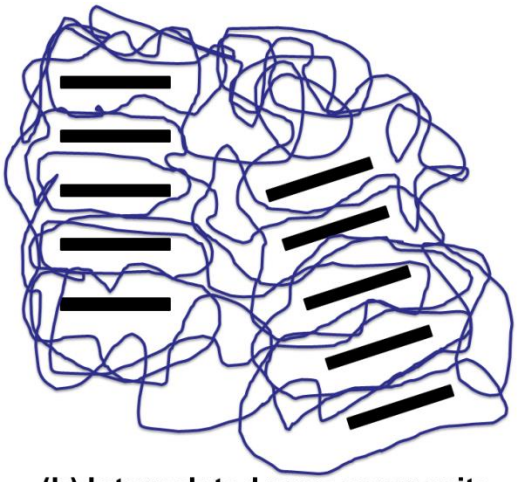

(b) Intercalated nanocomposite

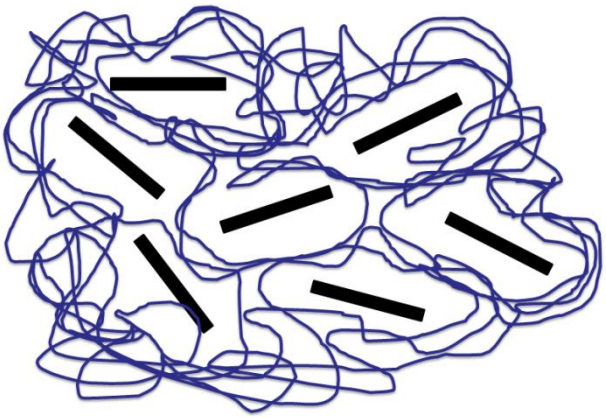

(c) Exfoliated nanocomposite

To prepare polymer/layered-material nanocomposites, four traditional processes were used: [11]

i. Exfoliation-adsorption: In this process, a solvent is used to disperse the layered silicates into single layers. If the polymer is also soluble in the solvent and it added, it can adsorb on the silicate layers. After the solvent is evaporated, the polymer chains are located between the aggregated silicate sheets, possibly forming an ordered intercalated structure. This method is used to obtain intercalated nanocomposites of water-soluble polymers, including poly(vinyl alcohol), [12, 13] poly(ethylene oxide), [13-17] poly(vinylpyrrolidone) [18] and poly(acrylic acid)[17]. The method can also be used with solvents other than water, which allowed one to obtain nanocomposites consisting of nitrile-based copolymer (Barex 210 E) and polyethylene-based polymer.[19] Ogata et al. used this technique to produce biodegradable polylactide [20] and poly(ε-caprolactone) nanocomposites. [21] For insoluble polymers (polyimide), Toyota research group has been the first one to report the possible route to produce nanocomposites, in which the soluble polymeric precursors were intercalated in the layered silicate. The subsequent polymerization rendered the nanocomposite product. [3(a)] Poly(methyl methacrylate) based nanocomposites have been produced first by using methyl methacylate added to delaminated Na-montmorillonite aqueous dispersion, which was followed by the emulsion polymerization. [22]

ii. In situ intercalative polymerization: In this process, the polymers are formed between the silicate layers by the polymerization initiated, for instance, by an initiator inside the interlayer space. Various thermoplastic nanocomposites can be prepared by in situ intercalative polymerization, such as nylon-6-based nanocomposites, [5a, 5b] polyurethane/clay nanocomposites [23] and polystyrene-based nanocomposites. [24] In the study of polystyrene-based nanocomposites, Akelah and Moet modified the clays by

cation-exchange with (vinylbenzyl)trimethyl ammonium to increase the interlayer spacing. [24] Doh and Cho extended this approach on the use of other modified montmorillonites and evaluated its effectiveness. [25] Tudor et al. have produced the polyolefin-based nanocomposites by coordination polymerization of propylene. [26] Polymerization-filling technique (PFT) has also been used to produce intercalated/exfoliated nanocomposites based on high density polyethylene. [27] In addition to the above thermoplastic nanocomposites, thermoset nanocomposites (such as epoxy-based nanocomposites) can also be produced by in situ intercalative polymerization. Messersmith and Giannelis have explored the formation of nanocomposites based on the diglycidyl ether of bisphenol A and a cation modified montmorillonite. [28] The synthesis of nanocomposites based on montmorillonite and unsaturated polyester was also demonstrated. [29] Elastomeric nanocomposites can also be obtained by this technique. Wang and Pinnavaia have obtained another type of an exfoliated structure where the layers were still organized in the elastomeric epoxy matrix. [30] They also developed the synthesis of intercalated elastomeric polyurethane/clay nanocomposites. [31] It should be noted that the nanocomposites synthesized during my PhD work were prepared through an in situ intercalative polymerization approach. The relevant literature will be overviewed in subsequent chapters.

iii. Melt intercalation: In melt intercalation, the layered silicates are heated to appropriately high temperatures and mixed with polymer in molten state. The process of formation of polystyrene-based or polystyrene derivatives-based nanocomposites by melt intercalation has been well studied in terms of thermodynamics, kinetics and morphologies. [32-34] The preparation of nylon-6 based nanocomposites have been also investigated by melt

intercalation, [35] although in situ intercalation is more commonly employed in this case. The other polymer/copolymer-based nanocomposites have been explored were polypropylene, [36-39] ethylene-vinyl acetate copolymers, [40] poly(styrene-b-butadiene) copolymers [41]and elastomers. [42]

iv. Template synthesis: In this case, the silicates are formed in situ in an aqueous solution in the presence of a polymer. The polymer facilitate the formation of the inorganic phase and is entrapped as the component grows. "This technique can be used for water soluble polymers but can also be implemented for other polymers such as poly(vinylpyrrolidone), hydroxyl-propylmethylcellulose, polyacrylonitrile, poly(dimethyldiallylammonium), and polyaniline". [43]

1.2. Properties of Nanoscale Organic-Inorganic Nanocomposites

Organic-inorganic nanocomposites often have improved properties even if a small proportion of the inorganic component is mixed with the organic matrix. Increases of modulus (tensile or flexural modulus) are observed for nanocomposites materials. Thermal stability and fire retardancy improvements have drawn a lot of attention, too. The layered-silica/polymer nanocomposite materials also attracted interests because of their barrier properties with respect to vapor/gas diffusion. Some nanocomposites also exhibit ionic conductivity.

The hydrogels containing silicate nanoparticles (Laponite) showed higher elongations and improved toughness when compared with the polymer part. [44] A dramatic increase of toughness and stiffness in poly(vinylidene fluoride) was also reported. [45] In a starch/poly(vinyl alcohol)/sodium montmorillonite nanocomposite, the increase of sodium montmorillonite content (0-20%) enhanced the tensile strength, but decreased elongation at break. [46] The relationship between the modulus enhancement and clay volume, as well as constrained polymer volume in nanocomposite has been investigated. [47] For the nanocomposite containing only 2.0 wt % montmorillonite, the tensile strength, Young's modulus and elongation at break increased markedly. [48]

Both intercalated and exfoliated poly(ε-caprolactone)/clay nanocomposites were degraded at higher temperature when compared with poly(ε-caprolactone) or poly(ε-caprolactone)/clay microcomposite. At 50% weight loss in thermal degradation patterns, a nanocomposite containing 5 wt % clay showed 25 ℃ higher temperature than the polymer degradation temperature. [49] Polystyrene/montmorillonite nanocomposite showed increased onset degradation temperature compared with polystyrene. [50] Glass transition temperature (T_g) change was

complicated in the nanocomposites. For exfoliated polyamide/organoclay nanocomposite, T_g increased when inorganic filler content was low, then T_g decreased with increasing filler content; however, intercalated polyamide/organoclay nanocomposite exhibited a linear T_g decrease with increasing inorganic filler content. [51] Polystyrene/montmorillonite nanocomposites showed a higher T_g when montmorillonite content was 1 or 3 or 5 wt %. [50] Intercalated polystyrene/lipophilized smectic clay nanocomposite displayed a 10 ℃ increase in T_g. [52] The glass transition temperature change will be discussed further in a subsequent chapter.

Some other interesting properties have been observed as well. Solvent uptake (swelling) in dispersed polysilozane/layered silicate nanocomposite was dramatically decreased when compared with conventional composites. [53] By using the quaternary alkylphosphonium salt, poly(methyl methacrylate)/clay nanocomposites showed enhanced anticorrosive property. [54] In coating applications, polymer/sodium montmorillonite nanocomposites exhibited an increase in the surface hardness, scratch resistance and flexibility. [55] Water vapor permeability was decreased in starch/poly(vinyl alcohol)/sodium montmorillonite nanocomposite when the inorganic filler content was increased from 0 to 20%. [46]

In general, the improved properties for nanocomposite materials family attract much more attention. The relationship between the structure and properties is worth further investigation.

1.3. Inorganic Fillers in Nanocomposites

1.3.1. Natural Inorganic Fillers

There is a variety of different types of inorganic fillers that can be used to prepare nanocomposites. Most of the fillers are natural materials, but some are synthetic materials. Some viable natural layered materials are: graphite [56], metal chalcogenides ($(PbS)_{1.18}(TiS_2)_2$ [57], MoS_2 [58]), metal phosphates ($ZrHPO_4$ [61]), clays and layered silicates (montmorillonite, hectorite, saponite, fluoromica, fluorohectorite, vermiculite, kaolinite, magadiite) and layered double hydroxides ($M_6Al_2(OH)_{16}CO_3 \cdot nH_2O$; M=Mg [62], or Zn [63]).[6a]

The nanocomposites based on clays or layered silicates (the type of nanocomposites with one dimension of the filler within the nanoscale range) have been well investigated. This is because the clay materials are commercially available of low cost and their intercalation mechanism is well known. [64, 65] The layered silicates typically used to prepare nanocomposites belong to the 2:1 phyllosilicate family (2:1 refers to two tetrahedral sheets and one octahedral sheet within the layer structure). In their crystal lattice, a central octahedral sheet (in which alumina or magnesia occupies the center space) is stacked between two silica tetrahedral sheets (one on the top, and one on the bottom). [6a] The structure is shown in Scheme 1.2. [66] The most commonly used commercial layered silicates, such as montmorillonite, hectorite and saponite, belong to this family, and montmorillonite is the most popular clay to prepare nanocomposite via cation exchange [49, 50, 54, 67a, 68-75] and covalent bonding [76a] (see chapter 1.5). The chemical formulas of the commonly used 2:1 phyllosilicates are: (a) montmorillonite ($M_x(Al_{4-x}Mg_x)Si_8O_{20}(OH)_4$), (b) hectorite ($M_x(Mg_{6-x}Li_x)Si_8O_{20}(OH)_4$) and (c) saponite ($M_xMg_6(Si_{8-x}Al_x)O_{20}(OH)_4$), where M is monovalent cation and x is the degree of isomorphous substitution (between 0.5 and 1.3). [6a]

Scheme 1.2. Structure of 2:1 Phyllosilicates. [66]

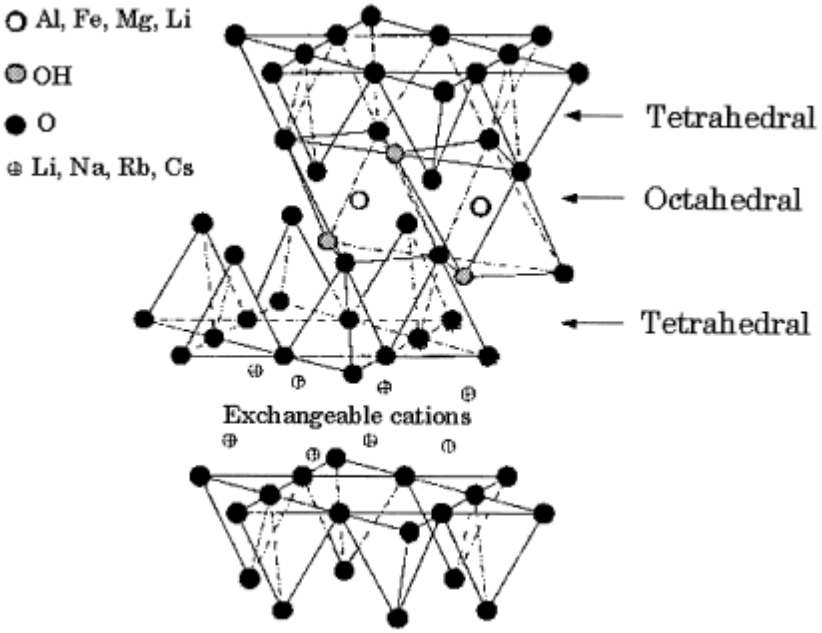

1.3.2. Synthetic Inorganic Fillers

1.3.2.1. Synthetic Clay

In addition to natural clays, a synthetic silicate is also a possible choice for serving as an inorganic filler to prepare nanocomposites. Laponite is a commercial available synthetic clay, which is uniform, disc-shaped, with discs of 25 nm in diameter and about 1 nm thickness. [77] The formula of laponite is $Na^{+}_{0.7}[(Si_8Mg_{5.5}Li_{0.3})O_{20}(OH)_4]^{-0.7}$. [77] Several research works have investigated the polymer-laponite nanocomposites. [44, 78-80] Unlike the cations on the clay surface, the silanol groups on the laponite disc edge provide possibility of covalent bonding using chlorosilanes or alkoxysilanes that react with silanol groups (-SiOH) on the clay edge. [79] Organic functional groups in the organosilane moiety such as primary amines, methacrylates, benzophenones, and tertiary bromines can serve as active sites for grafting polymer chains to or from the clay edge. [79, 80]

1.3.2.2. Mesoporous Silica MCM-50 with Lamellar Structures

Laponite clay has only small amount of silanol group on the edge, which limits the surface modification with organic molecules. Some work has been done to overcome the low reactivity by sol-gel process to synthesize organoclays using organoalkoxysilanes as silica source. [78, 81-84] But it may cause structure defects with the clay sheets or distortion. [78]

The surfactant-templated layered silica (lamellar phase) is a member in surfactant-templated nanostructured silica materials family. It can provide large amount of silanol groups on the surface, and it is the inorganic filler we have chosen in this dissertation. Ordered mesoporous materials have been developed two decades ago. In the early 1990s, the synthesis of mesostructured silicates was announced by Japanese scientists and later by U.S. scientists

working for Mobile Company. [85-87] Mobil's scientists prepared highly ordered mesoporous/mesostructured silicates under hydrothermal and basic conditions, which were referred to as M41S materials. Cationic quaternary ammonium surfactants such as cetyltrimethylammonium bromide ($C_{16}H_{33}N(CH_3)_3Br$, CTAB) were first used as surfactant templates. M41S materials broadened the achievable uniform pore size in periodic porous materials from the micropore-range (pore diameter less than 2 nm) to the mesoporous range (pore diameter between 2 to 50 nm). And the concept of "the template" was introduced in the synthesis of mesoporous silicate materials for the first time. [88]

Mesoporous molecular sieves (as they were often referred to after their discovery) or ordered mesoporous materials (as they are referred to in the current literature) are obtained via the organic-inorganic assembly process. The assembly is mediated by either weak noncovalent interactions such as hydrogen bondings and van der Waals forces or by the electrostatic interactions between inorganic species and the surfactant. After the assembly process is completed, OMMs with accessible pores could be obtained by removing the surfactants. Therefore, for the formation of highly ordered mesostructures, self-assembly with the surfactants is the key procedure. The mesoporous materials could be designed and the synthesis could be controlled based on current knowledge and technique of surfactants self-assembly. [88]

A large variety of mesoporous or nanostructured materials with different mesostructures (lamellar, [85, 86] two-dimensional (2D) hexagonal of space group *p*6*mm*, three-dimensional (3D) hexagonal, 3D cubic close packed, bicontinuous cubic, [85, 86] etc) and compostions (silica, metal oxides, [89-96] metal sulfides, [97, 98] metals, [99-102] and polymers and carbons [103, 104]) have been investigated. Some of the mesostructures are showed in Scheme 1.3.

Scheme 1.3. Structures of Mesoporous Materials: a) MCM-41 (2D hexagonal, space group *p*6*mm*; b) MCM-48 (cubic); c) MCM-50 (lamellar, space group *p*2).

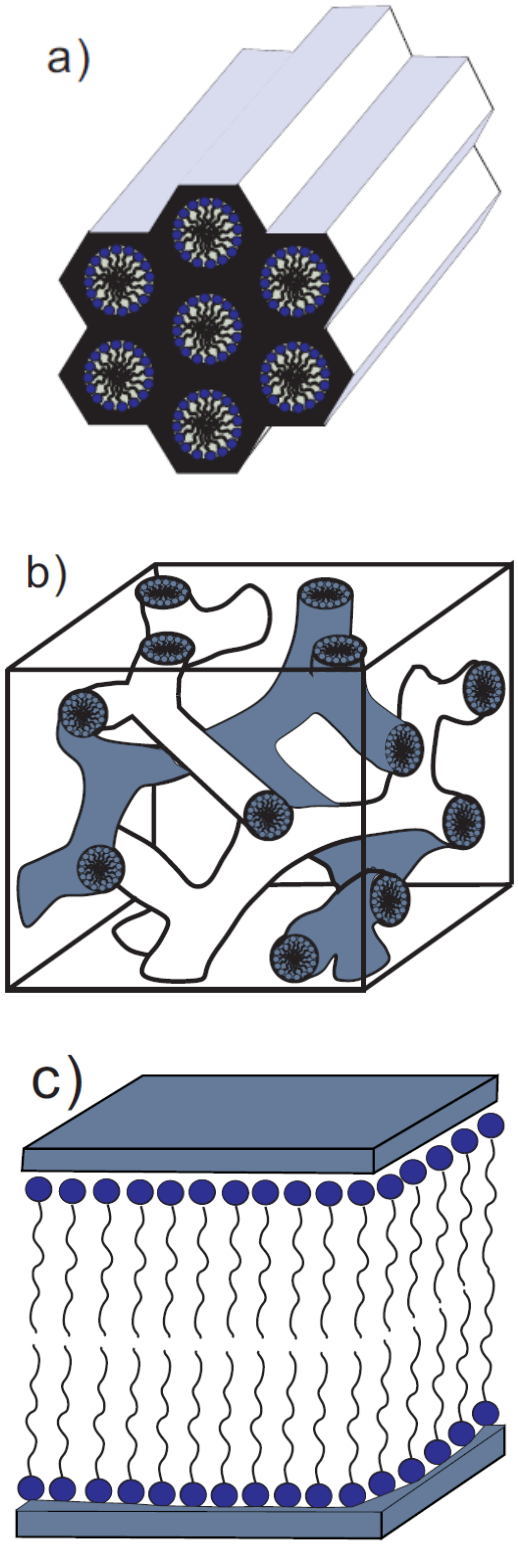

1.3.2.2.1. Surfactants

There are three types of surfactants frequently used: cationic, anionic and nonionic surfactants. [88] Some cationic quaternary ammonium surfactants are listed in Scheme 1.4. [88] Commercially available cetyltrimethylammonium bromide (CTAB) has been often used for the synthesis of ordered mesoporous silicate materials. Anionic salt surfactants includes carboxylates, sulfates, sulfonates, and phosphates. Nonionic surfactants are commercially available in a wide range of different structures. They are very attractive nowadays because of low cost, nontoxicity, biodegradability and possibilities of generating different geometries by self-assembly. Scheme 1.5 [88] illustrates some typical commercial nonionic surfactants. The main members are oligomeric alkyl poly(ethylene oxide) (PEO) surfactants (Brij family), amphiphilic block copolymers (Pluronic family, e.g., poly(ethylene oxide)-b-poly(propylene oxide)-b-poly(ethylene oxide) (PEO-PPO-PEO)), sorbitan esters, etc.

Scheme 1.4. Formula of Alkyltrimethyl Ammonium Surfactant. [88]

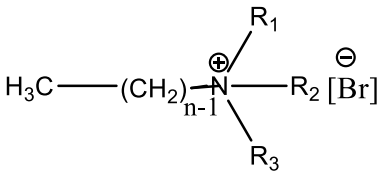

R_1, R_2, R_3 = CH_3

n = 8-22

Scheme 1.5. Commercially Available Nonionic Surfactants. [88]

Poly(alkylene oxide) block copolymer

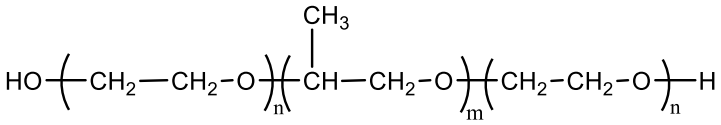

Pluronic PEO-PPO-PEO

Oligomeric alkyl poly(ethylene oxide)

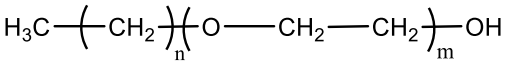

Brij

1.3.2.2.2. Cooperative Self-Assembly of Surfactants and Silica Source to Form Mesostructure

The self-assembly is established through the interactions between silicates and surfactants to form inorganic-organic mesostructured composites. [88] Among several mechanisms, the cooperative formation mechanism (Scheme 1.6 and 1.7 [88]) is accepted by most researchers, following Stucky and co-workers. [89, 105]

The interactions between the surfactants and silicates are typically classified as follows (Scheme 1.6 [106]): a) under basic conditions, the synthetic pathway is termed S^+I^- (S^+: cationic surfactant; I^-: inorganic precursor), and involves the assembly of polyacid anions and surfactant cations; b) under acidic conditions, the inorganic precursors are positively charged to interact with surfactant cations with the existence of a mediator ion X^- (Cl^-, Br^-, I^-, SO_4^{2-}, NO_3^-, etc), this pathway is called $S^+X^-I^+$; c) for pathway $S^-M^+I^-$, to ensure the interactions between negatively charged surfactants and inorganic precursors, it is necessary to add a mediator ion M^+; d) in contrast to pathway S^+I^-, S^-I^+ interactions also occurs between cationic precursors and surfactant anions such as the assembly of Keggin ion (Al_{13}^{7+}) and dodecyl benzenesulfonate; e) except electrostatic mechanism above, hydrogen bonding interactions between nonionic surfactants and uncharged inorganic precursors is termed S^0I^0 pathway (e.g., assembly with a long-chain amines or with poly(ethylene oxide)-based surfactants); f) $S^0(XI)^0$ is the pathway when the uncharged inorganic species are ion pairs. [88, 106]

Scheme 1.6. Common Synthetic Pathways for the Assembly of Surfactants and Inorganic Precursors under Basic, Acidic or Neutral Media (Adapted from Ref. 106).

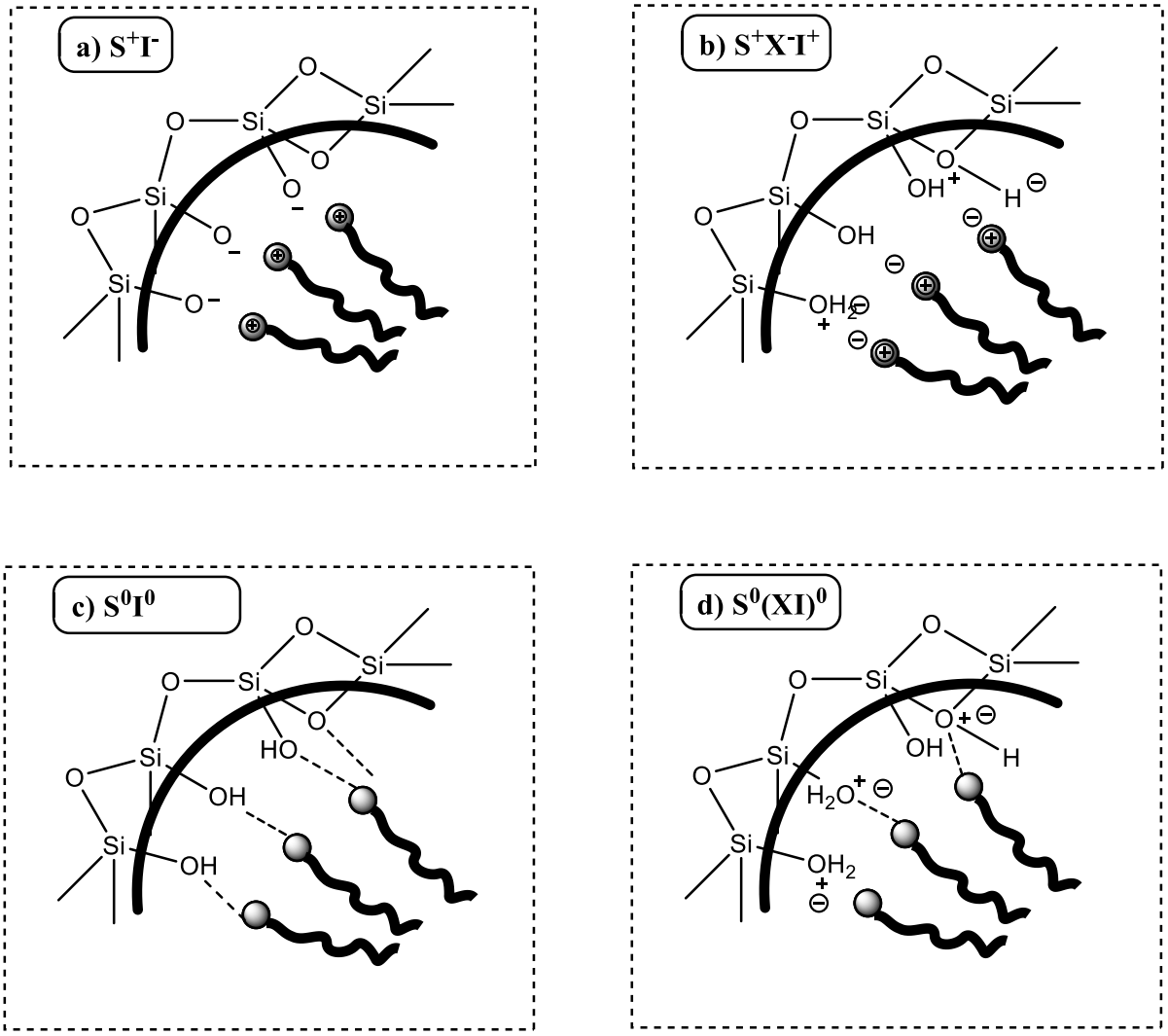

1.3.2.2.3. Liquid-Crystal Template Pathway

In addition to the cooperative self-assembly mechanism, the "true" liquid-crystal templating process (Scheme 1.7 [88]) is also considered as another possible pathway in the synthesis of ordered mesostructures. [107-110]

In "true" liquid-crystal templating processes, the surfactant concentration is very high, so a lyotropic liquid-crystalline phase is formed under specific conditions (temperature, pH) before the addition of the inorganic precursor (normally tetraethyl orthosilicate (TEOS) or tetramethylorthosilica (TMOS)). [111]

Scheme 1.7. Synthetic Strategies of Mesoporous Materials: (A) cooperative self-assembly; (B) "true" liquid-crystal templating process (Adapted from Ref. 88).

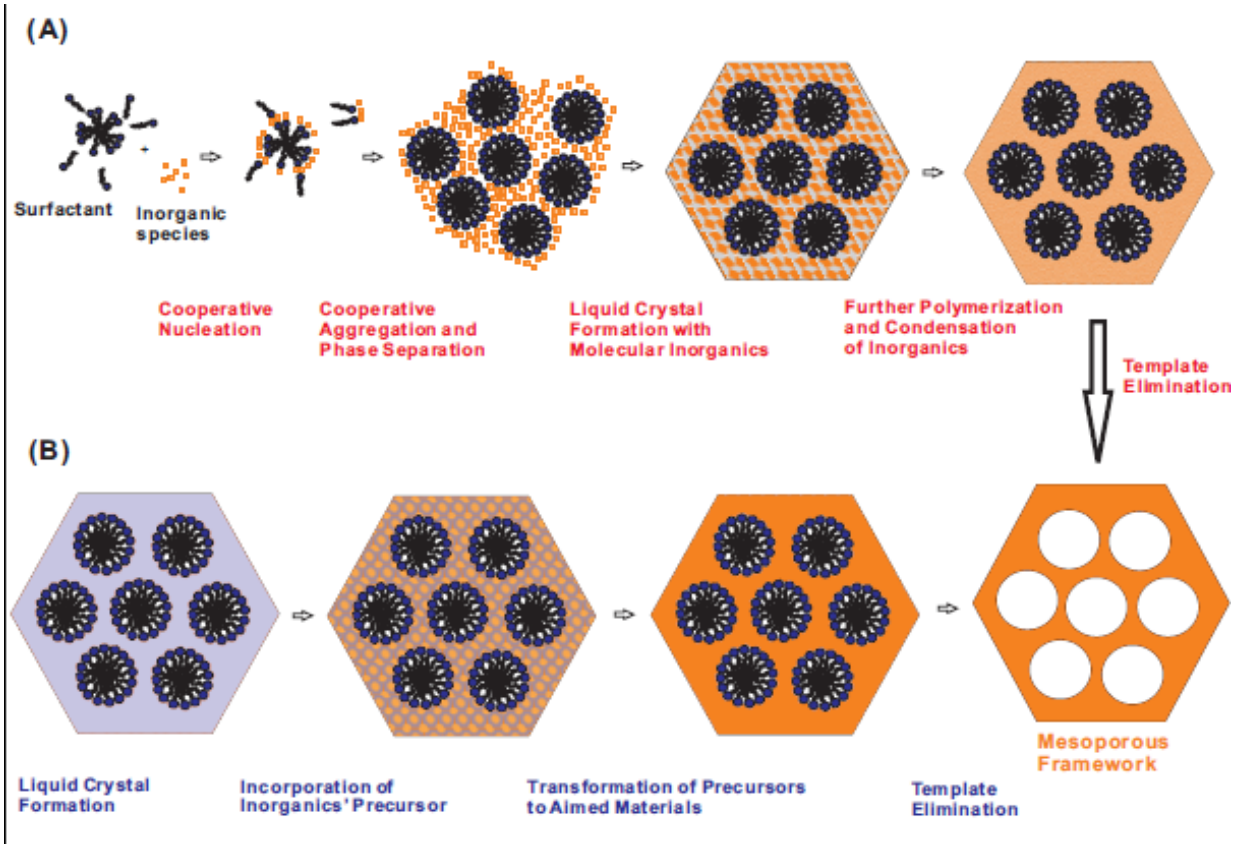

1.4. Polymerization Method in Nanocomposites Preparation

The interesting properties of nanocomposites have attracted a lot of attention from scientists; various polymers have been studied to prepare the nanocomposites with different types of layered inorganic fillers as mentioned in Chapter 1.1. The silanol groups on layered silica surface can be used to attach other functional moiety, which can serve as active sites for in situ polymerization. Comparing with other polymerization methods, controlled/living radical polymerization (CRP) can provide excellent molecular weight control and potentially well-defined nanocomposite architecture. It offers more freedom to adjust the loading of covalently bonded polymers in the nanocomposites. Therefore, the well-known living polymerization technique, atom transfer radical polymerization (ATRP), is further discussed here as a means for the controlled grafting of polymer from the surface of layered materials, which was explored in our study.

1.4.1. Normal Atom Transfer Radical Polymerization

A living polymerization is defined as the polymerization technique without irreversible chain transfer and chain termination.[112-114] Anionic, cationic, radical, coordination, and ring-opening polymerizations have all been explored in living polymerization research, both academic and industrial. Radical polymerizations are particularly attractive due to convenient conditions and wide variety of available monomers. [115] One of the methods of a controlled radical polymerization is atom transfer radical polymerization (ATRP) that involves transition metal catalysts. [115] ATRP has become very popular because of the use of common chemicals, convenient setup and its suitability for various well-defined macromolecular architectures. [115]

A general mechanism for atom transfer radical polymerization (ATRP) is shown in Scheme 1.8. [115] The radicals, or the active species, are generated through a reversible redox process catalyzed by a transition metal complex (M_t^n-Y/Ligand, where M_t^n is a transition metal and Y may be another ligand or a counterion), which undergoes a one electron oxidation with the abstraction of a halogen atom or pseudo-halogen atom (X) from a growing polymer chain in dormant form or from an initiator (R-X). This process builds equilibrium with an activation step (k_{act}) and a backward deactivation step (k_{deact}). The growth of polymer chains is similar as in a conventional radical polymerization which proceeds by adding the growing radicals to monomers, with the rate constant of propagation k_p. Termination reactions through radical coupling and disproportionation (k_t) also occur in ATRP, but in a well-controlled ATRP, no more than a few percent of the polymer chains undergo termination (at low or moderate extents of conversion). Some chains may terminate during the initial period of the polymerization before the concentration of deactivating species X-M_t^{n+1}-Y becomes sufficiently high (see below). This process leads to build-up of oxidized metal complexes, X-M_t^{n+1}, which reduces the concentration of growing radicals through deactivation process and thus minimizes termination.[116] A successful ATRP will not only result in a small portion of terminated chains, but also in a uniform growth of all the chains, which relies on fast initiation and rapid reversible deactivation. [115]

Scheme 1.8. Transition-Metal-Catalyzed ATRP. [115]

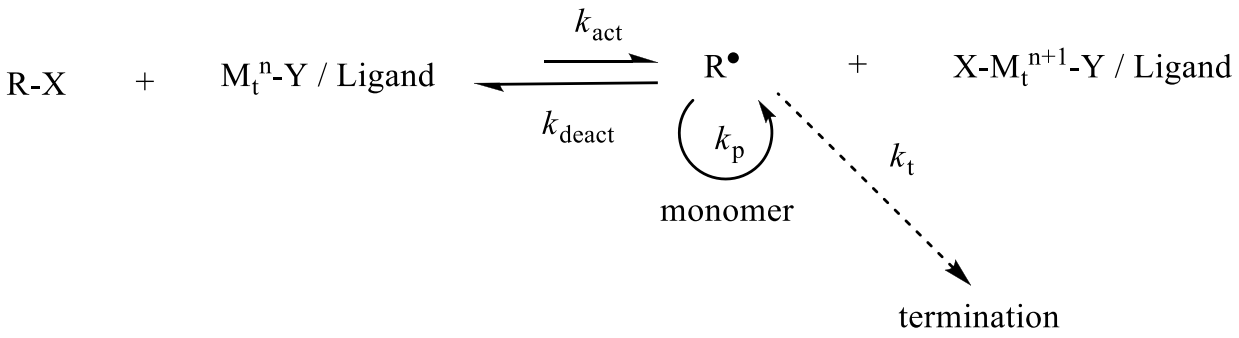

1.4.1.1. Components

The components in the ATRP system include monomers, an initiator with a transferable halogen or pseudo-halogen, and a catalyst (transition metal species combined with suitable ligand). They all affect the polymerization rate of ATRP (Equation 1.1 [115]), where k_p is the polymerization rate of monomers, K_{eq} is the rate constant of equilibrium in Scheme 1.8, [M] is the monomer concentration, $[I]_0$ is the initial initiator concentration, $[Cu^I]$ and $[X\text{-}Cu^{II}]$ refer to the catalyst and deactivating species concentration, respectively. For successful ATRP, in addition to the above main components, other factors such as additives, solvent and temperature also affect the system. [115]

Equation 1.1. Equation of Rate Law of ATRP. [115]

$$R_p = k_p[M][P^*] = k_pK_{eq}[M][I]_0 \text{ x } [Cu^I] / [X\text{-}Cu^{II}]$$

1.4.1.1.1. Monomers

ATRP has been successfully used to synthesize polymers from a lot of monomers. These monomers include styrenes, (meth)acrylates, (meth)acrylamides, and acrylonitrile, which have substituent groups in the structure to stabilize the propagating radicals.[117-119,] Scheme 1.9 and 1.10 illustrate some styrene and methacrylate derivatives polymerized by ATRP.[115] ATRP of styrene can be performed with different catalyst systems. It is often carried out in high temperature (>100 ℃) usually either in bulk or in a solvent, and styrenes with electron-withdrawing groups polymerize faster. [115] ATRP of methyl methacrylate (MMA) is usually carried out in a solution at 70-90 ℃, and it is also successful in many catalyst systems. [115]

Scheme 1.9. Various Styrenes Polymerized by ATRP. [115]

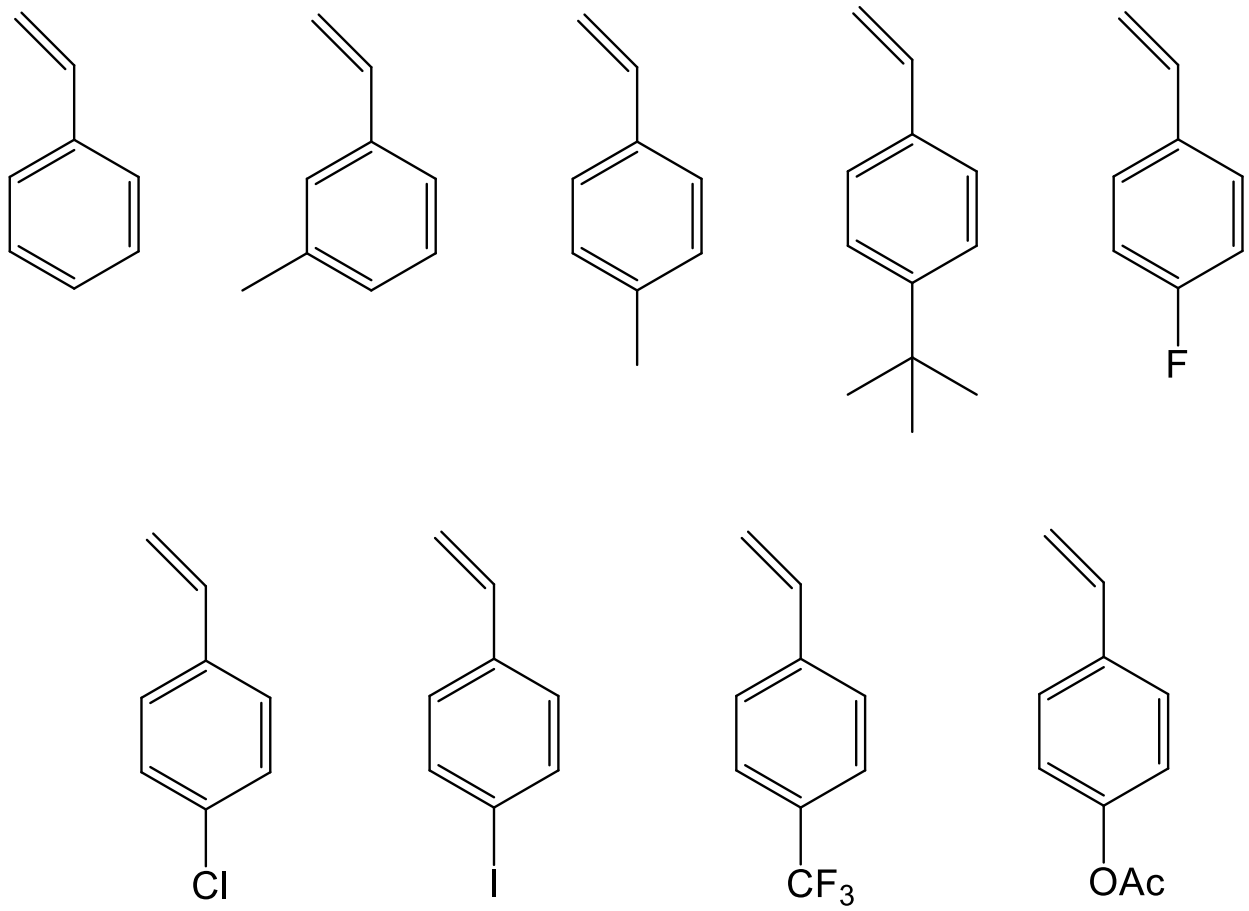

Scheme 1.10. Various Methacrylates Polymerized by ATRP. [115]

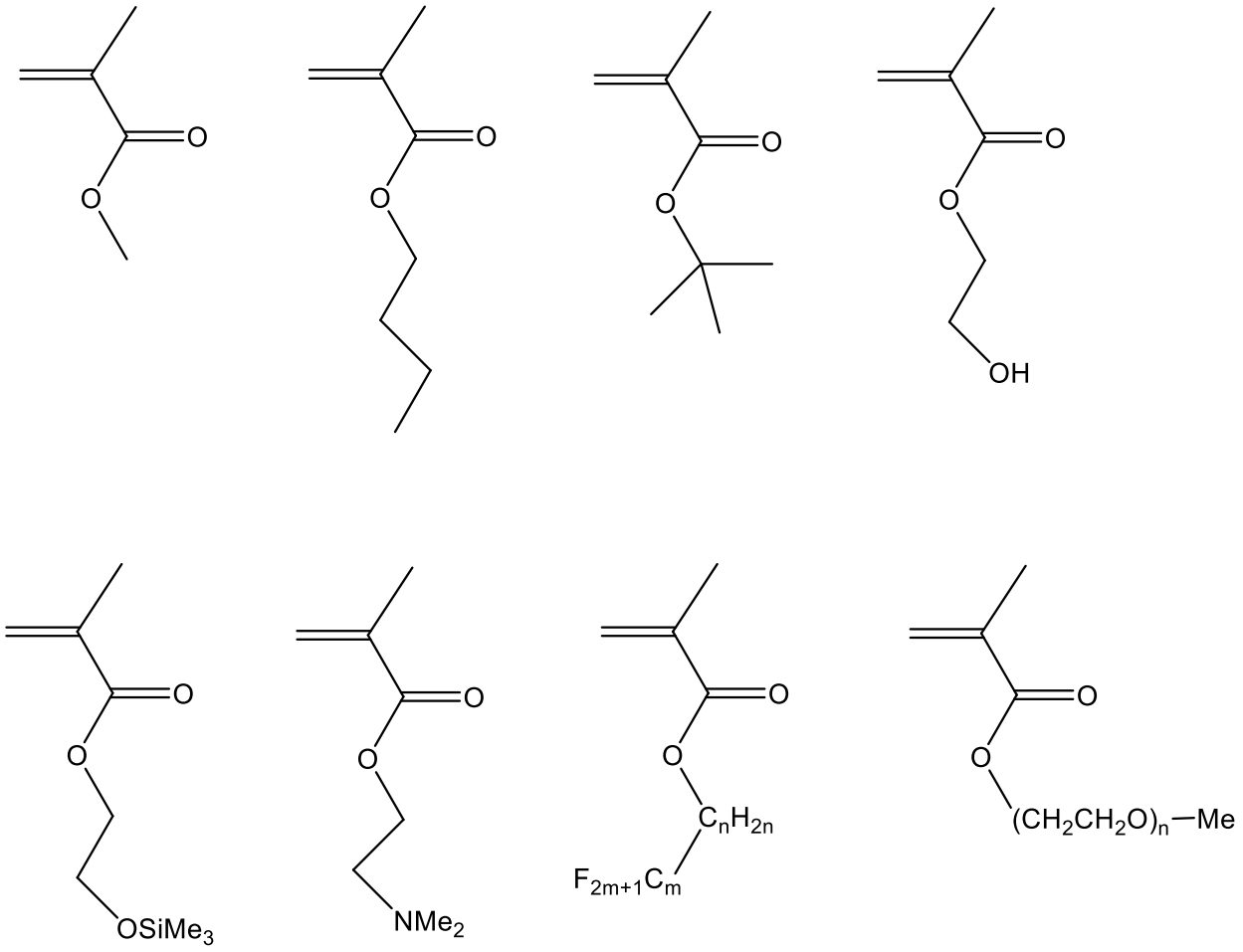

1.4.1.1.2. Initiators

The main function of an initiator is to initiate the polymerization, preferably in such a way that the growth of all chains is initiated at early stage of the polymerization when the propagation have not progressed to a considerable extent. The concentration of the initiator may determine the number of growing polymer chains. If the initiation is quantitative, the degree of polymerization (DP) is inversely proportional to the initial concentration of initiator $[initiator]_0$ in a living polymerization of polymeric species with a single initiator moiety (Equation 1.2).[115]

Equation 1.2. Equation for Degree of Polymerization. [115]

$$DP = [M]_0 / [Initiator]_0 \times conversion$$

where $[M]_0$ is the initial concentration of the monomer, and "conversion" is the extent of conversion defined as a fraction of monomer that has been consumed in the polymerization process, $[M]_0$ x conversion is the concentration of monomer already consumed in the polymerization process.

Various α-haloesters have been successfully used to initiate controlled ATRP. End-group functionalized α-haloesters can easily be synthesized through an esterification reaction of appropriate acid halides. As ATRP can tolerate various functional groups, well-defined polymers with functional end groups have been prepared without any protecting processes. Various functionalities, such as hydroxy, epoxy, allyl, vinyl, γ-lactone, and carboxylic acid have been attached onto the α-end of the polymer by using a functional initiator (Scheme 1.11).[115, 120-122]

Scheme 1.11. Representative Functional Initiators Derived from α-Haloesters. [115]

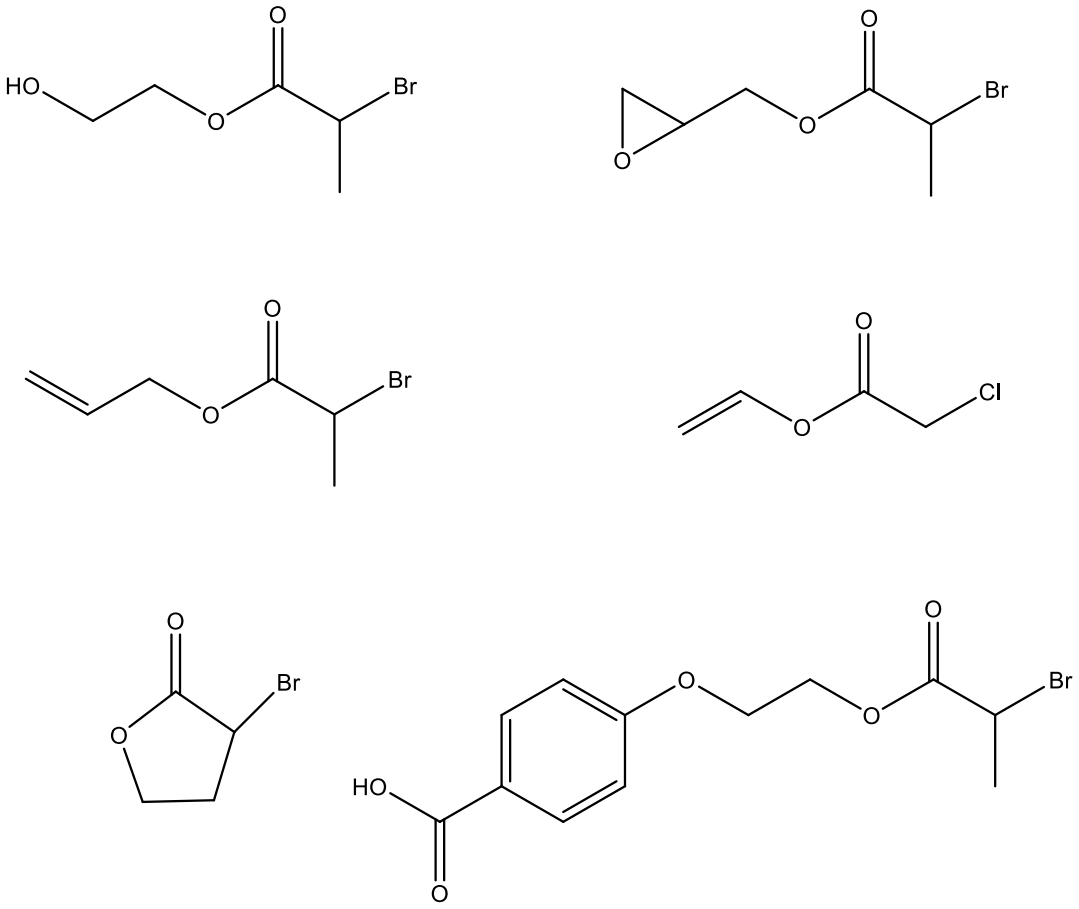

1.4.1.1.3. Catalysts

Copper catalysts are the most broadly used transition metal catalysts in ATRP. The catalyst consists of copper at the oxidation state of +1 complexed by an appropriate ligand (or ligands). In the case of copper, the ligands are typically bi, tri or tetradentate nitrogen-containing ligands. Styrenes, (meth)acrylate esters, amides, and acrylonitriles have all been successfully polymerized via copper-based ATRP.[117, 118, 123] Scheme 1.12 [115] illustrates some copper complex structures.

Scheme 1.12. Copper Complexes used as ATRP Catalysts. [115]

Catalyst complex

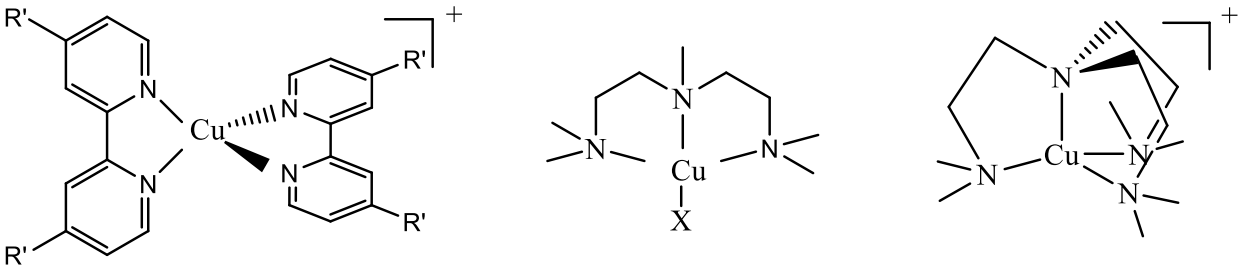

Corresponding deactivator

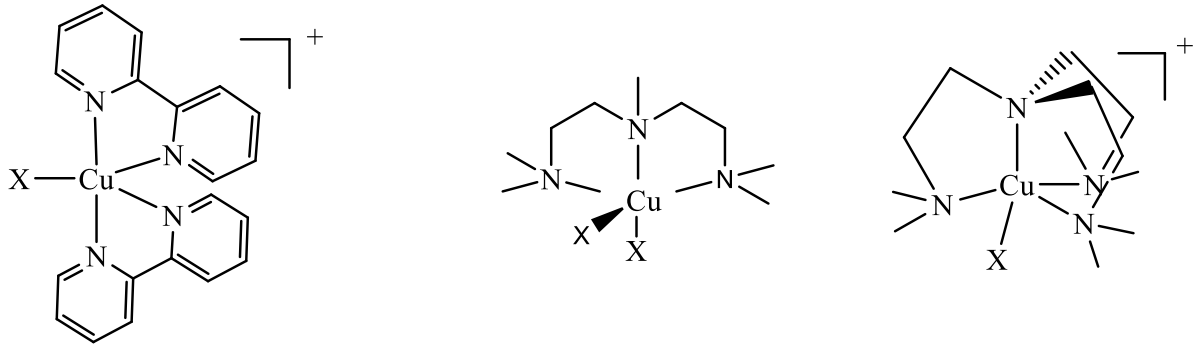

X = Br, Cl

1.4.1.1.4. Ligands

The main function of the ligand in ATRP is to make the transition-metal salt soluble in organic media, to tune the redox potential of the metal center for proper reactivity and dynamics and to ensure the stability of the catalyst complex.[124] Nitrogen ligands have been used with copper- and iron-based catalysts.[124, 125] For copper-catalyzed ATRP, nitrogen-based ligands work very well. Examples of some N-based ligands used successfully in Cu-based ATRP are shown in Scheme 1.13. [115]

Scheme 1.13. Examples of Ligands Used in Copper-Mediated ATRP. [115]

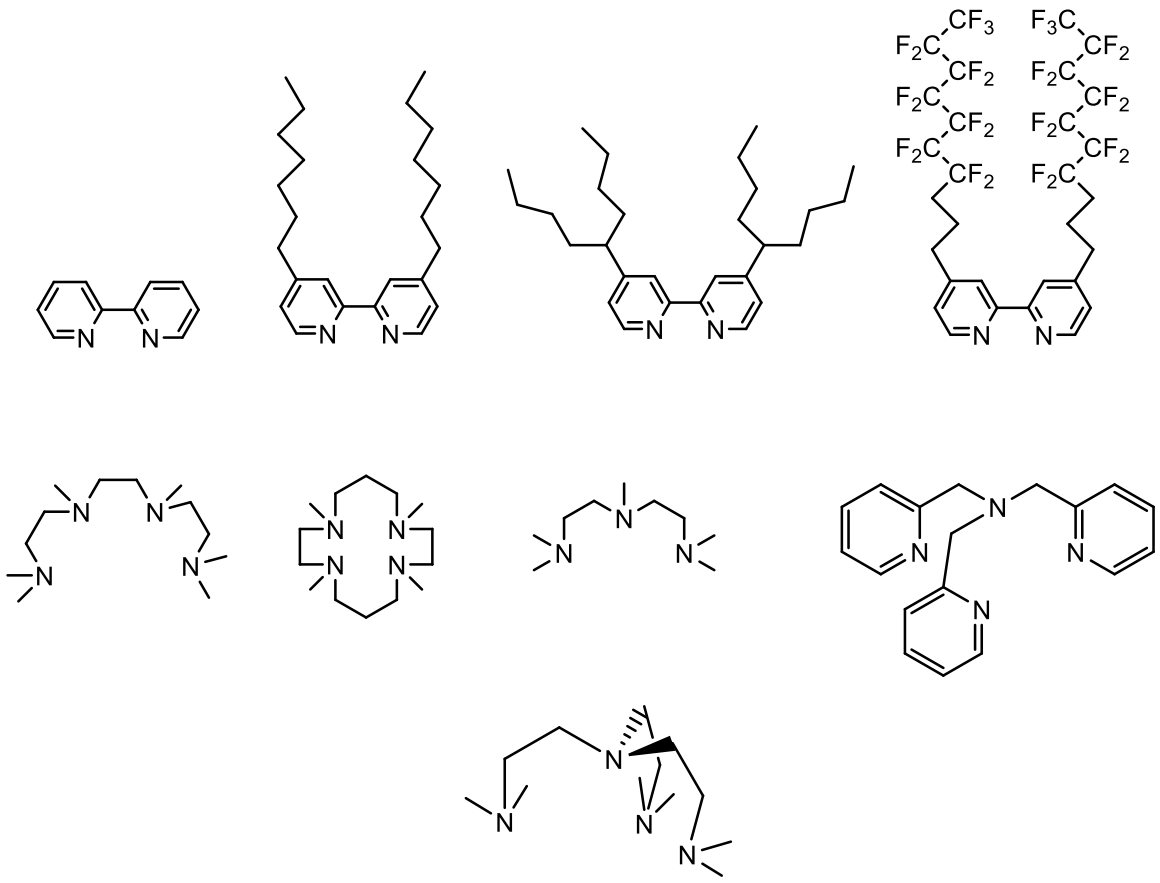

1.4.1.1.5. Solvents, Temperature, Reaction Time and Additives

ATRP can be carried out in bulk, solution, or heterogeneous systems (e.g., emulsion, suspension). Different solvents, such as benzene, toluene, anisole, diphenyl ether, ethyl acetate, acetone, dimethyl formamide (DMF), ethylene carbonate, alcohol, water, carbon dioxide, and many others, have been used for various monomers. A proper solvent is necessary especially when the obtained polymer is insoluble in its monomer (e.g., polyacrylonitrile). [115]

Higher temperature leads to higher rate of polymerization in ATRP, but chain transfer and other side reactions are more obvious at higher temperature, too.[126, 127] Generally speaking, temperature increase leads to increasing solubility of the catalyst, but catalyst decomposition may occur at the same time.[128, 129] The optimum temperature depends on several factors, such as the monomer, the catalyst, and the targeted molecular weight.[115]

When monomer conversions are high, the rate of propagation slows down, but the rate of any side reaction does not change too much. Longer reaction times leading to nearly complete monomer conversion may not increase the polydispersity of the final polymer to any appreciable extent, but will cause the loss of halogen-containing end groups.[130]

1.4.1.2. Molecular Weight and Molecular Weight Distribution

The average molecular weight of the polymer made by a well-controlled ATRP can be predicted by the ratio of consumed monomer and the initiator ($DP_n = \Delta[M]/[I]_o$, DP = degree of polymerization). A relatively narrow molecular weight distribution ($1.0 < M_w/M_n < 1.5$) is often observed.[115]

Scheme 1.14 [115] illustrates a linear relationship of molecular weights with conversion. At the same time, polydispersity (M_w/M_n) decreases with the conversion increase, depending on the relative rate of deactivation (Equation 1.3 [115]).

Scheme 1.14. Relationships of the Molecular Weight and Polydispersity with Conversion for a Living Polymerization. [115]

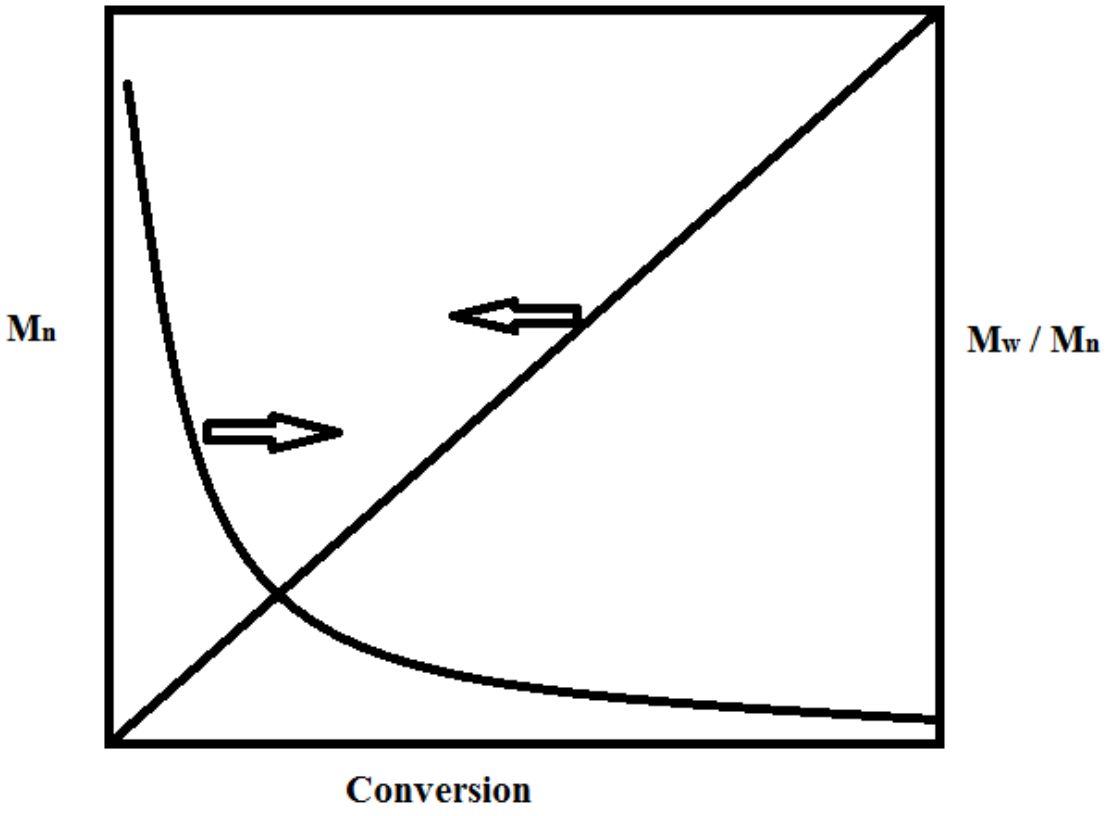

Polydispersity index (PDI, M_w/M_n) is the index indicating the breadth of the polymer molecular weight distribution. In a well-controlled polymerization, M_w/M_n can be 1.10 or even lower. Equation 1.3 shows how the polydispersity index in ATRP relates to the concentrations of initiator (RX) and deactivator (D) (such as Cu^{II} complex in copper catalyst system), the rate constants of propagation (k_p) and deactivation (k_{deact}), and the monomer conversion (p) in the absence of significant chain termination and transfer. [131] In ATRP, a small amount of Cu (II) complex (deactivator) can reduce the proportion of terminated chains and help in establishing the atom transfer equilibrium if added at the beginning of the polymerization.[115]

Equation 1.3. Equation that Describes Polydispersity in ATRP. [115]

$$M_w/M_n = 1 + \left(\frac{[RX]_0 k_p}{k_{deact}[D]}\right)(2/p - 1)$$

1.4.2. Activators ReGenerated by Electron Transfer Atom Transfer Radical Polymerization

In normal ATRP, as the propagating radicals can be rapidly trapped by oxygen, reaction mixtures must be rigorously deoxygenated to achieve successful polymerization. An additional problem is that copper (I) catalyst can be oxidized to copper (II) deactivator, causing a slow polymerization. The required procedure to get rid of oxygen in ATRP is by freeze-pump-thaw cycles, which not only requires special air-tight glassware, but also involves more effort to proceed. An alternative procedure is the passing of an inert gas (such as nitrogen) through the liquid reagents/solvents, the reaction mixture, which may involve the loss of volatile reagents/solvents and complicates the polymerization procedure.

Oxygen can be consumed by introducing a sufficient amount of reducing agents, such as tin(II) 2-ethylhexanoate (FDA approved) in an organic system or ascorbic acid in an aqueous system, in a process called activators generated by electron transfer (AGET) (Scheme 1.15).[119, 132, 133] In AGET, all Cu(II) species are quickly reduced to a Cu(I) state by the reducing agent, and normal ATRP takes place in the presence of more than 1000 ppm (>0.1 %) catalyst.[133] Unfortunately, it is not easy to estimate how much reducing agent is needed. If the amount is excessive, then the control over polymerization will be lost because nearly all of the deactivator (Cu(II) species) is reduced and at the same time a relatively large amount of activator (Cu(I)) exists in the system, leading to uncontrolled ATRP. On the other hand, an insufficient amount of reducing agent is not enough to consume all of the air and the polymerization will not start.[134]

Scheme 1.15. Proposed Mechanism for the AGET Process in ATRP. [119]

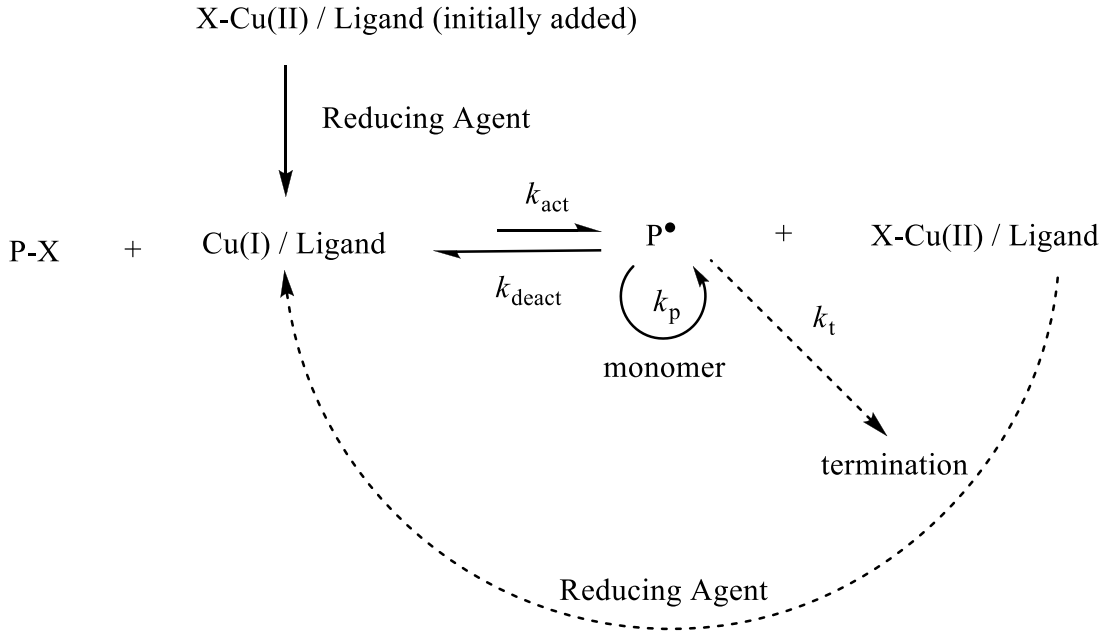

In an improved process, the catalyst amount can be lowered to several or several tens of ppm level while adding excess amount of reducing agent such as (tin(II) 2-ethylhexanoate). The activator (Cu(I) species) is regenerated continuously by electron transfer (this is why the process is referred to as activators regenerated by electron transfer, ARGET).[135] It is reported that ARGET ATRP can be successfully carried out in the presence of initial limited amounts of oxygen with an appropriate amount of a reducing agent. The oxygen is depleted in the polymerization mixture, as it oxidizes Cu (I) to Cu (II), which is reduced to Cu (I) by the -reducing agent. This oxidation-reduction cycle continues until concentration of oxygen is significantly decreased. Reactions can be carried out in flasks fitted with rubber septum or even in closed jars without any deoxygenation step other than that caused by the addition of the reducing agent.[134] The mechanism of ARGET ATRP is illustrated in Scheme. 1.16, while the redox process of Cu (II) to Cu (I) by tin(II) 2-ethylhexanoate is showed in Scheme 1.17.[135]

Scheme 1.16. Mechanism for Activators Regenerated by Electron Transfer Atom Transfer Radical Polymerization (ARGET ATRP). [135]

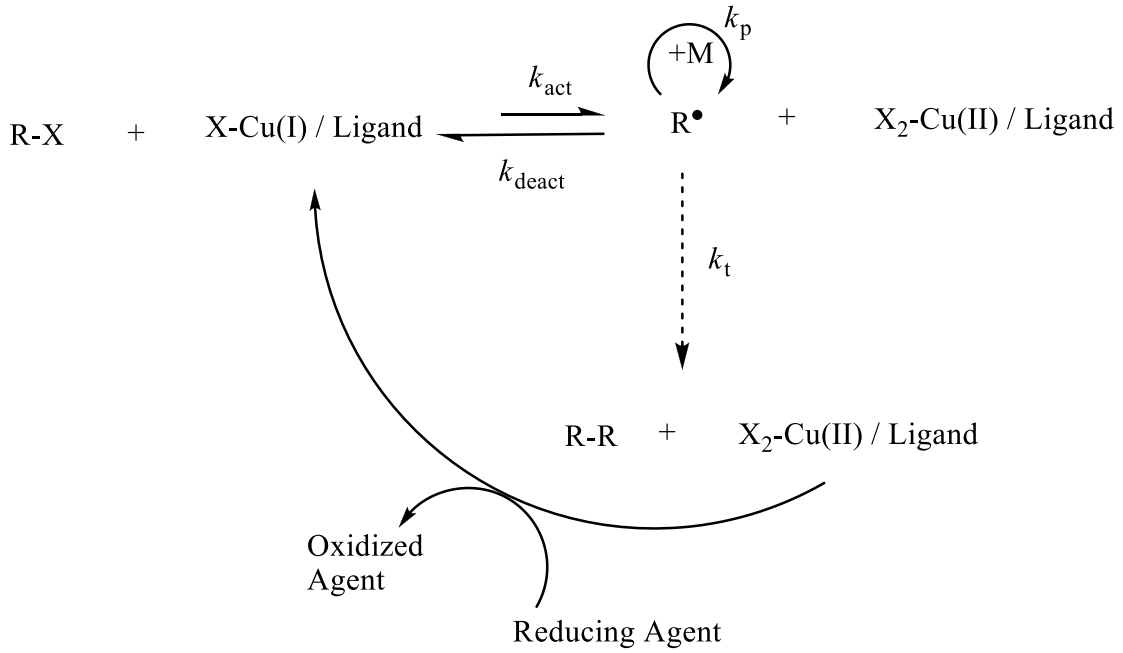

Scheme 1.17. Reduction of Cu(II) to Cu(I) by Tin(II) 2-Ethylhexanoate. [135]

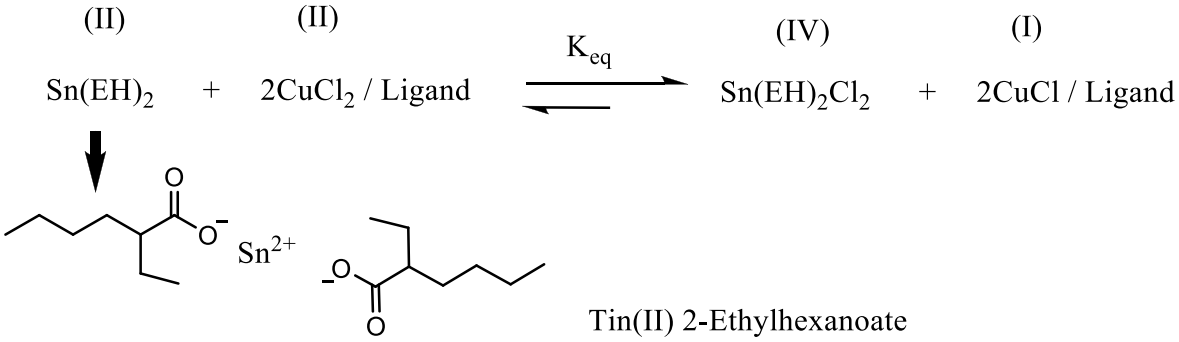

ARGET ATRP provides a convenient technique for living radical polymerization with low level of catalyst (10-100 ppm level). It is also proved that ARGET ATRP can be used to synthesize copolymers with much higher molecular weight, but with retained chain end functionality.[136, 137]

1.5. Recent Works on Preparation of Polymer- Inorganic Layered Filler Nanocomposites via Living Polymerization

1.5.1. Initiation Sites Introduced by Cation Exchange

The advantage of in-situ living polymerization to prepare polymer-(inorganic layered filler) nanocomposites is that the polymer chain length is controllable and the distance between inorganic filler layers is also under control.

The cation exchange is a well-known technique to graft initiator cations onto the surface of layered silicate. In 1999, it was reported that mica surface can be ion-exchanged to introduce peroxide radical initiator, thus allowing one to synthesize mica-polystyrene nanocomposite via uncontrolled radical polymerization. Also in 1999, the Sogah group reported the delaminated polystyrene/montmorillonite nanocomposite synthesis via living nitroxide-mediated free radical polymerization (NMP). [67a] After introducing the initiator cations, the interlayer spacing was enlarged from 1.26 nm to 2.35 nm. The fully dispersed architecture was confirmed by the absence of x-ray diffraction peak after polymerization and by the TEM images, which showed that the silicates were randomly dispersed. No glass transition temperature was detected by differential scanning calorimetry (DSC) for the nanocomposite. These results were noted to be the first example of a dispersed polystyrene/silicate nanocomposite. [67a] Later, Ha et al. [67b] showed that the aforementioned synthesis method is capable of affording intercalated polystyrene-clay nanocomposite with the interplanar spacing of 4.2 and 12.6 nm, suggesting an excellent ability to retain the ordered structure even with an appreciable polystyrene loading. It should be noted that NMP with TEMPO as an initiator is primarily suitable for styrene-type

monomers and some of their random copolymers, [67c] so an extension of this methodology on other polymer-clay compositions would require the use of a different initiator. Sogah and coworkers reported the exfoliated poly(styrene-*b*-caprolactone)/silicate nanocomposites later via one-pot, one-step in situ living polymerization by introducing the bifunctional initiator cations into silicate layers. XRD did not show any ordering pattern for this nanocomposite, and the dispersed silicates layers in the polymer matrix were observed in scanning transmission electron microscopy (STEM) image. DSC only showed the melting point for the polycaprolactone (PCL) segment, but no glass transition temperature was detected. [73] Behrens group applied ATRP method to synthesize the poly(methyl methacrylate)/montmorillonite nanocomposite. The cationic initiator was synthesized by a two-step procedure. The initiator-modified silica had an interlayer distance of 1.88 nm (which is significantly larger than 1.16 nm for the original clay). They reported a fully dispersed architecture as no X-ray diffraction peaks were seen for the nanocomposites after 1-4 hours of polymerization. There was only a weak diffraction peak at a 2θ angle smaller to that for the initiator in XRD pattern of the material obtained after 0.5 hour of polymerization for their nanocomposite. [68] The Shipp group has also done works on atom transfer radical polymerization initiated from the clay surface. In their research, the initiators were grafted via cation exchange. For the polystyrene/silicate nanocomposites, d_{001} peak in XRD patterns moved slightly to smaller angles (down to 2θ = ~3 °) with increasing monomer conversion and it disappeared after 6 hours of polymerization. Large clay particles and their aggregation were still present in the nanocomposites after 40 minutes of polymerization, as observed in TEM image. Even after 6 hours of polymerization, some areas in TEM image showed a relative high concentration of silicate, although some silicate layers were exfoliated in the polymer. Based on these results, mixed intercalated/exfoliated polystyrene/montmorillonite

nanocomposites were reported. [69] On the other hand, poly(methyl methacrylate)/montmorillonite nanocomposite was claimed to be more exfoliated than the polystyrene/montmorillonite nanocomposite, which was confirmed by TEM. [69] However, in both cases, intercalated structures with uniform d_{001} spacing giving rise to low angle peaks were not observed. Poly(styrene-*block*-butyl acrylate) copolymer/montmorillonite nanocomposite were also achieved, although it was not a completely homogenous dispersion of the silicate layers, which was showed in TEM. [70, 71] Shipp group also applied reversible addition-fragmentation chain transfer polymerization (RAFT), which is another controlled radical polymerization technique, to produce exfoliated polystyrene, poly(butyl acrylate), poly(methyl methacrylate)/montmorillonite nanocomposites via grafting through method. [72] An interesting hierarchical self-assembly phenomenon was found in poly(styrene-*block*-*tert*-butyl acrylate)/montmorillonite nanocomposites, which showed different architectures (layered or ellipsoidal), as seen from transmission electron microscopy (TEM). [75] To some extent, the silicate layers appeared to be bent, this also had been reported by Vaia group. [138] The graft density of polymer chains affected the kinetics of surface-initiated ATRP of polystyrene from montmorillonite. The Cochran group observed a seven-fold increase in the polymerization rate when the polymer chain graft density reached ~1 chain/nm^2. When the graft density was reduced, the polymerization process exhibited the same kinetics as in bulk system. [74] In this case, the initiator was introduced by cation-exchange and polydispersities of the graft polymer were found to be low.

While radical polymerization is particularly convenient in the synthesis of polymer-clay nanocomposites via surface-initiated polymerization, other methods, such as living anionic polymerization [67d, 67e] and ring opening polymerization [67f] can also be used.

1.5.2. Initiation Sites Introduced By Covalent Bonding

Due to the surface nature of clay silicate, the initiation sites appear to be more easily introduced by cation-exchange than covalently grafted on the surface. However, the covalent bonding would be more attractive from the point of view of stability, if it can uniformly modify the surface of the layered material.

In the research by Wei group, [139] ATRP initiation sites were introduced via a reaction of silanols on the clay surface with aminopropyl dimethyl ethoxysilane, which was then reacted with 2-bromopropionyl bromide. The resulting polystyrene/silicate nanocomposites were reported to be a mixed intercalated/exfoliated structure. The diffraction peak disappeared after 6 hours of polymerization, and the *d*-spacing was slightly enlarged to about 2.23 nm ($2\theta = 3.96°$) after 3 hours of polymerization (initiator-modified silicates had a *d*-spacing equaled to 1.64 nm). [139] As the silanol groups were located on the edge of clay, Mathias group investigated the synthesis of covalently functionalized laponites, which were capable of polymerization, photoinitiation and ATRP. [79] In other cases, the polymer was reported to be grafted on the edges of the clay layers. Lin group also modified the edge of montmorillonite with synthesized α-bromoester derivative moiety to produce poly(N-isopropylacrylamide)/montmorillonite nanocomposite. [76a] ATRP grafting from covalently bonded initiators on mica surface was also explored.[76b, 76c]

From these previous research works on the preparation of polymer/silicate nanocomposites, the challenge is to maintain a homogenous architecture. The ordering of intercalated morphology is easily destroyed during polymerization, which means that a uniformly periodic intercalated architecture is not easy to achieve. If the ordering is lost at early stages of the polymer grafting, it

is more difficult to understand the relation between the polymer loading and the interlayer distance and make inferences about uniformity of the polymer growth on the surface. The dispersion (exfoliation) of inorganic fillers (silicates) is not completely homogenous in most cases. The investigation of a new methodology that can control the architecture and achieve a homogenous dispersion of inorganic components in the nanocomposites is a very meaningful project.

Chapter II.

Synthesis of Surfactant-Templated Silica with Lamellar Structures

2.1. Lamellar Silica Synthesis Based on Cationic/Neutral Surfactants Mixture

The preparation was based on the method reported by Ryoo et al. [140] The silica source was an aqueous solution of sodium tetrasilicate (11.3 wt.% $Na_2Si_4O_9$ and 88.6 wt.% H_2O), which was prepared with colloidal silica Ludox HS40 (Sigma Aldrich) (22.9 wt.%), distilled water (74.2 wt.%), and NaOH (Acros Organics) (2.9 wt.%). [141] The mixture was magnetically stirred overnight at room temperature. The surfactant mixture was prepared by dissolving a cationic surfactant (hexadecyltrimethylammonium bromide, HTMABr (Alfa Aesar)) and a neutral surfactant (Brij ® 30, $C_{12}(EO)_4$ (Acros Organics)) simultaneously in distilled water (weight percentages were: 5.92 % cationic surfactant, 1.97 % neutral surfactant and 92.11 % distilled water in solution mixture) at 60 ℃, and then the surfactant solution was cooled to room temperature. At room temperature, the silica source was drop-wise added into the surfactant solution under stirring and the mixture was magnetically stirred vigorously overnight. The gel mixture thus obtained was hydrothermally treated under static conditions at 373 K in a closed polypropylene bottle in the oven for one day. The precipitated product (denoted "**1**") from the reaction mixture was then filtered, and dried in a vacuum oven at 333 K. The molar ratios in the synthesis mixture were: 5.0 SiO_2/1.25 Na_2O/0.25 $C_{12}(EO)_4$/0.75 HTMABr/400 H_2O.

Small-angle X-ray scattering (SAXS) patterns were acquired using a Bruker Nanostar U SAXS/wide-angle X-ray scattering (WAXS) system with a rotating anode X-ray source and Vantec-2000 area detector. The Nanostar U system had a sample-to-detector distance of 72 cm and was in high-flux configuration. The powder samples were secured in a hole of a sample holder plate by a Kapton or Scotch tape and put in a sample holder. The thermogravimetry was performed on TA Instruments 2950 Thermogravimetric Analyzer (TGA) under N_2 gas flow at 5 ℃/min with heating up to 800 ℃. FEI TECNAI Spirit Transmission Electron Microscopy

(TEM) instrument was used to examine the morphology of samples. The examined samples were dispersed in ethanol by sonication for an hour and deposited on a carbon-coated copper grid before imaging in TEM.

The weight loss of the surfactant-containing layered silica **1** powder was 65%, and the two degradation steps were around 213 °C (43% weight loss) and around 414 °C (15% weight loss) (Figure 2.1). It is suggested that these two steps corresponded to the weight loss of cationic surfactant ($HTMA^+$) and the neutral surfactant ($C_{12}(EO)_4$). The ordered lamellar structure was confirmed by SAXS pattern shown in Figure 2.2. Inter-layer spacing (001) was about 3.5 nm with the main peak at 2θ = 2.5 °($d_{001} = \frac{0.15418}{2\sin(\frac{2\theta}{2})}$ nm). After calcination under air at 550 ℃, the ordering features (001 and 002 peaks) were lost in the SAXS pattern (Figure 2.2), which meant that the lamellar structure collapsed during calcinations when the surfactants were removed from the space between silica layers. TEM image (Figure 2.3) provided some insight into the architecture of the layered silica, because some contrast differences in the edge area suggested the presence of overlapping plates. Based on the SAXS results, surfactant-templated layered silica **1** with 3.5 nm interlayer spacing was successfully synthesized.

Figure 2.1. Thermogravimetric Weight Change Curve of As-Synthesized Surfactant-Templated Layered Silica **1** under N_2 Atmosphere.

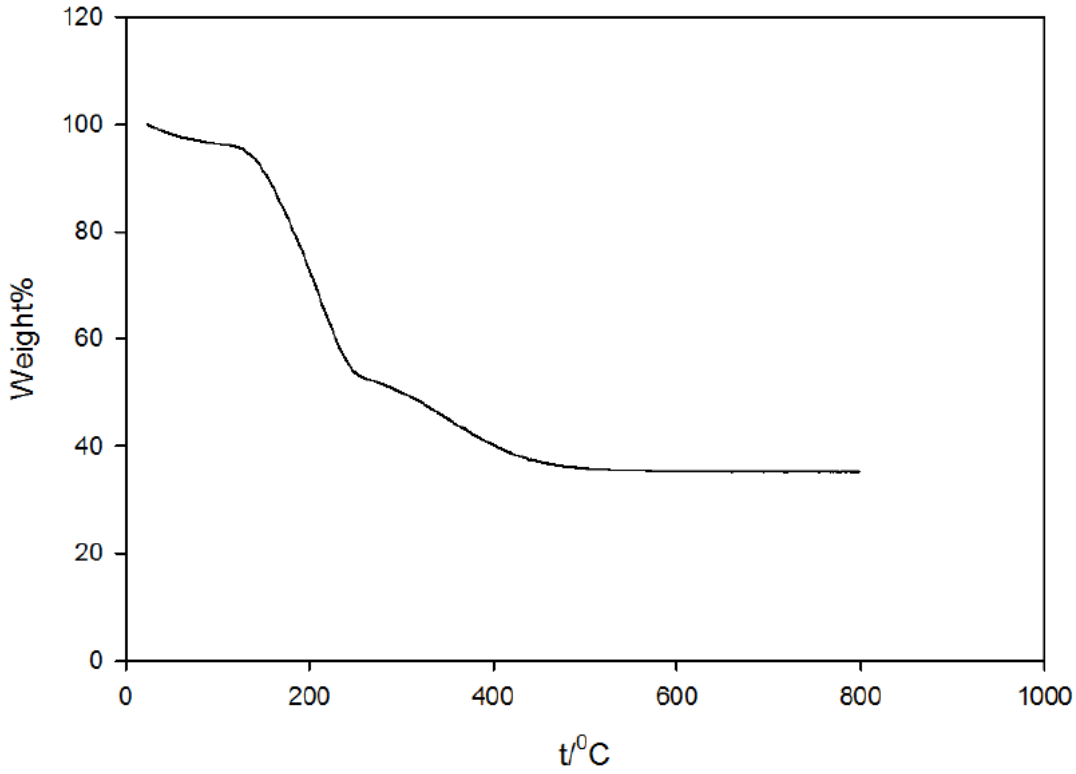

Figure 2.2. Small-Angle X-ray Scattering Patterns of As-Synthesized Surfactant-Templated Layered Silica **1** and Same Sample after Calcination under Air at 550 ℃**.**

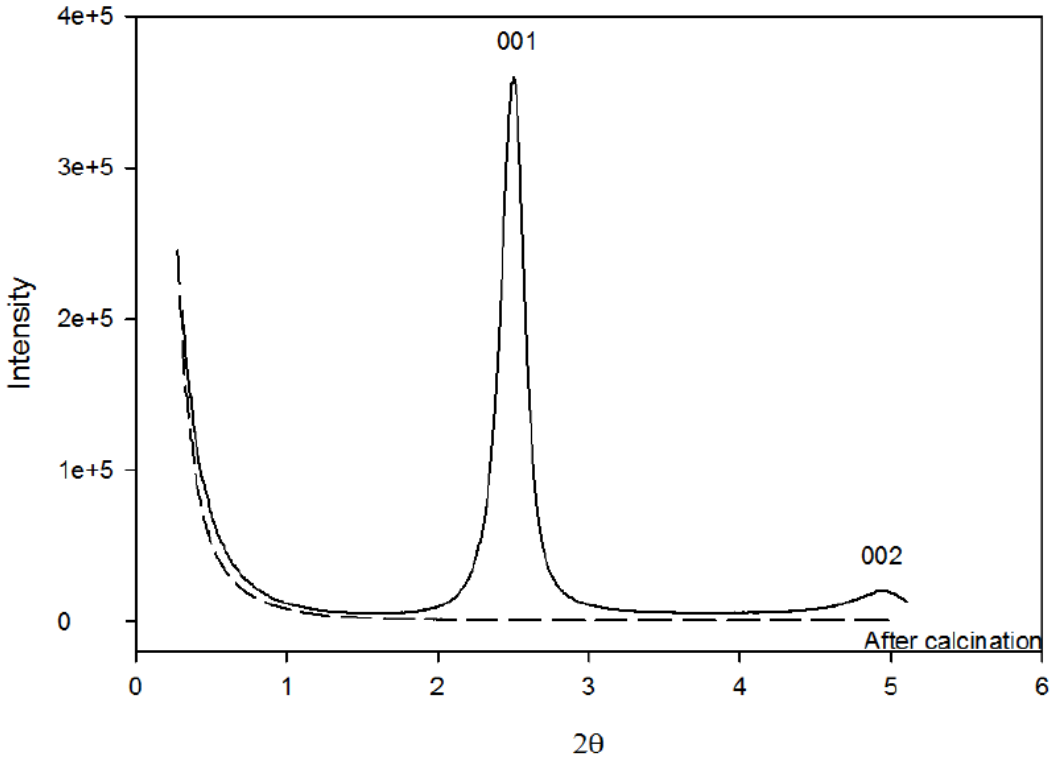

Figure 2.3. TEM Image of As-Synthesized Surfactant-Containing Layered Silica **1.**

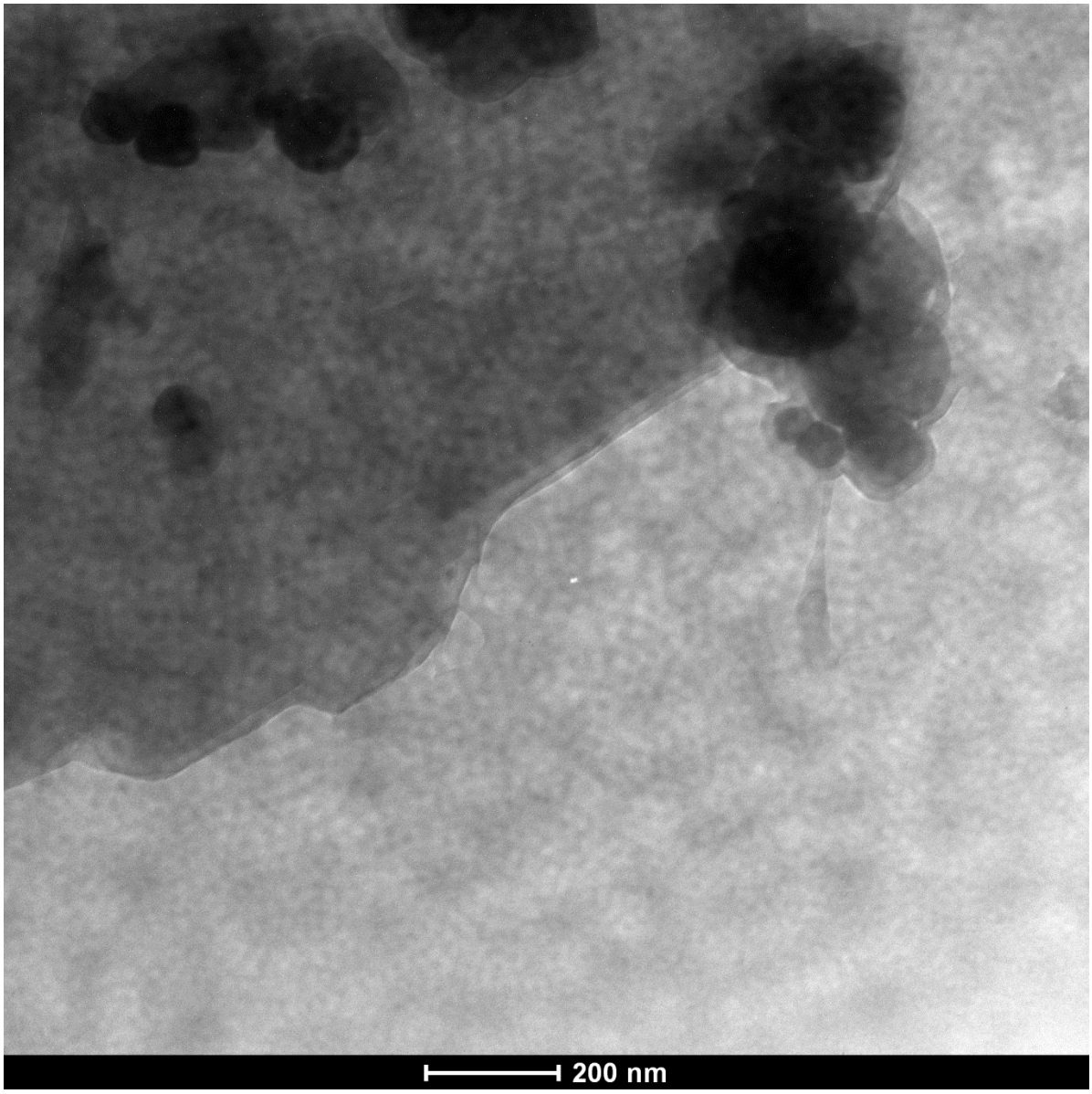

2.2. Lamellar Silica Synthesis Based on Neutral Surfactants Mixture

The preparation was performed as described in the literature. [142] In a typical synthesis, a 3.0 g mixture (Brij®(30) : dodecanol = 2.56 g : 0.45 g, molar ratio = 3 : 1) was dissolved in 57.4 g distilled water and stirred for 2 hours at room temperature. 8.80 g of sodium metasilicate was added under stirring, and the solution was stirred for another hour to achieve a clear solution. 17.7 g (15 ml) of concentrated HCl was quickly added under vigorous magnetic stirring. The reaction mixture was stirred for 24 hours at room temperature and was heated under static condition at 373 K for 24 hours in the oven. White silica product (denoted "**2**") was filtered and dried in a vacuum oven at 333 K. The material was characterized as described in chapter 2.1.

The weight loss of as-synthesized surfactant-templated layered silica **2** powder was 58% (Figure 2.4). The ordered lamellar structure was confirmed by SAXS pattern in Figure 2.5. Inter-layer spacing was about 5.4 nm because the main (001) peak was at $2\theta = 1.63°$. The morphology of layered silica **2** was illustrated in Figure 2.6 and 2.7, and the areas indicated by arrows illustrated ordering. Based on the scale bar in TEM images, the interplanar spacing was not constant (about 6-10 nm), which might be due to the surfactants between silica layers being washed out during one-hour sonication in ethanol before TEM imaging, resulting in a looser and less regular arrangement of the layers. TGA pattern showed that the weight loss for layered silica 2 after sonication dropped to only 21% (Figure 2.8). It is also possible that ethanol swelled the layered material. Based on SAXS, knowing the interlayer spacing of as-synthesized material from SAXS prior to sonication, one can conclude that the interplanar spacing was enlarged somewhat as a result of sonication as showed in TEM images. The details in the part of TEM image (Figure 2.7) clearly illustrated the ordering in layered silica **2**.

Figure 2.4. Thermogravimetric Weight Change Curve under N_2 Atmosphere of As-Synthesized Surfactant-Templated Layered Silica **2**.

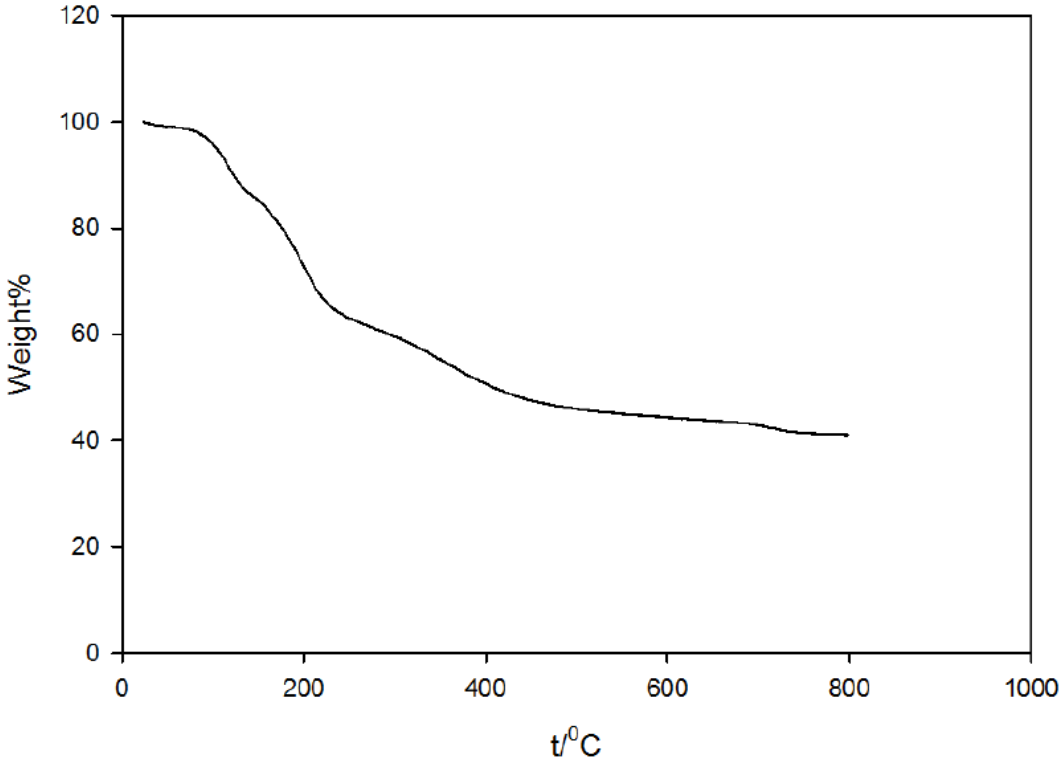

Figure 2.5. Small-Angle X-ray Scattering Pattern of As-Synthesized Surfactant-Templated Layered Silica **2.**

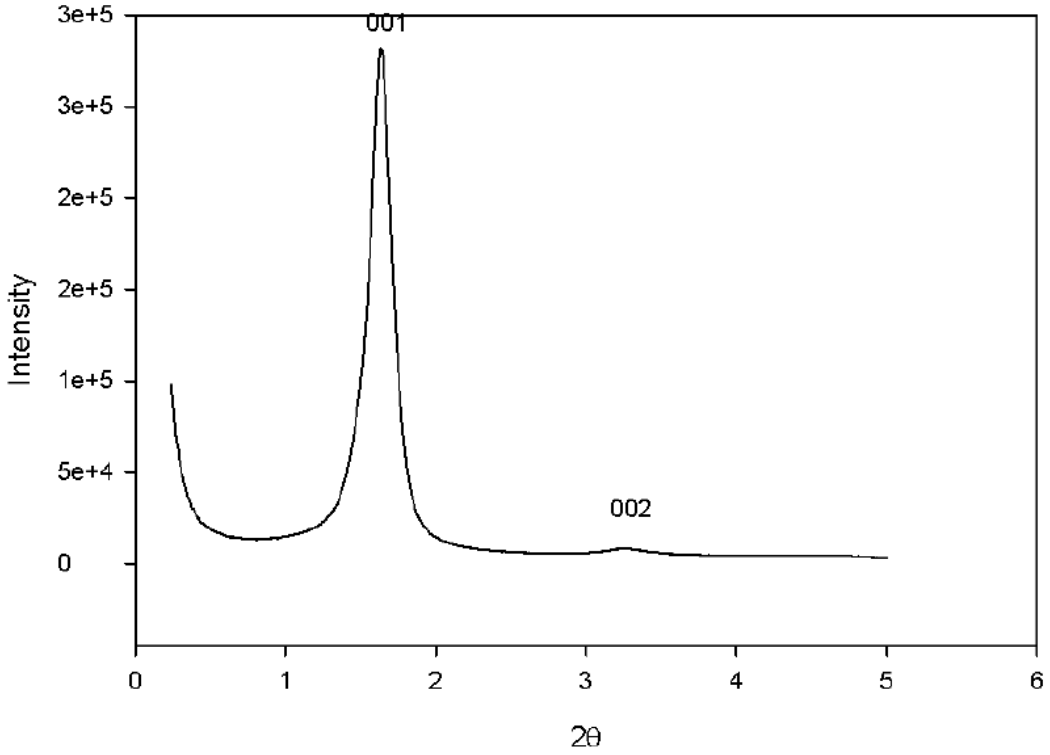

Figure 2.6. TEM Images of As-Synthesized Surfactant-Containing Layered Silica **2** (The Sample was Sonicated in Ethanol prior to Imaging)**.**

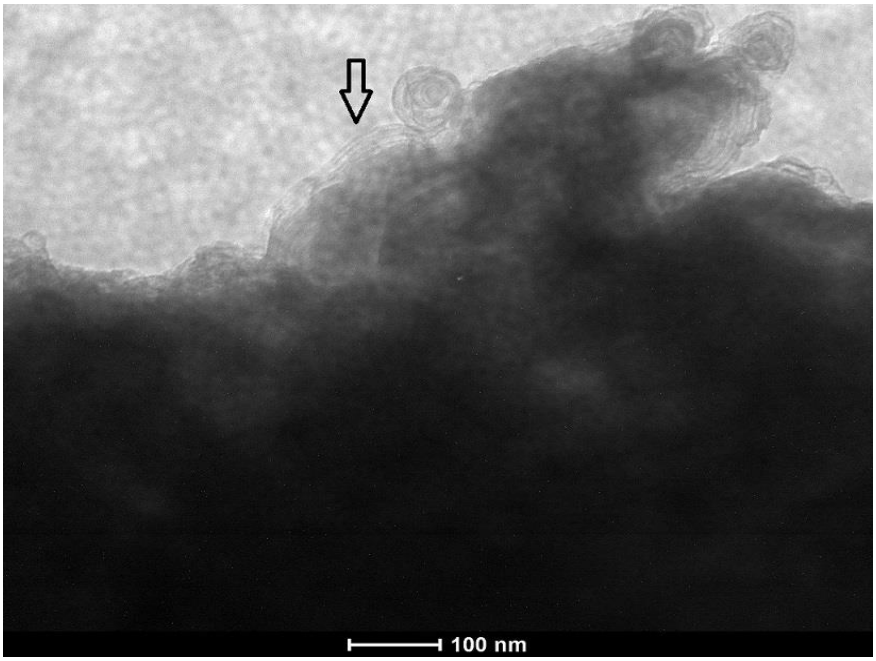

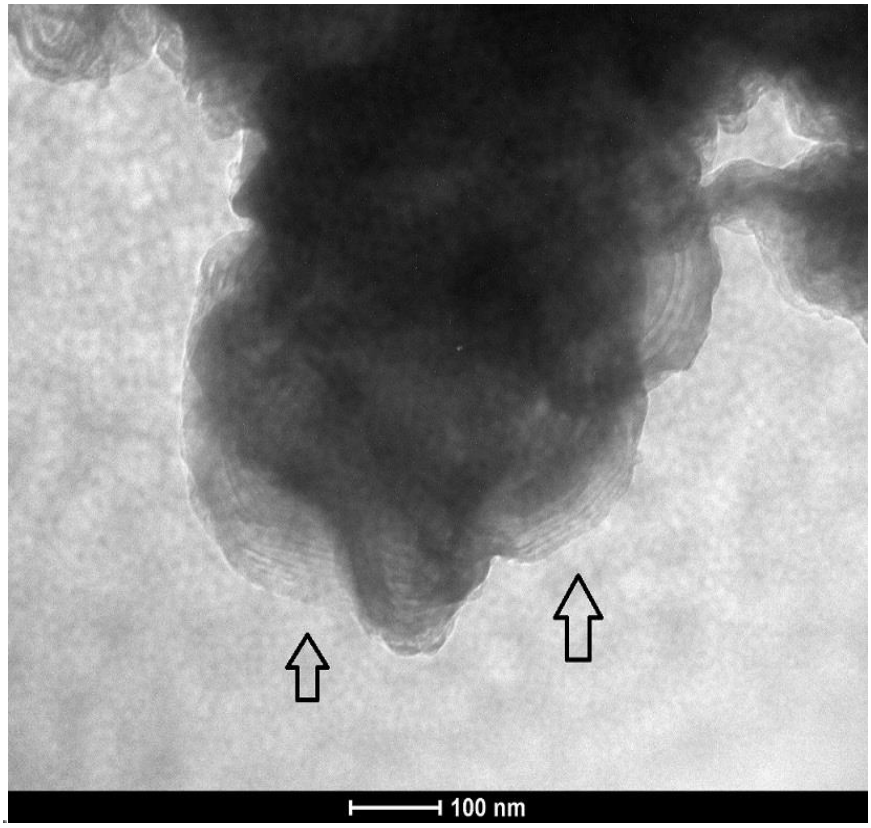

Figure 2.7. Enlarged Part of TEM Image of Layered Silica **2** (The Sample was Sonicated in Ethanol prior to Imaging).

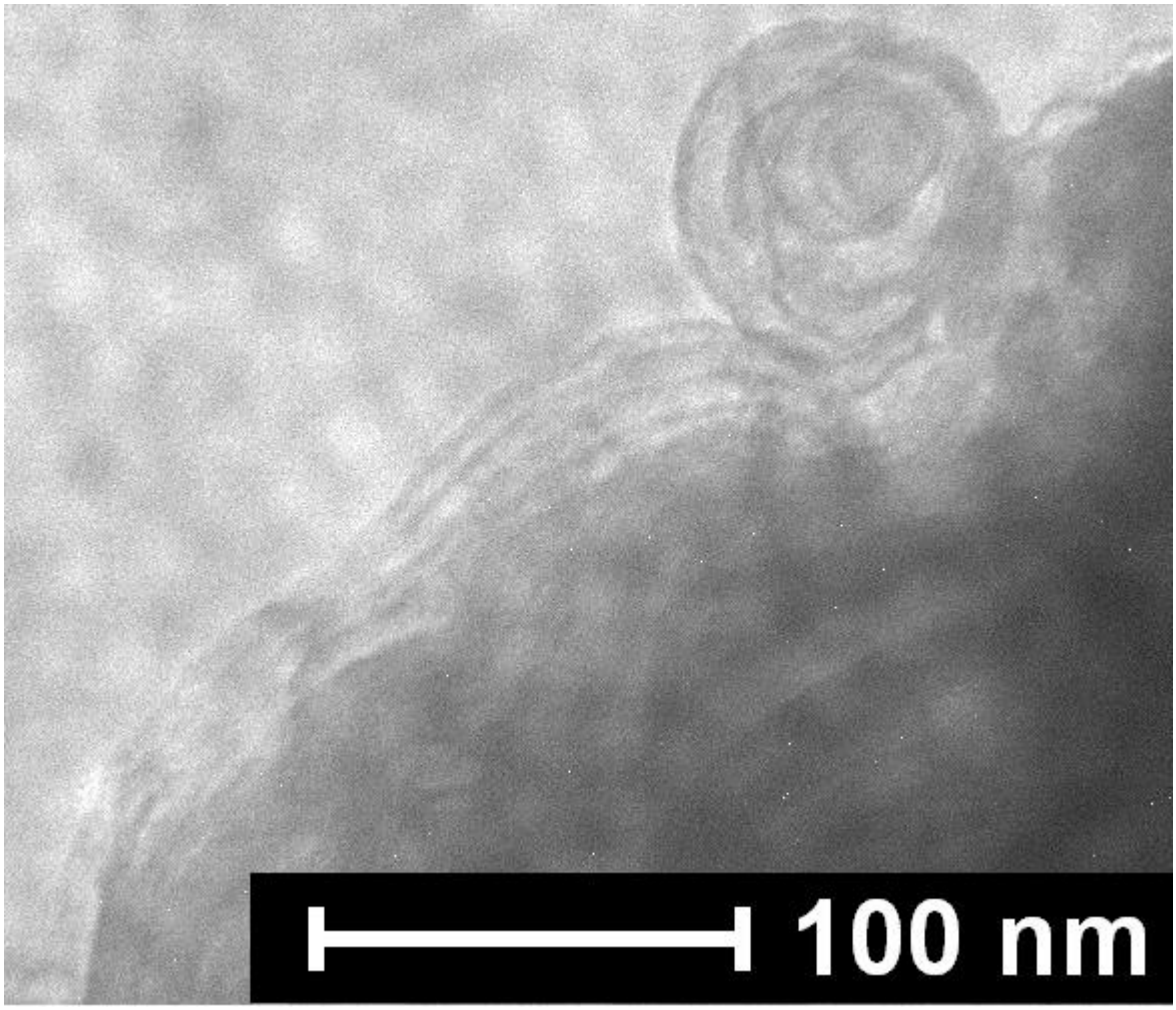

Figure 2.8. Thermogravimetric Weight Change Curves of Layered Silica **2** and after One-Hour Sonication in Ethanol.

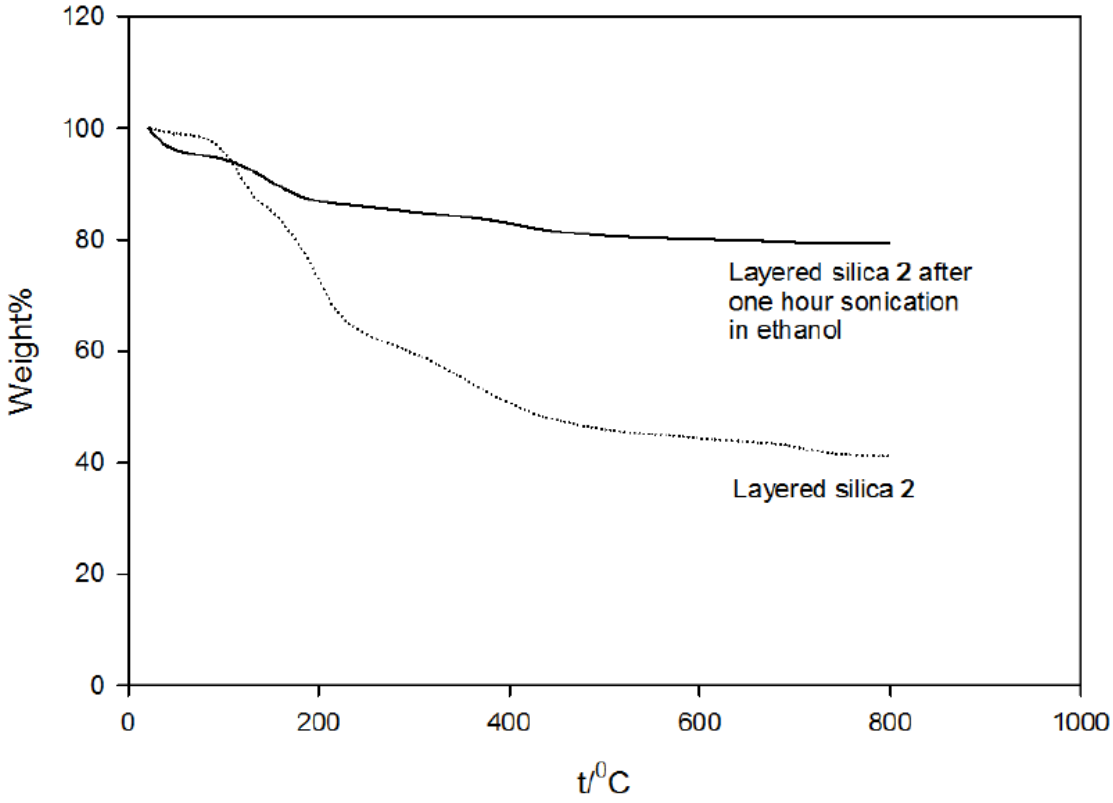

The results presented above show that layered silicas **1** and **2** were successfully prepared using cationic/nonionic surfactant mixture and neutral surfactant mixture following the literature procedures. The lamellar morphology was confirmed by SAXS and TEM. The interlayer spacing of silica/surfactant composites was 3.5 nm and 5.4 nm for layered silicas **1** and **2**, respectively. The surfactants were sandwiched between the silica layers, and they contributed to about 65% (layered silica **1**) and 58% (layered silica **2**) weight of the whole structure.

Chapter III.

Synthesis of Nanocomposites Using Surface-Initiated Normal Atom Transfer Radical Polymerization (ATRP)

3.1. Layered-Silica/Polymer Nanocomposite Synthesis Outline

Surface-initiated atom transfer radical polymerization (ATRP) was used to graft uniform layers of various polymers on concave surfaces of cylindrical silica mesopores (diameter 11 nm) and spherical silica mesopores (diameter ~14 nm). As shown in Scheme 3.1, a mesoporous silica support was modified by initiator (3-(chlorodimethylsilyl)propyl 2-bromo-2-methylpropanoate) and "inert" silane trimethylchlorosilane, and ATRP of different monomers was carried out. As a result, polymer chains were grafted on the surface of the mesopores.[143]

Scheme 3.1. Surface-Initiated Atom Transfer Radical Polymerization in Ordered Nanopores (reproduced from Reference 143 with permission). [143]

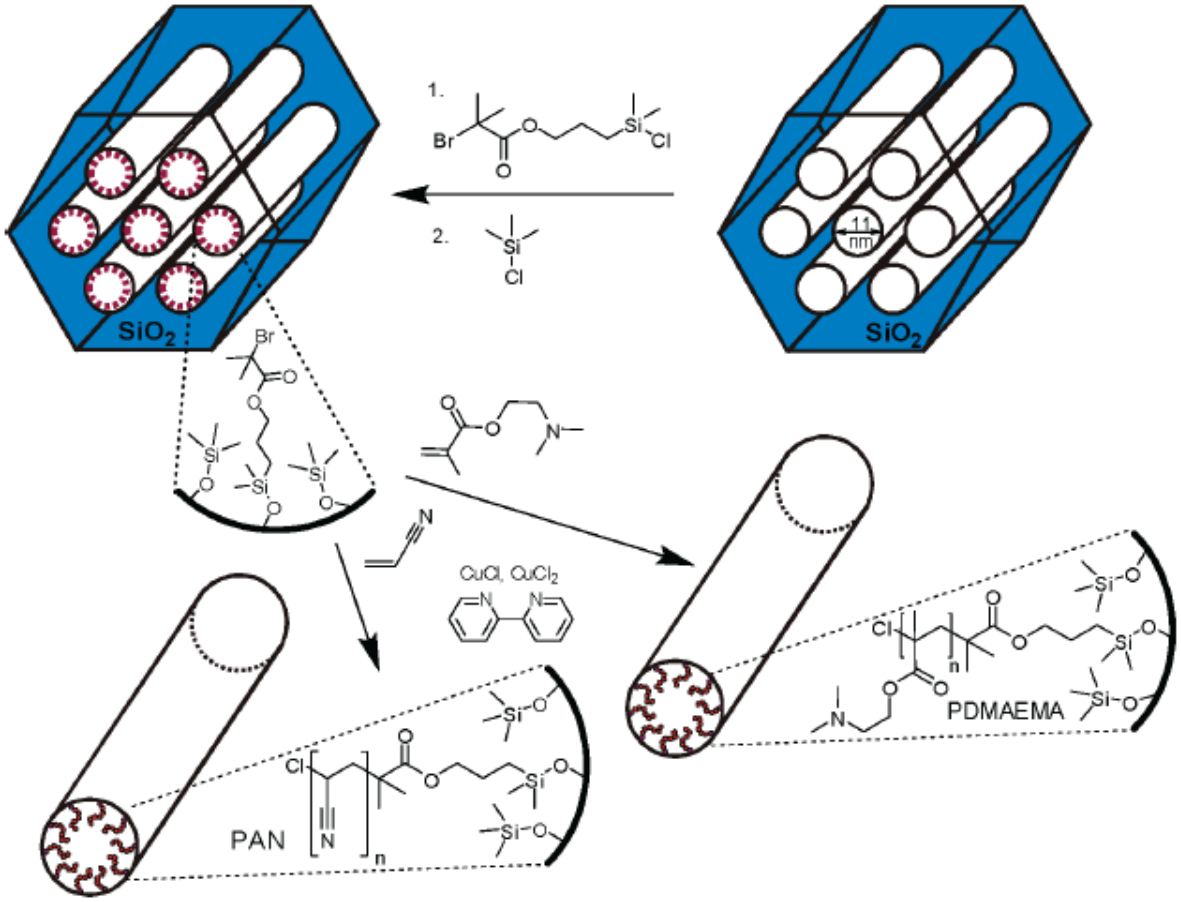

Although the polymerization in the mesopores appears at first to be very different from the polymerization on the surface of layered materials used to prepare the nanocomposites with nanoscale silica layers in the polymer matrix, the proposed synthetic route was similar, as illustrated in Scheme 3.2. First, a surfactant-templated nanoscale layered silica precursor was prepared as described in Chapter II; then the initiator (organosilane) was attached to the surface of the layered silica while removing (displacing) the surfactants; finally, polymer chains were grafted on the surface of layered silicas to achieve intercalated or exfoliated silica/polymer architectures. Despite the clear similarity in the synthesis approach, there are some important differences between the preparation of silica/polymer composites based on porous silicas and those involving layered materials. The first one is the need for the surface modification of the surfactant-containing layered silica, because if the surfactant is removed, the silica layers would collapse on one another and possibly covalently cross-link. The subsequent surface modifications would not be expected to result in efficient separation of the silica layers. The methods to modify surfactant-containing ordered mesoporous silicas have been established. [144a, 144b] The methods of surface modification of surfactant-intercalated clays are also known. [145a-145d] The method has been extended on surfactant-templated lamellar silicas that were successfully modified with trimethyl silyl, 2-glycidoxypropyl silyl and 2-(methoxy(polyethyleneoxy)propyl silyl groups. [145e-145h] Herein, we successfully implemented this method to functionalize surfactant-templated layered silicas with ATRP initiator. The second difference is that when polymer chains grow from the surface of ordered mesoporous silica support, typically the polymerization takes place in the pores (or outside particles of the material), without the change in the morphology of the silica structure. However, the surface-initiated polymerization on the surface of layers changes

their distance and may change their relative arrangement, because the silica layers do not constitute a continuous framework, but rather are separate nanoobjects.

Scheme 3.2. Proposed Synthetic Route to Prepare Well-Defined Layered-Silica/Polymer Nanocomposites.

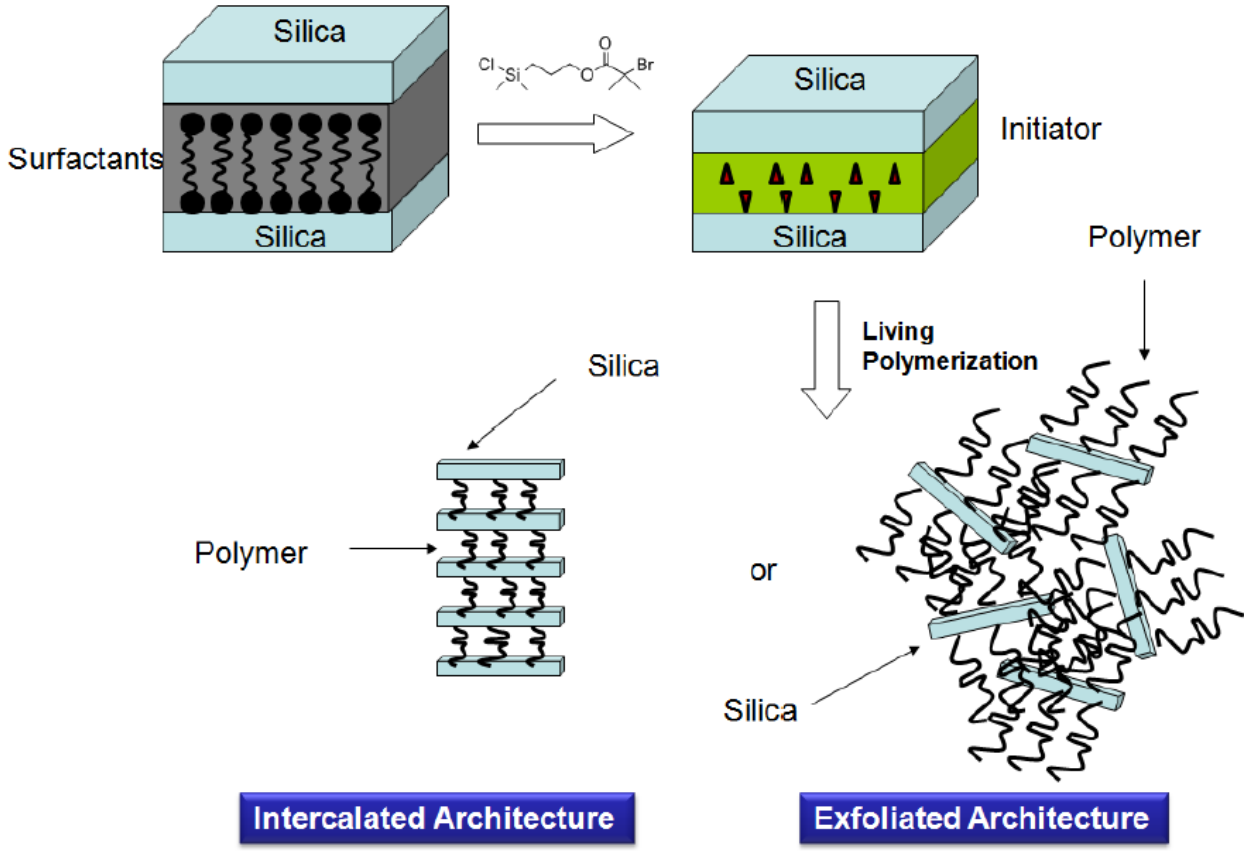

3.2. Functionalization of Silica Layers with Initiator

The following general surface modification procedure was used with all of organosilanes. In a typical synthesis, the surfactant-containing layered silica was dispersed in toluene (extra dry) under magnetic stirring. Pyridine was added (toluene/pyridine volume ratio 7:1), and then the organosilane in excess amount was introduced. The mixture was refluxed at 90 ℃ for 1 day under magnetic stirring. [146] The product was isolated by filtering and washing several times with ethanol. Then, the sample was dried in a vacuum oven at 60 ℃. The initiator-modified layered silicas used for polymerizations were denoted as 1-CDMSPBMP (for layered silica **1**) and 2-CDMSPBMP (for layered silica **2**).

The organosilanes (trimethylchlorosilane, n-butyldimethylchlorosilane, dimethyloctylchlorosilane, chloromethyl phenylethyl trichlorosilane, 2-(4-chlorosulfonyl phenyl) ethyl trichlorosilane) used to modify the surface of layered silica were used as received except 3-(chlorodimethylsilyl)propyl-2-bromo-2-methylpropanoate, which was synthesized as described elsewhere.[146]

The modification of silica surface is illustrated in Scheme 3.3. The procedure was to attach the initiator onto the layered silica surface via covalent bonding without loss of the layered morphology. To select a proper initiator to be attached on the surface of layered silica, a series of organosilanes were examined. Trimethylchlorosilane (TMCS), n-butyldimethylchlorosilane (BDMCS), dimethyloctylchlorosilane (DMOCS), chloromethyl phenylethyl trichlorosilane (CMPETS), 2-(4-chlorosulfonyl phenyl) ethyl trichlorosilane (CSPETCS), 3-(chlorodimethylsilyl)propyl 2-bromo-2-methylpropanoate (CDMSPBMP) (structures in Scheme 3.4) were used to modify layered silica **1**. Selected properties of the modified silicas were compared with those of unmodified layered silica **1** in Table 3.1. After the modification, the

weight loss and interlayer spacing decreased, indicating that the organosilanes replaced the surfactants and attached onto the silica surface with covalent bonds.

Scheme 3.3. Surface Modification of Surfactant-Templated Layered Silica.

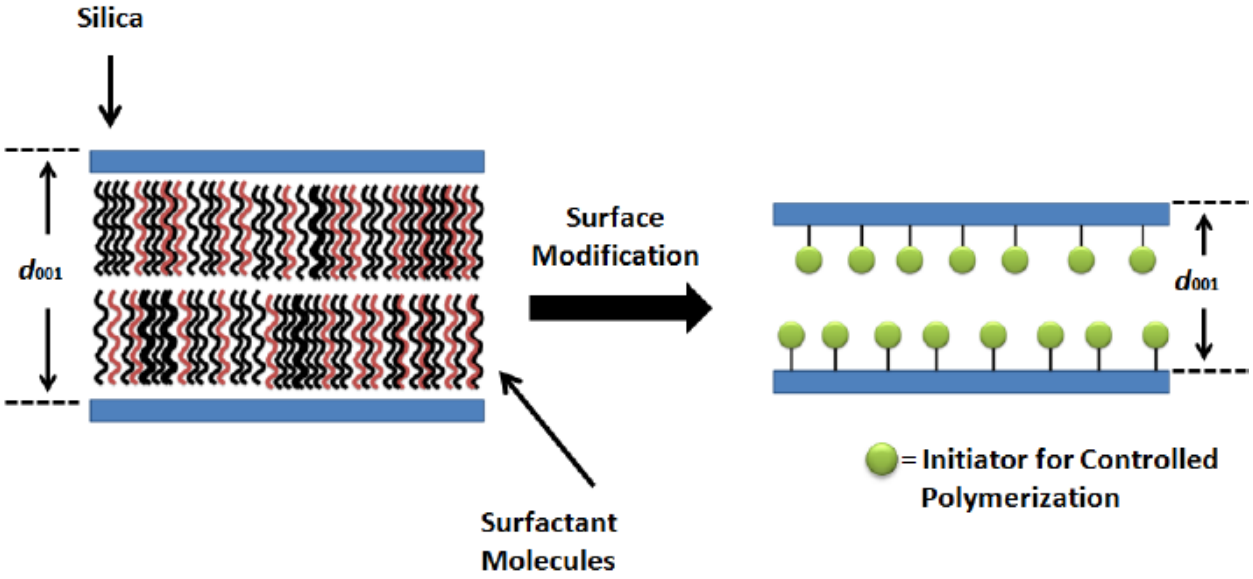

Scheme 3.4. Structures of Organosilanes Used in the Study.

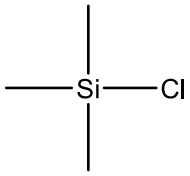

Trimethylchlorosilane (TMCS)

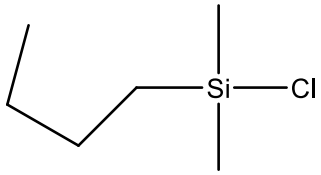

n-Butyldimethylchlorosilane (BDMCS)

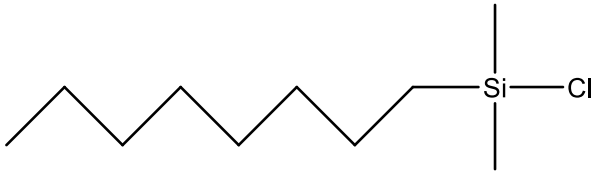

Dimethyloctylchlorosilane (DMOCS)

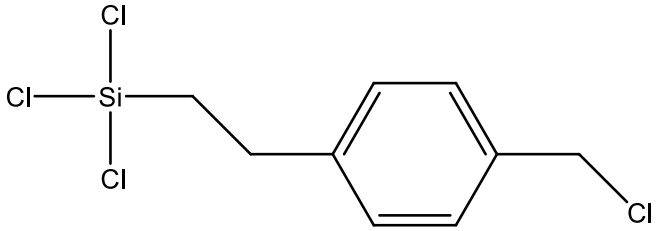

Chloromethyl phenylethyl trichlorosilane (CMPETS)

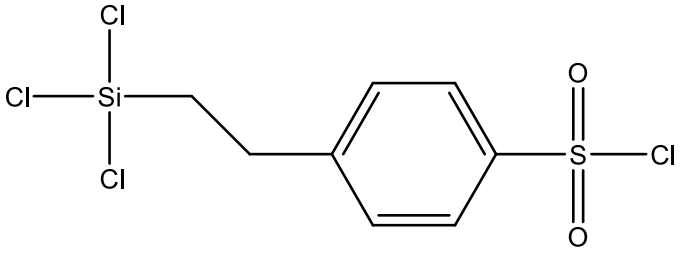

4-(2-(Trichlorosilyl)ethyl)benzene-1-sulfonyl chloride (CSPETCS)

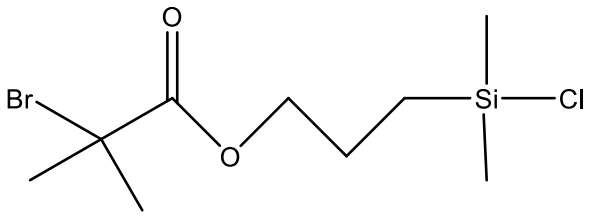

3-(Chlorodimethylsilyl)propyl 2-bromo-2-methylpropanoate (CDMSPBMP)

Table 3.1. Comparison of Organosilane-Modified Layered Silicas and Layered Silica **1** from Where They Were Derived**.**

Name	Organosilane	2θ	d_{001}/nm	Weight loss % (TGA)
Layered silica 1	**n/a**	**2.50**	**3.5**	**63**
1-TMCS	**Trimethylchlorosilane**	**4.73**	**1.87**	**15 (maybe some surfactant was present)**
1-BDMCS	**n-Butyldimethylchlorosilane**	**4.56**	**1.94**	**23**
1-DMOCS	**Dimethyloctylchlorosilane**	**3.54**	**2.5**	**35**
1-CMPETS	**Chloromethyl phenylethyl trichlorosilane**	**3.06**	**2.9**	**45**
1-CSPETCS	**2-(4-Chlorosulfonyl phenyl) ethyl trichlorosilane**	**3.15**	**2.8**	**45**
1-CDMSPBMP	**3-(Chlorodimethylsilyl)propyl 2-bromo-2-methylpropanoate**	**4.62**	**1.9**	**35**

TGA showed that the weight losses of the modified silicas increased with the increase of alkyl chain length of the organosilanes (Figure 3.1). 1-TMCS sample modified with the smallest organosilane showed the lowest weight loss % at 800 ℃, that is 15% (which in part can be related with residual surfactant). 1-BDMCS, 1-DMOCS samples with larger surface-bound organosilane groups showed increased weight loss. With the assumption that 1-TMCS, 1-BDMCS, 1-DMOCS had 3, 6, 10 carbons in the structure, the TGA weight loss % / residue % ratio gave good linear fit line, in which weight loss % mostly came from organic part and residue % came from inorganic part in the materials (Figure 3.2).

Figure 3.1. Thermogravimetric Weight Change Curves under N_2 for Various Organosilane-Modified Layered Silica **1**.

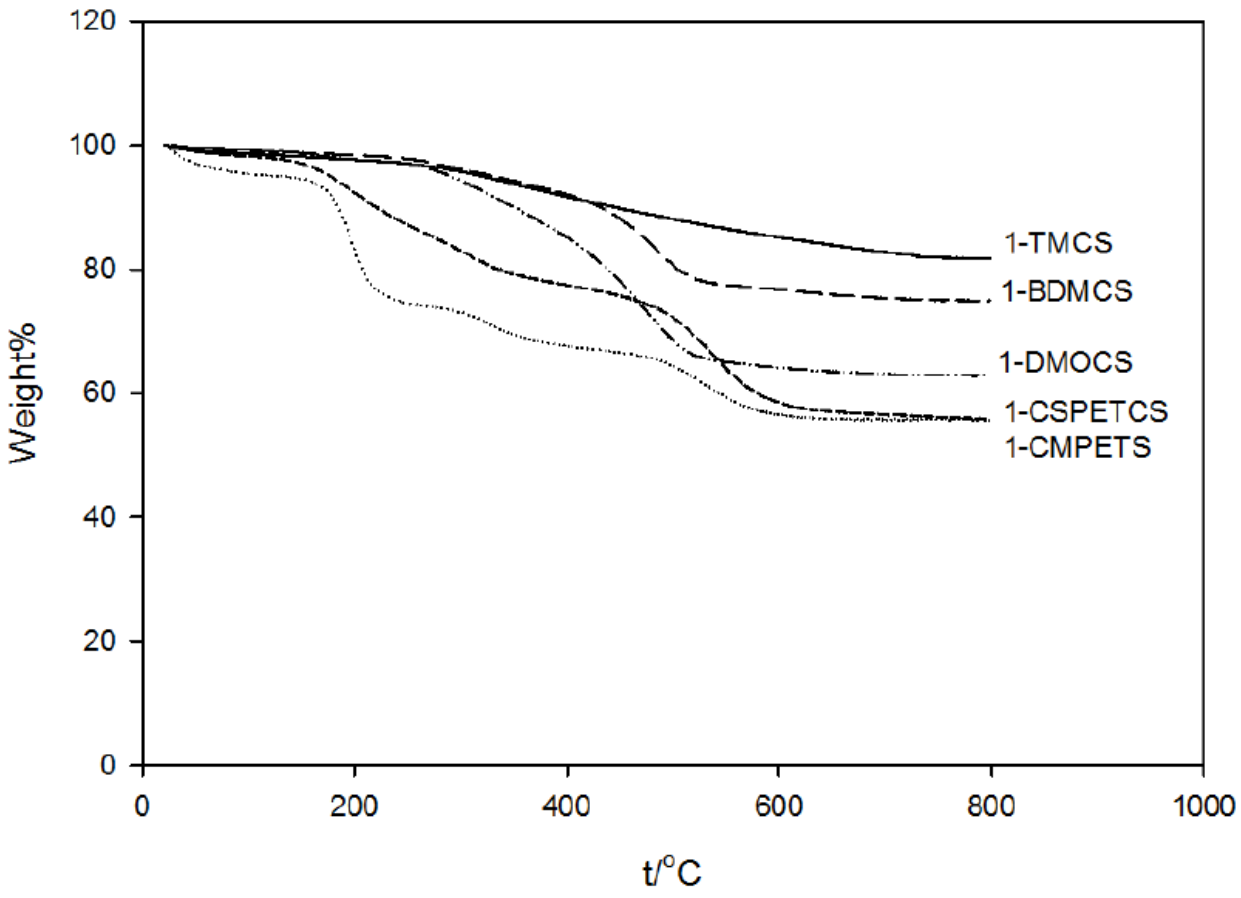

Figure 3.2. Number of Carbons of Surface-Grafted Organosilanes vs. Weight Loss %.

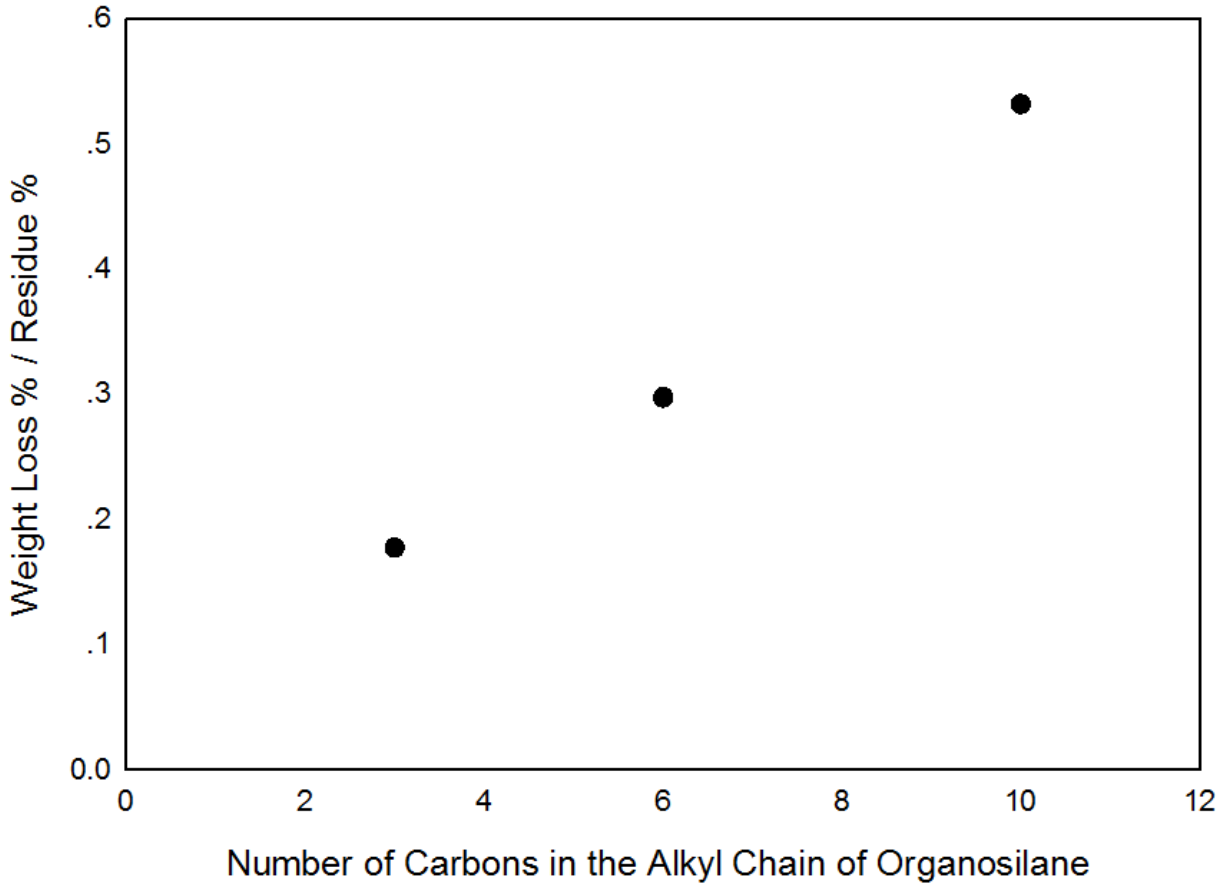

The interplanar spacing d_{001} values ranged from about 1.9 nm to 2.9 nm for organosilane-modified layered silicas (based on SAXS patterns shown in Figure 3.3). It should be noted that the variable interplanar spacing is a characteristic feature of layered materials. In contrast, ordered mesoporous silicas, whether surfactant-containing or surfactant-free, typically do not exhibit any major changes of the interplanar spacing after the surface modification, as expected from 3-dimensionally cross-linked nature of their frameworks. [144b] 1-CMPETS (chloromethyl phenylethyl trichlorosilane modified layered silica **1**) and 1-CSPETCS (2-(4-chlorosulfonyl phenyl) ethyl trichlorosilane modified layered silica **1**) had the largest distance between layers due to their bulky phenyl groups and perhaps also due to the presence of residual amounts of surfactant. Including the original layered silica **1**, d_{001} showed good linear relationship versus the TGA weight loss % (Figure 3.4). 1-CDMSPBM (3-(chlorodimethylsilyl)propyl 2-bromo-2-methylpropanoate modified layered silica **1**) showed some deviation from the straight line, possibly because the presence of heavy bromine atom that contributed to a higher density of the groups (smaller volume occupied by a particular mass of the groups).

Figure 3.3. Small-Angle X-Ray Scattering Patterns of Organosilane-Modified Layered Silica.

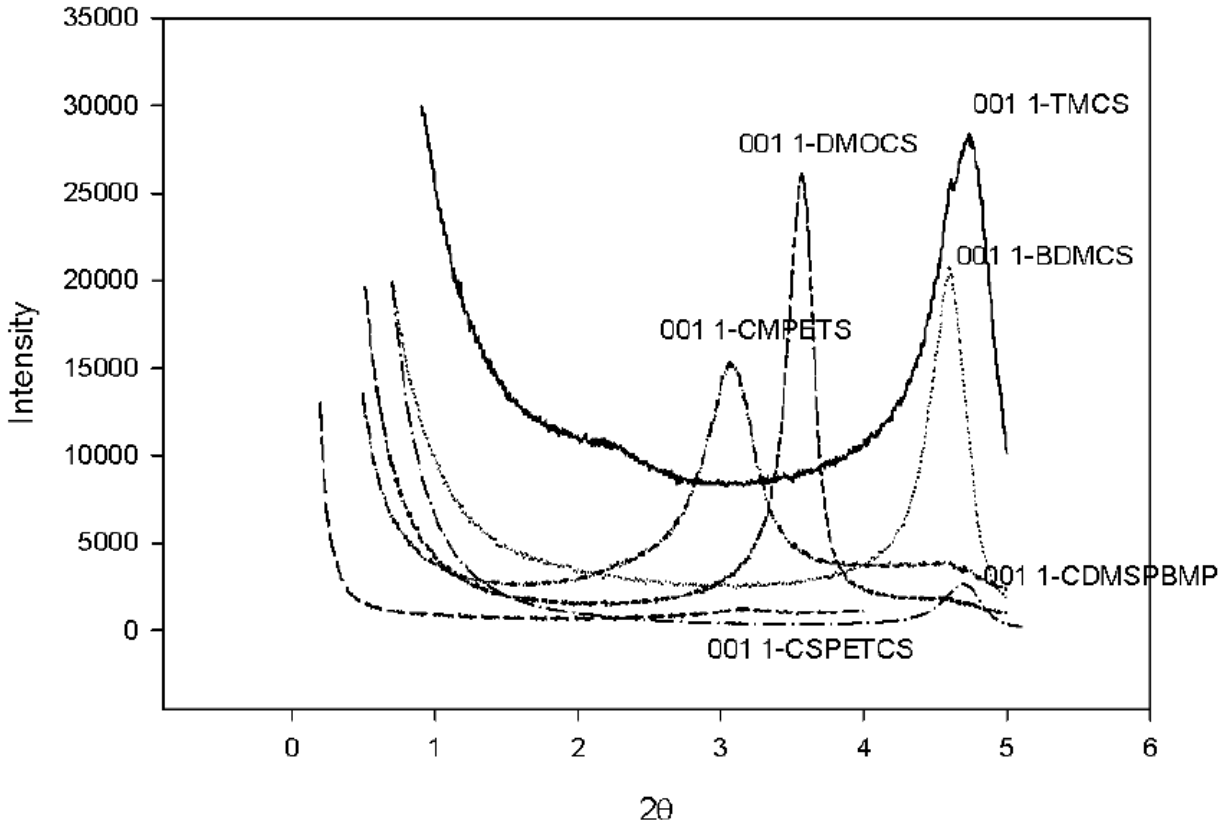

Figure 3.4. Interlayer Spacing vs. Weight Loss % for Organosilane-Modified Silicas.

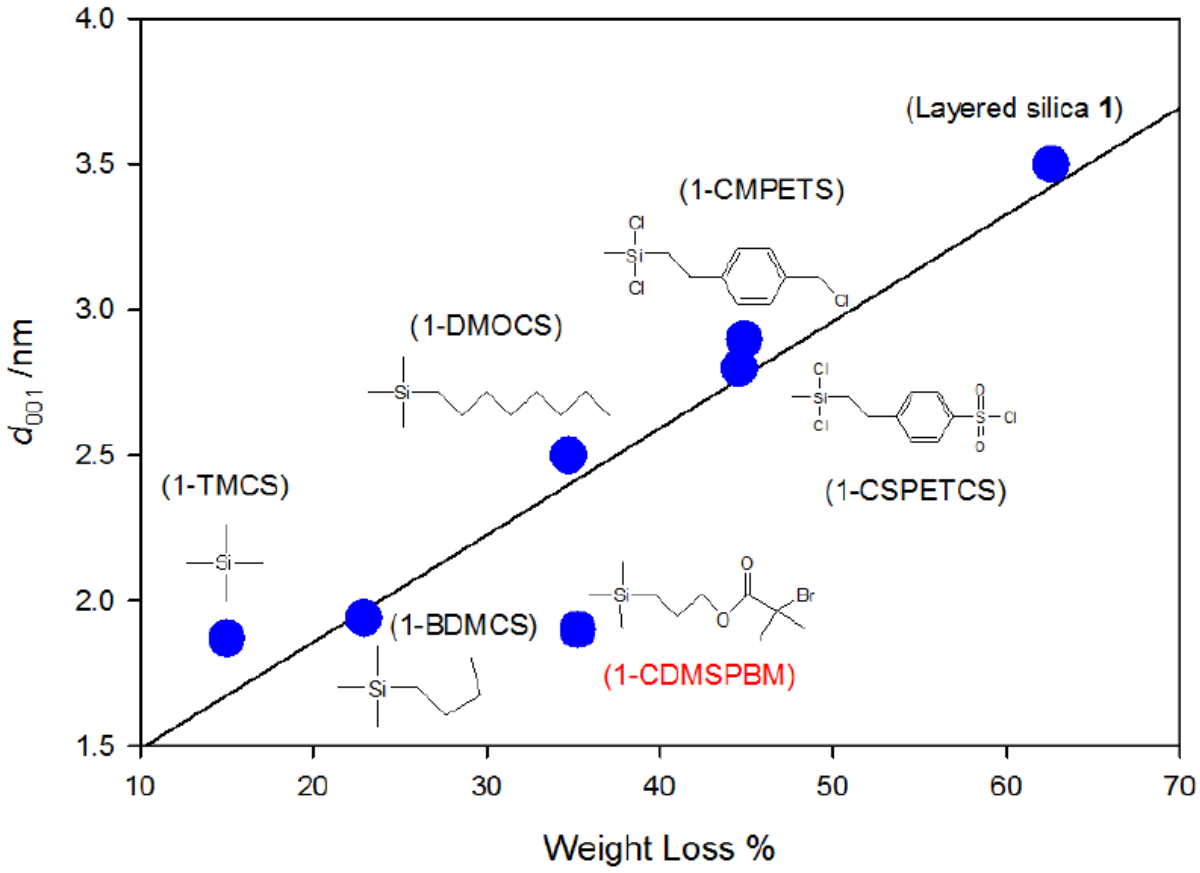

After modification, the peak intensity in SAXS of layered silica with surface-bonded organosilanes decreased a lot when compared with the original layered silica **1**. Our results confirmed that the layered structure can be modified by introducing organosilyl groups through the replacement of the surfactant. Also the good agreement between d_{001} and weight loss % supported the possibility for further modification (polymerization) to achieve the intercalated or exfoliated architectures. The halogen atoms at the end of the organosilanes (1-CMPETS (chloromethyl phenylethyl trichlorosilane modified layered silica **1**), 1-CSPETCS (2-(4-chlorosulfonyl phenyl) ethyl trichlorosilane modified layered silica **1**), 1-CDMSPBMP (3-(chlorodimethylsilyl)propyl 2-bromo-2-methylpropanoate modified layered silica **1**)) might serve as initiating centers for ATRP.

Based on the TGA weight loss patterns of 1-CMPETS and 1-CSPETCS (Figure 3.1), some surfactant might have remained in the materials, because the weight change patterns appeared to show multiple decomposition events. In the silica modified with trichloroorganosilanes (such as 1-CMPETS and 1-CSPETCS), the organosilane might be attached to the silica surface not only directly through one or more Si-O-Si bonds, but it is also possible for these organosilanes to be connected to each other with Si-O-Si bridging. As a result, some of the organosilane groups may be connected to other groups rather than to the surface, which could diminish the propensity of these organosilanes to replace the surfactant from layered silica **1**. Moreover, the cross-linking of organosilane molecules might have introduced a cross-linking between the silica layers, which may also hinder a complete surfactant displacement. 1-CDMSPBMP (3-(chlorodimethylsilyl)propyl 2-bromo-2-methylpropanoate modified layered silica **1**) showed a different behavior with a single step of degradation (Figure 3.5), which suggested that surfactant on the surface of layered silica **1** was displaced successfully by the organosilane with the

bromide end group. Therefore, the surface-initiated polymerization was performed using 1-CDMSPBMP (3-(chlorodimethylsilyl)propyl 2-bromo-2-methylpropanoate modified layered silica **1**), whereas 1-CMPETS and 1-CSPETCS were not used further.

2-CDMSPBMP (3-(chlorodimethylsilyl)propyl 2-bromo-2-methylpropanoate modified layered silica **2**) was prepared similarly to 1-CDMSPBMP (3-(chlorodimethylsilyl)propyl 2-bromo-2-methylpropanoate modified layered silica **1**). Its d_{001} was 2.6 nm (2θ angle= 3.4 °), and it exhibited 36% weight loss (Figure 3.6 & 3.7).

Figure 3.5. Thermogravimetric Weight Change Curve of Initiator-Modified Layered Silica 1-CDMSPBMP.

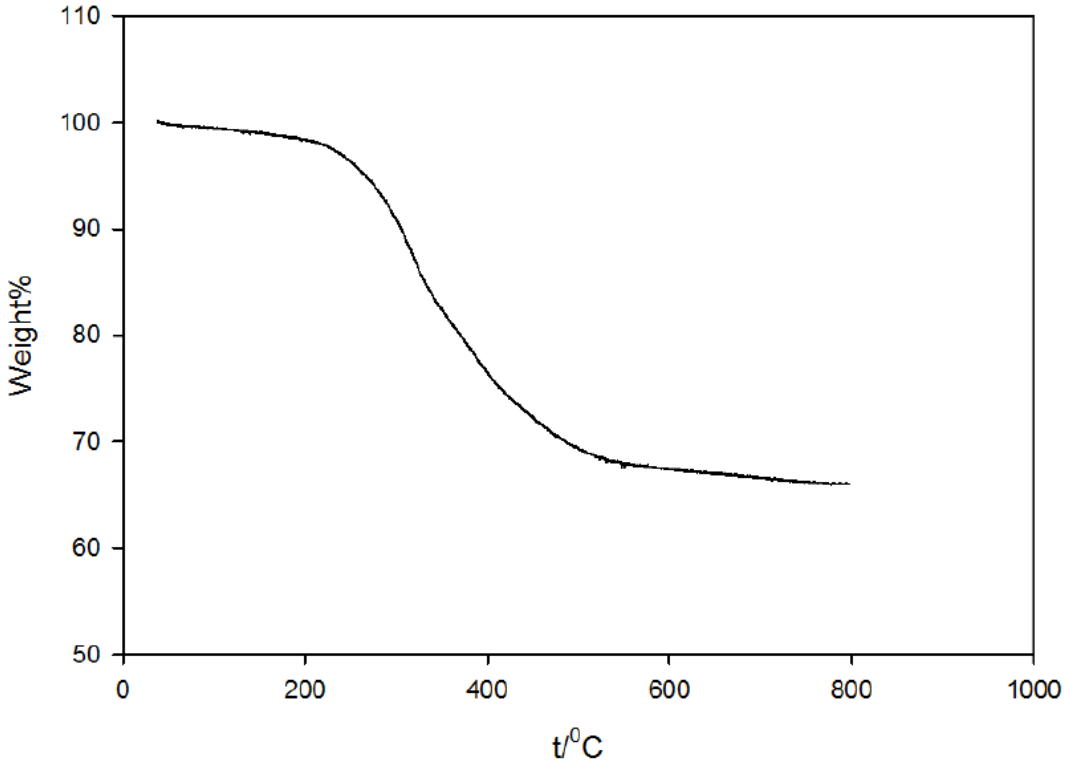

Figure 3.6. Small-Angle X-Ray Scattering Pattern of Initiator-Modified Layered Silica 2-CDMSPBMP.

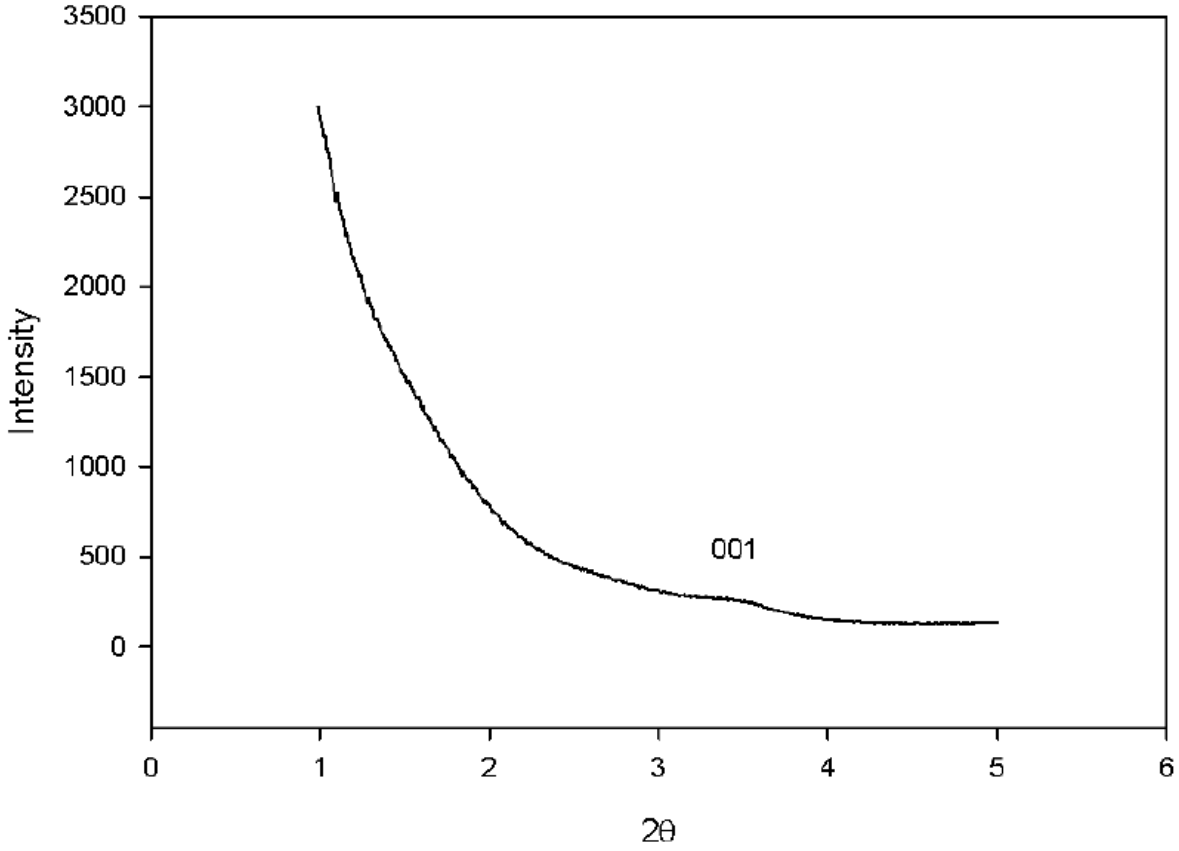

Figure 3.7. Thermogravimetric Weight Change Curve of Initiator-Modified Layered Silica 2-CDMSPBMP.

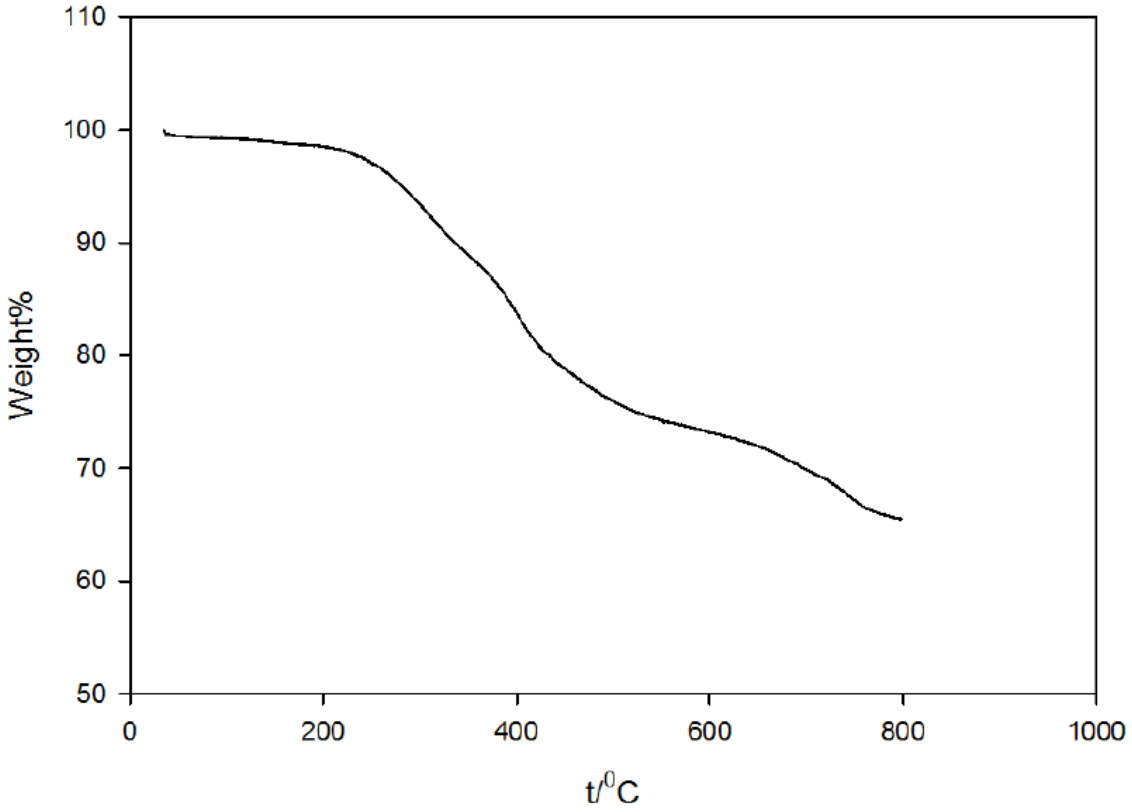

3.3. Surface-Initiated Atom Transfer Radical Polymerization

3.3.1. Experimental Section

Methyl methacrylate (MMA, 99%), Styrene (St) and acrylonitrile (AN) were purchased from Aldrich and purified by passing through a column filled with basic alumina. The ligands (tris[(2-pyridyl)methyl]amine (TPMA) (ATRP Solutions, Inc.) and 1, 1, 4, 7, 7-pentamethyl-diethylenetriamine (PMDETA) (Acros Organics)) were used as received. All other chemicals such as solvents (anisole, dimethyl sulfoxide (DMSO)), copper (I)/ (II) salts, pyridine, ethanol, and methanol were used as received.

In a typical normal ATRP, the initiator-modified layered silica (20 mg), monomers (1 ml MMA, 1 ml St or 615 μl AN), $CuBr_2$ (0.54 mg; $CuBr_2$ was dissolved in DMSO to be 10 mg/ml solution taken by micro-liter syringe as 54 μl solution contained 0.54 mg $CuBr_2$), ligand (5.4 μl PMDETA or 7.8 mg TPMA) and solvent (2.25 ml anisole for MMA and St or 2.25 ml DMSO for AN) were charged in Schlenk flask, followed by three freeze-pump-thaw cycles to get rid of oxygen dissolved in the reaction mixture. CuBr (about 3.7 mg) was introduced quickly to the system before the Schlenk flask was sealed with a rubber septum. The system was back-filled with N_2 gas, and stirred at a desired temperature (60 ℃ for MMA and AN, 90 ℃ for St). The polymerization was terminated by removing the rubber septum to expose the reaction mixture to the oxygen from the air, which converts Cu (I) catalyst complex to Cu (II) deactivator complex. The product was isolated by filtering and washing with toluene and methanol, and dried in a vacuum oven at 60 ℃.

The samples were characterized as described in chapter 2.1. In addition, the glass transition temperature of silica/polymer nanocomposite product was measured by TA Instruments Q100 Differential Scanning Calorimeter (DSC) under N_2 flow at 3 ℃/min heating up to 150 ℃.

3.3.2. Methyl Methacrylate Polymerization

Table 3.2 shows the reactant molar ratios for normal ATRP of methyl methacrylate using bromoisobutyrate-based initiator 1-CDMSPBMP, along with some characterization data for each sample. With the same composition of the polymerization mixture, samples 1-P1 and 1-P2 were collected after 4 and 17.5 hours since the reaction had started. With longer reaction time, 1-P1 showed higher polymer loading (27.49% vs. 47.78% silica residue, see Figure 3.8). The d_{001} spacing was enlarged from 1.9 nm (1-CDMSPBMP) to 3.2 nm for 1-P2 (Figure 3.9) and as high as 6.3 nm for 1-P1 (see SAXS data in Figure 3.10). While the formation of intercalated architectures with significantly enlarged interplanar spacing was sometimes reported earlier in the case of surface-initiated polymerization, [67b, 147a] such results have been uncommon. Also, we are not aware of achieving these kinds of architectures for PMMA/layered silica nanocomposites, as the above examples pertain to polystyrene. Polymer/Silica mass ratio was also calculated based on the residue % in TGA and subtracting the initiator weight percentage in the weight loss part. PMMA/silica ratios were 0.57:1 and 2.12:1 after the polymerization time 4 and 17.5 hours respectively. Figure 3.11 and Figure 3.12 showed the morphology of samples 1-P1 and 1-P2 observed by TEM. Although the layered structure is not immediately obvious, significant changes in degree of darkness along sharply defined lines could be easily explained if we assume that the images show platelets lying flat on the grid (perpendicular to electron beam). The changes in darkness would result from the changes in number of plates that stack on one another. The regions with the lowest number of plates (perhaps one plate) would be the lightest and as the number of plates in the stacks increases, the region would be darker. It should be noted that similar TEM images were reported by others for layered materials, [73, 147b] additionally supporting our interpretation of TEM images. As seen from SAXS, we achieved the intercalated

organic/inorganic nanocomposites, because the periodicity was retained after the polymer grafting, but the repeating distance significantly increased.

Table 3.2. Atom Transfer Radical Polymerization (ATRP) of Methyl Methacrylate (MMA) Initiated from Initiator-Modified Layered Silica 1-CDMSPBMP.

	1-CDMSPBMP	$CuBr_2$	CuBr	PMDETA	MMA	time/ hrs	residue%	polymer/ silica	d_{001}/nm	2θ (degree)
1-P1	**1**	**0.1**	**1**	**1.1**	**100**	**17.5**	**27.49**	**2.12**	**6.3**	**1.40**
1-P2	**1**	**0.1**	**1**	**1.1**	**100**	**4**	**47.78**	**0.57**	**3.2**	**2.72**
1-P3	**1**	**0.1**	**1**	**1.1**	**400**	**15**	**9.440**	**9.07**	**n/a**	**n/a**
1-P4	**1**	**0.1**	**1**	**1.1**	**400**	**22**	**3.510**	**27.0**	**n/a**	**n/a**
1-P5	**1**	**0.1**	**1**	**1.1**	**400**	**6**	**17.32**	**4.25**	**~12**	**0.7 (001, very weak); 1.405 (002, weak)**

Figure 3.8. Thermogravimetric Weight Change Curves of PMMA/Silica Composites 1-P1 to 1-P5.

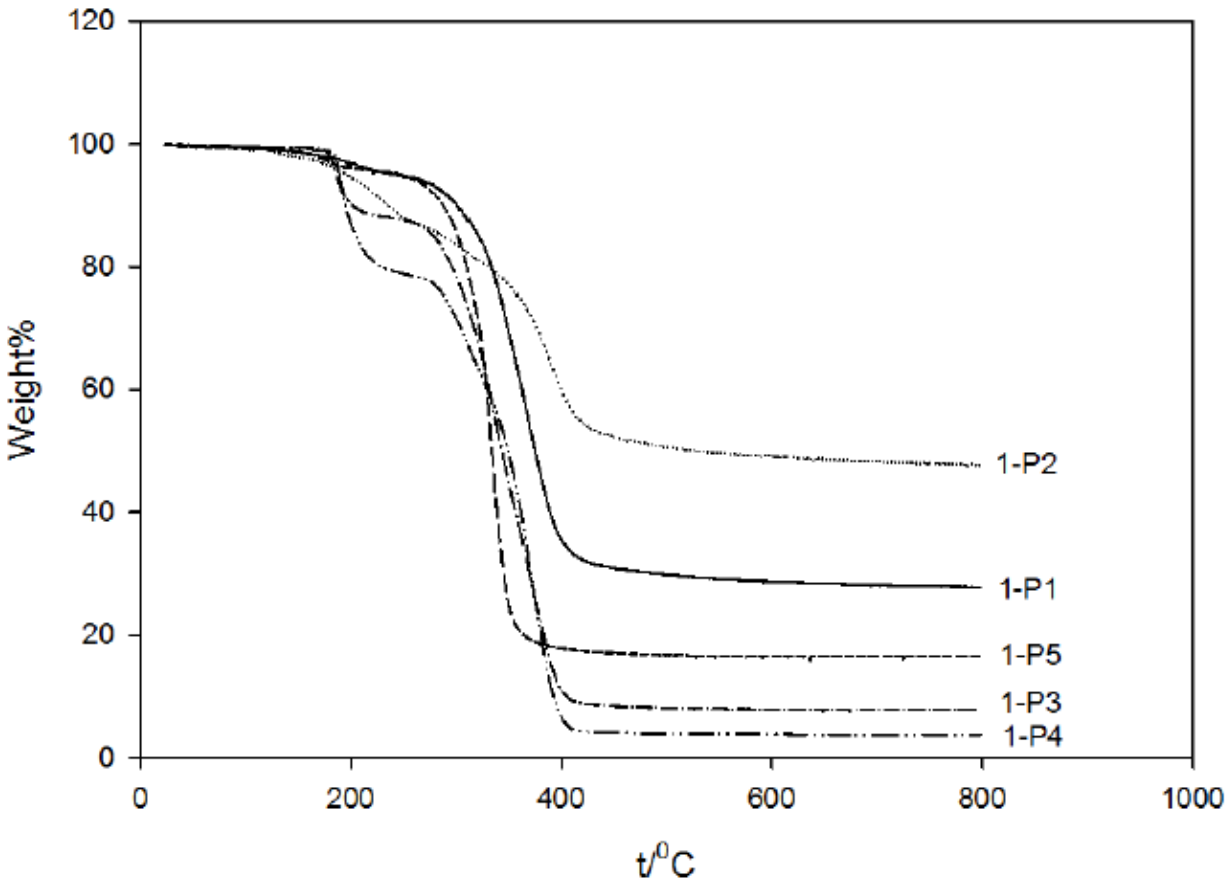

Figure 3.9. Small-Angle X-Ray Scattering Pattern of PMMA/Silica Composite 1-P2.

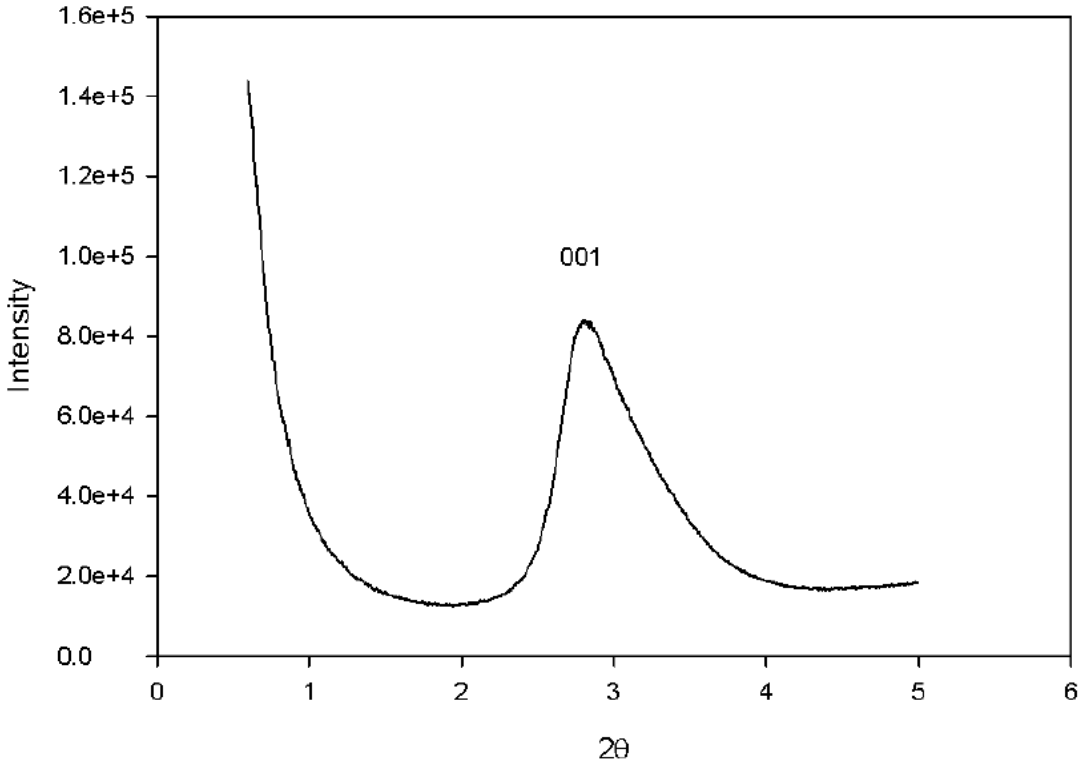

Figure 3.10. Small-Angle X-Ray Scattering Pattern of PMMA/Silica Composite 1-P1.

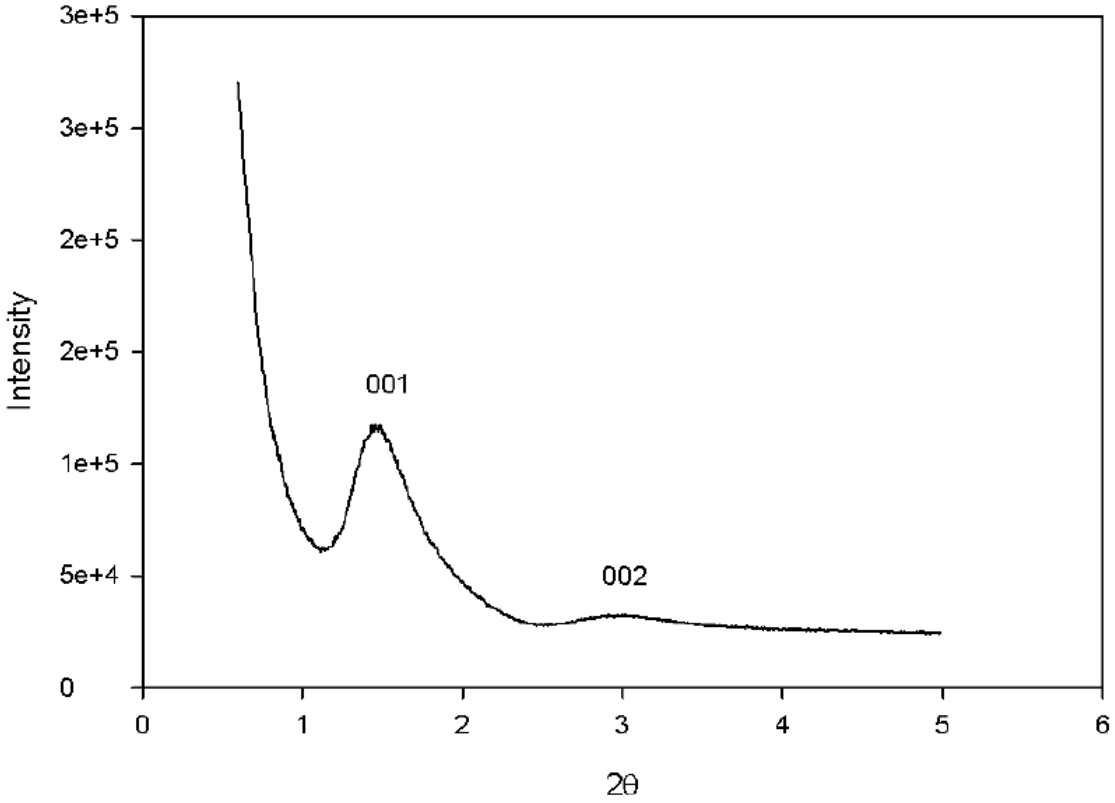

Figure 3.11. TEM Image of PMMA/Silica Nanocomposite 1-P1.

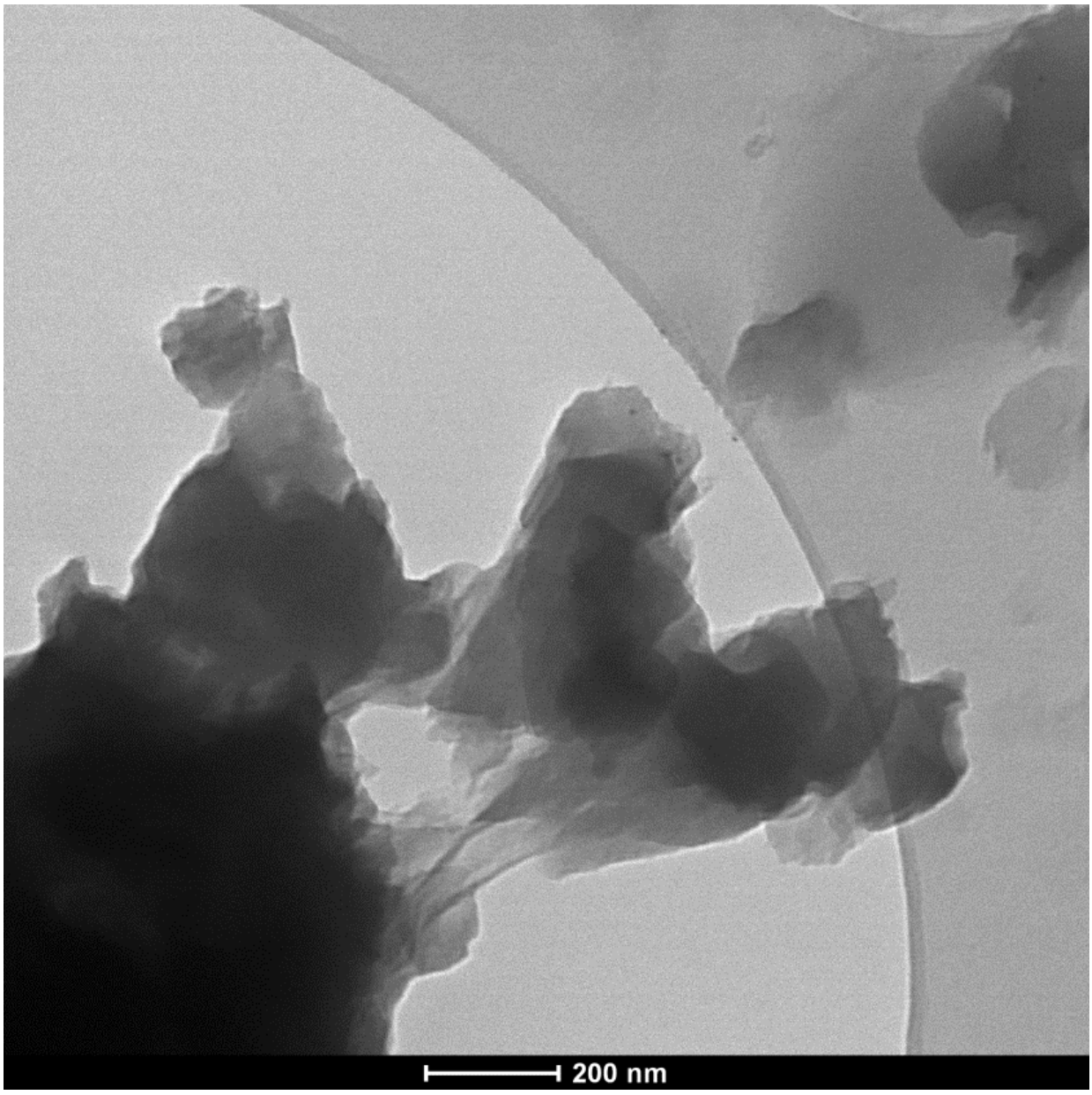

Figure 3.12. TEM Image of PMMA/Silica Nanocomposite 1-P2.

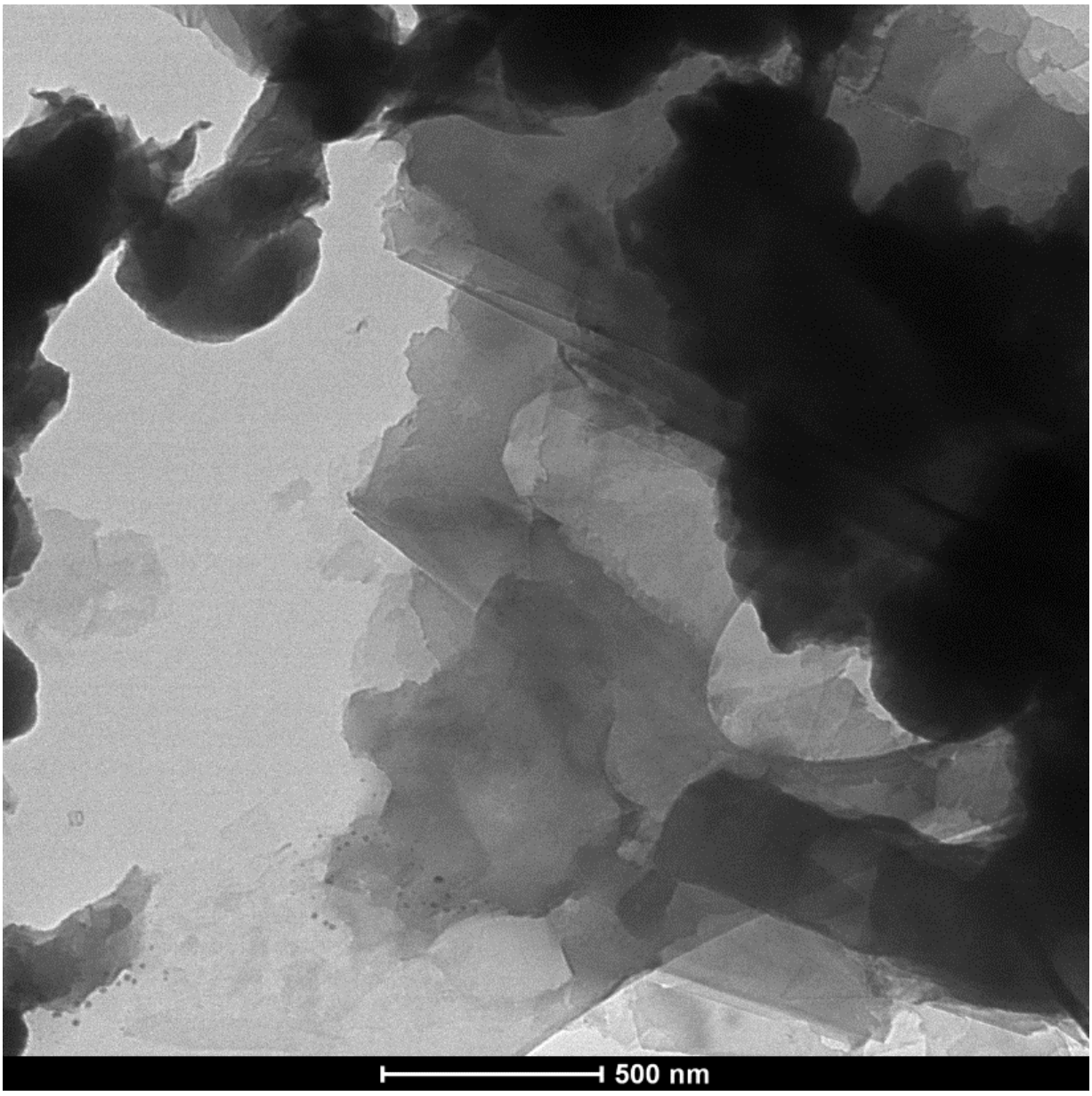

Not only the reaction time, but also the monomer concentration and/or monomer/initiator ratio affects the polymer loading. With a higher monomer concentration and higher monomer/initiator ratio (for 1-P1 and 1-P2, the initial molar concentration of MMA was about 2.35 mol/L; for 1-P3, 1-P4 and 1-P5, the initial molar concentration of MMA was about 2.89 mol/L (which is about 23% higher than 1-P1 and 1-P2)), 1-P4 showed increased polymer loading (3.510% residue, PMMA/Silica ratio of 27:1) after 22 hours reaction. This was the highest polymer/silica mass ratio in all normal ATRP polymerization products obtained in the current study, although longer polymerization times can be used to further increase the polymer loading. The morphology of the nanocomposite 1-P4 was investigated by TEM (Figure 3.13), showing features that can be attributed to the collection of layered structures, mostly seen from the side.

At higher monomer concentration and the resulting higher polymer loading, the ordered structure was no longer seen clearly by SAXS. 1-P3 and 1-P4 (PMMA/silica weight ratio = 9.07:1 and 27.0:1) did not show any features in their SAXS patterns, whereas 1-P5 (PMMA/silica weight ratio = 4.25:1) had a weak signal exhibiting two shoulders that suggest the interlayer spacing of 12.6 nm (Figure 3.14). As a result, higher polymer loading would result in a loss of an ordered architecture of organic/inorganic nanocomposites. Lower polymer loading needs to be selected if the intercalated structure of the product is preferred.

By comparing with literature results, Bottcher group witnessed a weak peak in X-ray diffraction (XRD) pattern for the poly(methyl methacrylate) (PMMA)/silicate nanocomposites prepared by surface-initiated atom transfer radical polymerization after 0.5 hour (5% conversion) reaction, and it disappeared after 1 hour (13% conversion) and 4 hours (52% conversion) reaction. They reported that they achieved fully exfoliated polymer silicate nanocomposites. [68] The PMMA/silicate prepared by Shipp group via surface-initiated atom transfer radical

polymerization exhibited a fully exfoliated architecture (no features indicating ordering in the XRD pattern) even when the molecular weight of PMMA was low (M_n = 4400). [69] In our methodology, based on the results shown above, the ordering feature of the PMMA/silica nanocomposites can be maintained to an extent that the interlayer spacing was 6.3 nm (1-P1) or even about 12 nm (1-P5). The architecture of the nanocomposites was controlled to achieve either an intercalated structure (for low polymer loading) or an exfoliated structure (for high polymer loading).

Figure 3.13. TEM Images of PMMA/Silica Nanocomposite 1-P4.

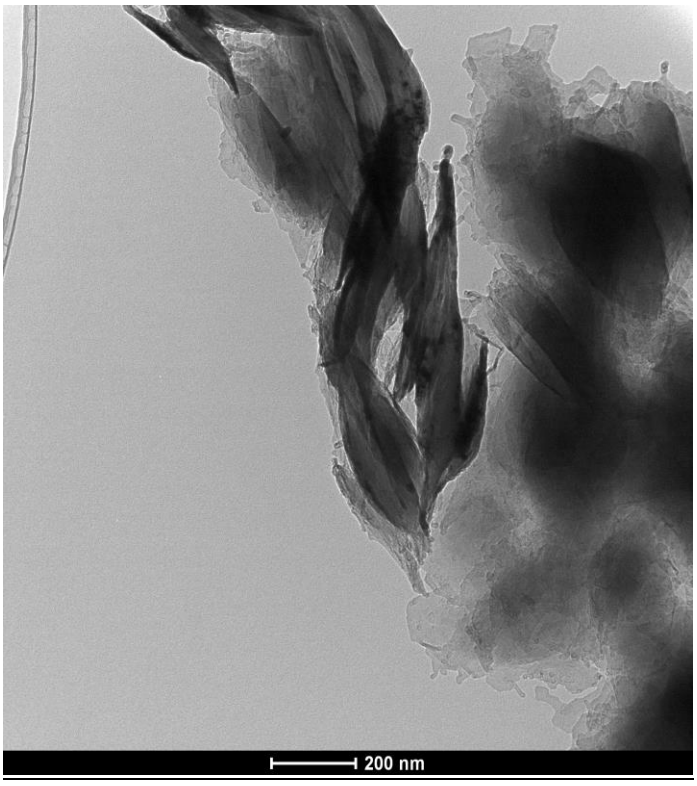

Figure 3.14. Small-Angle X-ray Scattering Pattern of PMMA/Silica Nanocomposite 1-P5.

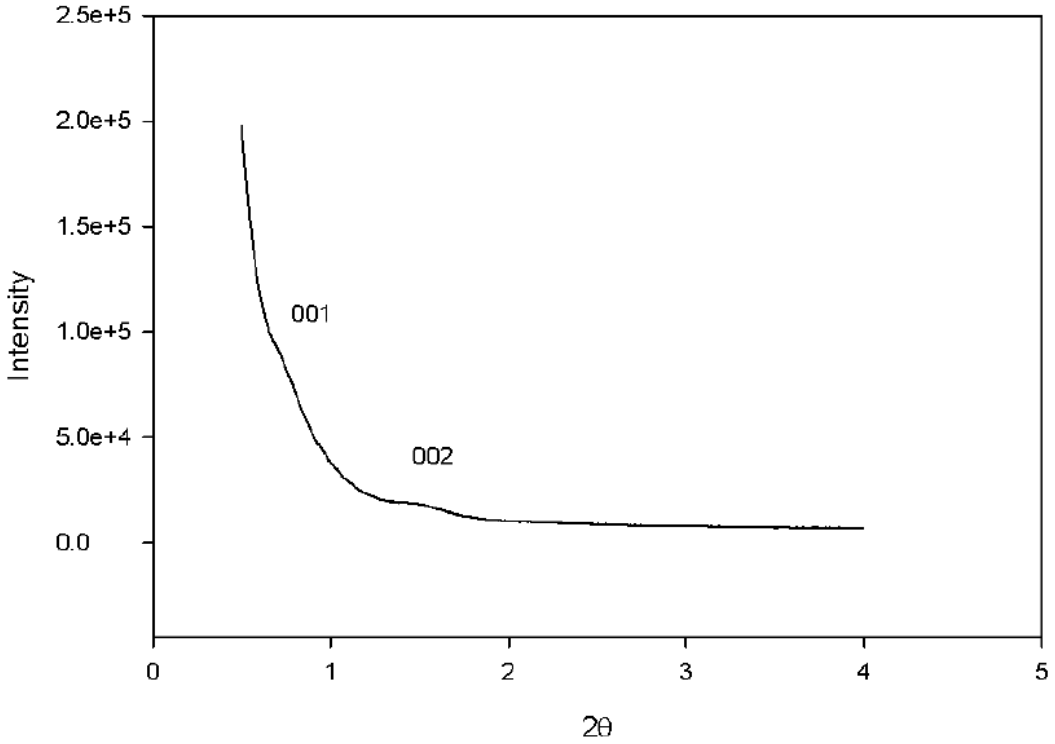

The glass transition temperatures (T_g) of the nanocomposites were examined by differential scanning calorimeter (DSC) (Figure 3.15). 1-P2, which had the lowest polymer loading, did not show any clear glass transition step, whereas T_g was 115.2, 125.5, 130.8 and 123.1 ℃ for 1-P1, 1-P3, 1-P4 and 1-P5. The T_g changed systematically with residue % for the nanocomposites, indicating that the glass transition temperature was increased by increasing the polymer loading, but the 1-P2 sample with the lowest polymer mass percentage had no observable glass transition.

Figure 3.15. Differential Scanning Calorimetry Traces of PMMA/Silica Nanocomposites 1-P1 to 1-P5.

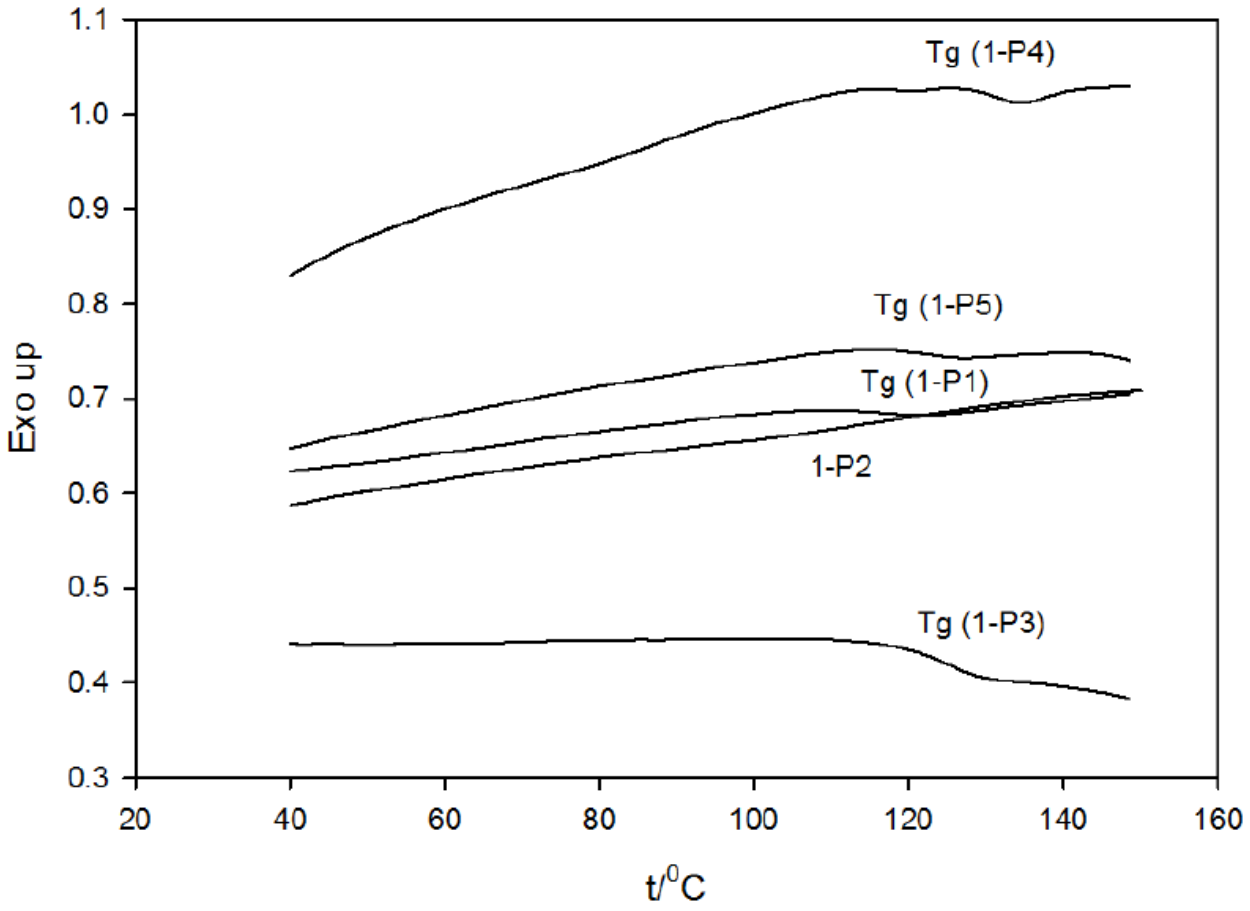

The glass transition temperature is a very important thermal property of a polymer. For poly(methyl methacrylate) (PMMA), T_g is highly depending on the tacticity. The glass transition temperatures of pure isotactic and syndiotactic PMMA were reported to be 52 °and 126 ℃. [148a] ATRP operates via a radical mechanism and it behaves similarly as conventional radical polymerization. [148b, 149] The T_g of PMMA prepared by free radical polymerization have been established as around 105 ℃. [150] Because of the fact that there was no means of controlling the tacticity in our living polymerization and all polymerizations were carried in a similar manner, we can conclude that there was no difference in tacticity between 1-P1 to 1-P5 and the tacticity was not the reason why these nanocomposites had different glass transition temperatures.

In nanocomposites based on PMMA, a T_g increase was reported in PMMA-clay nanocomposites. When the clay weight % was increased from 0 to 1, 3, 5 wt. %, the T_g changed from 109.7 ℃ (PMMA) to 111.0, 117.7 and 120.4 ℃. This T_g change trend is reverse to what is showed for 1-P1 to 1-P5 samples, but in their study, there was no covalent bonding between the layered material (clay) and PMMA. Other interesting results are that when the clay weight % increased to 18 and 22 wt. %, T_g was 124.5 and 122.5 ℃ respectively, which was different from the nanocomposites with lower clay weight %. The reason here may be due to the morphology, as in this report, their nanocomposites exhibited a combination of interacted and exfoliated structures, so it was not a homogeneous architecture, and some galleries of clay still existed in the nanocomposite (no polymer chains were sandwiched inside), leading to the complication of the thermal behavior for the nanocomposites. [54]

A nanocomposite consisting of spherical silica particles and PMMA showed a T_g increase from 91 ℃ (PMMA with COOH end group in polymer chain) to 104 ℃. The silica particles had a

mean size of 40 nm and the polymer chains were grafted to the surface of silica by ester bonds. [151]

When considering the glass transition temperature of layered silica/PMMA nanocomposites, we can compare it with the T_g in polymer thin films on a substrate. As for each silica platelet, the polymer chains were grafted onto both sides forming a thin polymer film, as inferred from the successful formation of intercalated nanocomposite architectures. Ultrathin polymer films (less than 100 nm) on a solid substrate have been investigated by many research groups. The glass transition temperatures for polymer thin films can increase or decrease, which is highly dependent on the interactions between the polymer chains and the solid substrate. [152-161] When polymer chains are freely standing (no interaction between the polymer chains and the substrate surface) on the substrate surface or contacting repulsive surface (repulsive interaction between the polymer chains and the substrate surface), the glass transition temperature will be lower than the one in bulk. [155-157] In contrast, if the interactions/attractions between polymer film and the substrate are strong, a T_g increase will be observed. [152] Thus for PMMA on a substrate, a stronger interaction between PMMA and substrate leads to a T_g increase, [162] whereas a weaker interaction leads to a T_g decrease. [163] Therefore, as the interactions between PMMA and layered silica in the nanocomposites were covalent bonds, an increased T_g is reasonable.

The thickness dependence of PMMA films/brushes on T_g on a substrate has been investigated. [160] The high-density PMMA brushes were grafted from a silicon wafer, and also PMMA films were spin-coated on a hydrophobically treated silicon wafer. Because the interactions between polymer chains and the silicon wafer were different (covalent vs. noncovalent), the thickness dependence of T_g exhibited opposite trends in these two cases, as shown in Figure 3.16. [160] The T_g of high-density PMMA brushes increased sharply with decreasing thickness when the

thickness was less than 50 nm, and T_g was almost constant when the thickness was larger than 50 nm. Our PMMA thin surface films appear to behave in an opposite way (Figure 3.16). At first, the high-density PMMA brushes on a silicon wafer appear to be very similar to our nanocomposites, but T_g of our nanocomposites increased with increasing thickness (as inferred on the basis of the polymer loading). However, the polymer brushes on a silicon wafer have the outer surface of the brush exposed to the air, whereas in our case, the brushes are sandwiched between the silica layers. The brushes grown on two different platelets may interpenetrate or exclude one another (or a combination thereof). So in fact, the environment of the brushes on a single flat surface and on multiple layers may be different. Moreover, the brush thickness studied in both cases may be quite different. If we assume: i) the silica density of 2.2 g/cm^3; ii) PMMA density of 1.2 g/cm^3; [164] iii) the thickness of silica platelet of 1 nm and iv) the coverage of both sides of the platelet with polymer, then average polymer film thickness = $\frac{1}{2}$ × thickness of silica $\times \frac{\frac{mass\ of\ PMMA}{density\ of\ PMMA}}{\frac{mass\ of\ silica}{density\ of\ silica}}$ = 0.5 nm × $\frac{2.2}{1.2}$ × $\frac{mass\ of\ PMMA}{mass\ of\ silica}$ = 0.92 nm × $\frac{mass\ of\ PMMA}{mass\ of\ silica}$. Using the polymer/silica ratios from Table 3.2, one can obtain PMMA film thickness values 0.52 nm for 1-P2, 1.95 nm for 1-P1, 3.9 nm for 1-P5, 8.3 nm for 1-P3 and 24.8 nm for 1-P4 (Figure 3.17). Only the last two values of the thickness fall within the range considered in Figure 3.16. Moreover, some cross-linking can develop at later stage of the synthesis (especially for 1-P4). If any cross-linking developed, a T_g increase could be expected. Such T_g increase in high-degree cross-linking polystyrene was reported by 70 ℃. [165] So it is difficult to conclusively compare the literature data with our results. It is notable that the above PMMA film thickness estimates for our samples are quite consistent with the (001) interplanar spacing from SAXS, because d_{001} is

expected to be equal to the platelet thickness + 2 times the polymer layer thickness + 2 times the thickness of initiator layer on the silica surface.

Figure 3.16. Plots of T_g vs L_d (PMMA layer thickness). The solid triangles and open circles represent the data for the polymer brushes and the polymer cast films, respectively, on a silicon wafer surface (reproduced from Reference 160 with permission). [160]

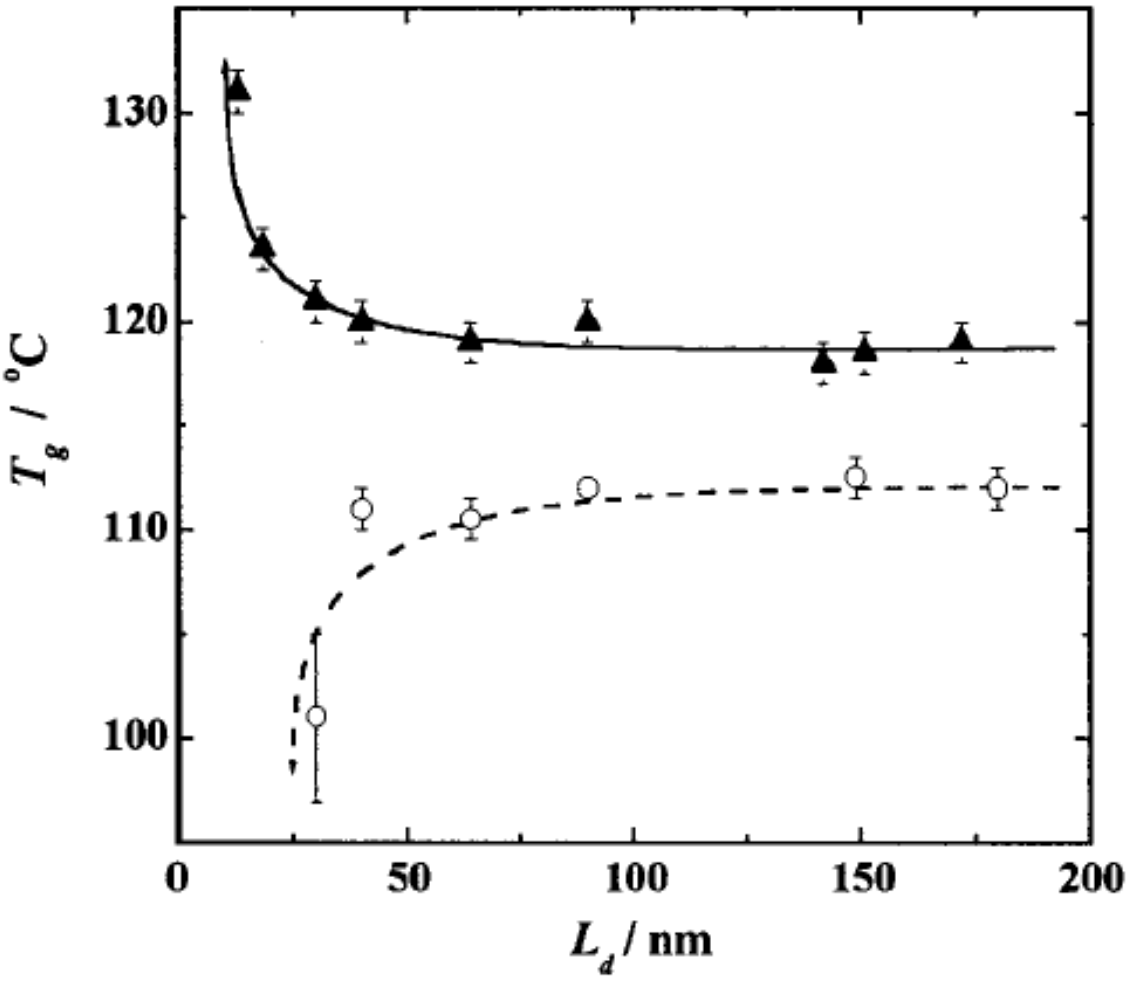

Figure 3.17. T_g vs. Estimated PMMA Layer Thickness of PMMA/Silica Nanocomposites.

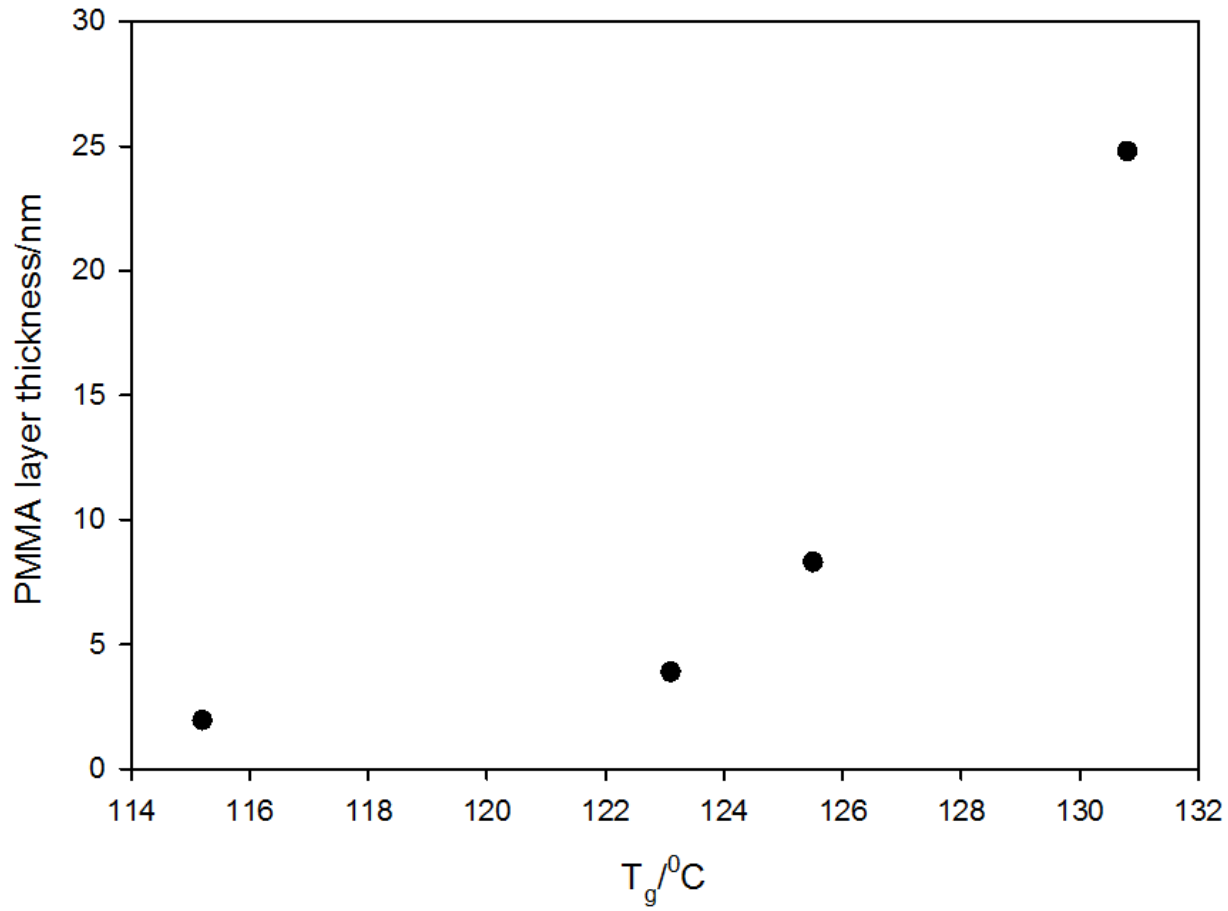

Normal ATRP of MMA from initiator-modified silica layers 2-CDMSPBMP (Table 3.3) was also successful. 2-P1 had 35% residue (Figure 3.18) and d_{001} = 8.4 nm (Figure 3.19). The glass transition temperature was 113.4 ℃ from the DSC pattern (Figure 3.20). Comparing with glass transition temperatures of 1-P1 to 1-P5 samples, 2-P1 has similar T_g to 1-P1, which has a similar polymer layer thickness, as inferred from (001) interplanar spacing of these materials. TEM image (Figure 3.21) illustrated some details on the edge, which can be explained as a result of an overlap of several layers.

Table 3.3. Atom Transfer Radical Polymerization of Methyl Methacrylate Initiated from Initiator-Modified Layered Silica 2-CDMSPBMP.

	2-CDMSPBMP	**$CuBr_2$**	**CuBr**	**PMDETA**	**MMA**	**time/hrs**	**residue%**	**polymer/silica**	**d_{001}/nm**	**2θ (degree)**
2-P1	**1**	**0.1**	**1**	**1.1**	**400**	**18**	**35**	**1.0**	**8.4**	**1.06**

Figure 3.18. Thermogravimetric Weight Change Curve of PMMA/Silica Nanocomposite 2-P1.

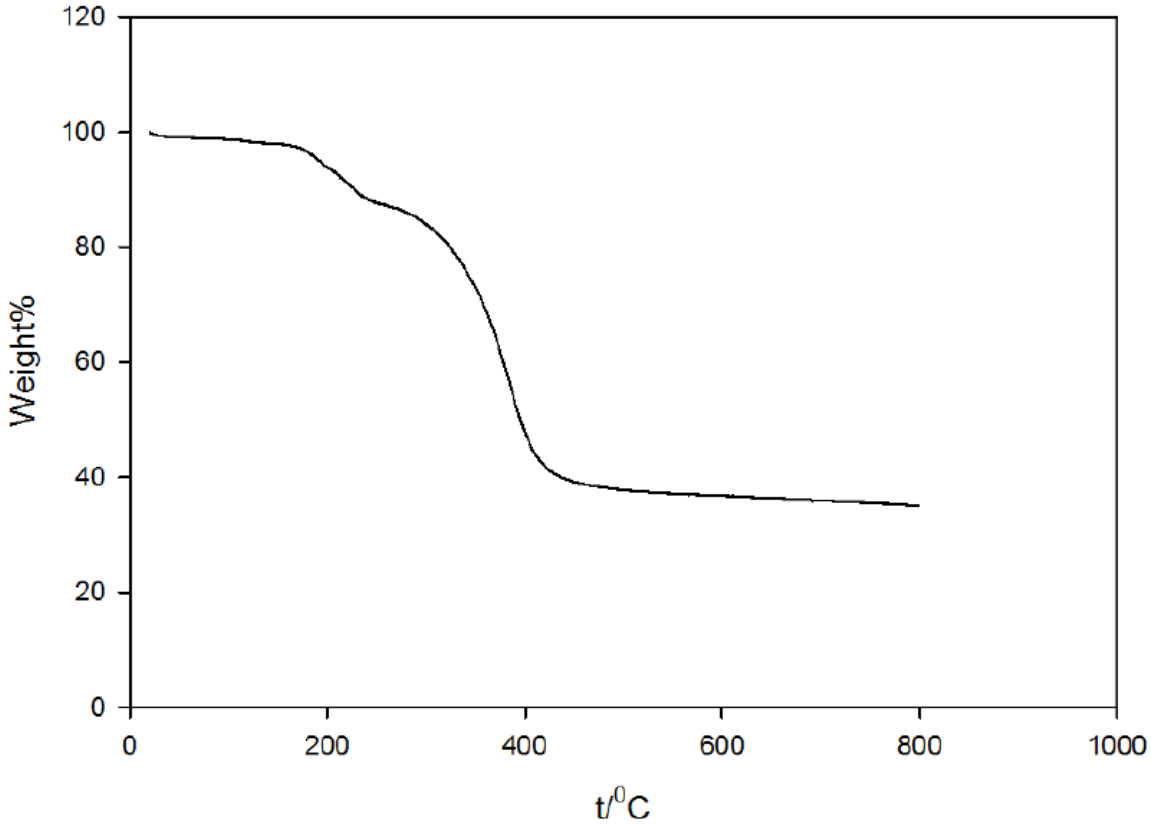

Figure 3.19. Small-Angle X-ray Scattering Pattern of PMMA/Silica Nanocomposite 2-P1.

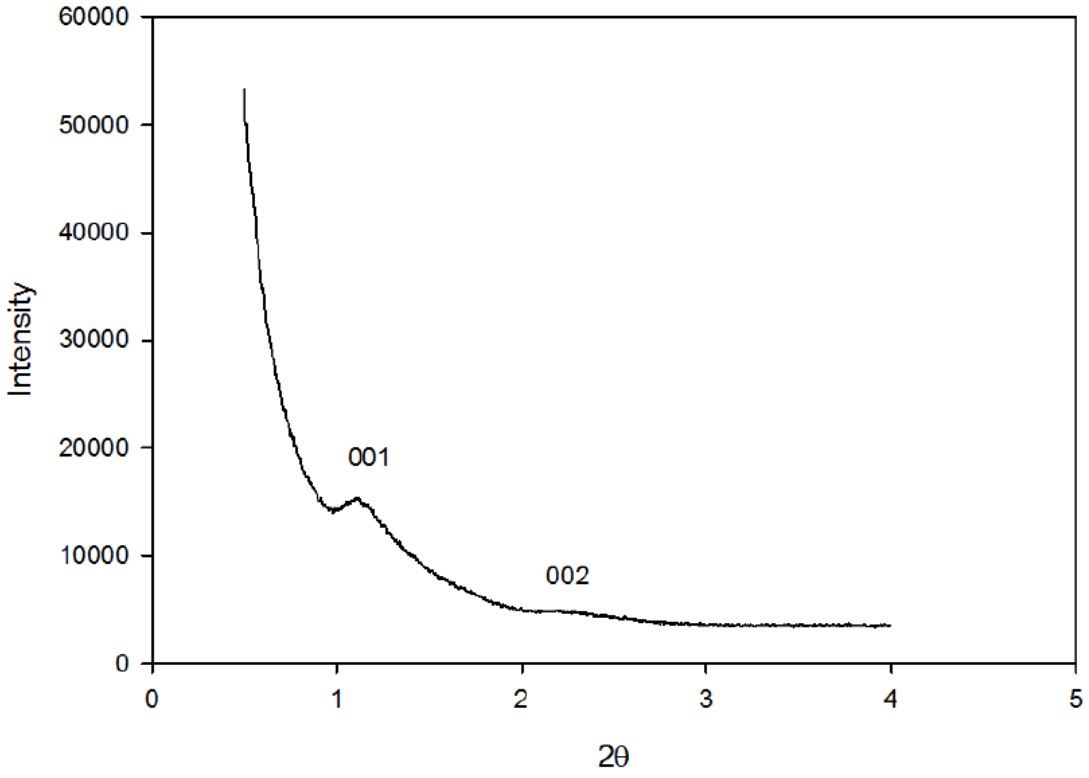

Figure 3.20. Differential Scanning Calorimetry Trace of PMMA/Silica Nanocomposite 2-P1.

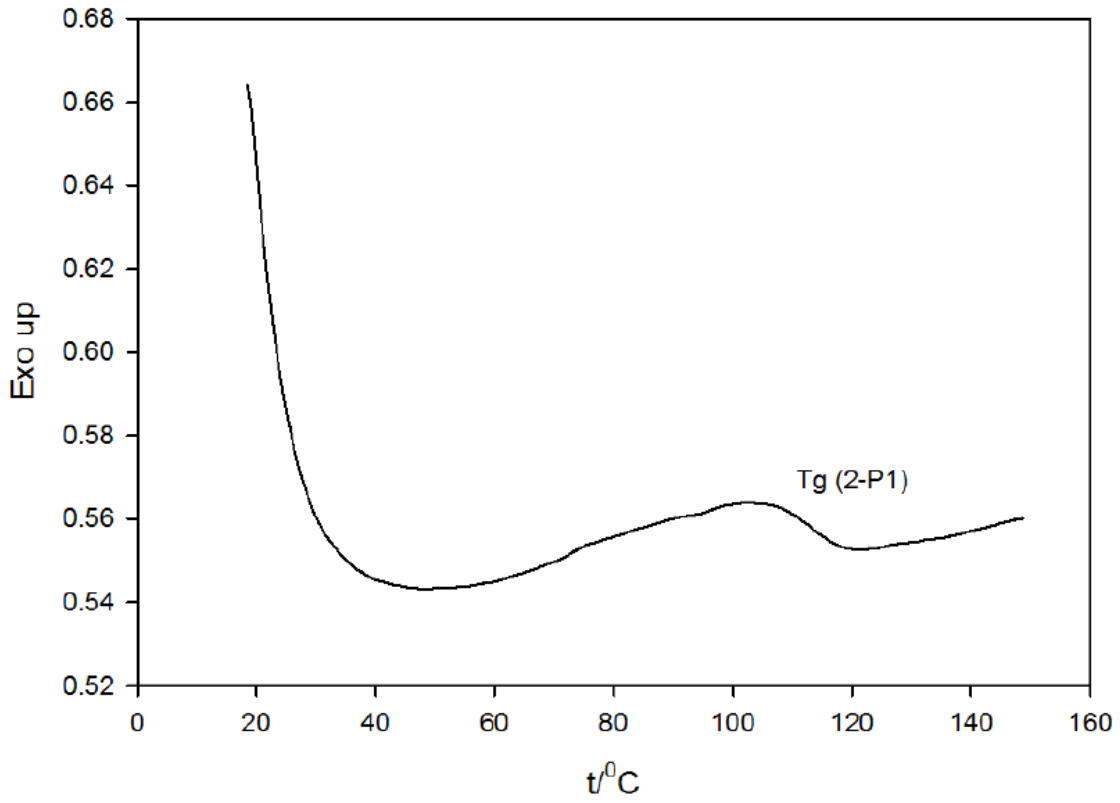

Figure 3.21. TEM Image of PMMA/Silica Nanocomposite 2-P1.

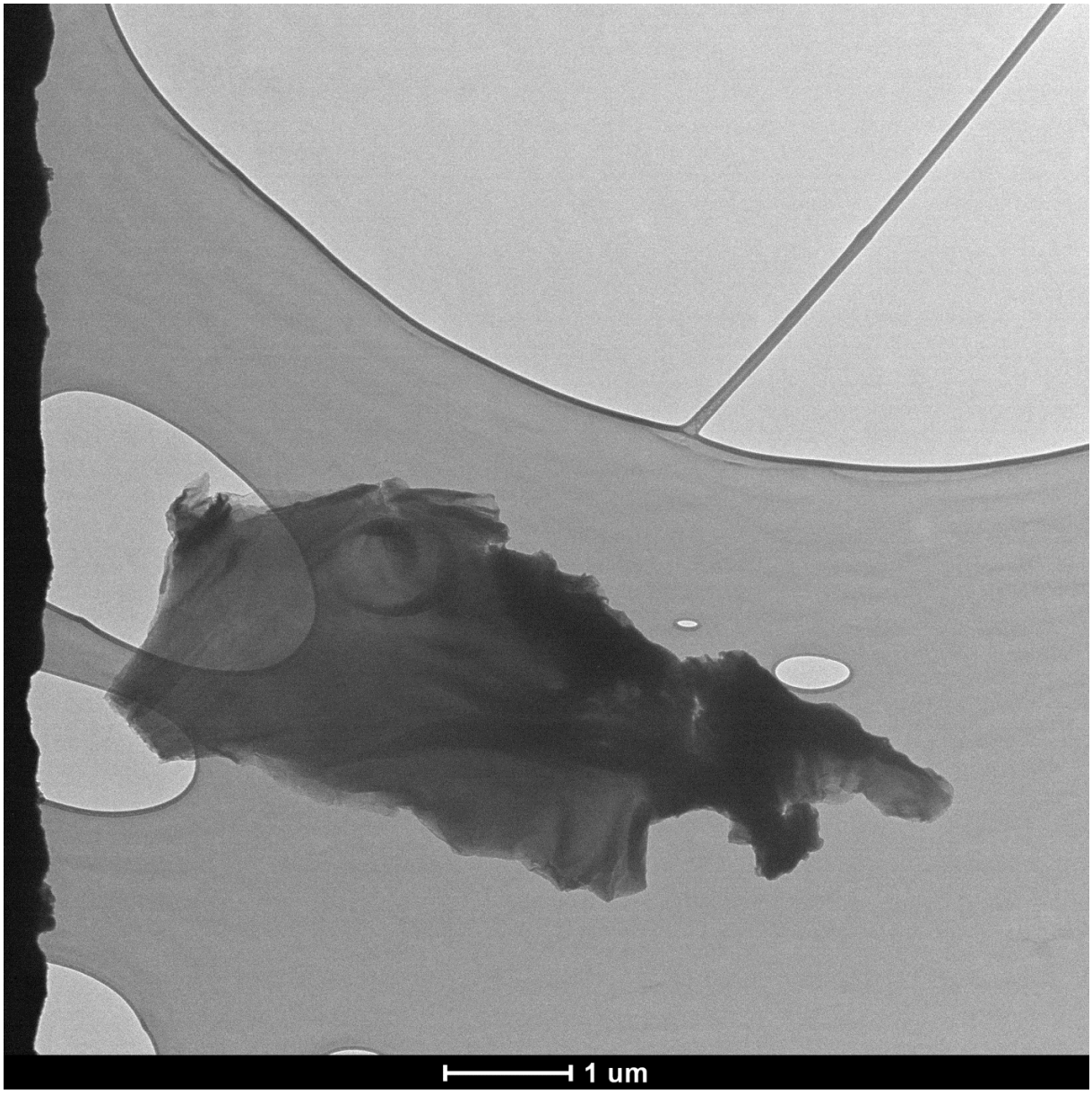

3.3.3. Acrylonitrile Polymerization

The series of acrylonitrile (AN) surface-initiated polymerizations by normal ATRP based on 2-CDMDPBMP initiator material is described in Table 3.4. The reactions were carried out in DMSO at 60^0C. Figure 3.22 shows the TGA weight change patterns under air flow for these samples. The air was chosen for thermogravimetric measurements, because PAN readily carbonizes under nitrogen atmosphere, [146] thus the weight loss under N_2 for PAN/silica composites may underestimate the PAN loading. After 44 hours of reaction, the weight loss % reached about 62% for 2-P4. The morphology of 2-P4 was illustrated by TEM image in Figure 3.23. The left side of the image appears to show twisted layers.

As shown in Figure 3.24, 3.25 and 3.26, d_{001} increased from 3.4 nm up to about 5 nm for PAN/silica nanocomposites. For 2-P4, there were two shoulders on the SAXS pattern (Figure 3.26). These shoulders are positioned in a way which suggests that they correspond to (001) and (002) reflections, but the resulting interplanar spacing appears to be too large (~10 nm) for a moderate polymer loading. Therefore, the feature of $2\theta \approx \sim 0.9°$ may be due to contamination and the actual interplanar spacing is likely to be ~5 nm.

Table 3.4. Atom Transfer Radical Polymerization of Acrylonitrile Initiated from Initiator-Modified Layered Silica 2-CDMSPBMP.

	2-CDMDPBMP	$CuBr_2$	CuBr	TPMA	AN	time/ hrs	residue% (SiO_2)	polymer/ silica	d_{001} (nm)	2θ
2-P2	**1**	**0.1**	**1**	**1.1**	**400**	**22**	**61.70%**	**0.1**	**3.4**	**2.56**
2-P3	**1**	**0.1**	**1**	**1.1**	**400**	**28**	**44.13%**	**0.75**	**4.6**	**1.92**
2-P4	**1**	**0.1**	**1**	**1.1**	**400**	**44**	**37.54%**	**1.17**	**5.2 or 10.4**	**1.7 or 0.9**

Figure 3.22. Thermogravimetric Weight Change Curves of PAN/Silica Nanocomposites 2-P2, 2-P3 and 2-P4 under Air.

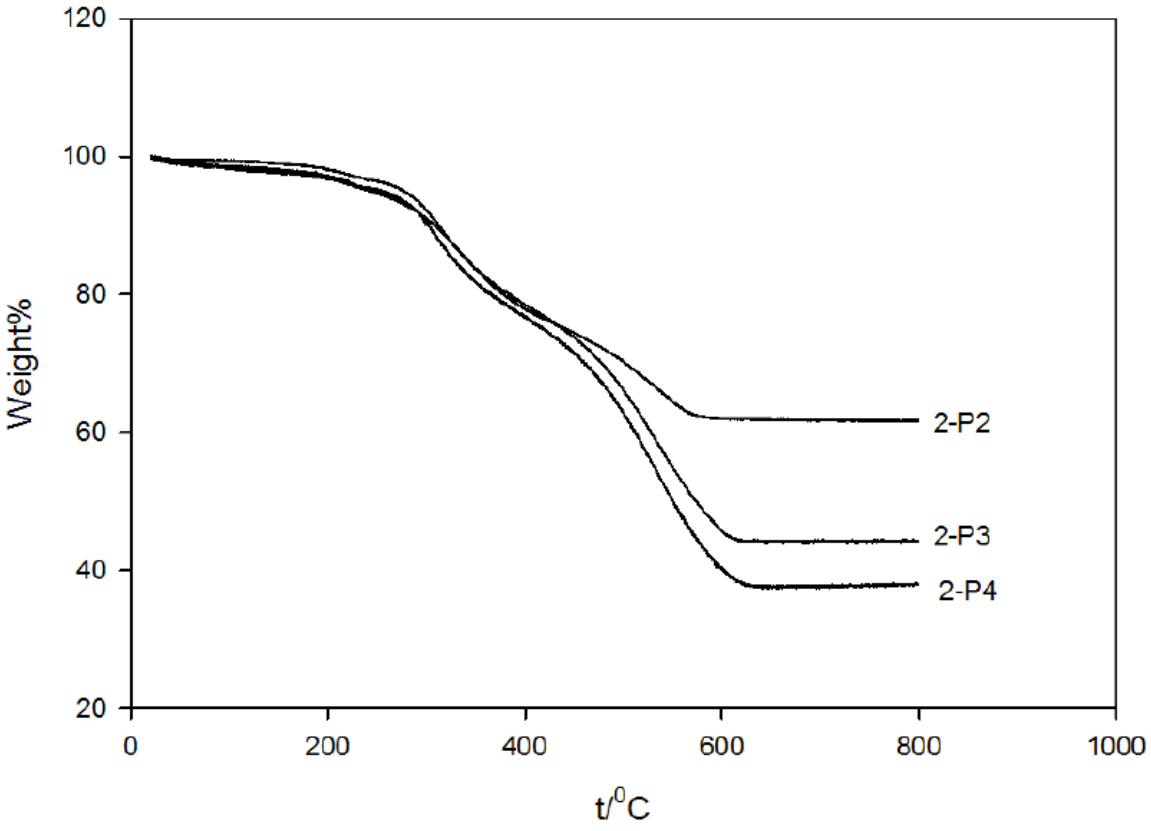

Figure 3.23. TEM Image of PAN/Silica Nanocomposite 2-P4.

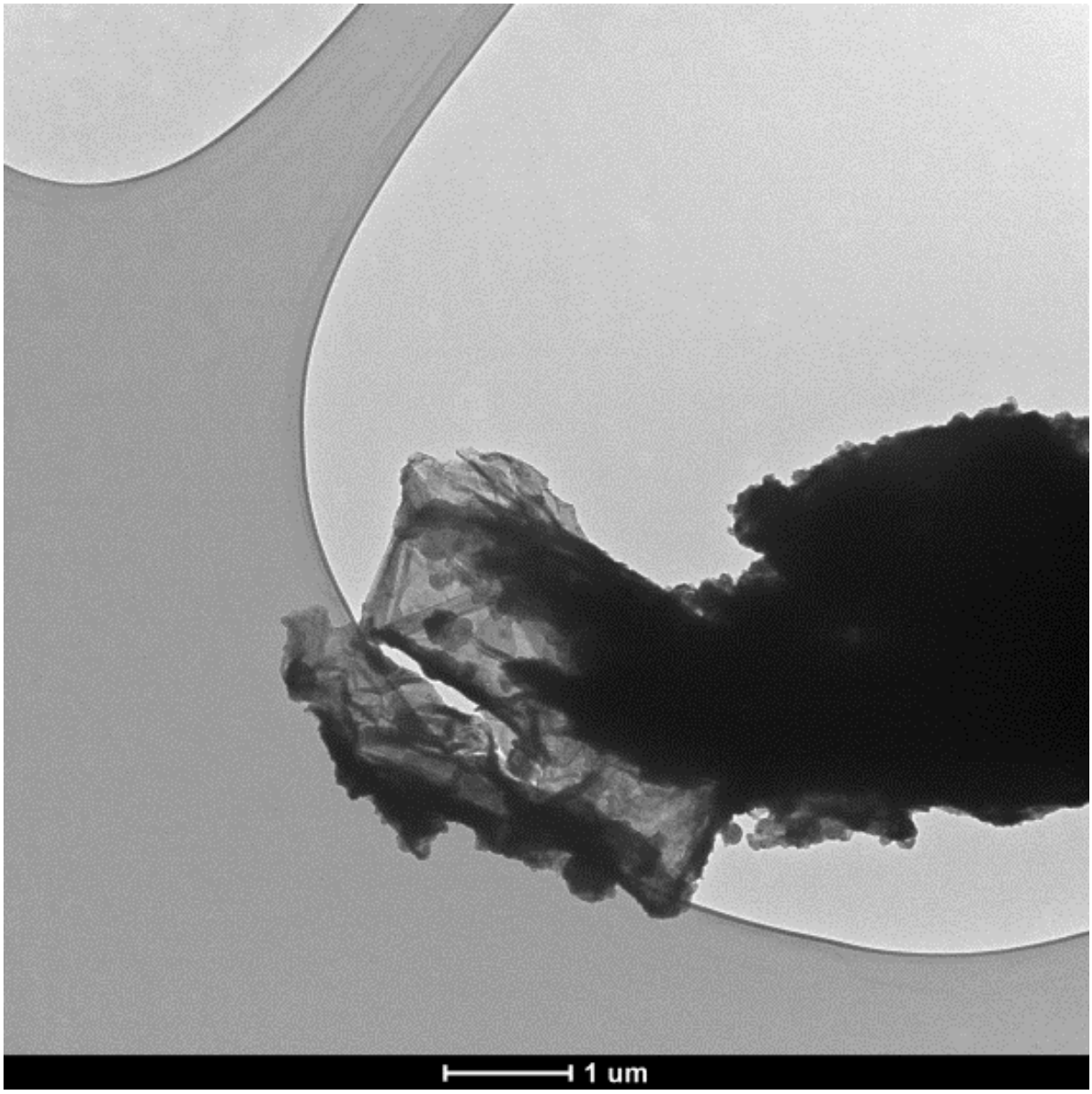

Figure 3.24. Small-Angle X-ray Scattering Pattern of PAN/Silica Nanocomposite 2-P2.

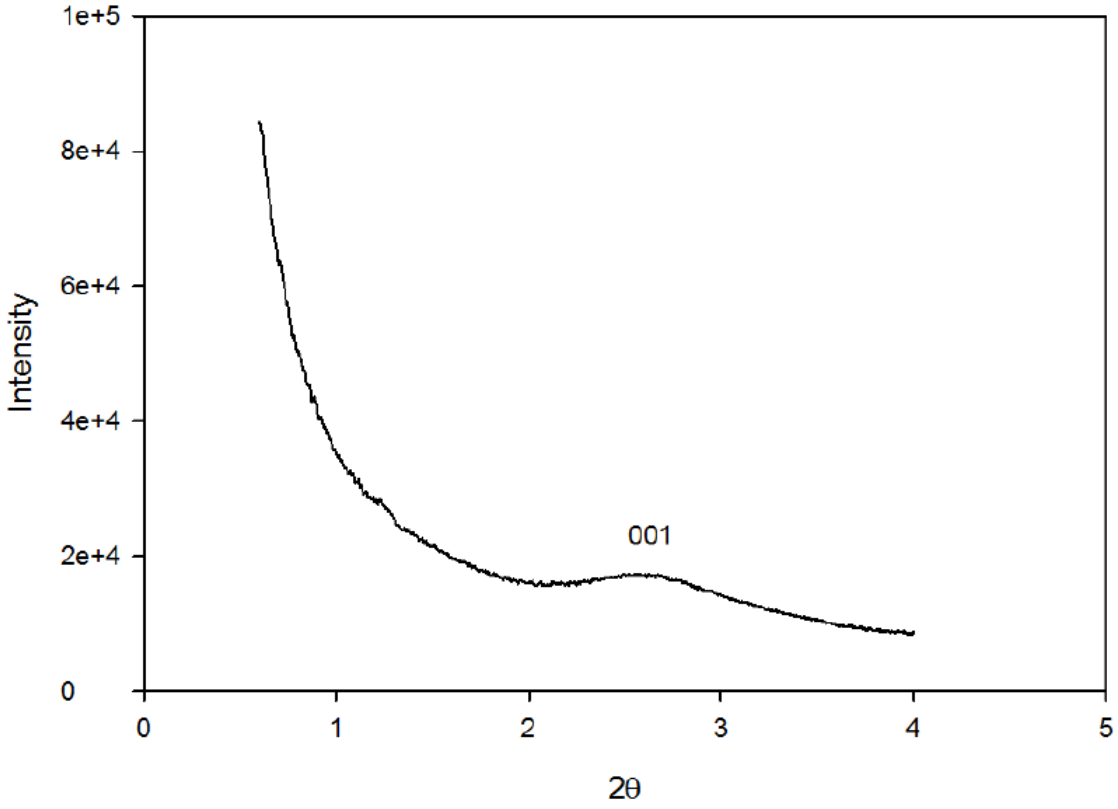

Figure 3.25. Small-Angle X-ray Scattering Pattern of PAN/Silica Nanocomposite 2-P3.

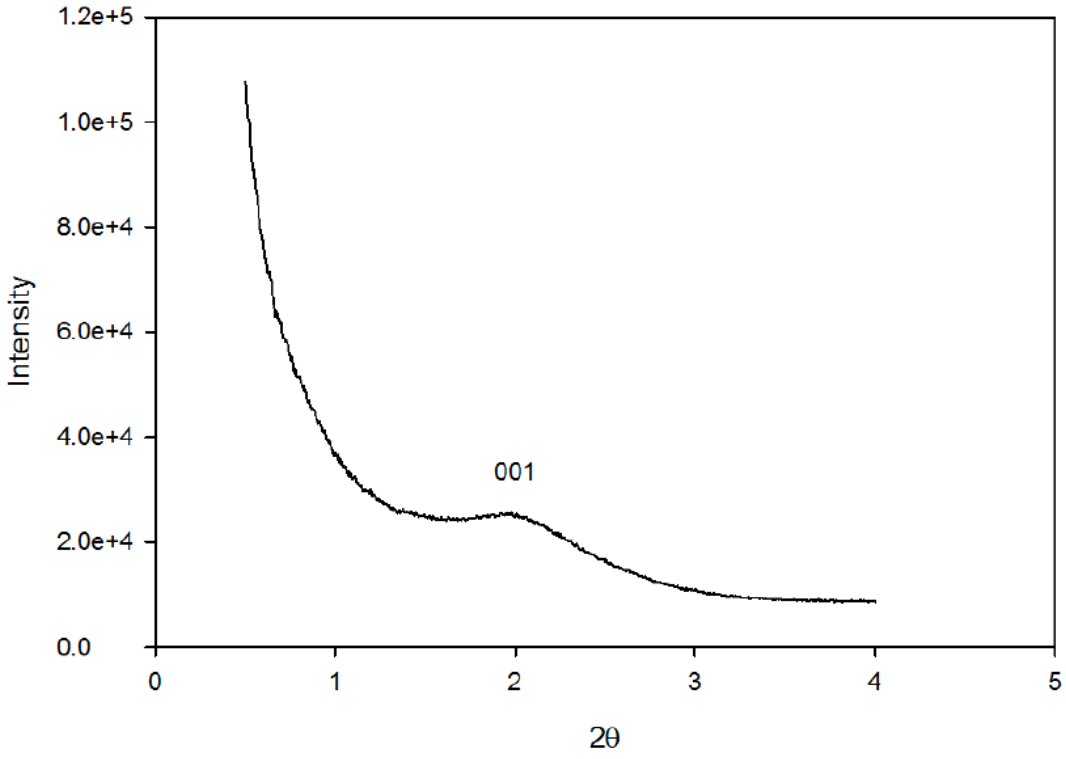

Figure 3.26. Small-Angle X-ray Scattering Pattern of PAN/Silica Nanocomposite 2-P4.

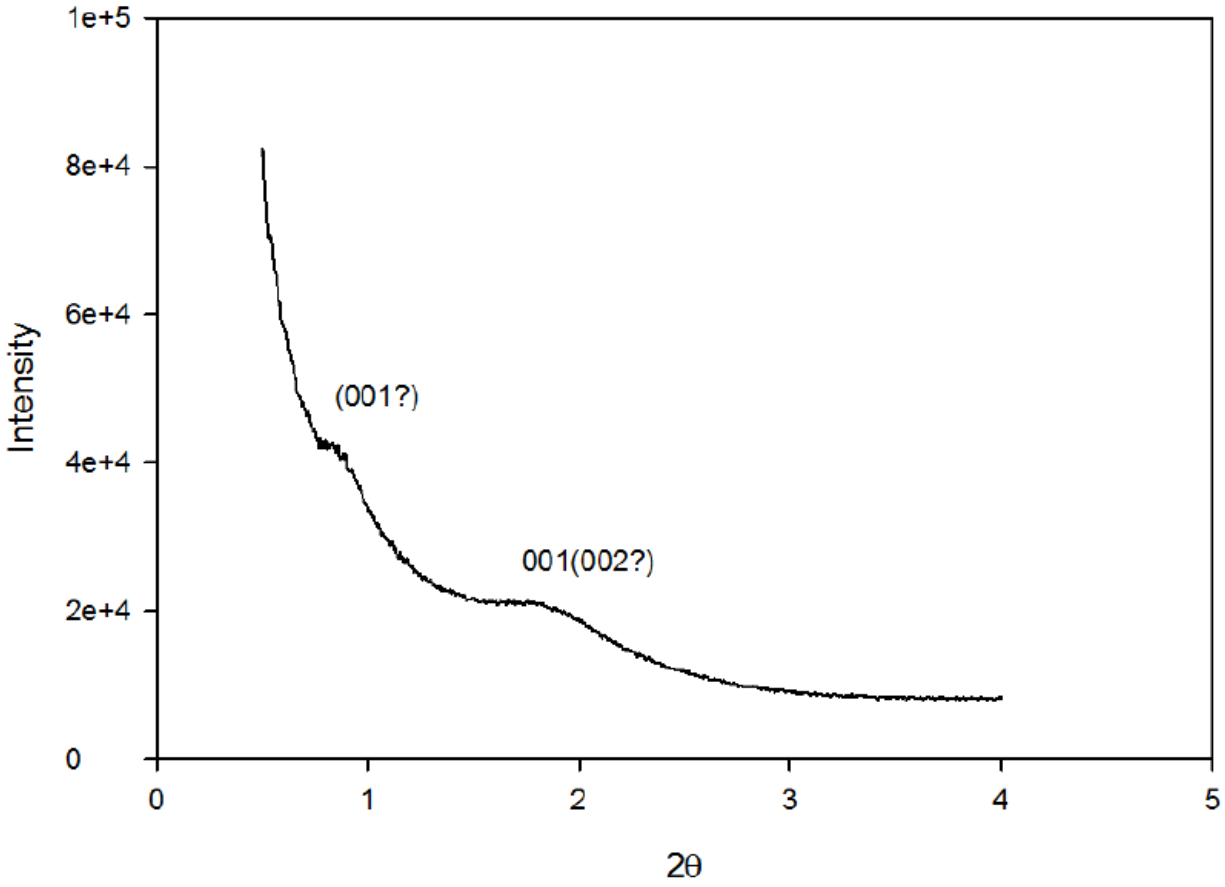

3.3.4. Styrene Polymerization

Styrene polymerization results obtained using normal ATRP are summarized in Table 3.5. After almost two days of the reaction, d_{001} was enlarged to 5.3 nm (Figure 3.27) with 31.40% silica residue (Figure 3.28). It should be noted that nitroxide-mediated polymerization was already shown to afford similar or even larger *d*-spacing in PS-clay nanocomposites. [67b]

Table 3.5. Atom Transfer Radical Polymerization of Styrene Initiated from Initiator-Modified Layered Silica 1-CDMSPBMP.

	1-CDMSPBMP	$CuBr_2$	CuBr	PMDETA	St	time/ hrs	residue%	polymer/ silica	d_{001}/nm	2θ (degree)
1-P6	**1**	**0.1**	**1**	**1.1**	**370**	**25.5**	**43.31**	**0.79**	**3.4**	**2.61**
1-P7	**1**	**0.1**	**1**	**1.1**	**370**	**47**	**31.40**	**1.66**	**5.3**	**1.66**

Figure 3.27. Small-Angle X-ray Scattering Patterns of PS/Silica Nanocomposites 1-P6 and 1-P7.

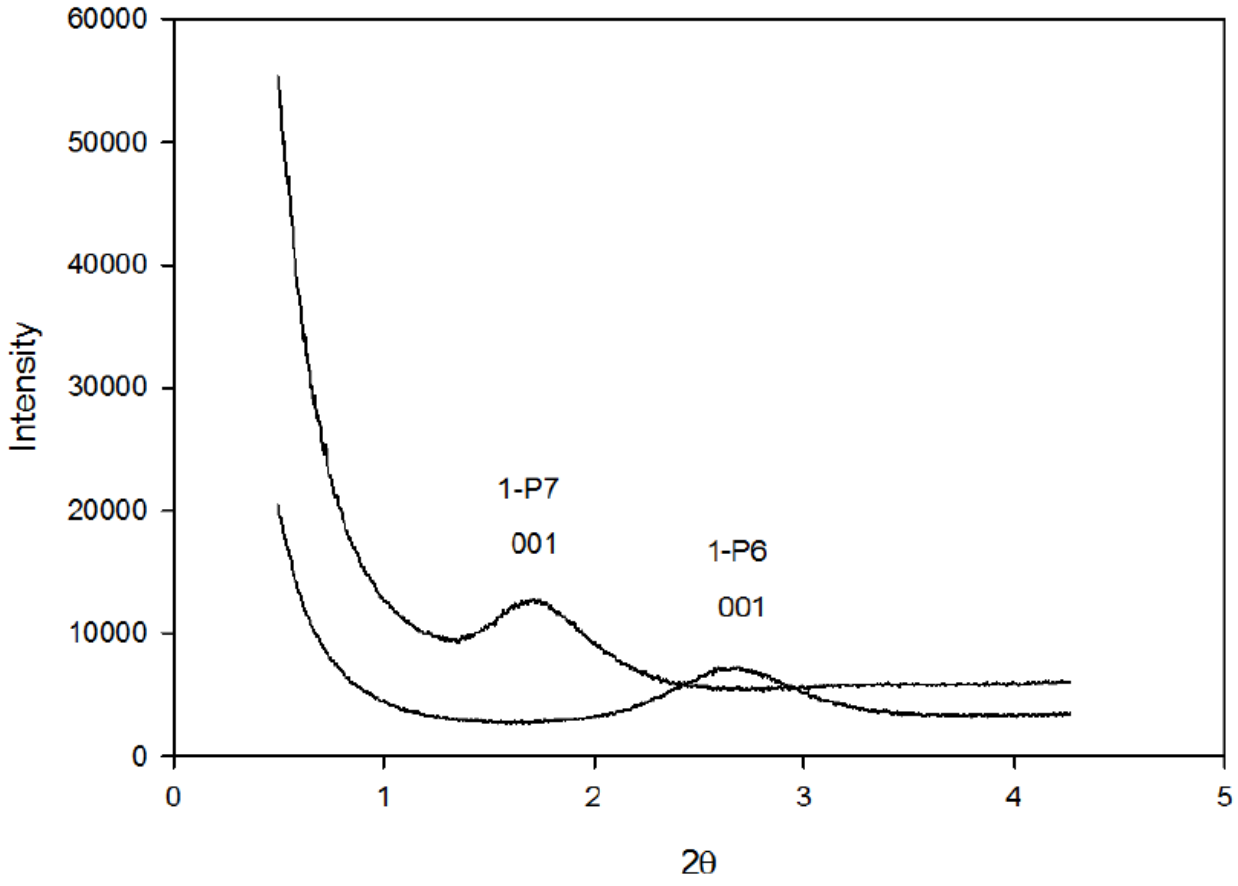

Figure 3.28. Thermogravimetric Weight Change Curves of PS/Silica Nanocomposites 1-P6 and 1-P7.

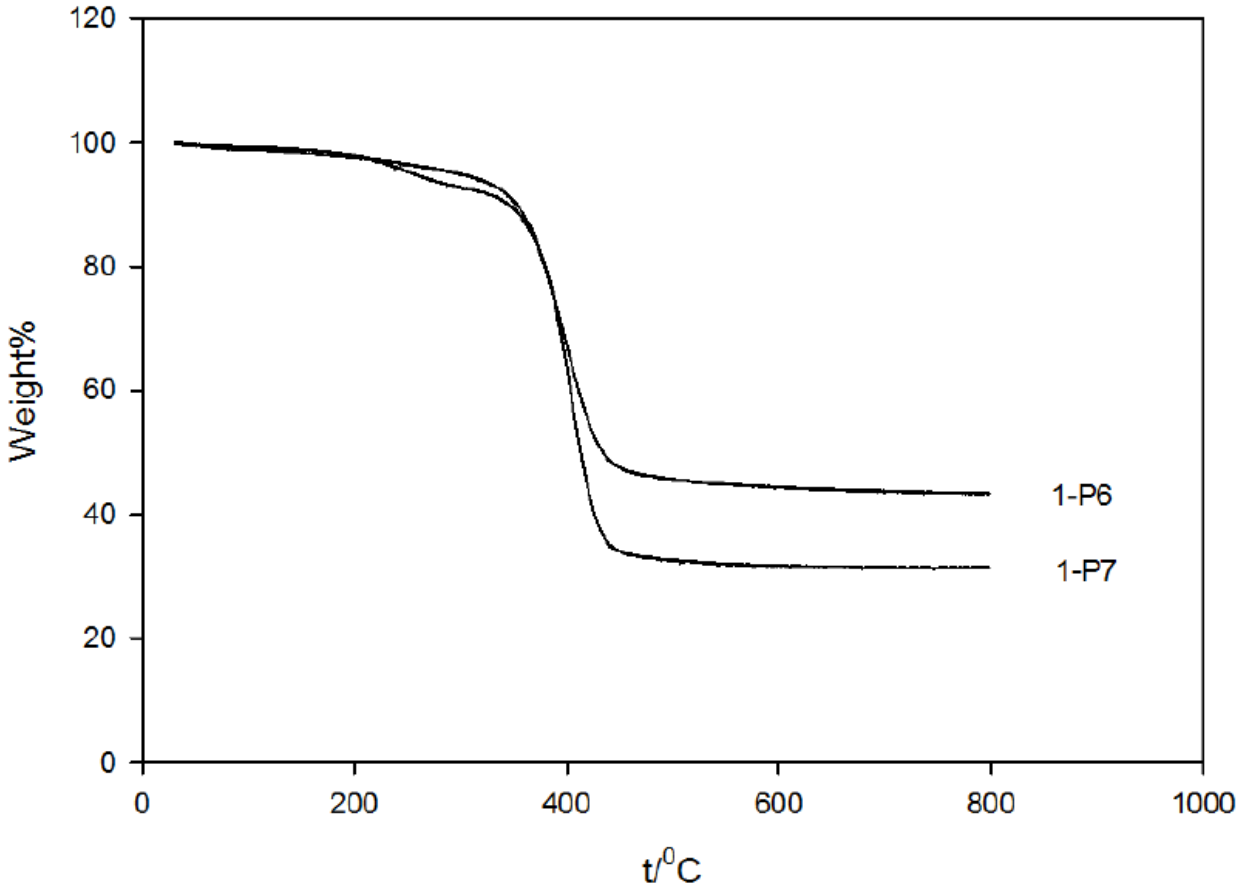

Glass transition temperature of 1-P7 was 102 ^{0}C (Figure 3.29), which is 2 ℃ higher than bulk polystyrene T_g, [150] and 1-P6 did not have an indication of the transition. TEM image in Figure 3.30 exhibited features that suggest a layered structure of the material.

Figure 3.29. Differential Scanning Calorimetry Trace of PS/Silica Nanocomposite 1-P7.

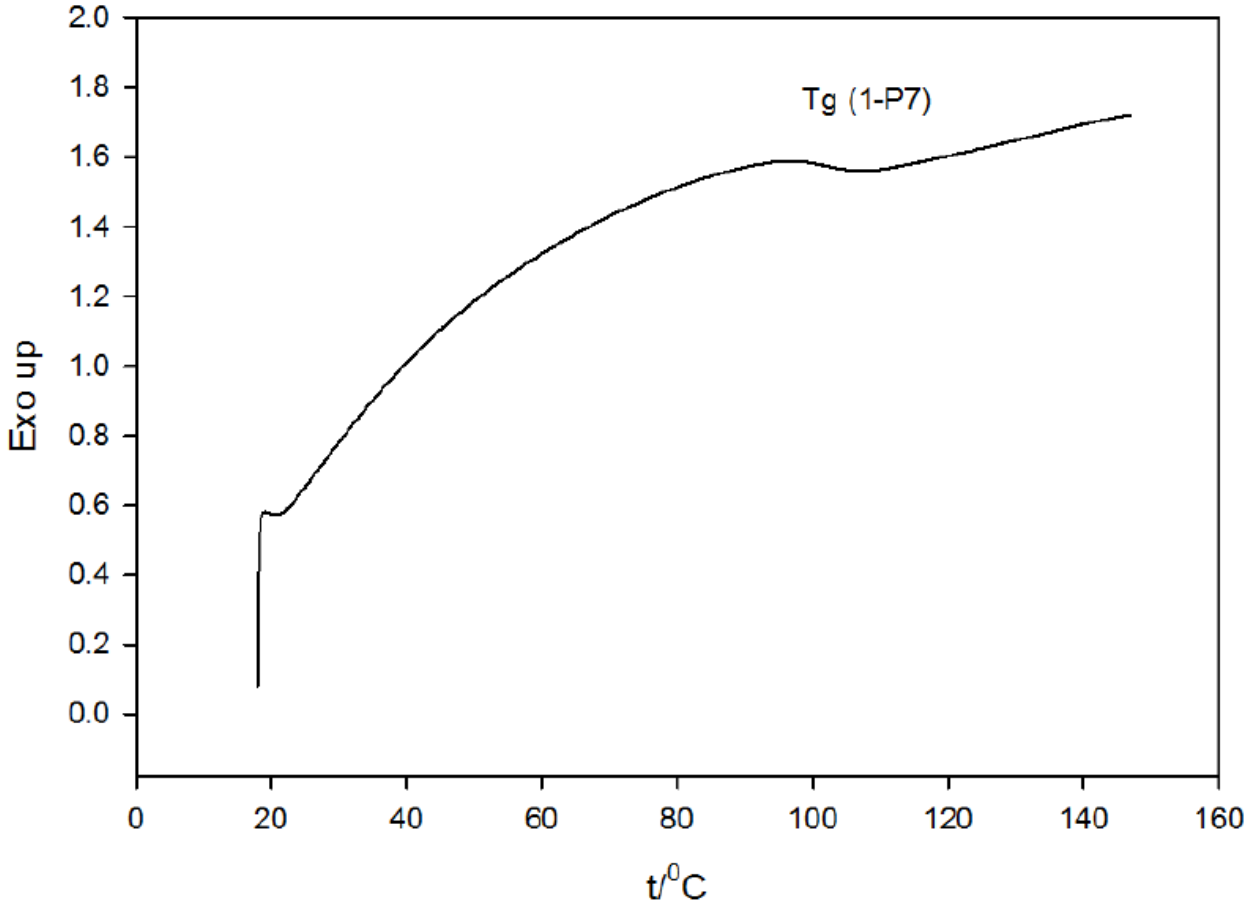

Figure 3.30. TEM Image of PS/Silica Nanocomposite 1-P7.

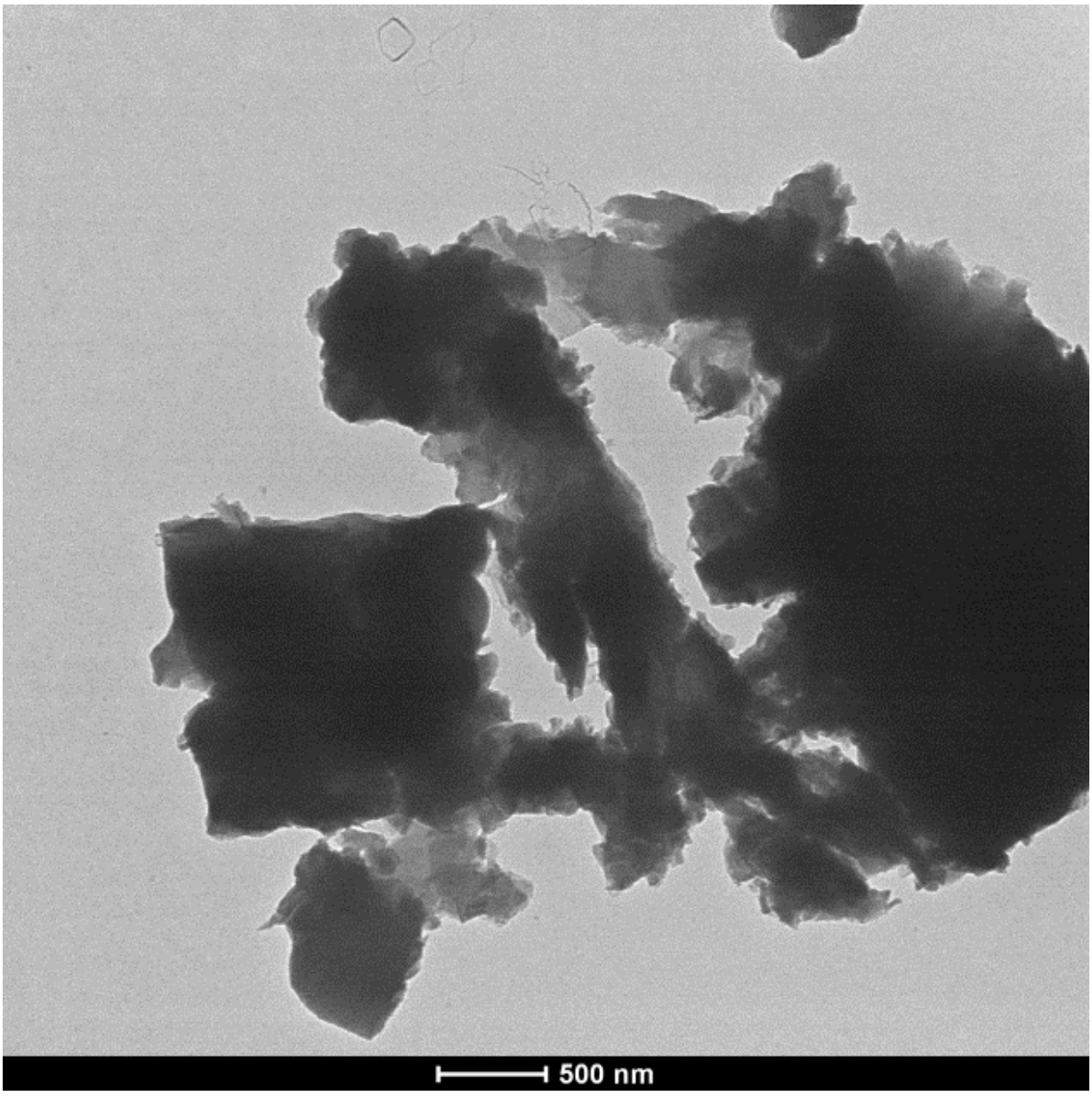

When compared with the literature results, the polystyrene (PS)/silicate nanocomposite prepared by Sogah group via nitroxide-mediated radical polymerization initiated from silicate-anchored initiator was identified as exfoliated architecture, which did not show any X-ray diffraction (XRD) peaks. This PS/silicate nanocomposite did not exhibit glass transition behavior observable in DSC. [67a] Shipp group investigated the PS/silicate nanocomposites prepared by atom transfer radical polymerization. Their results indicated that the polymer loading was controlled by reaction duration and the molecular weight increased with reaction time, while the polydispersity decreased. From XRD patterns for their samples, d_{001} peak moved slightly to smaller angles with increasing monomer conversion, which meant the interplanar spacing was slightly increased. d_{001} peak was lost after 81.8% conversion (360 min reaction), but TEM images showed some domains containing high concentration of silicate, which meant it may not be a fully exfoliated nanocomposite. [69] Our PS/silica nanocomposites had ordered intercalated architectures, and the interplanar spacing was significantly enlarged by polymer loading. PS/silica nanocomposite 1-P7 showed glass transition temperature of 102 ℃, which meant that sufficiently large PS domains existed in the dispersed nanocomposite architecture.

It can be concluded that normal atom transfer radical polymerization (ATRP) can be successfully used in the synthesis of intercalated and exfoliated nanocomposites with nanoscale silica layers dispersed in different polymer matrixes (PMMA, PAN, PS). The loading of the polymer grafted from the silica surface can be controlled. The ordering that the periodic layered intercalated architecture can be maintained to some loading level (polymer/silica at least 1:1, but sometimes even 4:1) until the exfoliated structure forms, but the impurities (copper species) level is high for the nanocomposites prepared via normal ATRP (because one recovers colorful

products, as seen in Figure 3.31). MMA-based nanocomposites exhibited interesting glass transition trend, where T_g was increased with increasing polymer loading.

Figure 3.31. Appearance of PMMA/Silica nanocomposite 1-P5 Prepared via Normal ATRP.

Chapter IV.

Synthesis of Nanocomposites Using Surface-Initiated Activators Regenerated by Electron Transfer Atom Transfer Radical Polymerization (ARGET ATRP)

4.1. Experimental Section

A typical ARGET ATRP reaction was carried out in a 4 ml vial without prior deoxygenation. The initiator-modified layered silica (1-CDMSPBMP or 2-CDMSPBMP, about 10-30 mg), ligand (3.6 μl 1, 1, 4, 7, 7-pentamethyl-diethylenetriamine (PMDETA) for MMA or St, 5 mg tris[(2-pyridyl)methyl]amine (TPMA) for AN), 0.094 or 0.032 mg $CuCl_2$ ($CuCl_2$ was dissolved in DMSO to be 10 mg/ml solution taken by micro-liter syringe (3.2 μl solution contained 0.032 mg $CuCl_2$)), monomer (MMA, St or AN), and solvent (0.6 ml anisole for MMA or St, 0.62 ml DMSO for AN) were charged to the vial, finally the reducing agent solution (50 mg tin (II) 2-ethylhexanoate ($Sn(EH)_2$) dissolved in 1.0 ml anisole for MMA or St, or 1.0 ml DMSO for AN) was transferred into the vial. The vial was capped and stirred in the oil bath at 60 °C for MMA or AN, 90 °C for St.

The reaction was terminated at a selected time by opening the cap to expose the polymerization mixture to oxygen from the air (to convert ATRP catalyst to deactivator). The polymerization product was filtered and washed with methanol and toluene, dried in a vacuum oven at 60 °C overnight. The samples were characterized as described in Chapter 2.1 and 3.3.

4.2. Methyl Methacrylate Polymerization by ARGET ATRP

Table 4.1 shows two series of MMA ARGET ATRP results based on initiator-modified layered silica 1-CDMSPBM. Samples 1-P8~1-P12 synthesized with initiator/MMA molar ratio of 1:90 series reached residue% as low as 11.53% (1-P12) after 24 hours of reaction (Figure 4.1), which corresponds to PMMA/silica weight ratio of 7.2:1. Samples 1-P8 and 1-P9 with low or moderate polymer loading obtained after 4 and 6 hours reaction showed ordered structures with the (001) interplanar spacings of 2.1 nm and 4.6 nm (Figure 4.2). The polymer loadings for samples 1-P8 to 1-P12 indicate that there might be an "induction" period in which oxygen was depleted in the polymerization mixture, after which the polymerization started. This might have been 3-4 hours for this series, because the polymer loading in 1-P8 was very low as seen in Figure 4.3. From SAXS patterns (Figure 4.2), the interlayer spacing was enlarged for 1-P10 sample (residue of 22.98%) in comparison to samples 1-P8 and 1-P9, but the SAXS pattern for 1-P10 featured a broad shoulder, which does not provide good basis to calculate the interplanar spacing. For a higher polymer loading, 1-P11 and 1-P12 samples did not have clear peaks or shoulders on SAXS patterns.

For 1-P13~1-P18 samples, the polymerizations were carried with larger monomer/initiator molar ratio (270:1, which is threefold higher comparing with the previous series) and a higher reducing agent molar ratio, which increased the propagation rate compared to the products discussed above. The PMMA/silica weight ratio reached 22.9 for sample 1-P18 after 41 hours polymerization reaction (Table 4.1, Figure 4.4). The higher amount the polymer loaded, the higher the viscosity of the crude product appeared to be, and the purified products had different physical properties changing from fine powders to rock-like crystals. This series of products

showed featureless SAXS patterns, which was similar as in the case of normal ATRP PMMA/silica products with high polymer loading.

When comparing PMMA/silica nanocomposites with similar polymer loadings synthesized via normal ATRP and ARGET ATRP, 1-P1 (normal ATRP, residue = 27.49%) had a quite narrow peak on the SAXS pattern, but 1-P9 and 1-P10 (ARGET ATRP, residue = 28.53% and 22.98%) exhibited either broad peak or a broad shoulder. The interplanar spacings for these samples were similar (4.6-6.3 nm). When considering polydispersity index (PDI) difference for polymers prepared from normal ATRP and ARGET ATRP, as described in Chapter I, normal ATRP offers lower PDI comparing to ARGET ATRP. This was also confirmed by studies of ATRP and ARGET ATRP initiated from surfaces of mesopores. [166-167] Therefore, the polymer growth in ARGET ATRP was apparently less controlled, which led to a less uniform growth of the polymer initiated from the surface of the layers, making it more difficult to preserve their parallel orientation as the polymer chains grow. This led to broader features (peaks or shoulders) in SAXS patterns.

Table 4.1. ARGET ATRP of Methyl Methacrylate Initiated from Initiator-Modified Layered Silica 1-CDMSPBMP.

	1-CDMDPBMP	$CuCl_2$	PMDETA	MMA	Sn(II)	time/hrs	residue%	Polymer /Silica	d_{001}(nm)	2θ (degree)
1-P8	**1**	**0.02**	**0.4**	**90**	**3**	**4**	**58.01%**	**0.20**	**2.1**	**4.3**
1-P9	**1**	**0.02**	**0.4**	**90**	**3**	**6**	**28.53%**	**2.0**	**4.6**	**2.0**
1-P10	**1**	**0.02**	**0.4**	**90**	**3**	**8**	**22.98%**	**2.8**	**n/a**	**1.2-2.5 (weak and broad)**
1-P11	**1**	**0.02**	**0.4**	**90**	**3**	**18**	**13.49%**	**5.9**	**n/a**	**n/a**
1-P12	**1**	**0.02**	**0.4**	**90**	**3**	**24**	**11.53%**	**7.2**	**n/a**	**n/a**
1-P13	**1**	**0.02**	**1.2**	**270**	**9**	**6**	**23.57%**	**2.7**	**n/a**	**n/a**
1-P14	**1**	**0.02**	**1.2**	**270**	**9**	**8**	**17.41%**	**4.2**	**n/a**	**n/a**
1-P15	**1**	**0.02**	**1.2**	**270**	**9**	**15**	**9.491%**	**9.0**	**n/a**	**n/a**
1-P16	**1**	**0.02**	**1.2**	**270**	**9**	**22**	**6.790%**	**13.2**	**n/a**	**n/a**
1-P17	**1**	**0.02**	**1.2**	**270**	**9**	**30**	**4.695%**	**19.8**	**n/a**	**n/a**
1-P18	**1**	**0.02**	**1.2**	**270**	**9**	**41**	**4.088%**	**22.9**	**n/a**	**n/a**

Figure 4.1. Thermogravimetric Weight Change Curves of PMMA/Silica Nanocomposites 1-P8 to 1-P12.

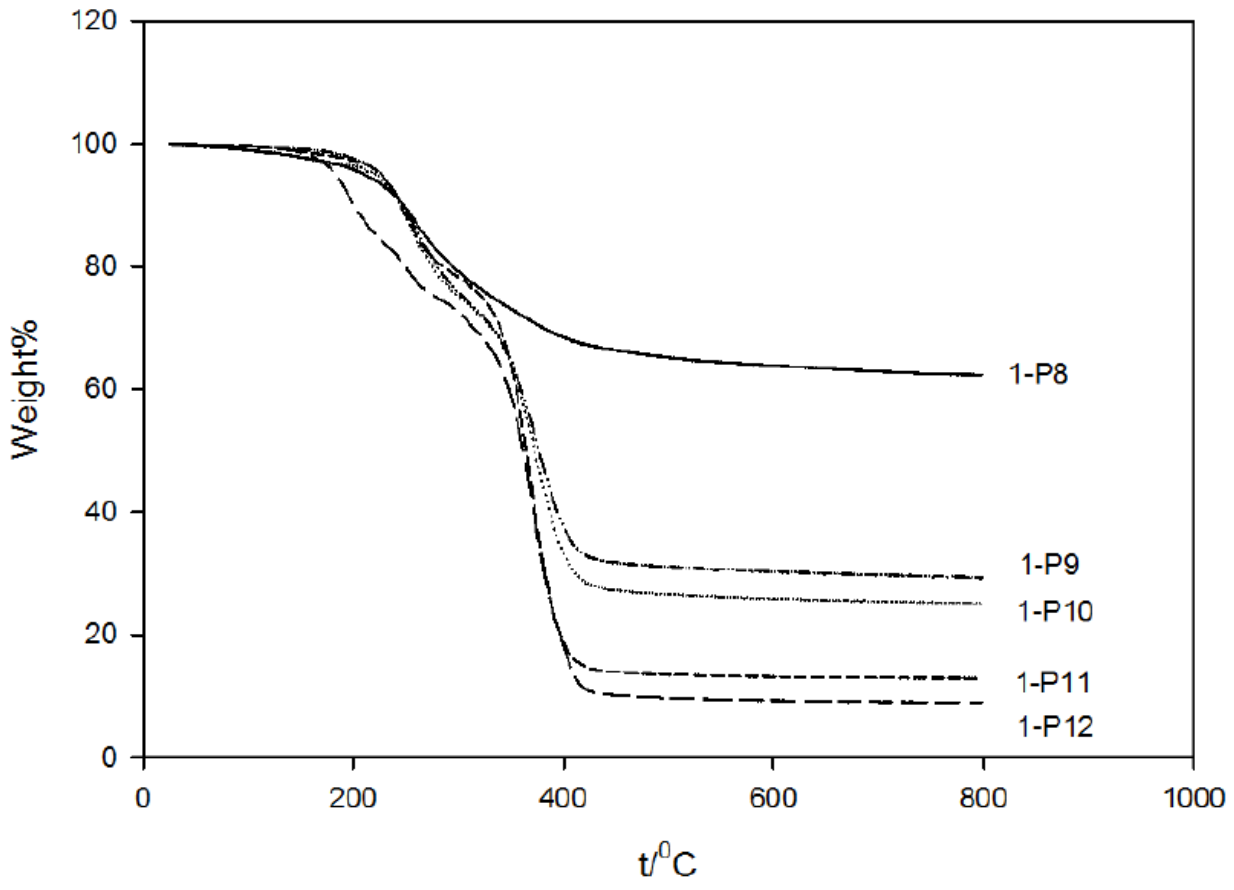

Figure 4.2. Small-Angle X-ray Scattering Patterns of PMMA/Silica Nanocomposites 1-P8, 1-P9 and 1-P10.

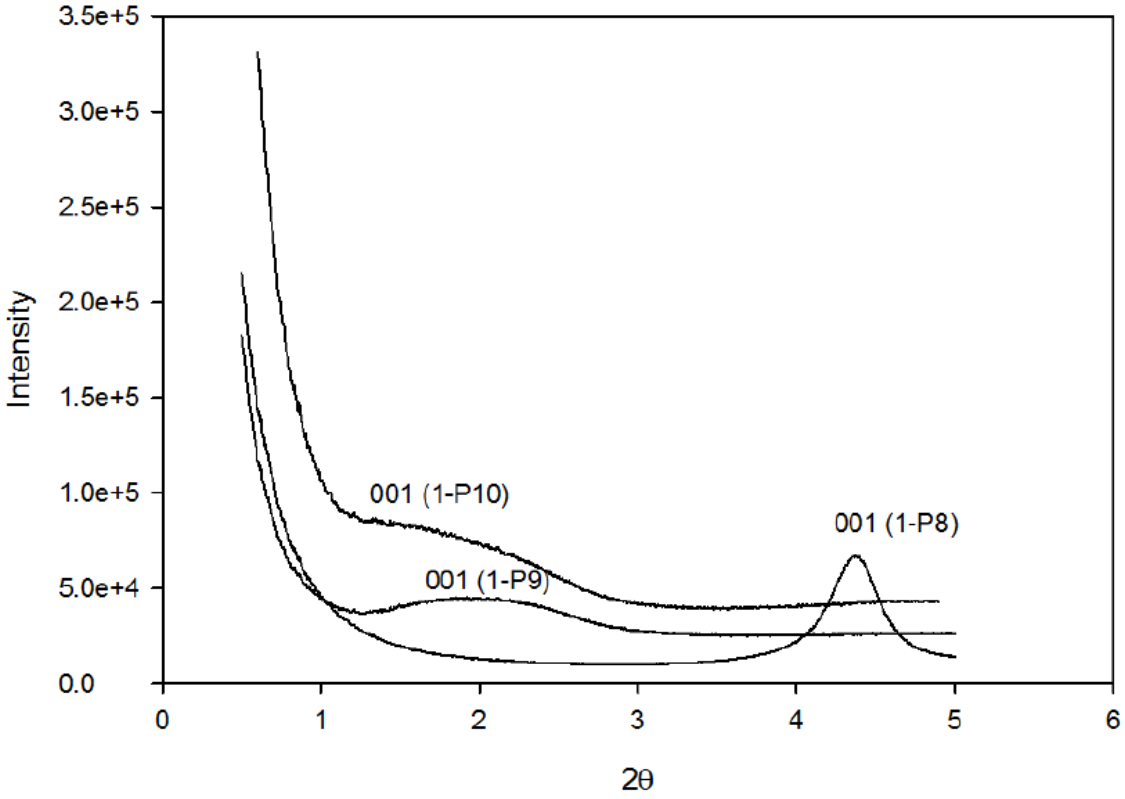

Figure 4.3. Polymer/Silica Mass Ratio vs. Polymerization Time of PMMA/Silica Nanocomposites 1-P8 to 1-P12.

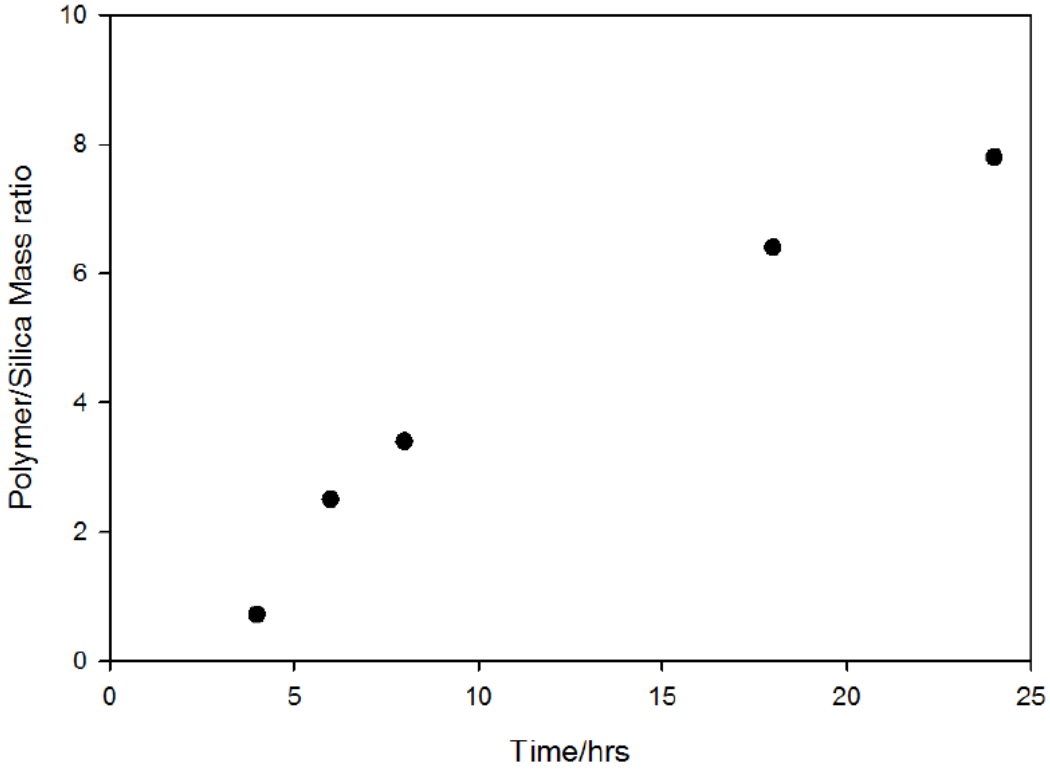

Figure 4.4. Thermogravimetric Weight Change Curves of PMMA/Silica Nanocomposites 1-P13 to 1-P18.

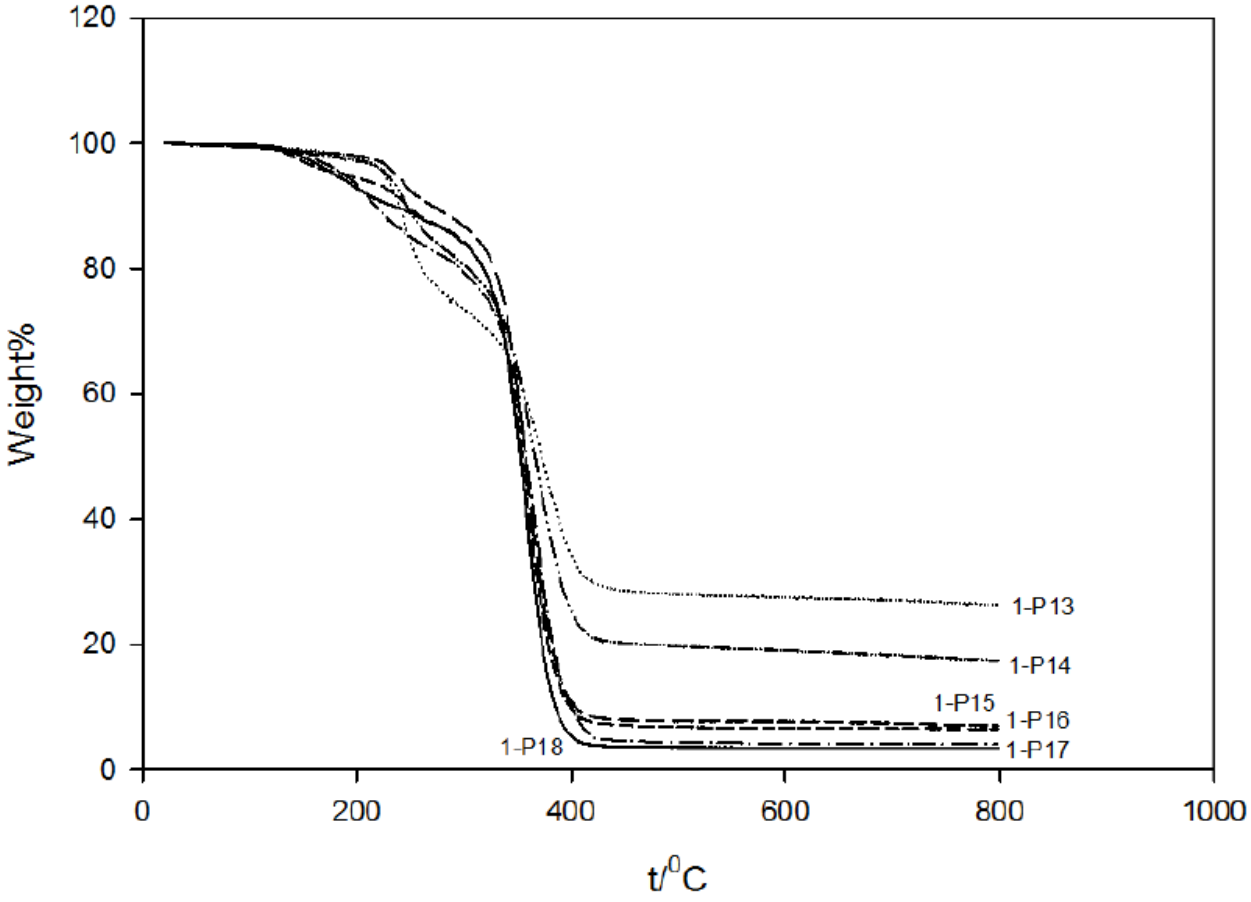

Glass transition temperatures for ARGET ATRP PMMA/silica nanocomposites were interesting (Table 4.2, Figure 4.5, and Figure 4.6). Generally, there was no clear trend in T_g as a function of the polymer loading, in contrast to the results from normal ATRP. The glass transition temperatures were about 122-129 ℃ for the current series of samples. The reason might be due to the lower ordering of nanocomposites synthesized by ARGET ATRP, which made the environment of polymer chains less homogenous. 1-P17 and 1-P18 samples exhibited unusually low temperatures at which glass transition was indicated by DSC (99 and 86 ℃), and the possible reason might be some monomers left in the system during the isolation of the product. In the synthesis, the reaction mixture turned to gel (via crosslinking of the polymer), and monomer might have been trapped inside the materials. The morphologies of 1-P8 and 1-P18 nanocomposites were illustrated in Figure 4.7 and Figure 4.8. The details in the edge of 1-P8 sample seemed like a stacking of several platelets, which was more obvious in sample 1-P18.

Table 4.2. Glass Transition Temperatures of PMMA/Silica Nanocomposites 1-P8 to 1-P18.

	1-P8	1-P9	1-P10	1-P11	1-P12	1-P13	1-P14	1-P15	1-P16	1-P17	1-P18
T_g/°C	**none**	**125.4**	**122.1**	**127.5**	**127.3**	**127.9**	**n/a[a]**	**128.5**	**125.1**	**98.9[b]**	**86.4[b]**

[a] The sample amount for 1-P14 was not enough to complete the DSC test, so no DSC test was performed.

[b] Possibly, these thermal event may be related to the monomer left in the apparently cross-linked matrix.

Figure 4.5. Differential Scanning Calorimetry Traces of PMMA/Silica Nanocomposites 1-P8 to 1-P12.

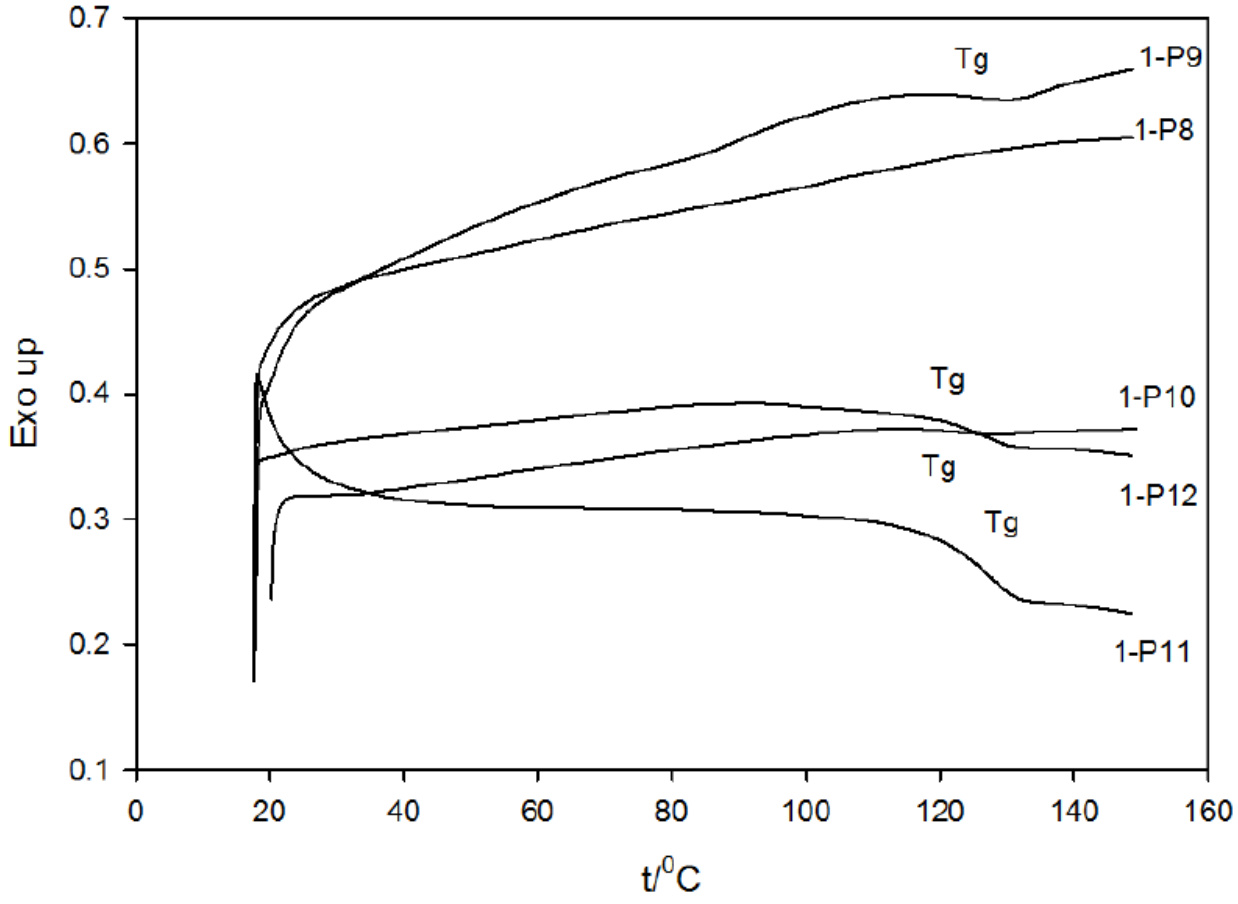

Figure 4.6. Differential Scanning Calorimetry Traces of PMMA/Silica Nanocomposites 1-P13, and 1-P15 to 1-P18.

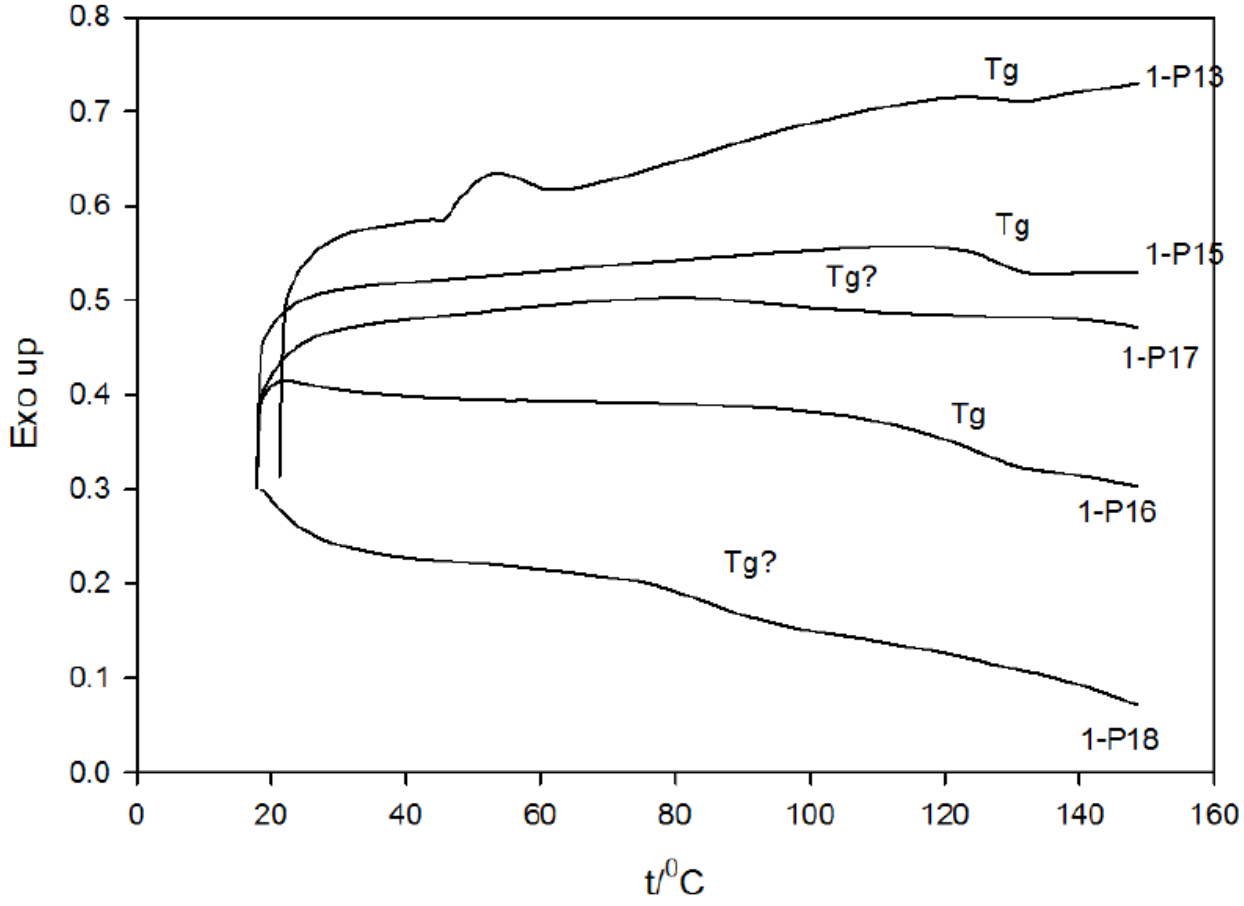

Figure 4.7. TEM Image of PMMA/Silica Nanocomposite 1-P8.

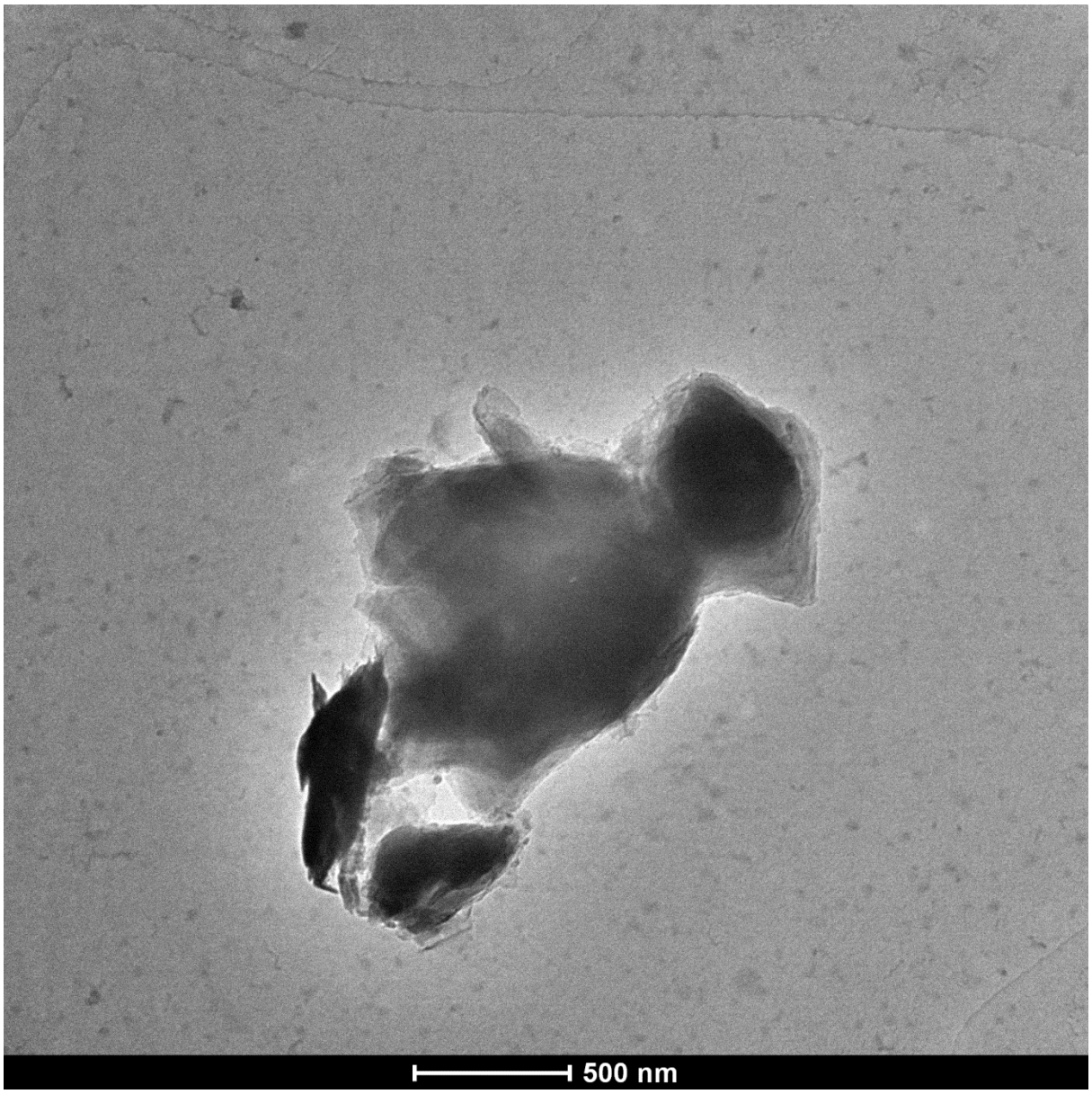

Figure 4.8. TEM Image of PMMA/Silica Nanocomposite 1-P18.

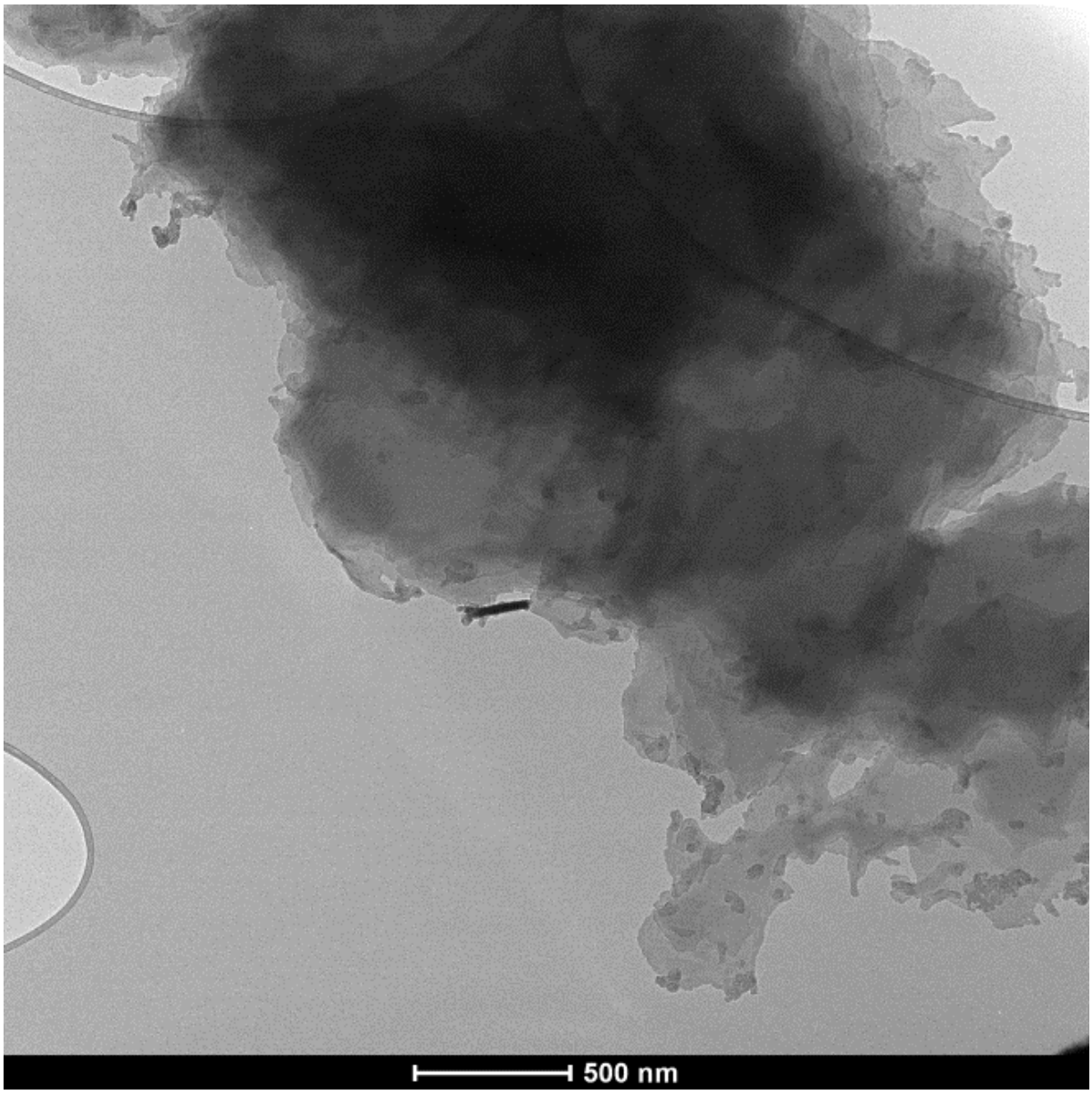

The results of MMA polymerizations by ARGET ATRP based on initiator-modified layered silica 2-CDMSPBMP are shown in Table 4.3. SAXS pattern did not have any peaks for this series of products. The weight change patterns are shown in Figures 4.9, and the polymer loadings reached high levels, as there was only 5.23% residue of silica for PMMA/silica nanocomposite 2-P9.

Table 4.3. ARGET ATRP of Methyl Methacrylate Initiated from Initiator-Modified Layered Silica 2-CDMSPBMP.

	2-CDMDPBMP	$CuCl_2$	PMDETA	MMA	Sn(II)	time/hrs	residue%	Polymer /Silica	d_{001}(nm)	2θ (degree)
2-P5	**1**	**0.02**	**1.2**	**270**	**9**	**8**	**22.59%**	**2.6**	**n/a**	**n/a**
2-P6	**1**	**0.02**	**1.2**	**270**	**9**	**15.5**	**8.42%**	**10.0**	**n/a**	**n/a**
2-P7	**1**	**0.02**	**1.2**	**270**	**9**	**18**	**7.95%**	**10.7**	**n/a**	**n/a**
2-P8	**1**	**0.02**	**1.2**	**270**	**9**	**21**	**5.85%**	**15.2**	**n/a**	**n/a**
2-P9	**1**	**0.02**	**1.2**	**270**	**9**	**25**	**5.23%**	**17.3**	**n/a**	**n/a**

The results for 2-CDMSPBMP initiator-functionalized layers are comparable to those for 1-CDMSPBMP initiator-functionalized layers (Table 4.1, entries of 1-P13 to 1-P18), suggesting the facile reproducibility of the method for different layered silica starting materials.

Figure 4.9. Thermogravimetric Weight Change Curves of PMMA/Silica Nanocomposites 2-P5 to 2-P9.

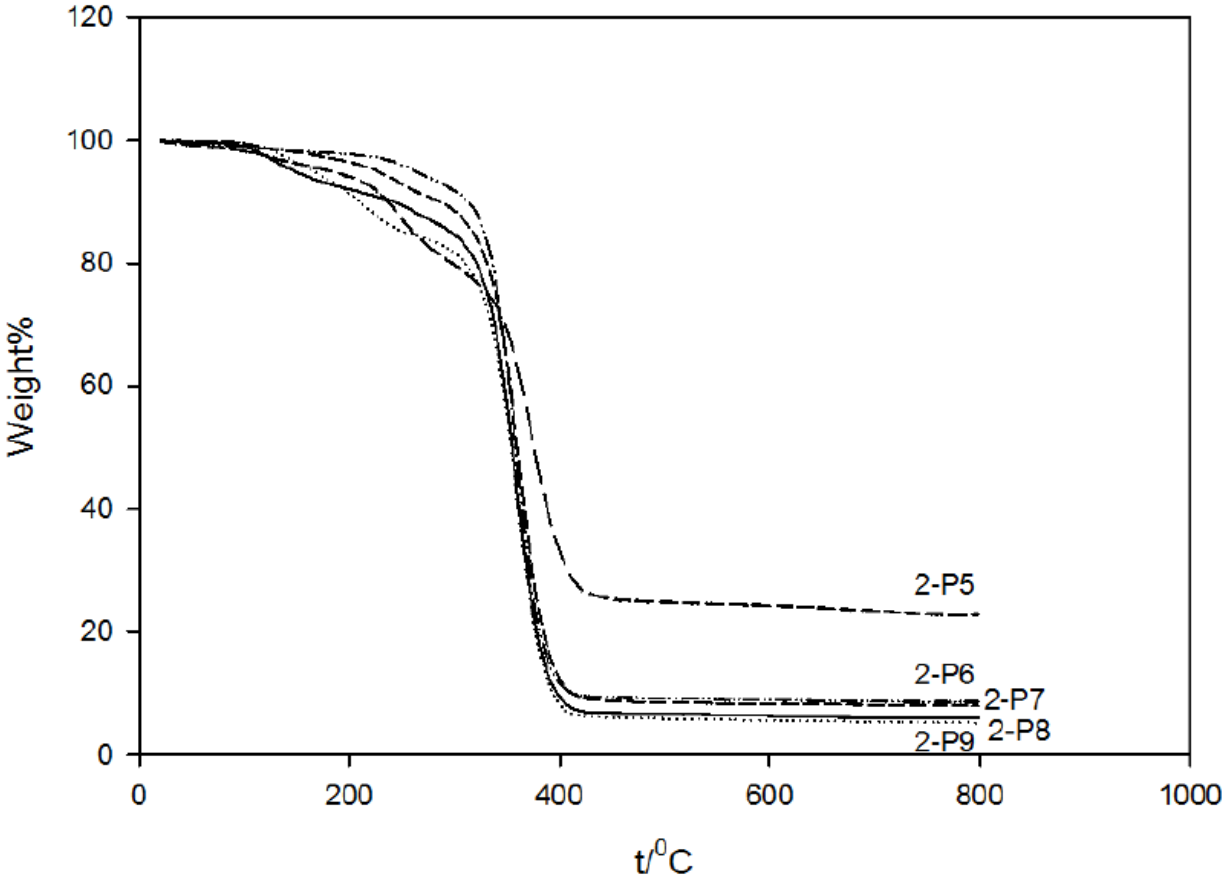

DSC results for the considered series of samples were similar to those for ARGET ATRP series prepared using initiator-modified layered silica 1-CDMSPBM. No major change of T_g with the polymer loading (Figure 4.10, Table 4.4) was observed. The glass transition temperatures were about 123-127 ℃ for this series of samples, and they were very close to those for 1-P8 to 1-P16 series of samples (122-129 ℃), which meant the PMMA/silica nanocomposites prepared via ARGET ATRP exhibited similar glass transition behavior even though two different layered silica sources were used. TEM images of sample 2-P5 are shown in Figure 4.11. Some details on the first image suggest the overlap of several layers, whereas the second image shows morphologies similar to those seen in the layered silica **2** and initiator-modified layered silica 2- CDMDPBMP, which can be interpreted as layers parallel to the electron beam.

Table 4.4. Glass Transition Temperatures of PMMA/Silica Nanocomposites 2-P5 to 2-P9.

	2-P5	**2-P6**	**2-P7**	**2-P8**	**2-P9**
Tg/°C	**123.0**	**125.7**	**126.9**	**126.0**	**126.0**

Figure 4.10. Differential Scanning Calorimetry Traces of PMMA/Silica Nanocomposites 2-P5 to 2-P9.

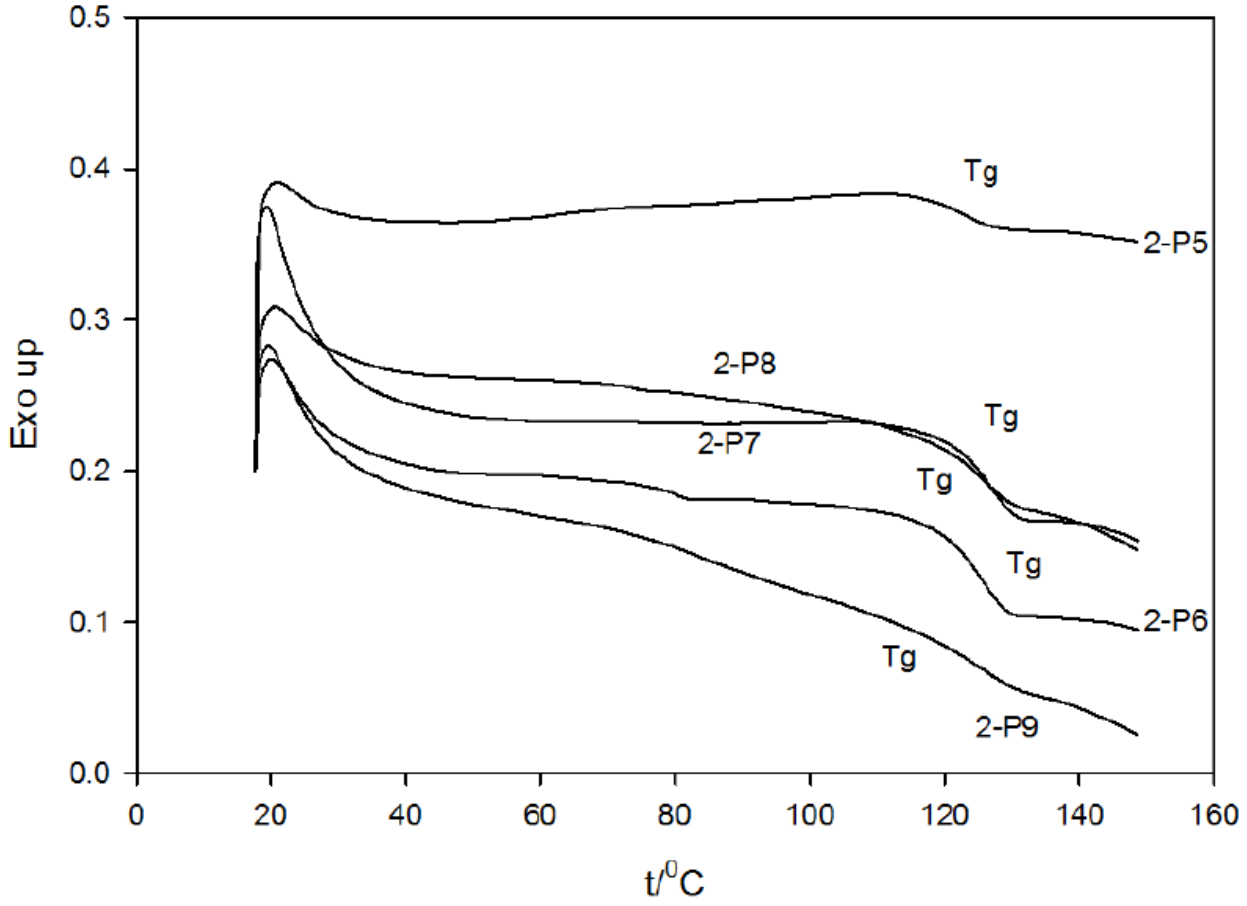

Figure 4.11. TEM Images of PMMA/Silica Nanocomposite 2-P5.

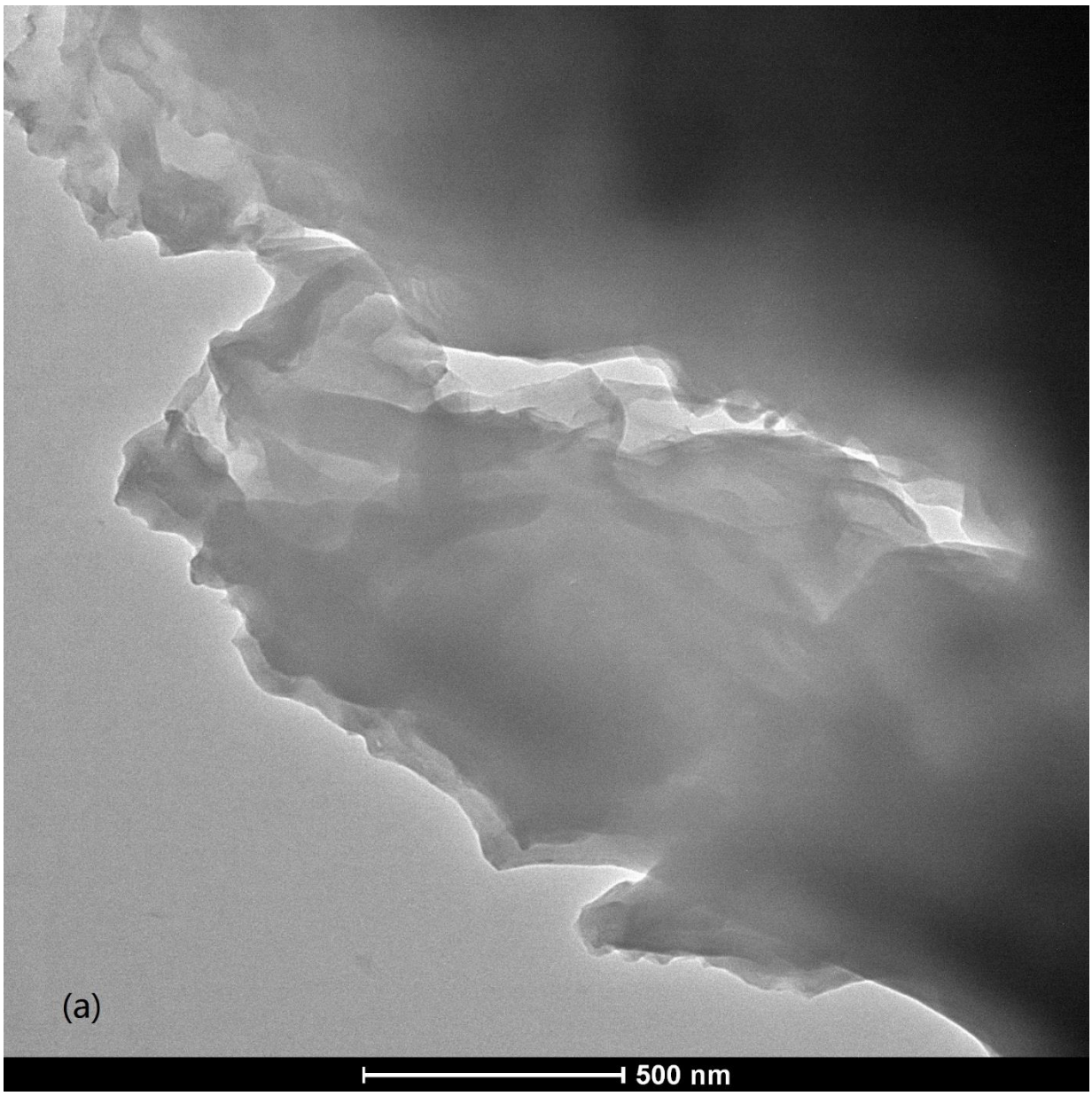

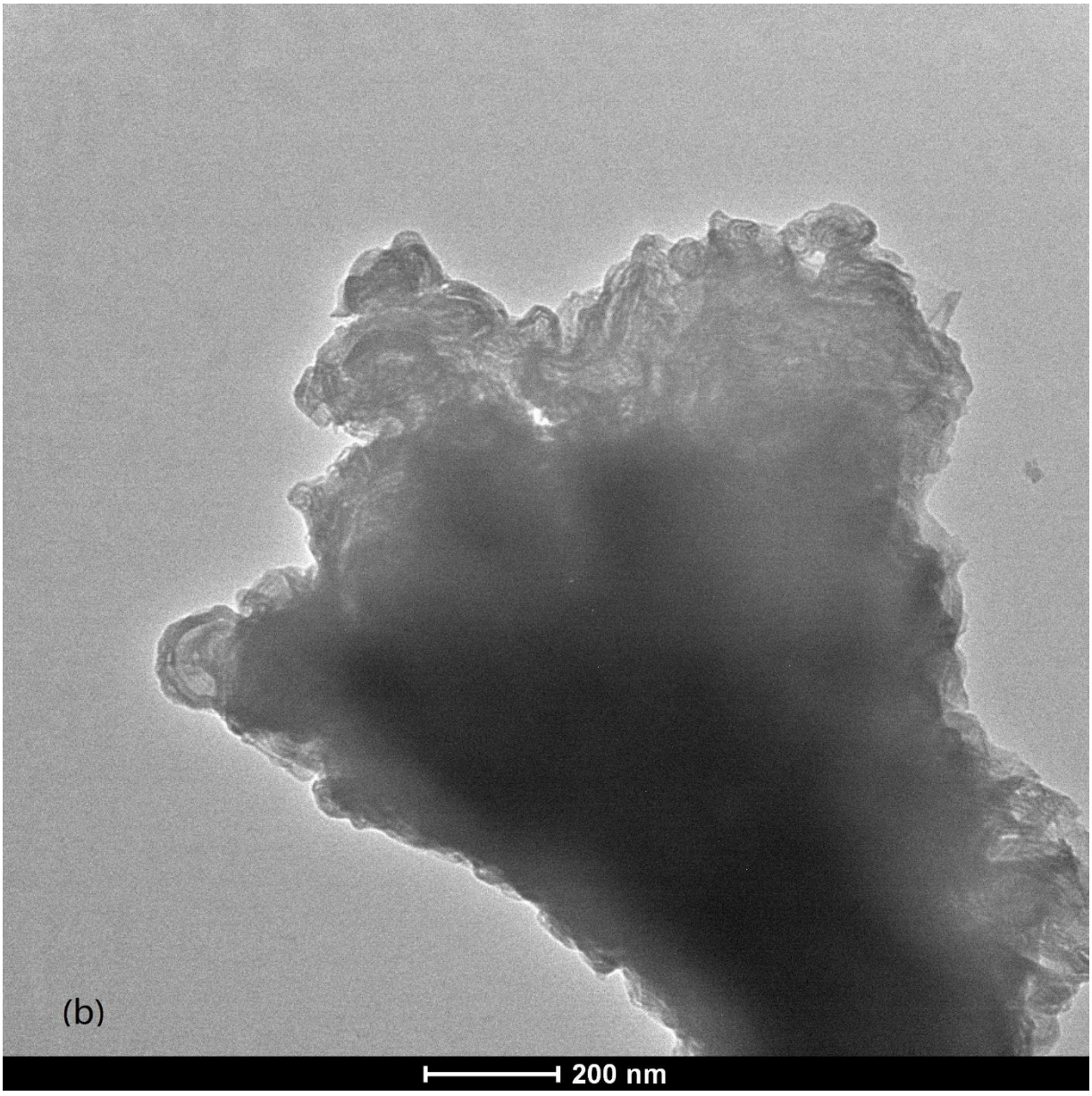
(b)
200 nm

4.3. Styrene Polymerization by ARGET ATRP

The series of styrene (St) polymerizations by ARGET ATRP initiated by initiator-modified layered silica 1-CDMDPBMP is presented in Table 4.5. The ordered architecture was apparently still maintained after 3 hours polymerization with d_{001} =~ 6 nm for 1-P19, but the SAXS showed a weak shoulder (Figure 4.12), which meant the structure was weakly ordered. For higher polystyrene loading (up to residue=1.63%), the ordered architecture was no longer evident from SAXS patterns. Figure 4.13 shows the weight changes upon the thermal degradation of the nanocomposites under N_2. The polymer/silica mass ratio vs. reaction time (Figure 4.14) indicated that the "induction" period was ~2.5 hours in which oxygen dissolved in the reaction mixture was depleted.

Table 4.5. ARGET ATRP of Styrene Initiated from Initiator-Modified Layered Silica 1-CDMSPBMP.

	1-CDMDPBMP	$CuCl_2$	PMDETA	St	Sn(II)	time/ hrs	residue% (SiO_2)	polymer/ silica	d_{001} (nm)	2θ (degree)
1-P19	**1**	**0.02**	**1.2**	**270**	**9**	**3**	**24.75%**	**2.52**	**~6**	**~1.4**
1-P20	**1**	**0.02**	**1.2**	**270**	**9**	**5**	**8.02%**	**10.9**	**n/a**	**n/a**
1-P21	**1**	**0.02**	**1.2**	**270**	**9**	**7**	**6.12%**	**14.8**	**n/a**	**n/a**
1-P22	**1**	**0.02**	**1.2**	**270**	**9**	**19**	**2.21%**	**43.7**	**n/a**	**n/a**
1-P23	**1**	**0.02**	**1.2**	**270**	**9**	**24**	**1.63%**	**59.8**	**n/a**	**n/a**

Figure 4.12. Small-Angle X-ray Scattering Pattern of PS/Silica Nanocomposite 1-P19.

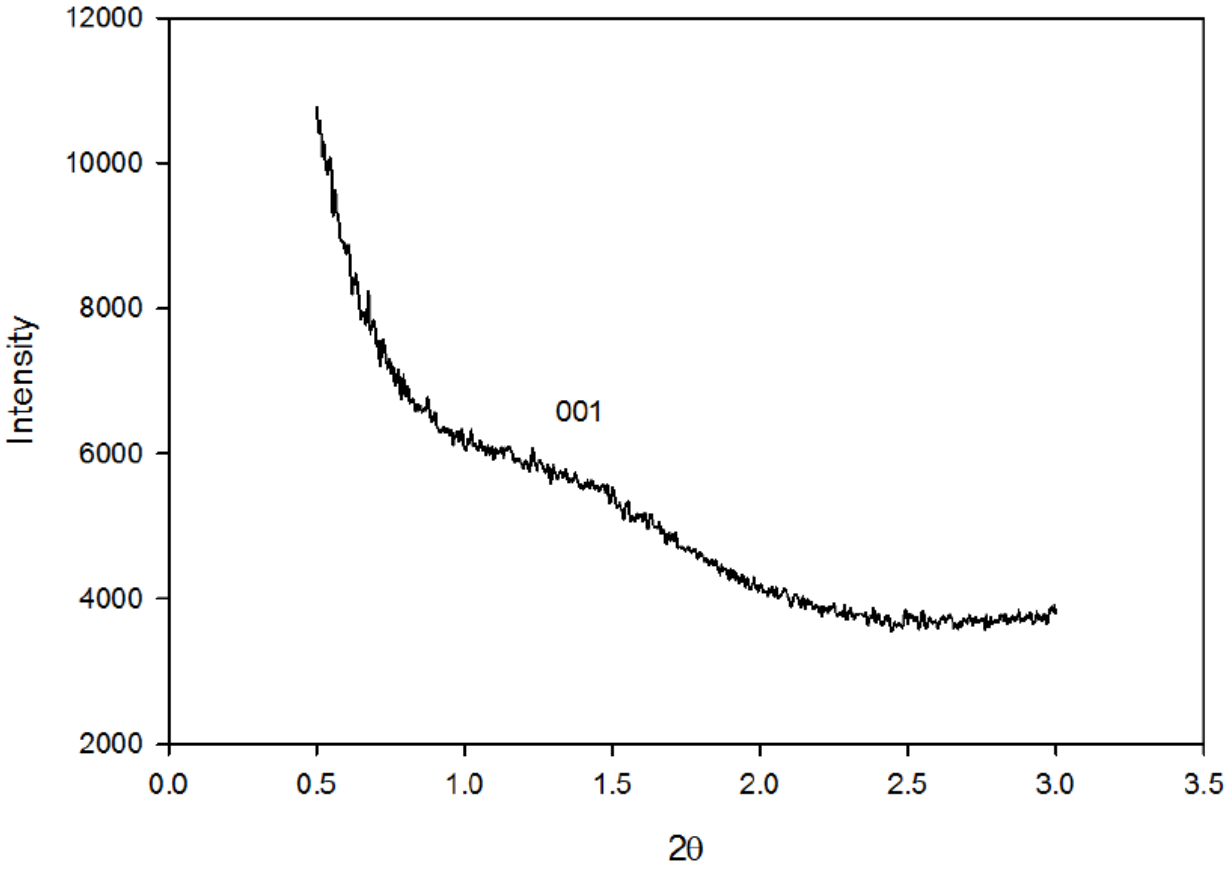

Figure 4.13. Thermogravimetric Weight Change Curves of PS/Silica Nanocomposites 1-P19 to 1-P23.

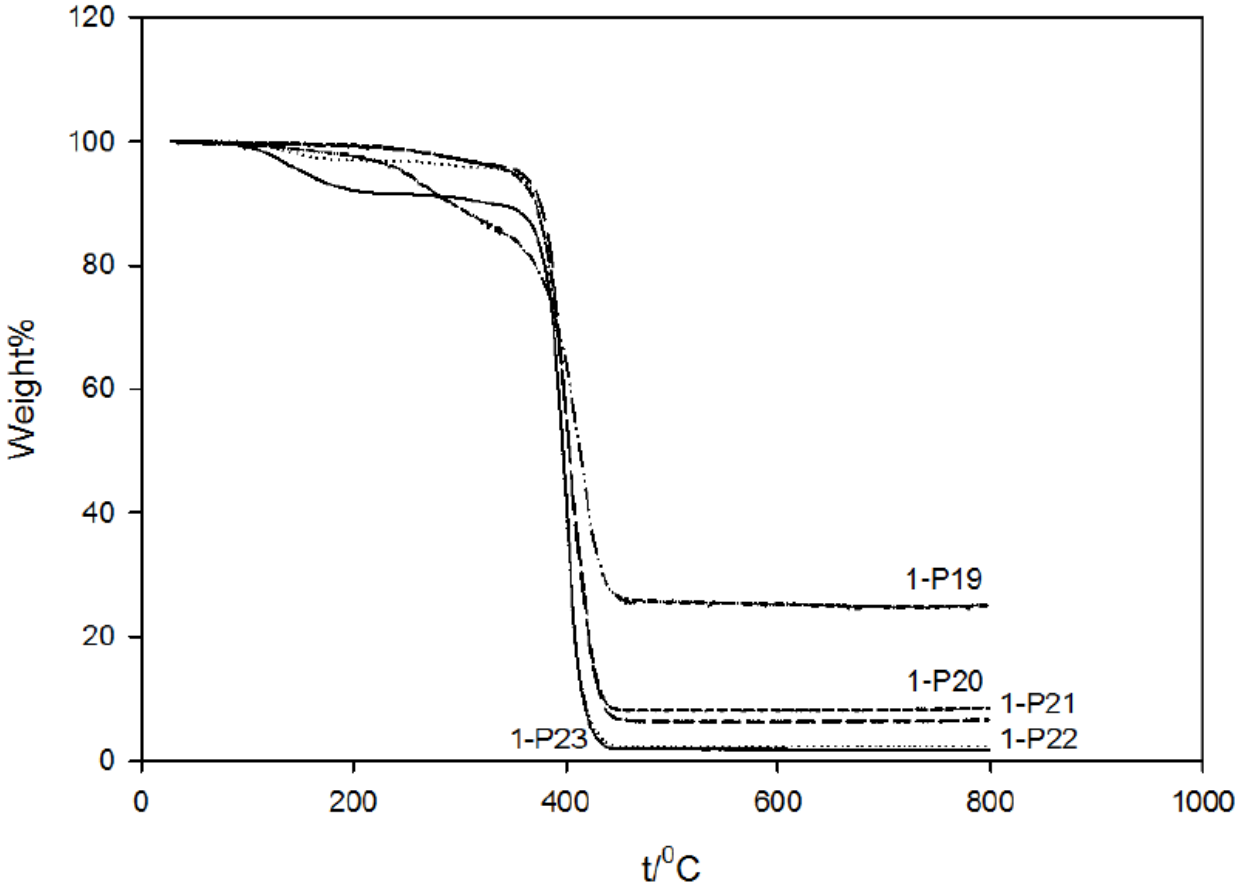

Figure 4.14. Polymer/Silica Mass Ratio vs. Polymerization Time of PS/Silica Nanocomposites 1-P19 to 1-P23.

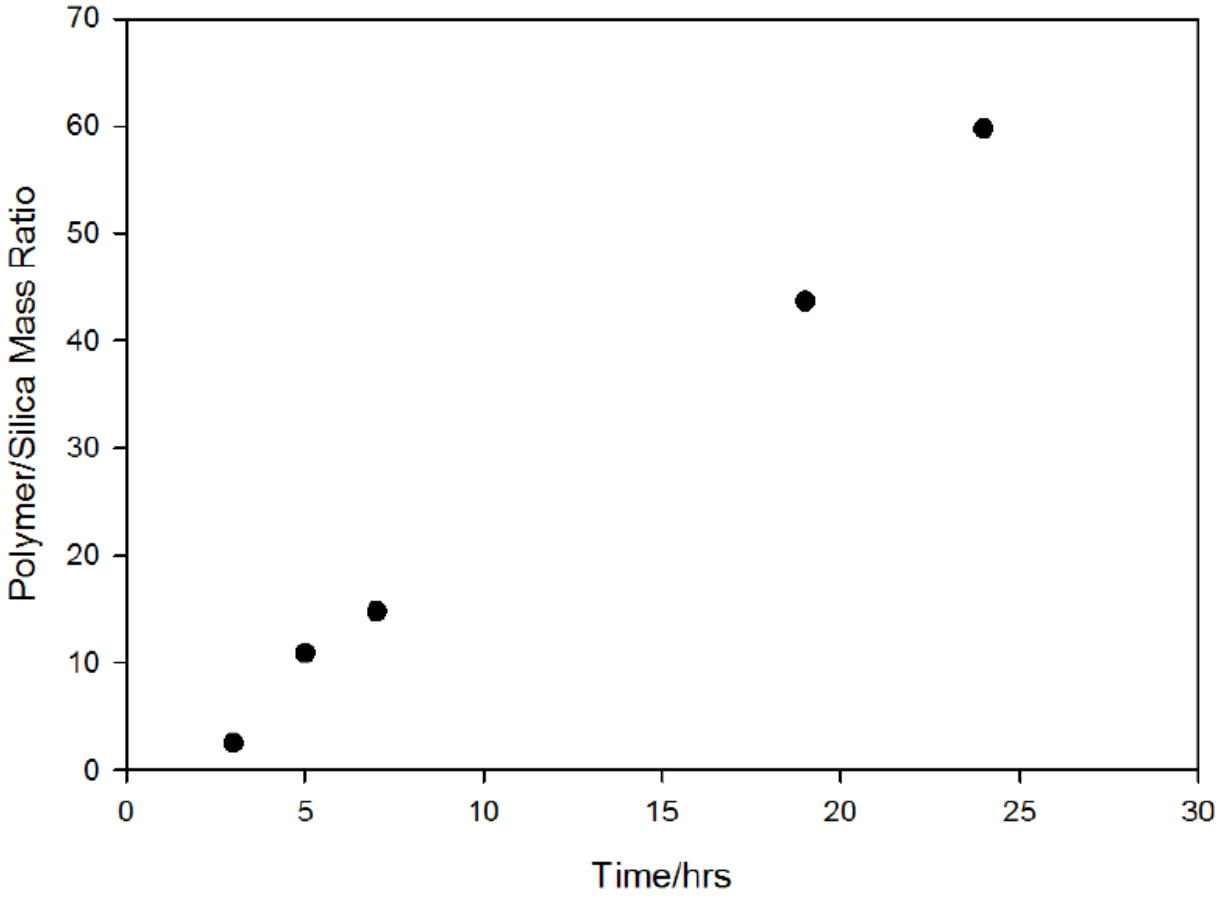

Glass transition temperatures for polystyrene-based nanocomposites synthesized via ARGET ATRP were from 100 to 106 °C (Table 4.6., Figure 4.15), T_g was several degrees higher for samples with higher polymer loading when comparing with the lowest loading sample 1-P19. The PS/silica nanocomposites 1-P20 to 1-P23 exhibited about 5-6 ℃ higher T_g than that of bulk polystyrene (100 ℃ [150]). The morphologies of 1-P19 and 1-P23 were seen in TEM images in Figures 4.16 and 4.17. The stacki of several layers were observed at the edges.

Table 4.6. Glass Transition Temperatures of PS/Silica Nanocomposites 1-P19 to 1-P23.

	1-P19	**1-P20**	**1-P21**	**1-P22**	**1-P23**
Tg/°C	**100**	**105**	**106**	**106**	**106**

Figure 4.15. Differential Scanning Calorimetry Traces of PS/Silica Nanocomposites 1-P19 to 1-P23.

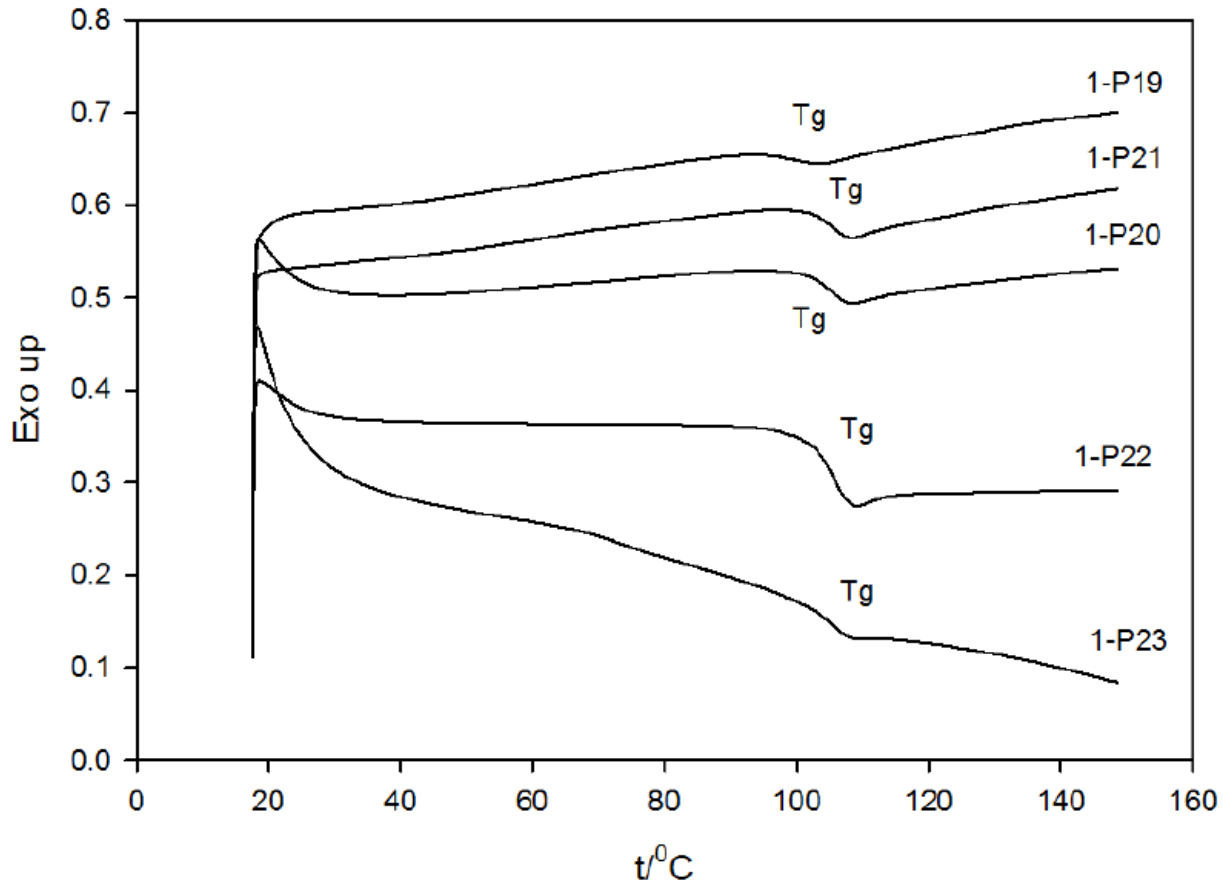

Figure 4.16. TEM Image of PS/Silica Nanocomposite 1-P19.

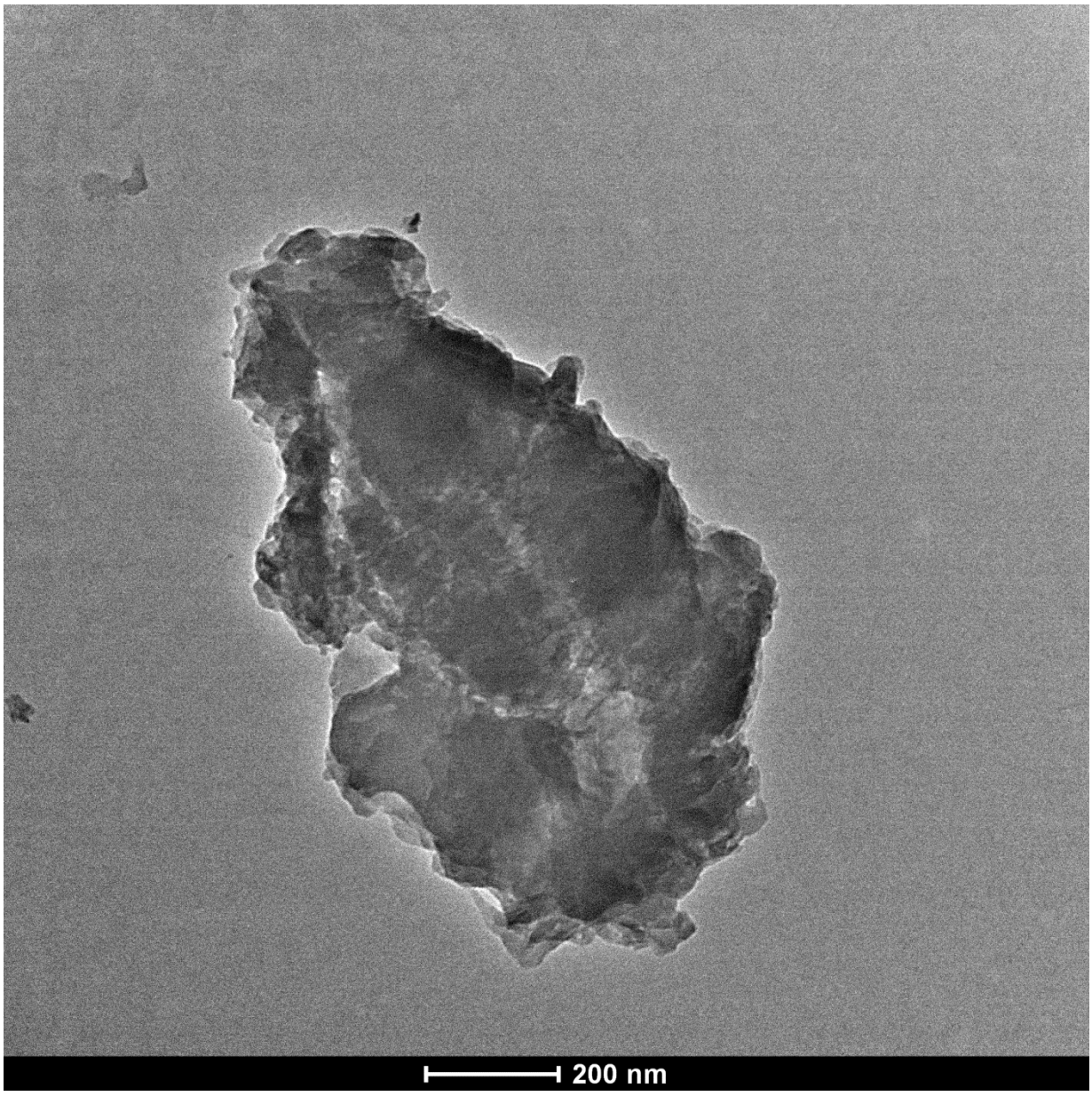

Figure 4.17. TEM Image of PS/Silica Nanocomposite 1-P23.

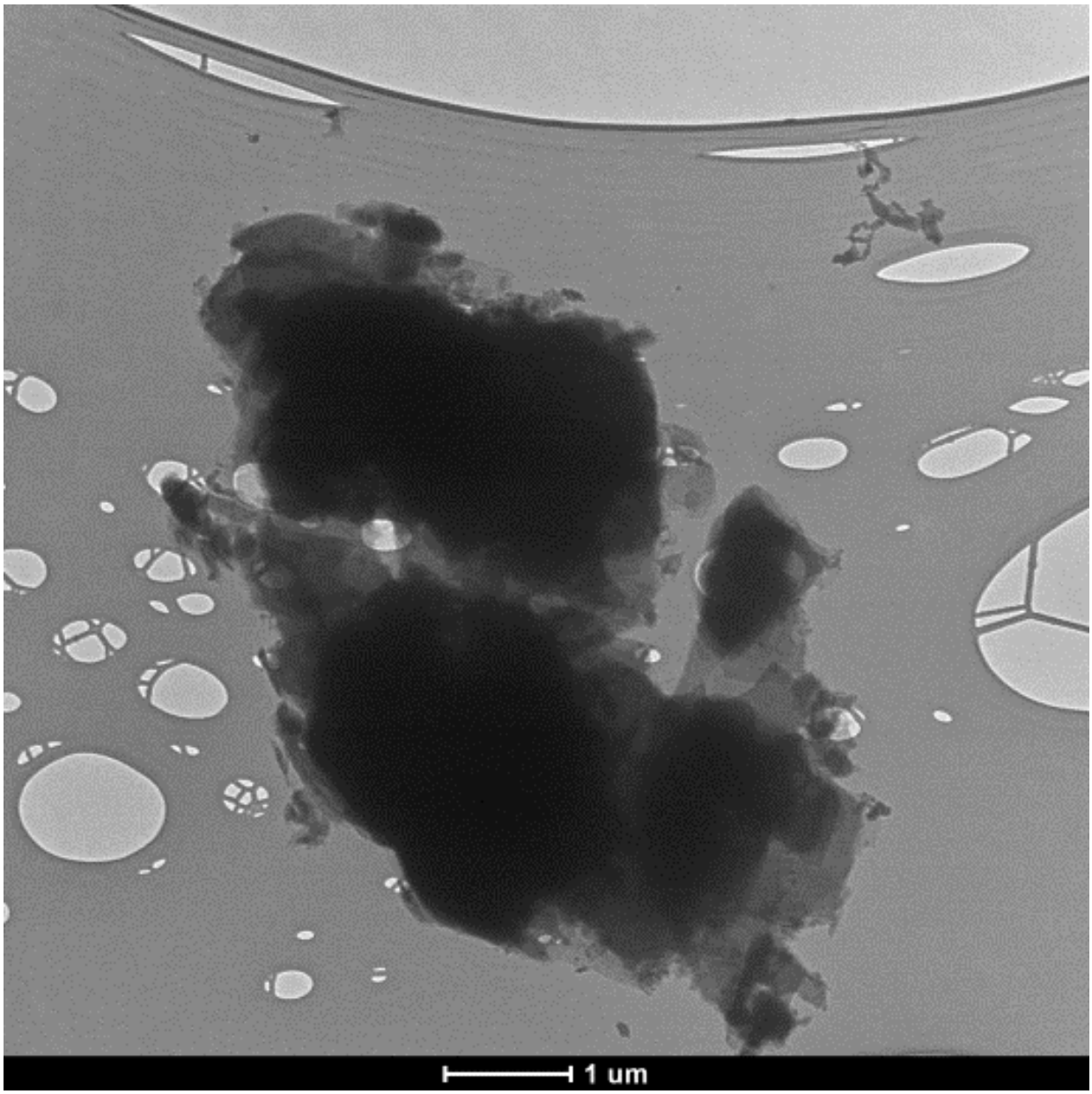

The results of styrene polymerizations by ARGET ATRP based on initiator-modified layered silica 2-CDMDPBMP are shown in Table 4.7. The SAXS pattern for the resulting materials did not have any features, indicating that these are exfoliated nanocomposites. The weight change curves are shown in Figures 4.18. If we compare the polymer loadings for the considered series of samples and for the previously discussed series synthesized samples using initiator-functionalized silica layers 1-CDMSPBMP, one can see that in the present case, the loading of polymer increased with time about two times slower. However, in both cases, the loading systematically increased with time and was high after about one day of polymerization. DSC patterns are shown in Figure 4.19, the glass transition temperatures were in range 104-106^{0}C (Table 4.8). Considering T_g for 1-P20 to 1-P23 samples prepared using the other initiator-functionalized silica layers (1-CDMSPBMP), the results indicate that the glass transition temperatures for polystyrene-based exfoliated nanocomposites prepared by surface initiatied ARGET ATRP are essentially constant if the polymer loading is high enough (for silica residues from 17.85% (2-P10) to 1.63% (1-P23)). The morphology of 2-P10 sample is shown in TEM images (Figure 4.20). Several layers seemed to overlap at the particle edges.

Table 4.7. ARGET ATRP of Styrene Initiated from Initiator-Modified Layered Silica 2-CDMSPBMP.

	2-CDMDPBMP	$CuCl_2$	PMDETA	St	Sn(II)	time/hrs	residue% (SiO_2)	polymer/ Silica	d_{001} (nm)	2θ (degree)
2-P10	**1**	**0.02**	**1.2**	**270**	**9**	**6**	**17.85%**	**2.7**	**n/a**	**n/a**
2-P11	**1**	**0.02**	**1.2**	**270**	**9**	**17**	**5.02%**	**17.1**	**n/a**	**n/a**
2-P12	**1**	**0.02**	**1.2**	**270**	**9**	**18.5**	**3.83%**	**23.2**	**n/a**	**n/a**
2-P13	**1**	**0.02**	**1.2**	**270**	**9**	**20**	**3.55%**	**25.3**	**n/a**	**n/a**

Table 4.8. Glass Transition Temperatures of PS/Silica Nanocomposites 2-P10 to 2-P13.

	2-P10	2-P11	2-P12	2-P13
Tg/°C	104	106	106	106

Figure 4.18. Thermogravimetric Weight Change Curves of PS/Silica Nanocomposites 2-P10 to 2-P13.

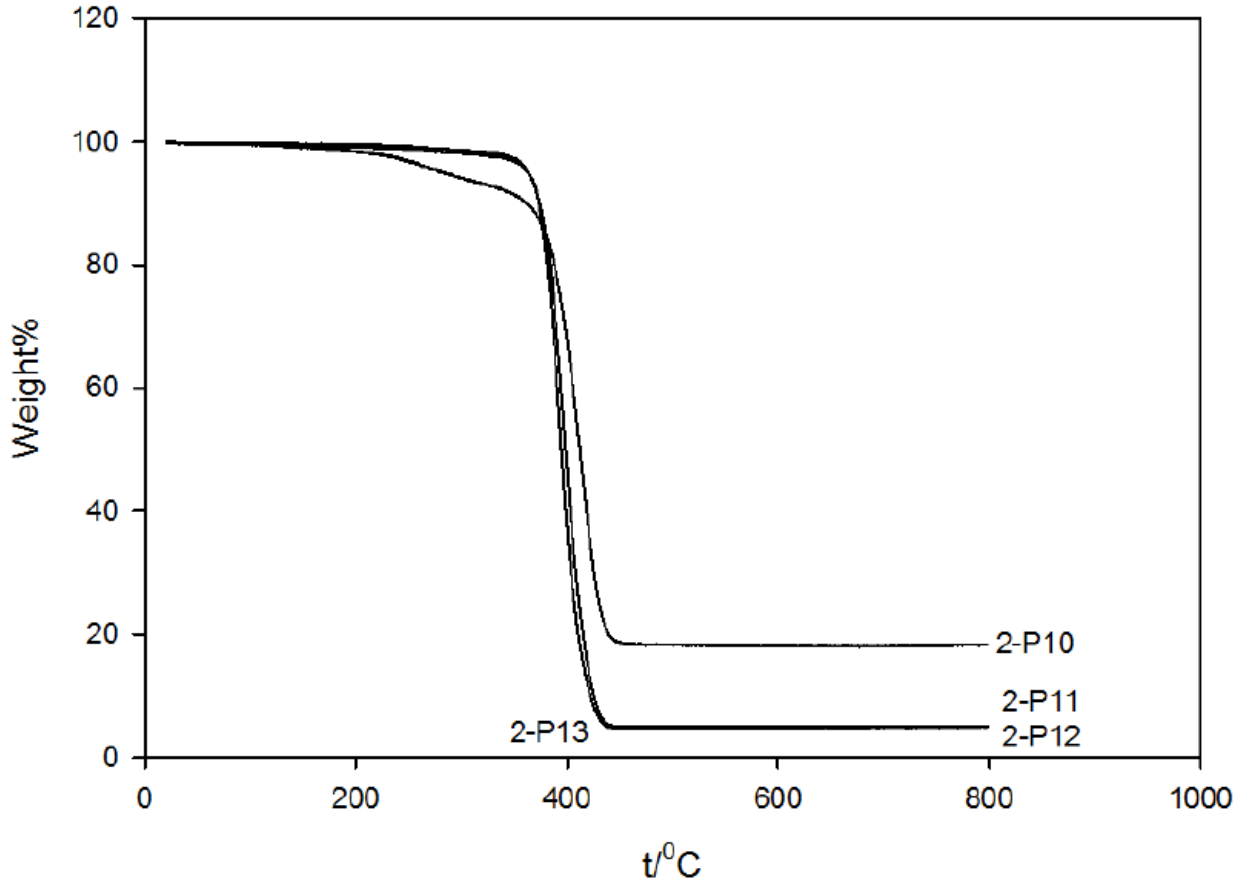

Figure 4.19. Differential Scanning Calorimetry Traces of PS/Silica Nanocomposites 2-P10 to 2-P13.

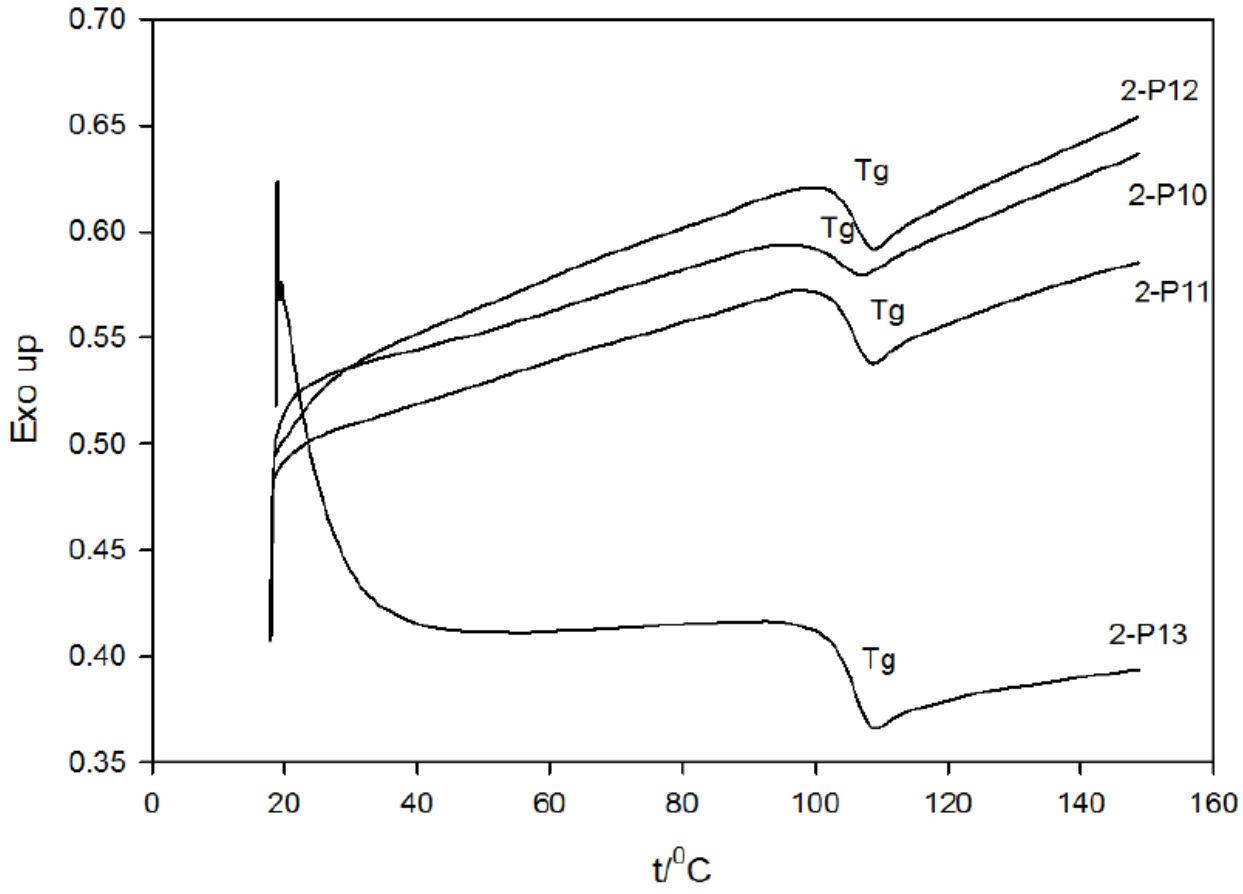

Figure 4.20. TEM Images of PS/Silica Nanocomposite 2-P10.

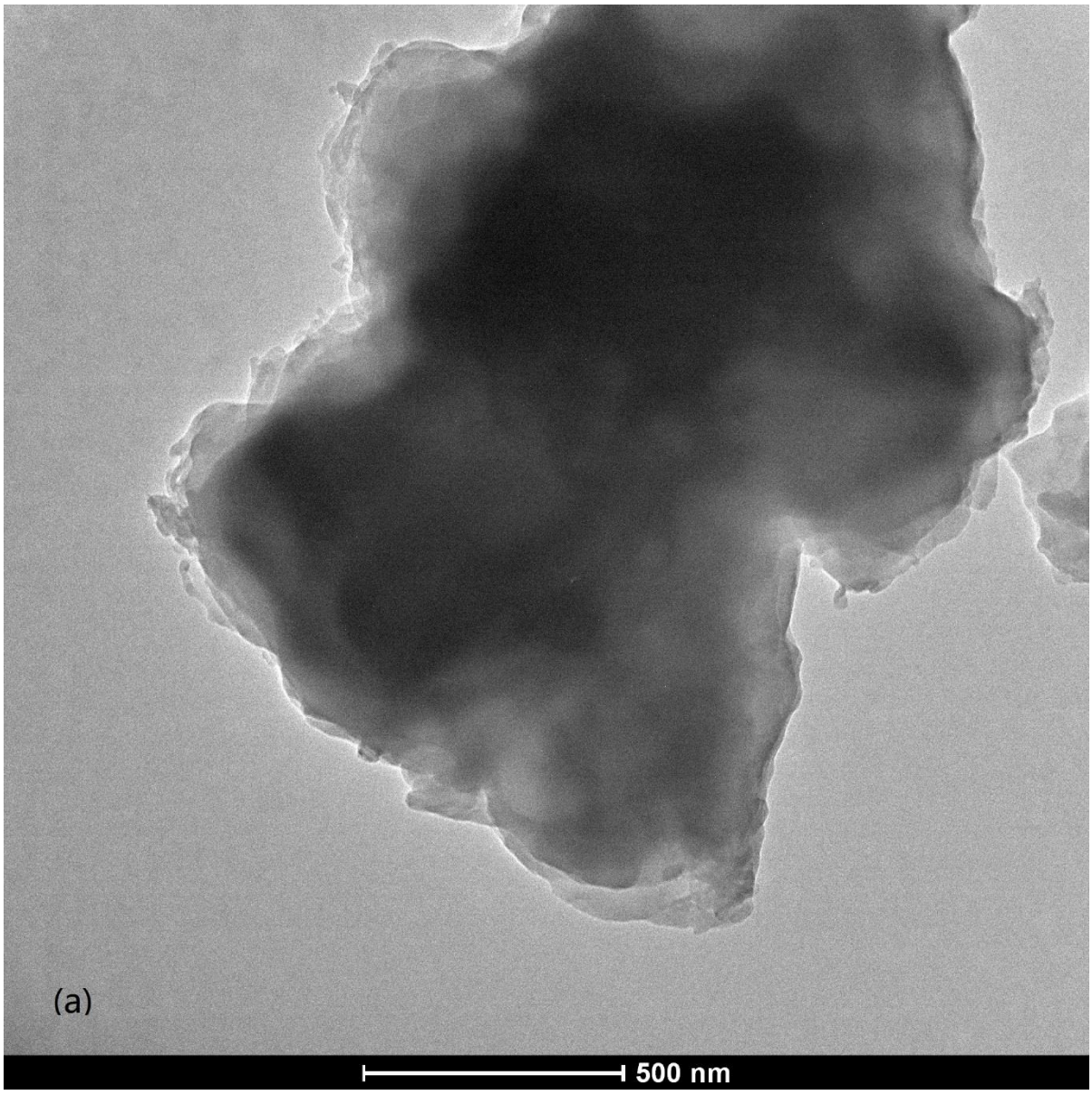

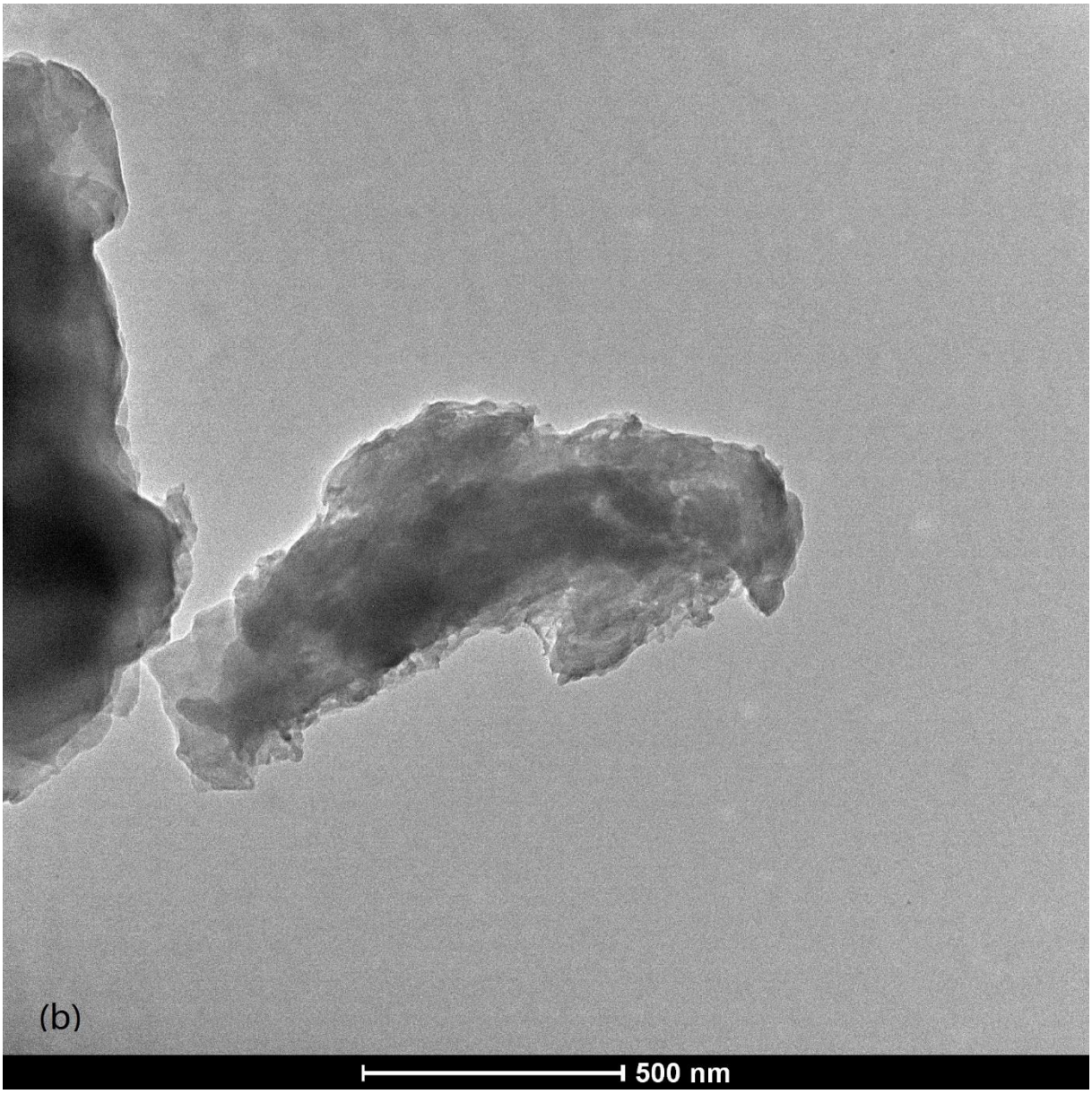
(b)
500 nm

4.4. Acrylonitrile Polymerization by ARGET ATRP

The polymerization conditions and characterization data for the series of acrylonitrile (AN) polymerizations by ARGET ATRP initiated by initiator-modified layered silica 1-CDMDPBMP are presented in Table 4.9. The ordered structure was lost even after 6 hours of polymerization, with no peaks or shoulders observed in the SAXS pattern. The ordering was lost with such a low loading for 1-P24 sample that the grafting of polymer chains had to be very nonuniform in the early stages of polymerization. Perhaps the process led to some cross-linking between the layers of an early stage, which made it impossible to stack the silica layers even for a low polymer loading. Alternatively, the spatial distribution of grafted polymer chains might have been highly nonuniform and the PAN tendency to crystallize might have created local "bumps" of polymer, which made it impossible for the layers to pack. Figure 4.21 shows the degradation curves under air for the products. The glass transition temperatures were about 97-98 °C for 1-P26 and 1-P27 samples (Table 4.10), and 1-P24 sample did not have a thermal event in DSC pattern that could be related to the glass transition, which was possibly due to too low polymer loading in the sample (Figure 4.22). Due to the very limited amount for isolated 1-P25 sample, DSC trace was not acquired for this sample. The morphology of PAN/silica nanocomposite 1-P27 is illustrated in Figure 4.23. Some fragments of layers were apparently seen for this sample on its TEM image.

Table 4.9. ARGET ATRP of Acrylonitrile Initiated from Initiator-Modified Layered Silica 1-CDMSPBMP.

	1-CDMDPBMP	$CuCl_2$	TPMA	AN	Sn(II)	time/hrs	residue% (SiO_2)	polymer/ silica	d_{001} (nm)	2θ
1-P24	**1**	**0.02**	**1.2**	**270**	**9**	**6**	**60.14%**	**0.14**	**n/a**	**n/a**
1-P25	**1**	**0.02**	**1.2**	**270**	**9**	**16.5**	**36.35%**	**1.23**	**n/a**	**n/a**
1-P26	**1**	**0.02**	**1.2**	**270**	**9**	**20**	**23.79%**	**2.65**	**n/a**	**n/a**
1-P27	**1**	**0.02**	**1.2**	**270**	**9**	**24.5**	**19.85%**	**3.52**	**n/a**	**n/a**

Table 4.10. Glass Transition Temperatures of PAN/Silica Nanocomposites 1-P24 to 1-P27.

	1-P24	1-P25	1-P26	1-P27
Tg/°C	none	n/a	98	97

Figure 4.21. Thermogravimetric Weight Change Curves of PAN/Silica Nanocomposites 1-P24 to 1-P27 under Air.

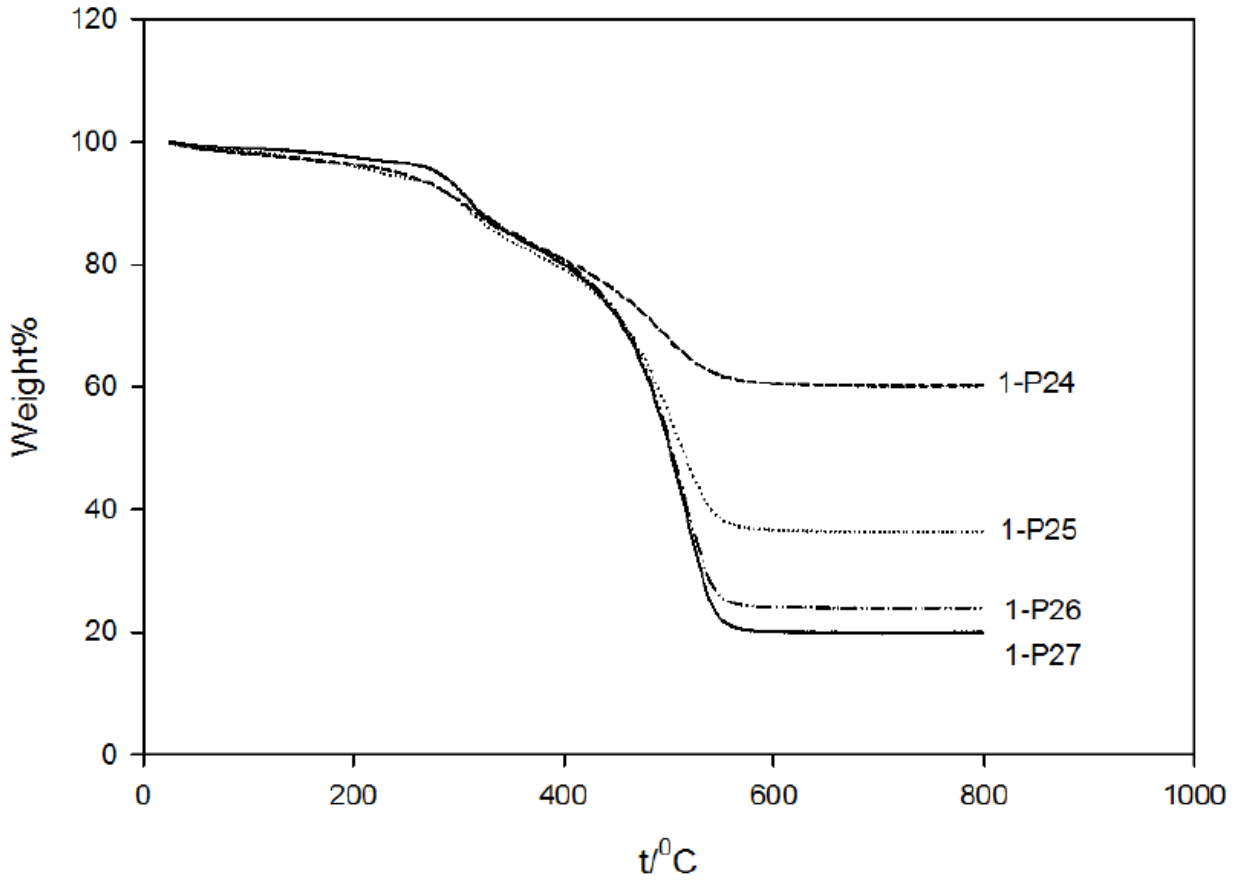

Figure 4.22. Differential Scanning Calorimetry Traces of PAN/Silica Nanocomposites 1-P24, 1-P26 and 1-P27.

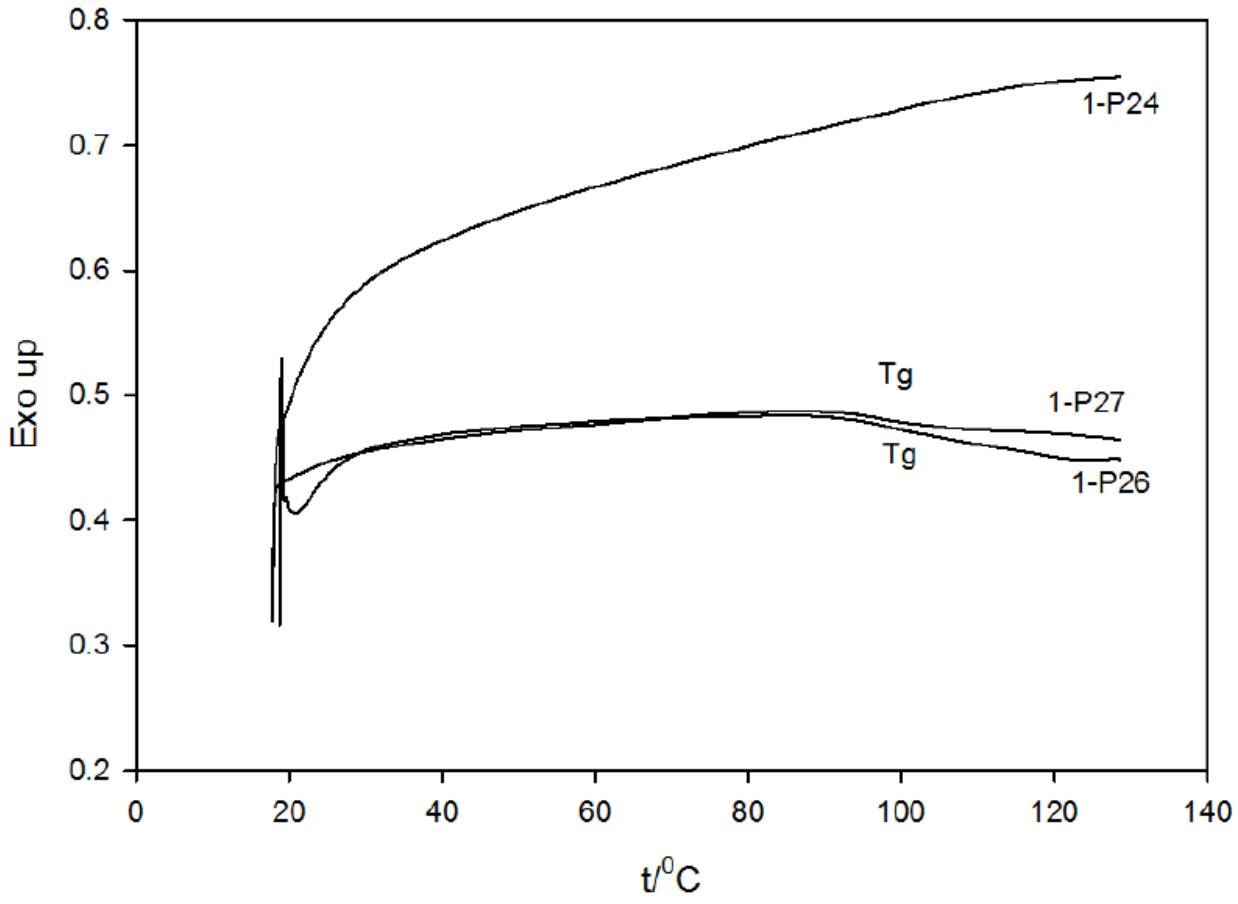

Figure 4.23. TEM Image of PAN/Silica Nanocomposite 1-P27.

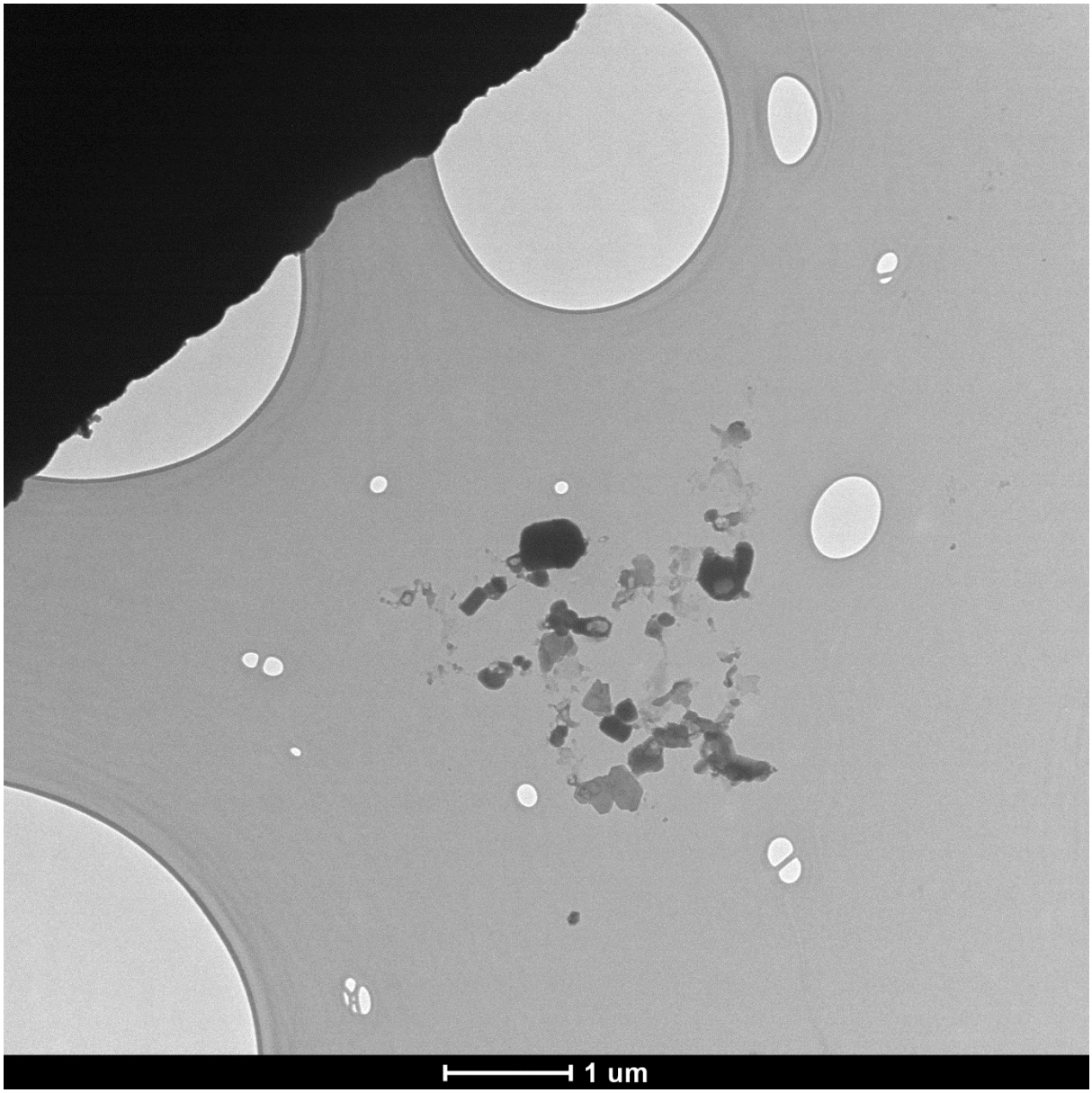

The conditions and results of AN polymerizations by ARGET ATRP based on initiator-modified layered silica 2-CDMDPBMP are shown in Table 4.11. SAXS patterns did not have any peaks or shoulders for this series of products. The weight change curves are shown in Figures 4.24. The DSC patterns are shown in Figure 4.25, and the thermal events related to the glass transition are listed in Table 4.12. The transition at 97 °C in DSC pattern was clearly observed only for 2-P17 sample. Although the DSC pattern of 2-P16 seemed to have a transition feature around the same temperature, but it was not well visible. The determination of the glass transition temperature of PAN is complicated and its estimated value depends on the instrumentation used and crystallinity of the samples. T_g of PAN was reported to be 82 and 140 ℃ for paracrystalline and amorphous region for PAN fibres. [150] The commercial available PAN powder from Sigma Aldrich has a T_g of 85 ℃ for 150,000 molecular weight. When comparing with the PAN/silica nanocomposite samples prepared using initiator-modified layered silica 1-CDMSPBMP and 2-CDMSPBMP, they showed very similar properties, which meant the synthetic procedures worked well with different layered silica precursors.

Table 4.11. ARGET ATRP of Acrylonitrile Initiated from Initiator-Modified Layered Silica 2-CDMSPBMP.

	2-CDMDPBMP	$CuCl_2$	TPMA	AN	Sn(II)	time/hrs	residue% (SiO_2)	polymer/ silica	d_{001} (nm)	2θ
2-P14	**1**	**0.02**	**1.2**	**270**	**9**	**6**	**45.86%**	**0.69**	**n/a**	**n/a**
2-P15	**1**	**0.02**	**1.2**	**270**	**9**	**19**	**26.27%**	**2.32**	**n/a**	**n/a**
2-P16	**1**	**0.02**	**1.2**	**270**	**9**	**23**	**21.63%**	**3.13**	**n/a**	**n/a**
2-P17	**1**	**0.02**	**1.2**	**270**	**9**	**44**	**17.33%**	**4.28**	**n/a**	**n/a**

Table 4.12. Glass Transition Temperatures of PAN/Silica Nanocomposites 2-P14 to 2-P17.

	2-P14	2-P15	2-P16	2-P17
Tg/°C	n/a	none	none	97

Figure 4.24. Thermogravimetric Weight Change Curves under Air of PAN/Silica Nanocomposites 2-P14 to 2-P17.

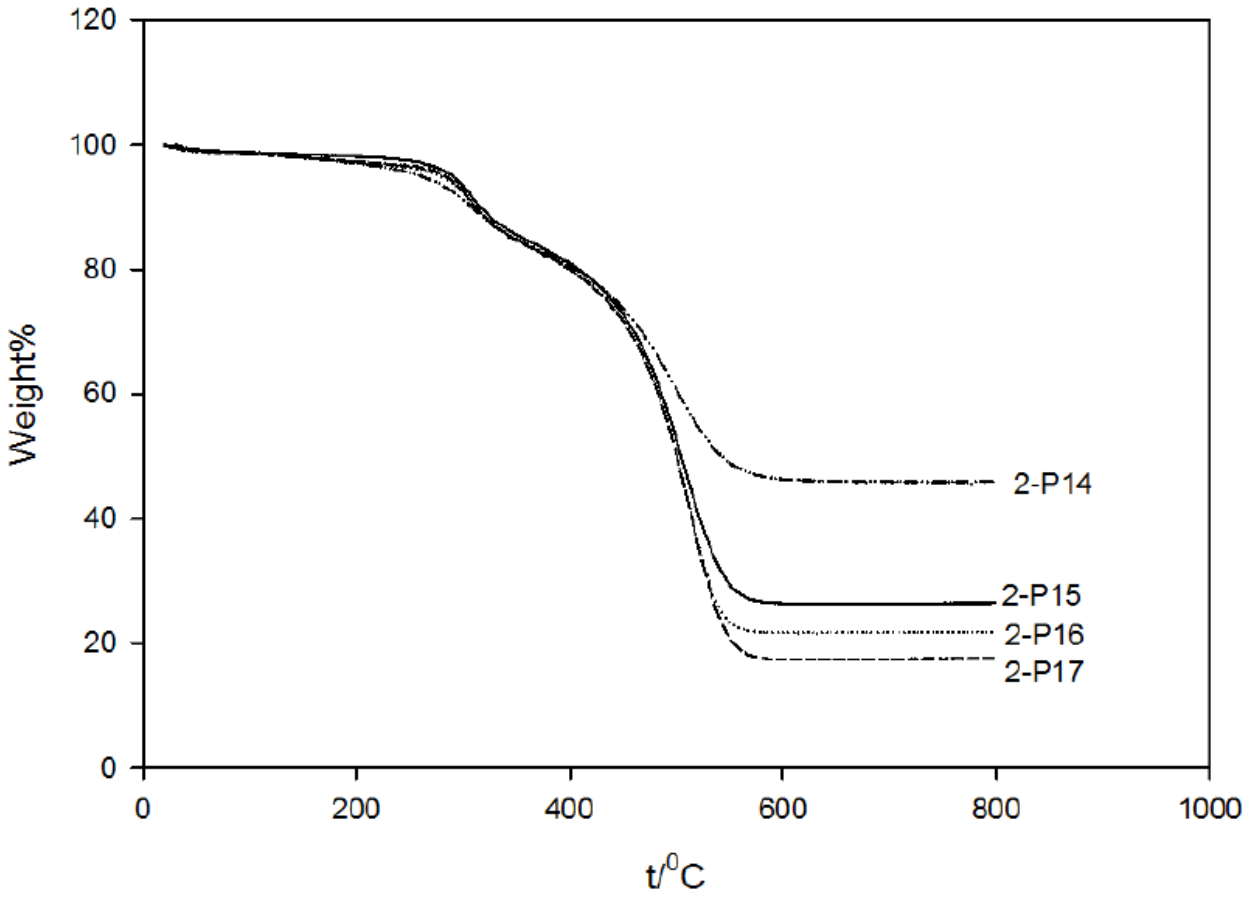

Figure 4.25. Differential Scanning Calorimetry Traces of PAN/Silica Nanocomposites 2-P15 to 2-P17.

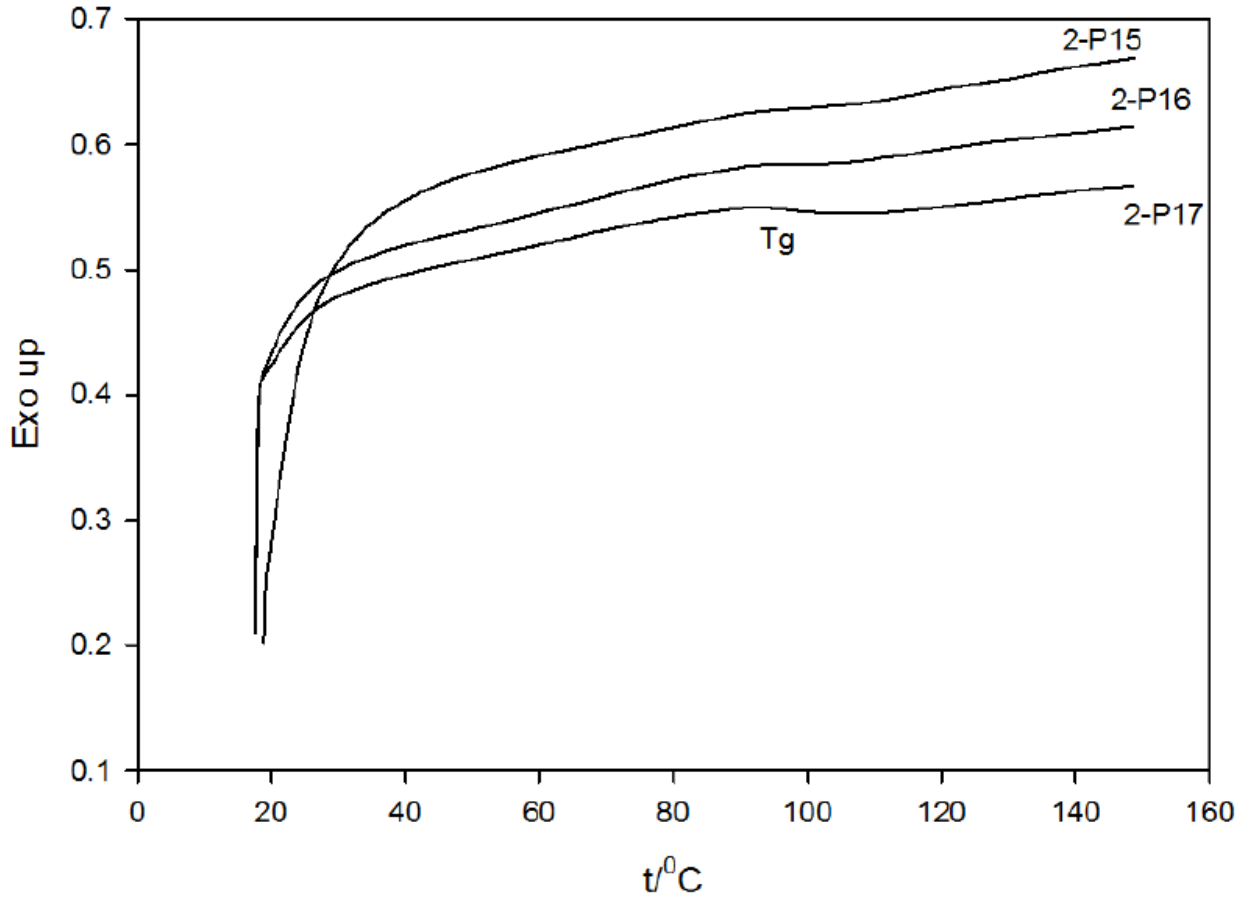

4.5. Block Copolymerization by ARGET ATRP

Copolymers (or mixed brushes) grafted on silica layers were also prepared. Table 4.13 shows the types of (co)polymer products and the silica/polymer 1/polymer 2 mass ratio (polymer 1 refers to the polymer grafted first (PMMA or PAN); polymer 2 refers to the second grafted polymer, which was polystyrene) based on TGA results. The glass transition temperatures were around 105-106 ℃ as seen from DSC patterns and these can be attributed to the polystyrene component. The corresponding molar ratios of the reagents are shown in Table 4.14. Figures 4.26, 4.27 and 4.28 show the weight change patterns of the copolymer/silica nanocomposites compared with the starting homopolymer/silica nanocomposites. The residue percentages for 1-P10, 1-P16 and 1-P26 samples were 22.98%, 6.79% and 23.79% under air. Based on the weight loss increases (and silica residue decreases), the second block (polystyrene), was most likely introduced. In principle, the polymerization may be initiated from: (i) the halogen-containing chain end of the homopolymer initially grafted on the surface, giving rise to a block copolymer, or (ii) the unreacted initiator on the surface. The second possibility arises, because the surface-initiated polymerization usually has a moderate efficiency, which is lower than 100%, [143] and thus some unreacted initiator is expected to remain on the surface after the grafting of the first polymer. However, it is not clear whether these initiating sites are accessible in the second polymerization process if the layer of the first polymer is sufficiently thick. Therefore, one can expect the formation of block copolymers or block copolymers mixed with surface-initiated homopolymer. This primarily pertains to the use of PMMA/silica nanocomposites as initiators. However, in the case of PAN/silica nanocomposites, the evidence of nonuniform distribution of PAN was discussed earlier, and thus the chances for initiation of styrene polymerization from residual initiator on the silica surface are higher.

Table 4.13. Characterizations of Copolymer (or Mixed Brush)/Silica Nanocomposites 1-CP1 to 1-CP3.

	Initiator	2nd Monomer	residue%	Silica	Polymer 1	Polymer 2	Tg/°C
1-CP1	1-P10(MMA)	St	1.42%	1	2.8	65	105
1-CP2	1-P16(MMA)	St	2.41%	1	13	27	106
1-CP3	1-P26(AN)	St	7.64%	1	2.6	8.7	105

Table 4.14. Conditions of ARGET ATRP Used for Copolymer (or Mixed Brush)/Silica Nanocomposites 1-CP1 to 1-CP3.

	Initiator	$CuCl_2$	PMDETA	St	Sn(II)	time/hours
1-CP1	1	0.2	14	6000	50	23
1-CP2	1	0.8	55	22000	200	24
1-CP3	1	0.2	16	6300	56	24

Figure 4.26. Thermogravimetric Weight Change Curve of Copolymer (or Mixed Brush)/Silica Nanocomposite 1-CP1 in Comparison to the Curve for the Starting PMMA/Silica Nanocomposite 1-P10.

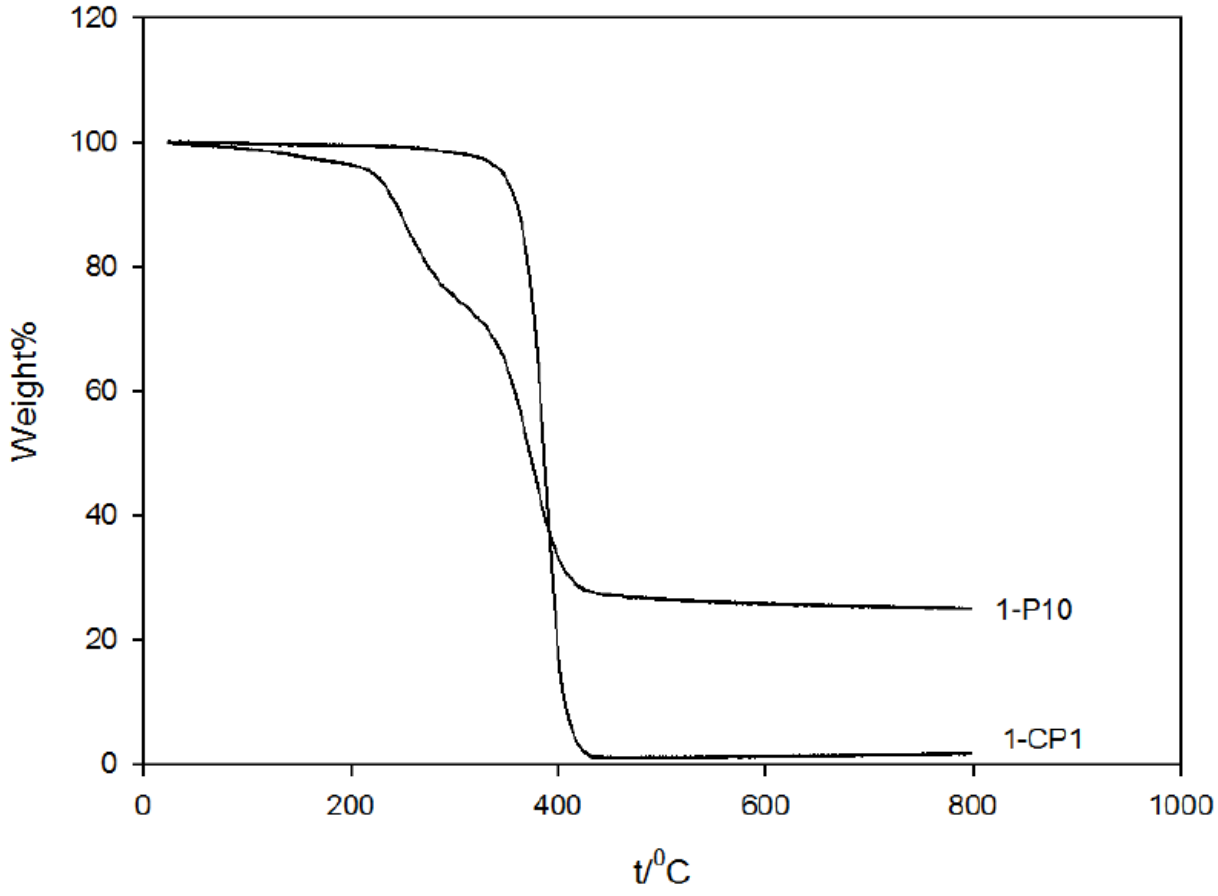

Figure 4.27. Thermogravimetric Weight Change Curve of Copolymer (or Mixed Brush)/Silica Nanocomposite 1-CP2 in Comparison to the Curve for the Starting PMMA/Silica Nanocomposite 1-P16.

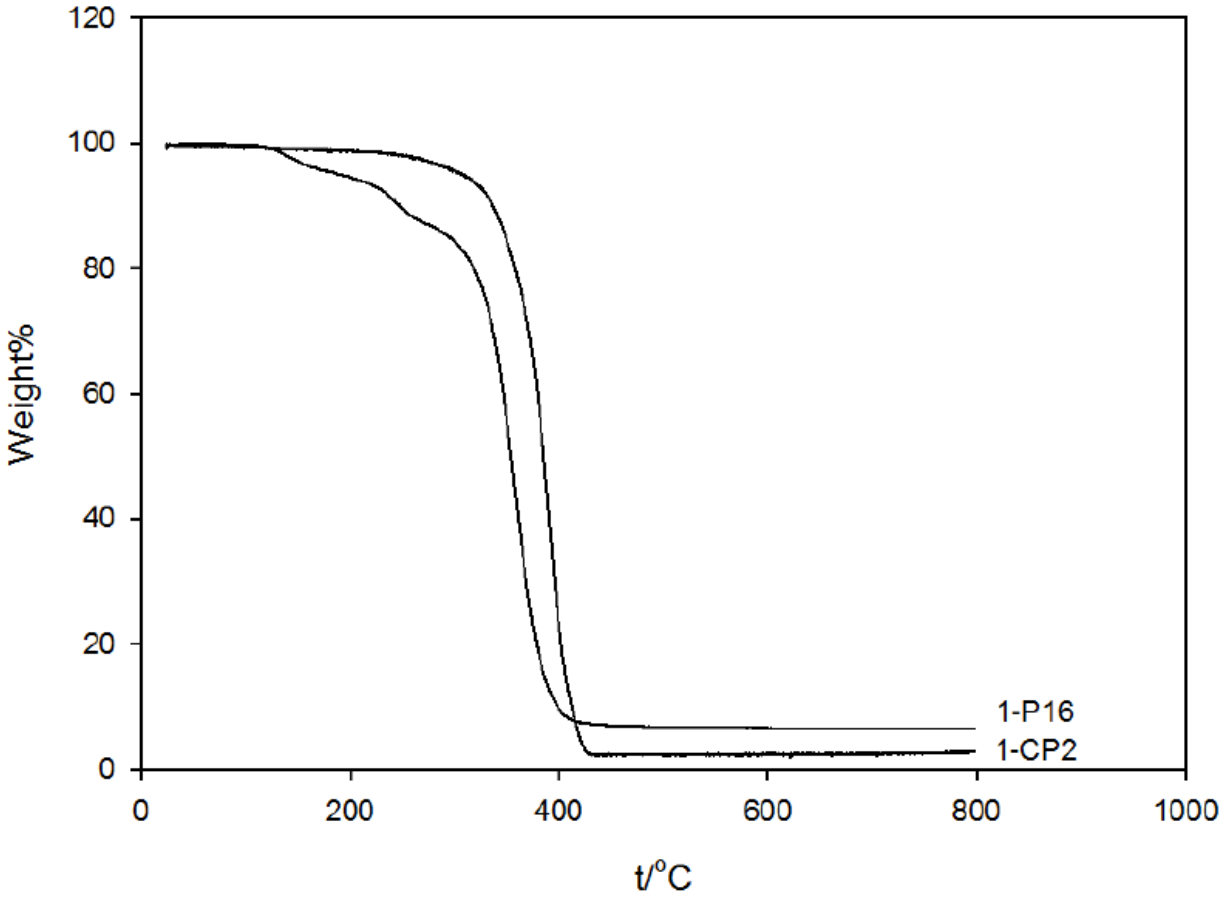

Figure 4.28. Thermogravimetric Weight Change Curve of Copolymer (or Mixed Brush)/Silica Nanocomposite 1-CP3 in Comparison to the Curve for the Starting PAN/Silica Nanocomposite 1-P26.

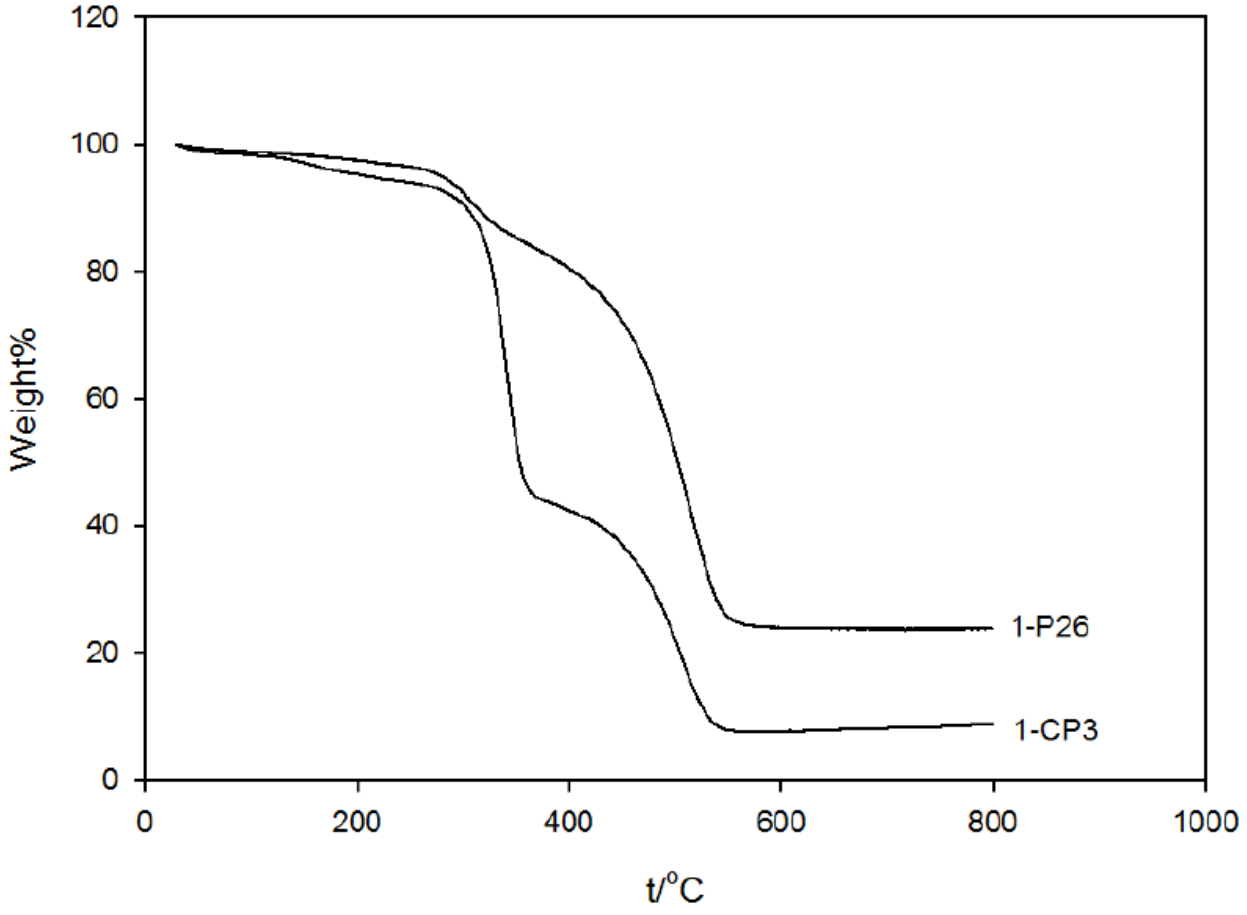

DSC patterns of the resulting samples are shown in Figure 4.29, and the comparison figures of DSC patterns for homopolymer/silica nanocomposites and copolymer/silica nanocomposites are showed in Figures 4.30, 4.31 and 4.32. The observed thermal event at 105-106 ℃ corresponds to T_g of polystyrene (PS) block. This indicates that PS (or at least part of it) is separated from PMMA or PAN matrix. This is consistent with the block extension model for second polymer grafting (otherwise a mixed brush may have no T_g). The DSC curves at Figure 4.29 show no strong evidence of T_g of PMMA or PAN, although weak indications of thermal events in the temperature range 120-140 ℃ can be observed. It is not fully clear whether the lack of clearly visible thermal event related to T_g of PMMA is due to the formation of a mixed PMMA/PS brush or due to low loading of PMMA or restrictions on the mobility of PMMA blocks after grafting of PS. (see discussion of Ref. 70 below)

The morphologies of PMMA-PS/silica nanocomposite 1-CP1 and PAN-PS/silica nanocomposite 1-CP3 are reflected on TEM images in Figures 4.33 and 4.34. Figure 4.33 can be interpreted as the evidence of stacking of many layers for 1-CP1. Figure 4.34 (1-CP3) also appears to show stacks layers, with some darker edges potentially arising from curved layers and their outer part parallel to the electron beam.

When comparing with literature results, Shipp group claimed a mixed exfoliated/intercalated architecture of poly(styrene-*block*-butyl acrylate) block copolymer (PSBA)/silicate nanocomposites. The polystyrene (PS) block was grafted on the silicate surface first via atom transfer radical polymerization (ATRP), and poly(butyl acrylate) (PBA) block was attached to PS block via ATRP. The free block copolymer (PSBA) detached from the silicate surface showed two glass transition temperatures (-40 ℃ and 93 ℃ corresponding to PBA and PS blocks) in DSC pattern, but the PSBA/silica nanocomposite showed a T_g at -40 ℃ and a shallow

hump around 93 ℃. The thermal transition behavior of PS block in the nanocomposites was explained as the limiting movement of PS segments due to the direct linkage of polystyrene chains and the silicate surface. In the contrast, PBA block in the nanocomposites had some freedom to show the characteristic glass transition. [70]

Sogah group had investigated the preparation of exfoliated block copolymer/silicate nanocomposites by one-pot, one-step living polymerization from a silicate anchored bifunctional initiator. Polystyrene (PS) and polycaprolactone (PCL) chains were attached to the silicate surface at the junction (initiator) between the two blocks. There was no glass transition temperature visible in DSC patterns for their nanocomposites, only the melting point of PCL block was shown. [73]

Based on these literature results, the glass transition behavior of our block copolymer (or mixed brush)/silica nanocomposites was very similar to that of the copolymer/silicate nanocomposite prepared by Shipp group.

Figure 4.29. Differential Scanning Calorimetry Traces of Copolymer/Silica Nanocomposites 1-CP1, 1-CP2 and 1-CP3.

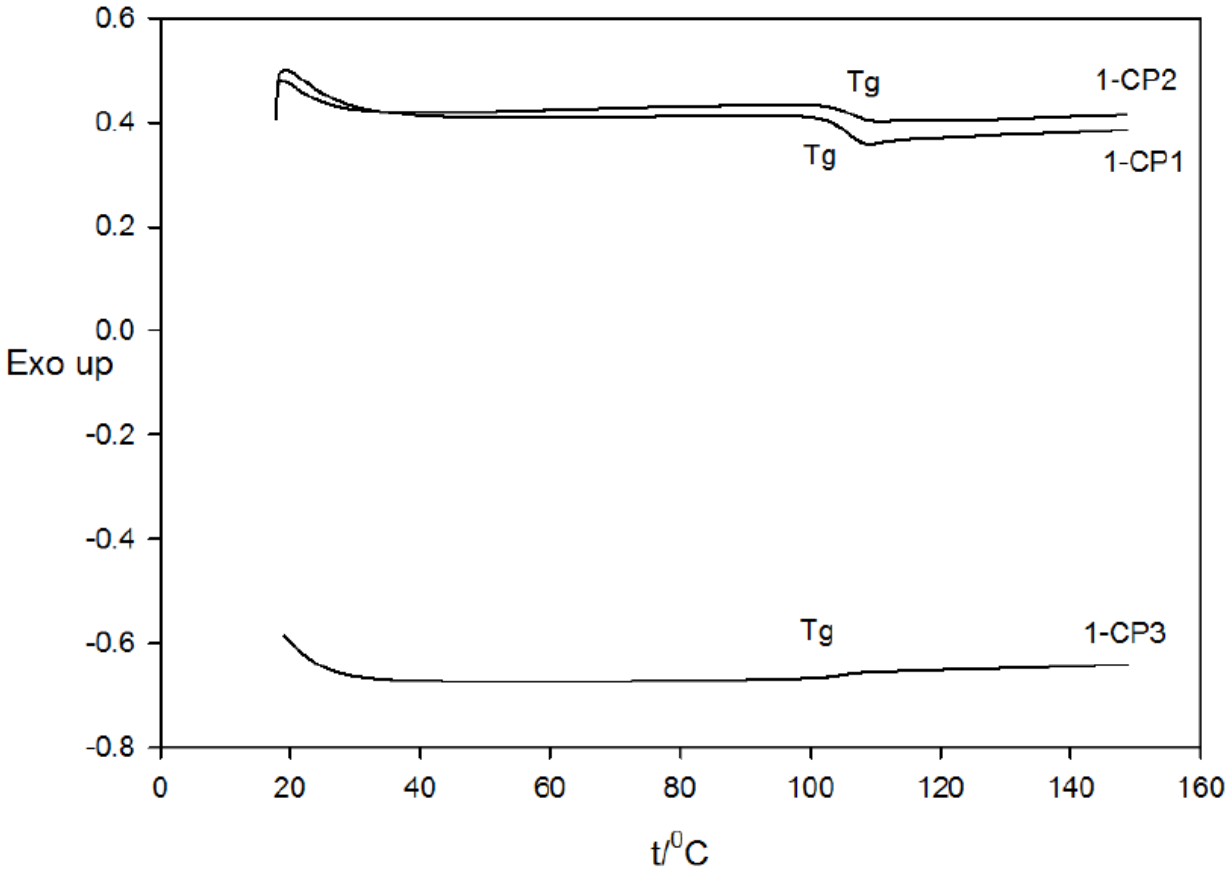

Figure 4.30. Differential Scanning Calorimetry Traces of PMMA/Silica Nanocomposite1-P10 and PMMA-PS/Silica Nanocomposite 1-CP1.

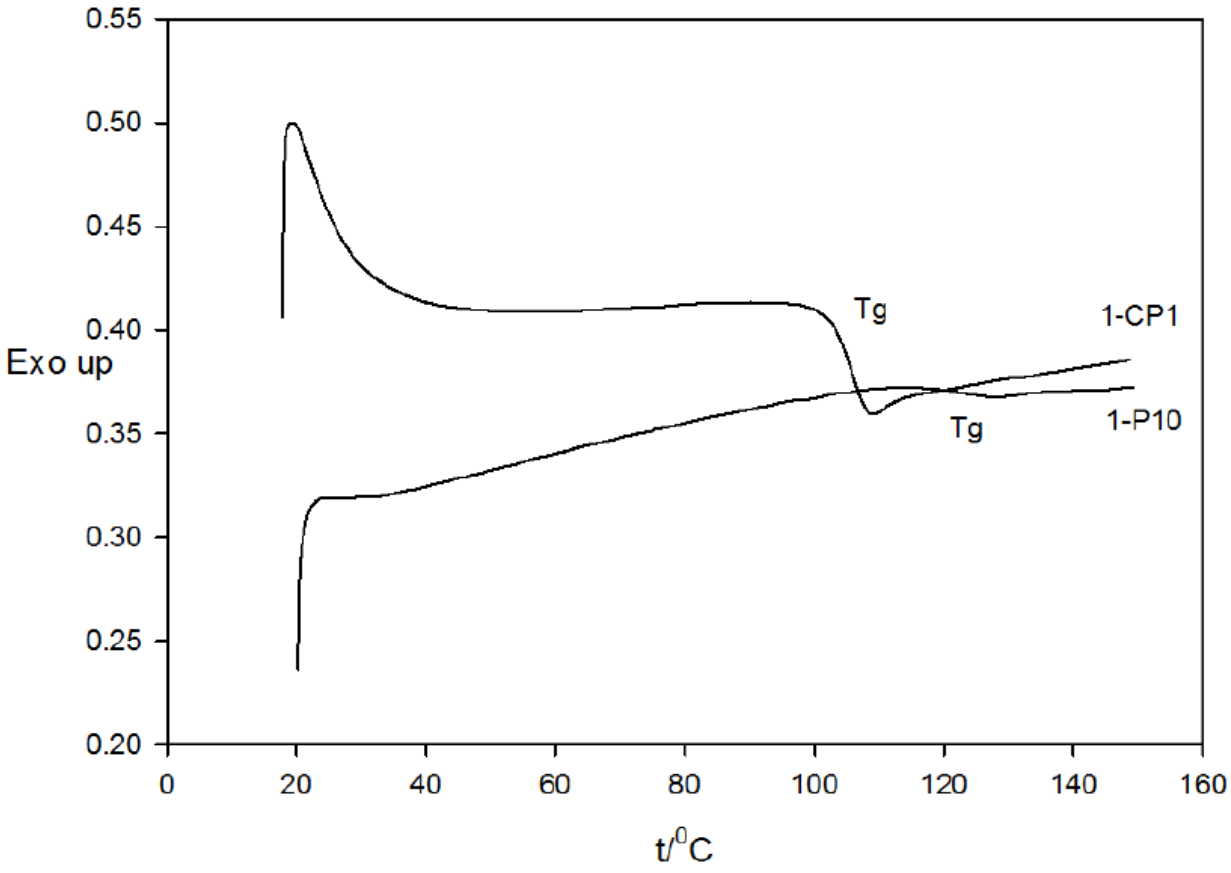

Figure 4.31. Differential Scanning Calorimetry Traces of PMMA/Silica Nanocomposite 1-P16 and PMMA-PS/Silica Nanocomposite 1-CP2.

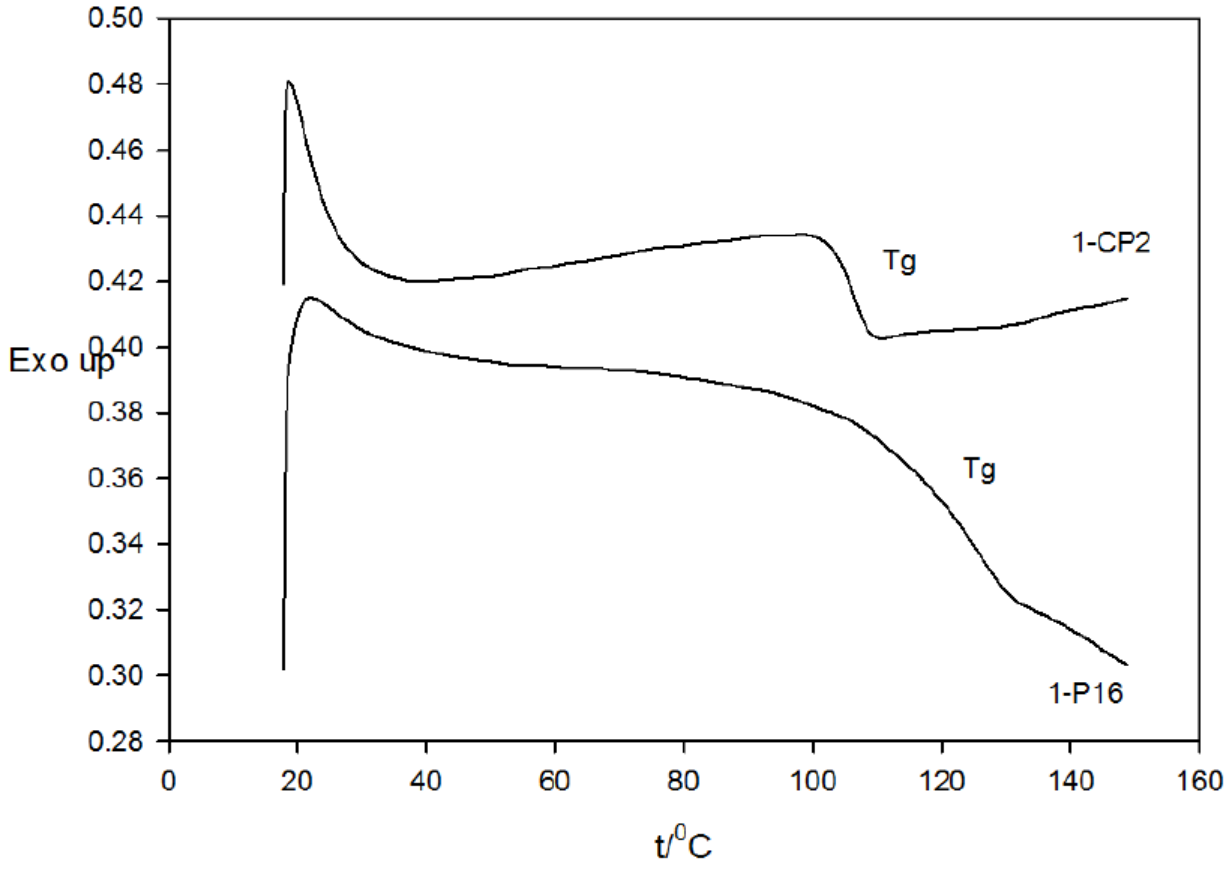

Figure 4.32. Differential Scanning Calorimetry Traces of PAN/Silica Nanocomposite 1-P26 and PAN-PS/Silica Nanocomposite 1-CP3.

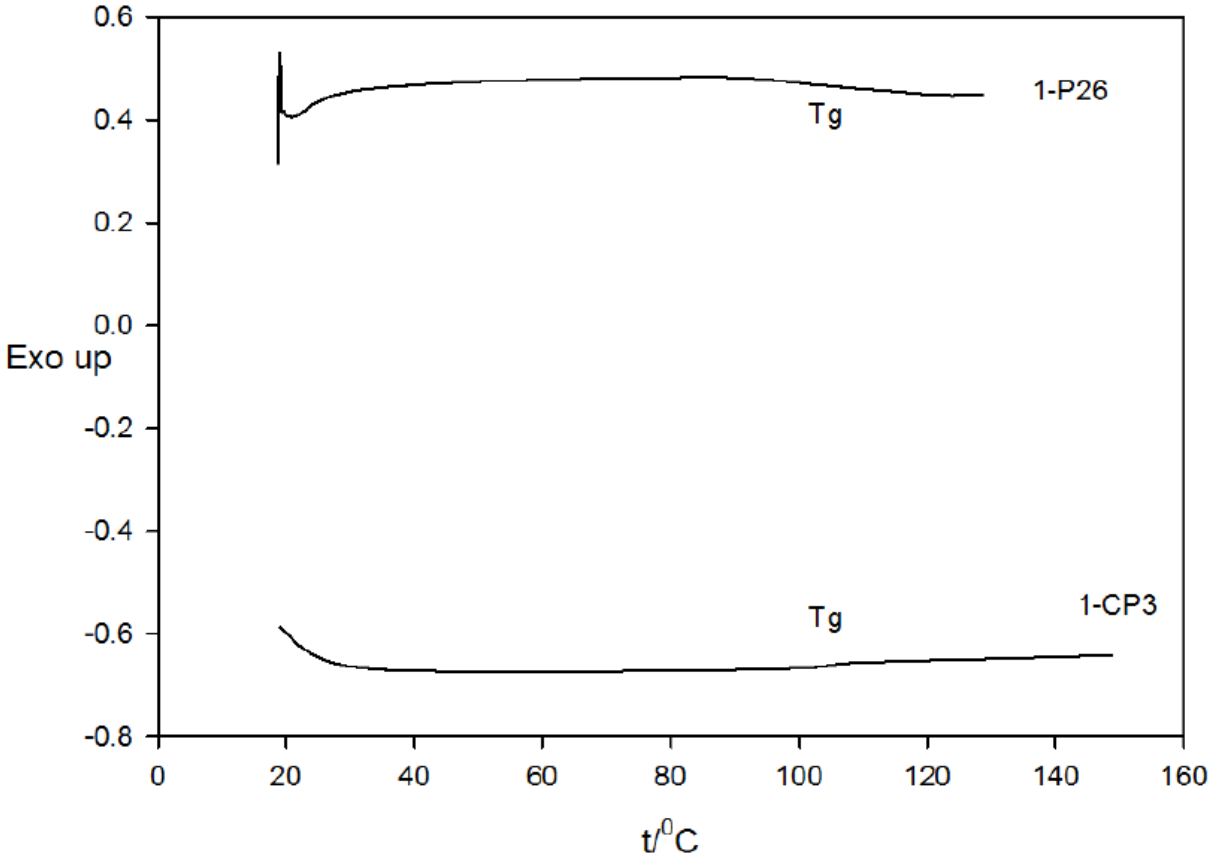

Figure 4.33. TEM Images of PMMA-PS/Silica Nanocomposite 1-CP1.

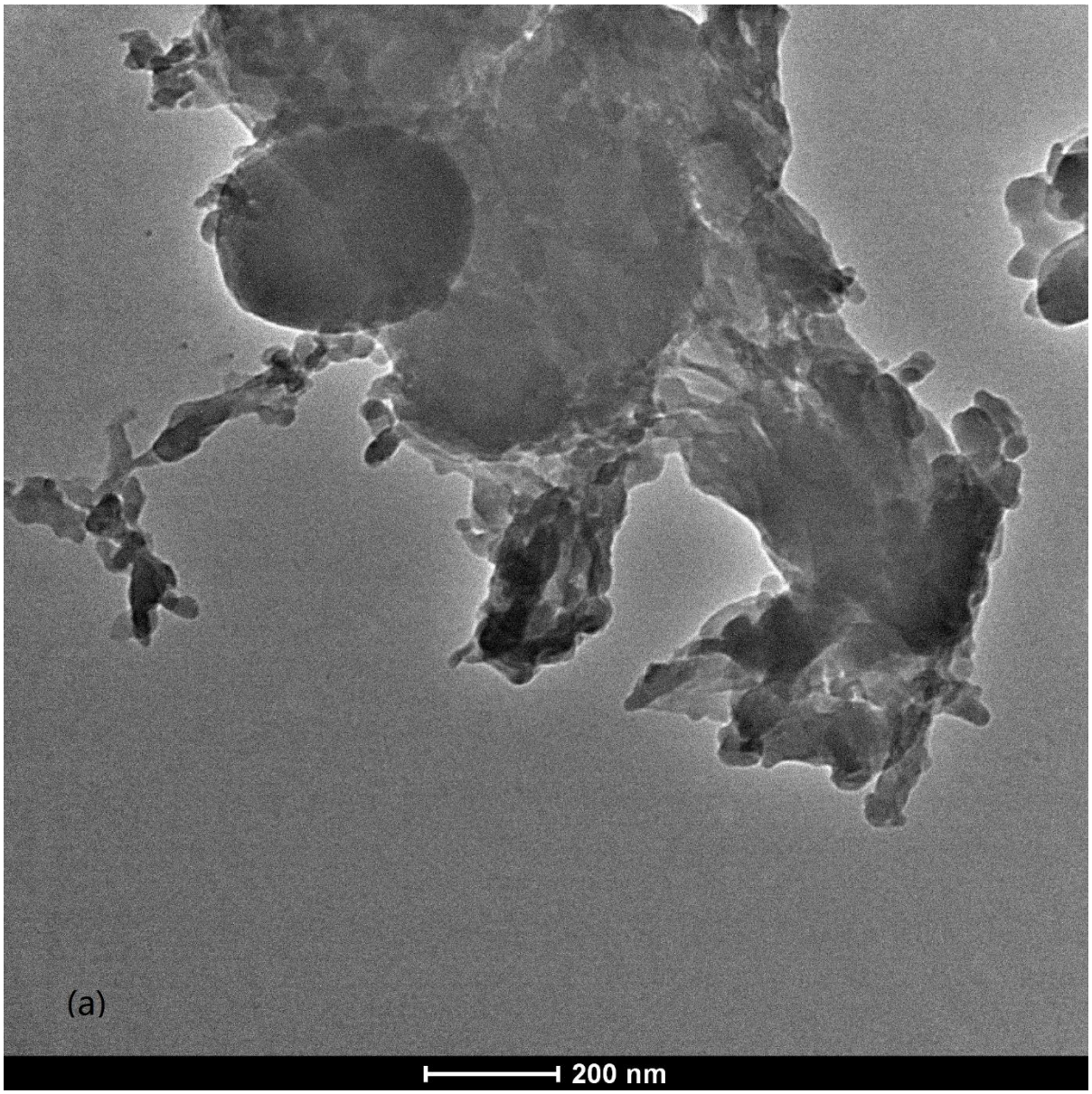

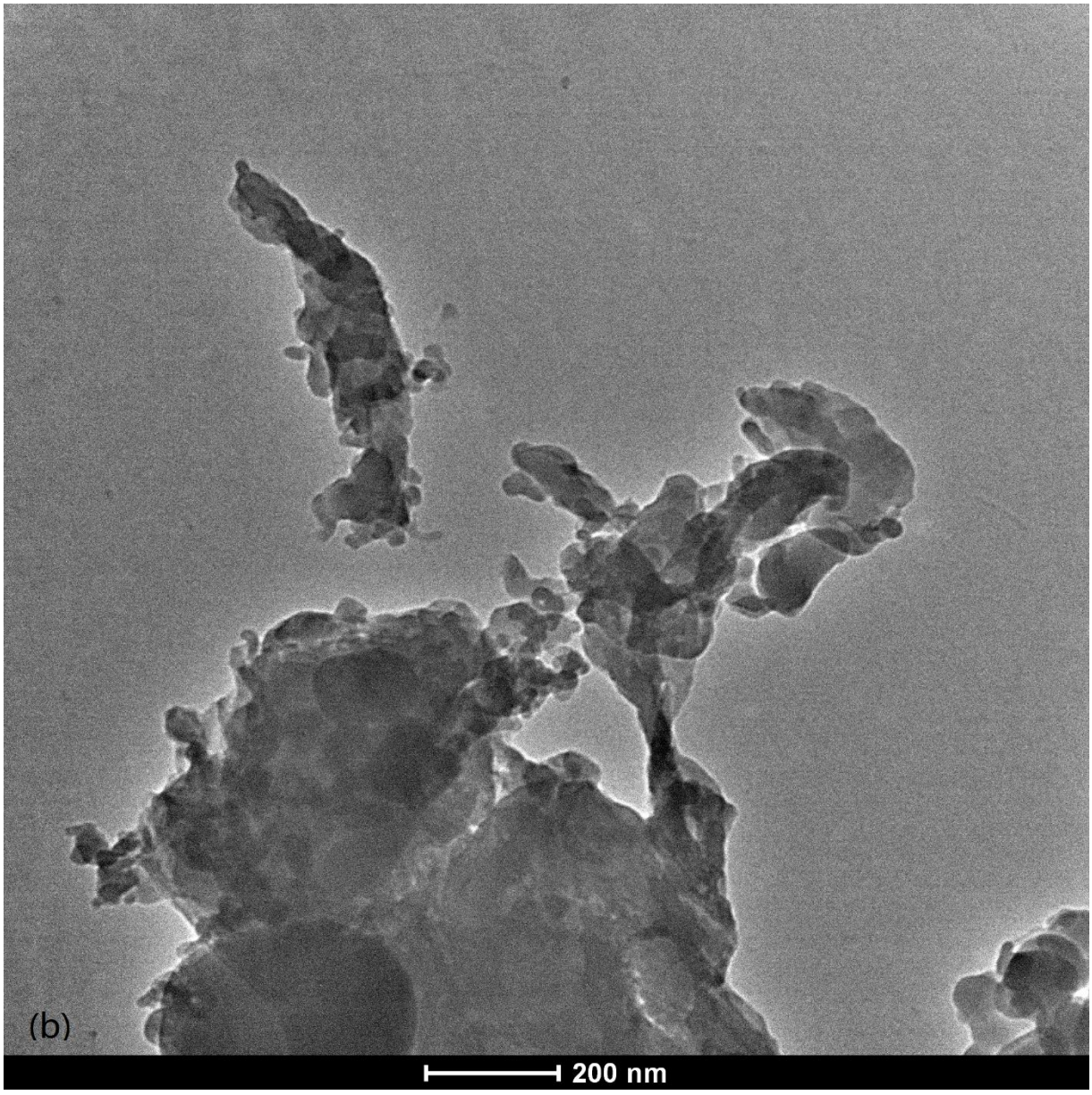
(b)
200 nm

Figure 4.34. TEM Images of PAN-PS/Silica Nanocomposite 1-CP3.

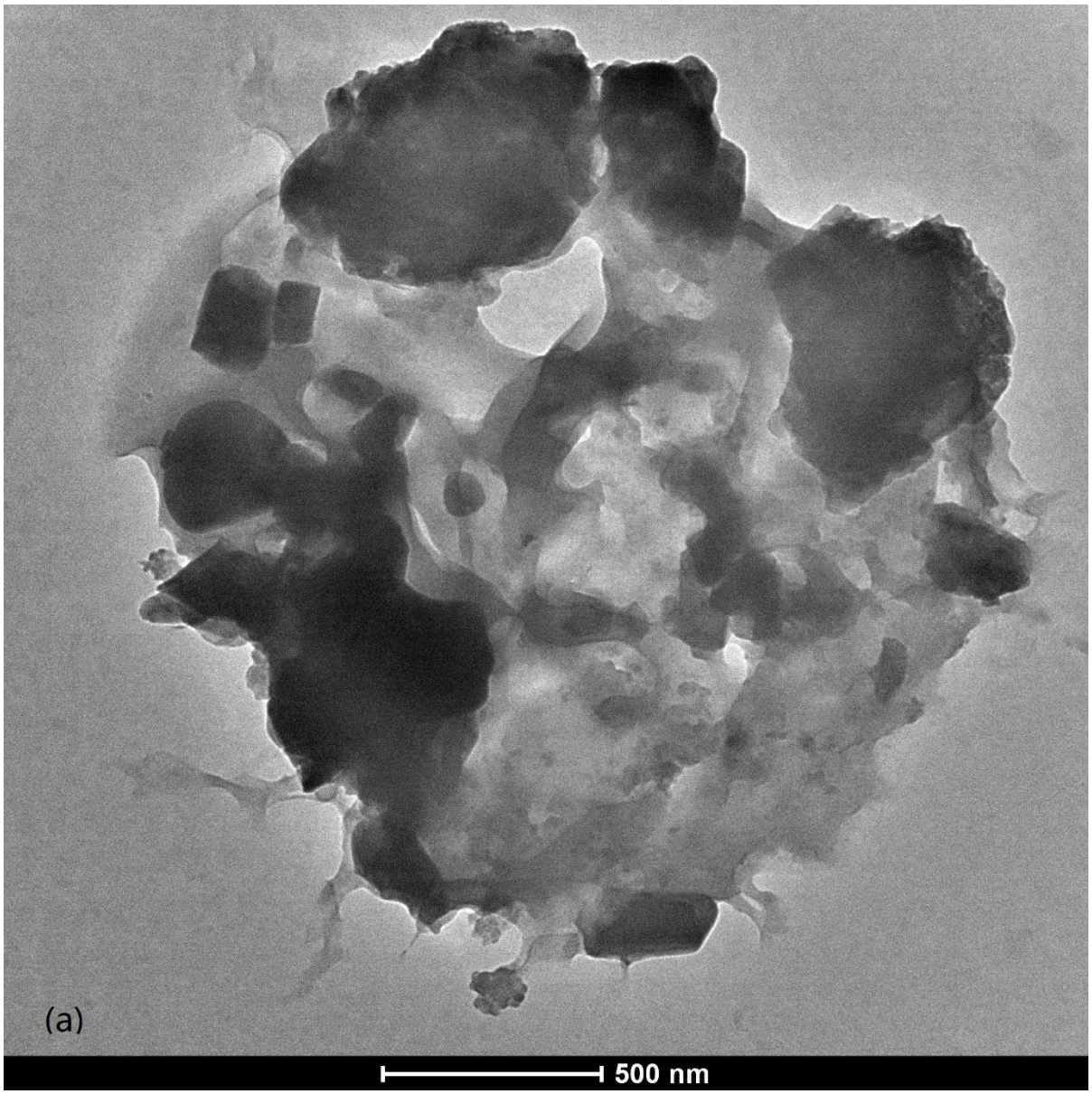

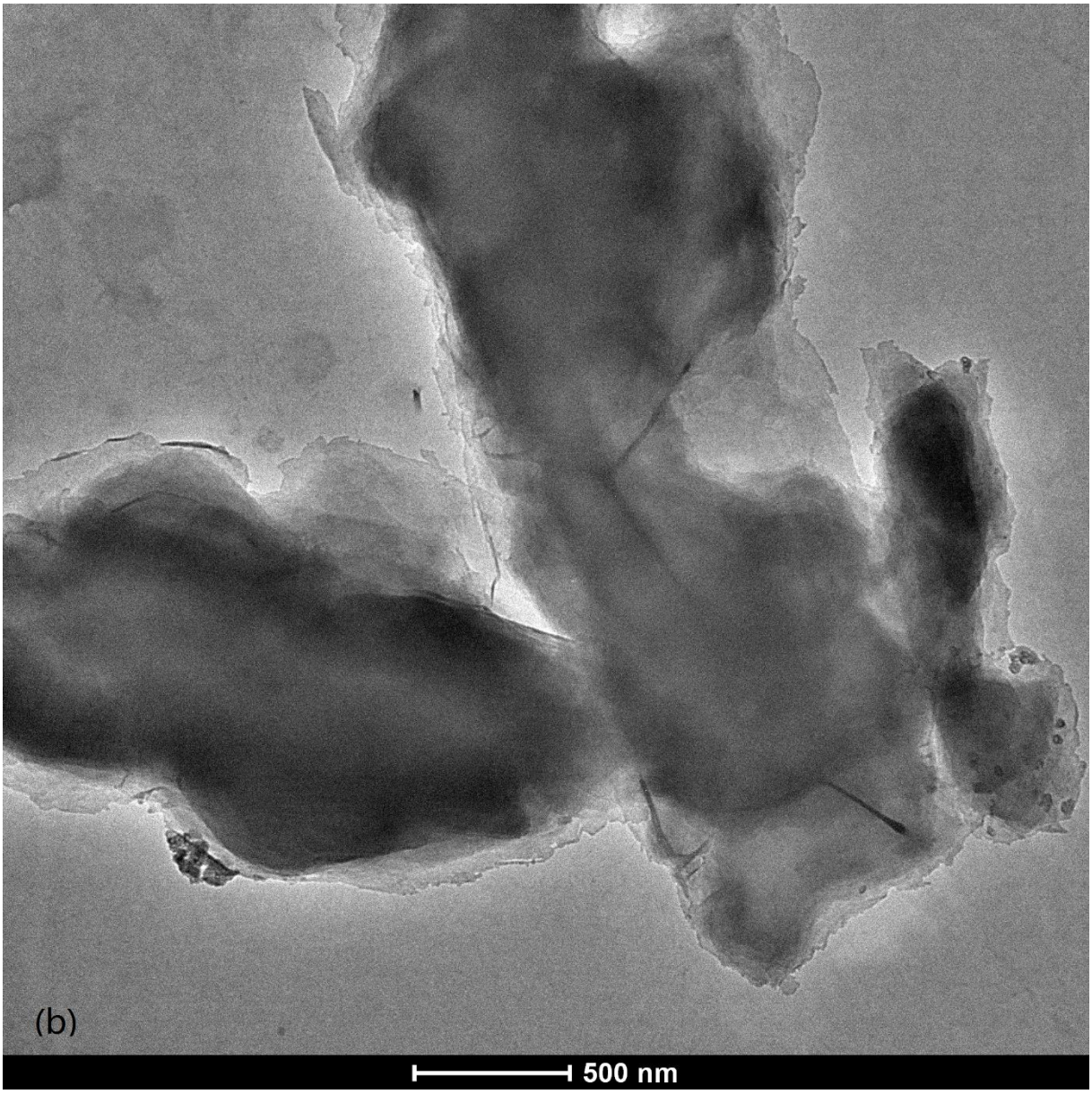
(b)
500 nm

The polymerization on the surface of mesopores via ARGET ATRP were investigated by other lab members in our research group. Poly(methyl methacrylate), [166] polystyrene, [166] poly(*N*-isopropylacrylamide) [168] and poly(2-(dimethylamino)ethyl methacrylate) [168] were attached onto the surface of SBA-15 successfully. From all these results, it can be concluded that activators regenerated by electron transfer atom transfer radical polymerization (ARGET ATRP) can be successfully used in the synthesis of nanocomposites with different silica precursors (including nanoscale-dispersed layered silicas) in different polymer matrixes (including copolymers).

TGA and SAXS confirmed the loading of polymer on the layered silica surface, but the ordering was difficult to preserve (more difficult than in normal ATRP). At the same time, the nanocomposites prepared via ARGET ATRP had very low level of impurities (they were white products, as seen in Figure 4.35), which is an advantage over ATRP (Figure 3.31) if one is concerned about the copper impurity level in the product. There was evidence of glass transition of the second block (PS) in copolymer/silica nanocomposite.

Figure 4.35. Appearance of PS/Silica Nanocomposite 1-P21 via ARGET ATRP.

4.6. Summary and Conclusions

The organic-inorganic nanocomposites with silica layers dispersed in polymer matrixes were successfully prepared. Our new synthesis route involved the atom transfer radical polymerization initiator covalently attached on the surfaces of lamellar (layered) silicas, the latter being prepared through surfactant templating. The covalent bonding between the layered silica surface and the initiator provided a strong interaction between the surface of inorganic substrate and the polymer chains, thus providing a way to improve thermal stability comparing with the ionic interactions between the quaternary ammonium cation initiators grafted via cation exchange to the silicate surface in many other polymer/clay nanocomposites. This methodology was expected to provide us with the opportunity to better control the architecture of the polymer/silica nanocomposites, and indeed in many cases we were able to obtain either intercalated or exfoliated structures by controlling the polymer loading.

The layered silica precursors were prepared successfully following the literature procedures, using a mixture of cationic and neutral surfactants (precursor **1**), or a mixture of neutral surfactants (precursor **2**). Both SAXS and TEM confirmed the lamellar morphology of these silica precursors, whose interlayer spacings were 3.5 nm (layered silica **1**) and 5.4 nm (layered silica **2**). The templating surfactants were present in the samples, and they were sandwiched between the silica layers.

A series of organosilanes were examined to understand the organic group grafting with concomitant surfactant displacement and to select a proper initiator for the surface-initiated polymerization. Trimethylchlorosilane (TMCS), n-butyldimethylchlorosilane (BDMCS), dimethyloctylchlorosilane (DMOCS), (chloromethyl-phenyl)ethyl trichlorosilane (CMPETS), 2-

(4-chlorosulfonyl phenyl) ethyl trichlorosilane (CSPETCS), and 3-(chlorodimethylsilyl)propyl 2-bromo-2-methylpropanoate (CDMSPBMP) were used to modify the layered silica **1**. The weight loss changes and the interlayer spacing changes to 1.9 nm and 2.9 nm for the organomonochlorosilane-modified layered silica samples **1** and **2**, indicating the surfactants were displaced by the organomonochlorosilanes. (3-(Chlorodimethylsilyl)propyl 2-bromo-2-methylpropanoate modified layered silica **1**was successfully prepared, because the organosilane displaced the surfactant. However, the weight change patterns of 1-CMPETS (chloromethyl phenylethyl trichlorosilane modified layered silica **1**) and 1-CSPETCS (2-(4-chlorosulfonyl phenyl) ethyl trichlorosilane modified layered silica **1**) indicated that some surfactants remained in the structure after the reaction with the silane. For the trichloroorganosilane-modified layered silicas (1-CMPETS and 1-CSPETCS), these organosilanes might not only be attached on the silica surface via Si-O-Si bonds, but also connected to each other via Si-O-Si bridges. Moreover, the cross-linking of organosilane molecules might have introduced a cross-linking between the silica layers, which also might have hindered a complete surfactant displacement. 3-(Chlorodimethylsilyl)propyl 2-bromo-2-methylpropanoate (CDMSPBMP) was selected as an initiator to modify the layered silica **1** and **2**, and the corresponding initiator-modified layered silicas had interplanar spacings of 1.9 nm (for 1-CDMSPBMP) and 2.6 nm (for 2-CDMSPBMP). It was thus demonstrated that the reaction of surfactant-templated layered silicas with suitable organosilanes provides general avenue to obtain initiator-functionalized silica layers.

The polymerizations of methyl methacrylate, styrene and acrylonitrile via atom transfer radical polymerization (ATRP) and activators regenerated by electron transfer (ARGET) ATRP were successful. In PMMA/silica nanocomposites preparation via ATRP from initiator-functionalized layered silica 1-CDMSPBMP, the polymer loading can be controlled by adjusting

polymerization time and initial monomer concentration. The intercalated architecture can be maintained to an appreciable extent, reaching interplanar spacing of 6 nm, or perhaps even about 12 nm for sample with 17% of silica residue. At a higher polymer loading, no ordering was evident from SAXS patterns, and we can conclude that the exfoliated architectures for PMMA/silica nanocomposites were achieved. The glass transition temperatures evaluated by DSC of the intercalated PMMA/silica nanocomposites showed an increase with increasing polymer loading. These glass transition temperatures were higher than T_g of PMMA prepared via conventional free radical polymerization (105 ℃). The T_g differences are likely to be related to the covalent bonding of polymer chains to the surface and possibly to the interactions between the polymer chains and the surface of silica layers. If the interactions are strong, glass transition temperatures are expected to increase, which was observed in our nanocomposites perhaps due to the covalent interactions between the polymer chains and the silica surface. The T_g trend for our PMMA/silica nanocomposites was opposite comparing with literature results. However, the difference of the architecture from our intercalated nanocomposites and the possible cross-linkings in the structure of the polymer layer make the comparison difficult. The PMMA/silica nanocomposite prepared via ATRP from initiator-functionalized layered silica 2-CDMSPBMP had an intercalated architecture with interplanar spacing of 8.4 nm (with 35% silica residue), and the T_g of this sample was about 113 ℃ (higher than PMMA T_g in bulk). This confirms that the present method can readily afford intercalated PMMA-silica nanocomposites with quite large interplanar spacings, thus suggesting the PMMA grafting uniformity.

The interplanar spacing of the PAN/silica nanocomposites prepared via ATRP from initiator-functionalized layered silica 2-CDMSPBMP was about 5 nm (38% silica residue) after 44 hours polymerization. With about 31% silica residue, the PS/silica nanocomposite (prepared from 1-

CDMSPBMP) had an interplanar spacing of about 5 nm. The glass transition temperature for this nanocomposite was about 102 ℃ in DSC pattern, which is slightly higher than the T_g of bulk polystyrene. The results for PAN and PS suggest the good ability of ATRP to render intercalated nanocomposites of silica lay9layereders with different grafted polymers with controlled polymer loading.

These finding for PMMA-(layered silica) and PAN-(layered silica) nanocomposites are particularly notable, because we are not aware of prior successful synthesis of such ordered intercalated composites. PAN-(layered silica) nanocomposites have not been reported earlier as far as we know.

ARGET ATRP was found suitable to synthesize well-defined polymer-(layered silica) nanocomposites with controlled polymer loading. We are not aware of any prior demonstration of that in the scientific literature. In general, ARGET ATRP led to higher polymer loadings in the polymer/silica nanocomposites. However, as normal ATRP is known to offer lower polydispersity index (PDI) than ARGET ATRP, the polymer growth in ARGET ATRP was apparently less uniform. In particular, ordering was lost at lower polymer loadings for composite samples prepared via ARGET ATRP, and the peaks/shoulders in SAXS patterns were broader when compared to the SAXS patterns of the nanocomposites prepared via normal ATRP with similar polymer loading. On the other hand, ARGET ATRP greatly decreased copper content in the products.

The silica residue of the PMMA/silica nanocomposites prepared via ARGET ATRP from initiator-functionalized layered silica 1-CDMSPBMP reached as low as about 4%. The glass transition temperatures of these nanocomposites were in the range of 122-129 ℃, and there was

no T_g trend in contrast to the results from normal ATRP, which is possibly due to the less homogeneous polymer chains in the nanocomposites. In the preparation of PMMA/silica nanocomposites via ARGET ATRP, the results for 2-CDMSPBMP initiator-functionalized layers are comparable to those for 1-CDMSPBMP initiator-functionalized layers, suggesting the facile reproducibility of the method for different layered silica starting materials.

The PS/silica nanocomposites initiated from 1-CDMSPBMP and 2-CDMSPBMP via ARGET ATRP were comparable. At high polystyrene loadings (about 1-18% silica residue), these nanocomposites exhibited similar T_g of about 104-106 ℃, which suggests essentially glass transition temperatures of exfoliated PS/silica nanocomposites are constant if the polymer loading is high enough.

PAN/silica nanocomposite samples prepared using initiator-modified layered silicas 1-CDMSPBMP or 2-CDMSPBMP via ARGET ATRP showed very similar properties, which meant that the synthetic procedure worked well with different layered silica precursors. The ordering was lost at very low PAN loading for these nanocomposites. Perhaps the process led to some cross-linking between the layers at an early stage, which made it impossible to stack the silica layers even for a low polymer loading. Alternatively, the spatial distribution of grafted polymer chains might have been highly nonuniform and the PAN tendency to crystallize might have created local “bumps” of polymer, which made it impossible for the layers to pack. Some of the PAN/silica nanocomposites with high PAN loadings prepared via ARGET ATRP exhibited T_g around 97-98 ℃, which is higher than the T_g (85 ℃) of the commercially available PAN powders.

The copolymers were also synthesized by ARGET ATRP, although the exact nature of the polymer layer requires further studies.

It was thus demonstrated that surface-initiated ATRP and ARGET ATRP allows one to obtain intercalated and/or exfoliated polymer-(layered silica) architectures with controlled polymer loading. The layered silica materials can be synthesized via surfactant templating and functionalized with initiator through a reaction with a suitable organosilane. The strategy offers flexibility in choice of the polymer matrix and layered silica component.

References

(1) (a) Giannelis, E. P. *Ad*v. *Mater.* **1996,** *8*, 29; (b) Wong, S.; Vaia, R.; Vasudevan, S.; Giannelis, E. P.; Zax, D. B. *J. Am. Chem. Soc.* **1995**, *117*, 7568; (c) Vaia, R. A.; Vasudevan, S.; Karwiec, W.; Scanlon, L. G.; Giannelis, E. P. *Ad*v. *Mater.* **1995**, *7*, 154; (d) Krishnamoorti, R.; Vaia, R. A.; Giannelis, E. P. *Chem. Mater.* **1996**, *8*, 1728.

(2) (a) Pinnavaia, T. J. *Science* **1983**, *220*, 365; (b) Lan, T.; Kaviratna, P. D.; Pinnavaia, T. J. *Chem. Mater*. **1995**, *7*, 2144. (c) Solomon, D. H.; Hawthorne, D. G. *Chemistry of Pigments and Fillers*; Wiley: New York, 1983; pp 136-144.

(3) (a) Kojima, Y.; Usuki, A.; Kawasumi, M.; Okada, A.; Kurauchi, T.; Kamigaito, O. *J. Polym. Sci., Part A: Polym. Chem*. **1993**, *31*, 983; (b) Kojima, Y.; Usuki, A.; Kawasumi, M.; Okada, A.; Fukushima, Y.; Kurauchi, T.; Kamigaito, O. *J. Mater. Res.* **1993**, *8*, 1185.

(4) Ozin, G. *Ad*v. *Mater.* **1992**, *4*, 612.

(5) (a) Usuki, A.; Kawasumi, M.; Kojima, Y.; Okada, A.; Kurauchi, T.; Kamigaito, O. *J. Mater. Res.* **1993**, *8*, 1174; (b) Usuki, A.; Kojima, Y.; Kawasumi, M.; Okada, A.; Fukushima, Y.; Kurauchi, T.; Kamigaito, O. *J. Mater. Res*. **1993**, *8*, 1179.

(6) (a) Alexandre, M.; Dubois, P. *Mater. Sci. Eng.* **2000**, *R28*, 1. (b) Zanetti, M.; Lomakin, S.; Camino, G. *Macromol. Mater. Eng*. **2000**, *279*, 1.

(7) Biswas, M.; Ray, S. S. *Adv. Polym. Sci*. **2001**, *155*, 167.

(8) (a) Mark, J. E. *Polym. Eng. Sci.* **1996**, 36, 2905; (b) E. Reynaud, C. Gauthier, J. Perez, *Rev. Metall./Cah. Inf. Tech.* **1999**, *96*, 169.

(9) P. Calvert, Potential applications of nanotubes, in: T.W. Ebbesen (Ed.), *Carbon Nanotubes,* CRC Press, Boca Raton, FL, **1997**, pp. 277.

(10) Piazza, D.; Lorandi, N. P.; Pasqual, C. I.; Scienza, L. C.; Zattera, A. J. *Mat. Sci. Eng.: A,* **2011**, *528*, 6769.

(11) C. Oriakhi, *Nano sandwiches*, *Chem. Br.* **1998**, *34*, 59.

(12) D.J. Greenland, *J. Colloid Sci*. **1963,** *18,* 647.

(13) N. Ogata, S. Kawakage, T. Ogihara, *J. Appl. Polym. Sci.* **1997,** *66,* 573.

(14) R.L. Parfitt, D.J. Greenland, *Clay Mineral* **1970**, *8*, 305.

(15) X. Zhao, K. Urano, S. Ogasawara, *Colloid Polym. Sci*. **1989**, *267*, 899.

(16) E. Ruiz-Hitzky, P. Aranda, B. Casal, J.C. Galván, *Adv. Mater.* **1995**, *7*, 180.

(17) J. Billingham, C. Breen, J. Yarwood, *Vibr. Spectrosc.* **1997**, *14*, 19.

(18) R. Levy, C.W. Francis, *J. Colloid Interface Sci.* **1975**, *50*, 442.

(19) H.G. Jeon, H.-T. Jung, S.W. Lee, S.D. Hudson, *Polym. Bull.* **1998**, *41*, 107.

(20) N. Ogata, G. Jimenez, H. Kawai, T. Ogihara, *J. Polym. Sci.: Part B: Polym. Phys.* **1997**, *35*, 389.

(21) G. Jimenez, N. Ogata, H. Kawai, T. Ogihara, *J. Appl. Polym. Sci*. **1997**, *64*, 2211.

(22) D.C. Lee, L.W. Jang, *J. Appl. Polym. Sci.* **1996**, *61*, 1117.

(23) T.K. Chen, Y.I. Tien, K.H. Wei, *J. Polym. Sci.: Part A Polym. Chem.* **1999**, *37*, 2225.

(24) A. Akelah, A. Moet, *J. Mater. Sci.* **1996**, *31*, 3589.

(25) J.G. Doh, I. Cho, *Polym. Bull.* **1998**, *41*, 511.

(26) J. Tudor, L.Willington, D. O'Hare, B. Royan, *Chem. Commun.* **1996**, 2031.

(27) P. Dubois, M. Alexandre, F. Hindryckx, R. Jerôme, *J. Macromol. Sci.: Rev. Macromol. Chem. Phys.* **1998**, *C38*, 511.

(28) P.B. Messersmith, E.P. Giannelis, *Chem. Mater.* **1994**, *6*, 1719.

(29) X. Kornmann, L.A. Berglund, J. Sterte, *Polym. Eng. Sci.* **1998**, *38*, 1351.

(30) Z. Wang, T.J. Pinnavaia, *Chem. Mater.* **1998**, *10*, 1820.

(31) Z. Wang, T.J. Pinnavaia, *Chem. Mater.* **1998**, *10*, 3769.

(32) R.A. Vaia, H. Ishii, E.P. Giannelis, *Chem. Mater.* **1993**, *5*, 1694.

(33) R.A. Vaia, K.D. Jandt, E.J. Kramer, E.P. Giannelis, *Macromolecules* **1995**, *28*, 8080.

(34) R.A. Vaia, K.D. Jandt, E.J. Kramer, E.P. Giannelis, *Chem. Mater.* **1996**, *8*, 2628.

(35) L.M. Liu, Z.N. Qi, X.G. Zhu, *J. Appl. Polym. Sci.* **1999**, *71*, 1133.

(36) M. Kato, A. Usuki, A. Okada, *J. Appl. Polym. Sci*. **1997**, *66*, 1781.

(37) M. Kawasumi, N. Hasegawa, M. Kato, A. Usuki, A. Okada, *Macromolecules* **1997,** *30*, 6333.

(38) N. Hasegawa, M. Kawasumi, M. Kato, A. Usuki, A. Okada, *J. Appl. Polym. Sci.* **1998**, *67*, 87.

(39) D. Wolf, A. Fuchs, U. Wagenknecht, B. Kretzschmar, D. Jehnichen, L. Häussler, Nanocomposites of polyolefin clay hybrids, in: Proceedings of the Eurofiller'99, Lyon-Villeurbanne, 6-9 September **1999**.

(40) M. Alexandre, G. Beyer, C. Henrist, R. Cloots, A. Rulmont, P. Dubois, *Macromolecular Rapid Communications*, **2001**, *22*, 643.

(41) M. Laus, O. Francesangeli, F. Sandrolini, *J. Mater. Res.* **1997**, *12*, 3134.

(42) S.D. Burnside, E.P. Giannelis, *Chem. Mater.* **1995**, *7*, 1597.

(43) K.A. Carrado, L.Q. Xu, *Chem. Mater.* **1998**, *10*, 1440.

(44) Wu, C. J.; Gaharwar, A. K.; Chan, B. K.; Schmidt, G. *Macromolecules* **2011**, *44*, 8215.

(45) Shah, D.; Maiti, P.; Gunn, E.; Schmidt, D. F.; Jiang, D. D.; Batt, C. A.; Giannelis, E. P. *Adv. Mater.* **2004**, *16*, 1173.

(46) Ali, S. S.; Tang, X. Z.; Alavi, S.; Faubion, J. *J Agric. Food. Chem.* **2011**, *59*, 12384.

(47) Rao, Y. Q.; Pochan, J. M. *Macromolecules* **2007**, *40*, 290.

(48) Dai, X. H.; Xu, J.; Guo, X. L.; Lu, Y.L.; Shen, D. Y.; Zhao, N.; Luo, X. D.; Zhang, X. L. *Macromolecules* **2004**, *37*, 5615.

(49) Lepoittevin, B.; Pantoustier, N.; Devalckenaere, M.; Alexandre, M.; Kubies, D.; Calberg, C.; Jerome, R.; Dubois, P. *Macromolecules* **2002**, *35*, 8385.

(50) Uthirakumar, P.; Nahm, K. S.; Hahn, Y. B.; Lee, Y. S. *Eur. Polym. J.* **2004**, *40*, 2437.

(51) Zhang, X. G.; Loo, L. S. *Macromolecules* **2009**, *42*, 5196.

(52) Okamoto, M.; Morita, S.; Taguchi, H.; Kim, Y. H.; Kotaka, T.; Tateyama, H. *Polymer* **2000**, *41*, 3887.

(53) Burnside, S. D.; Giannelis, E. P. *J. Polym. Sci.: Part B: Polym. Phys.* **2000**, *38*, 1595.

(54) Yeh, J. M.; Liou, S. J.; Lin, C. Y.; Cheng, C. Y.; Chang, Y. W.; Lee, K. R. *Chem. Mater.* **2002**, *14*, 154.

(55) Fogelstrom, L.; Malmstrom, E.; Johansson, M.; Hult, A. *Appl. Mater. Interfaces* **2010**, *2*, 1679.

(56) H. Shioyama, *Carbon*. **1997**, *35*, 1664-1665.

(57) L. Hernan, J. Morales, J. Santos, *J. Solid State Chem.* **1998**, *141*, 327.

(58) D.J. Harris, T.J. Bonagamba, K. Schmidt-Rohr, *Macromolecules*.**1999**, *32*, 6718.

(59) Y. Matsuo, K. Tahara, Y. Sugie, *Carbon.* **1996**, *34*, 672.

(60) Y. Matsuo, K. Tahara, Y. Sugie, *Carbon.* **1997**, *35*, 113.

(61) Y. Ding, D.J. Jones, P. Maireles-Torres, *Chem. Mater.* **1995**, *7*, 562.

(62) O.C. Wilson Jr., T. Olorunyolemi, A. Jaworski, L. Borum, D. Young, A. Siriwat, E. Dickens, C. Oriakhi, M. Lerner, *Appl. Clay Sci.* **1999**, *15*, 265.

(63) C.O. Oriakhi, I.V. Farr, M.M. Lerner, *Clays and Clay Minerals.* **1997**, *45*, 194.

(64) B.K.G. Theng, *The Chemistry of Clay-Organic Reactions*, Wiley, New York, **1974**.

(65) M. Ogawa, K. Kuroda, *Bull. Chem. Soc. Jpn.* **1997**, *70*, 2593.

(66) E.P. Giannelis, R. Krishnamoorti, E. Manias, *Adv. Polym. Sci.* **1999**, *138*, 107.

(67) (a) Weimer, M. W.; Chen, H.; Giannelis, E. P.; Sogah, D. Y. *J. Am. Chem. Soc.* **1999**, *121*, 1615; (b) Ha, Y. H.; Kwon, Y.; Breiner, T.; Chan, E. P.; Tzianetopoulou, T.; Cohen, R. E.; Boyce, M. C.; Thomas, E. L., *Macromolecules* **2005**, *38*, 5170; (c) Hawker, C. J.; Bosman, A. W.; Harth, E. *Chem. Rev.* **2001**, *101*, 3661; (d) Fan, X. W.; Zhou, Q. Y.; Xia, C. J.; Cristofoli, W.; Mays, J.; Advincula, R. *Langmuir* **2002**, *18*, 4511; (e) Zhou, Q. Y.; Fan, X. W.; Xia, C. J.; Mays, J.; Advincula, R. *Chem. Mater.* **2001**, *13*, 2465; (f) Lepoittevin, B.; Pantoustier, N.; Alexandre, M.; Calberg, C.; Jérôme, R.; Dubois, P. *J. Mater. Chem.* **2002**, *12*, 3528.

(68) Böttcher, H.; Hallensleben, M. L.; Nuß, S.; Wurm, H.; Bauer, J.; Behrens, P. *J. Mater. Chem.* **2002**, *12*, 1351.

(69) Zhao, H. Y.; Argoti, S. D.; Farrell, B. P.; Shipp, D. A. *J. Polym. Sci.: Part A: Polym. Chem.* **2004**, *42*, 916.

(70) Zhao, H. Y.; Shipp, D. A. *Chem. Mater.* **2003**, *15*, 2693.

(71) Zhao, H. Y.; Farrell, B. P.; Shipp, D. A. *Polymer* **2004**, *45*, 4473.

(72) Salem, N.; Shipp, D. A. *Polymer Preprints* **2005**, *46*, 339.

(73) Di, J. B.; Sogah, D. Y. *Macromolecules* **2006**, *39*, 5052.

(74) Behling, R. E.; Williams, B. A.; Staad, B. L.; Wolf, L. M.; Cochran, E. W. *Macromolecules* **2009**, *42*, 1867.

(75) Behling, R. E.; Wolf, L. M.; Cochran, E. W. *Macromolecules* **2010**, *43*, 2111.

(76) (a) Chen, Y. M.; Lin, H. C.; Hsu, R. S.; Hsieh, B. Z.; Su, Y. A.; Sheng, Y. J.; Lin, J. J. *Chem. Mater.* **2009**, *21*, 4071; (b) Lego, B.; Skene, W. G.; Giasson, S. *Langmuir* **2008**, *24*, 379; (c) Lego, B.; François, M.; Skene, W. G.; Giasson, S. *Langmuir* **2009**, *25*, 5313.

(77) Laponite® Technical Brochure. http://www.scprod.com/pdfs/laponite.pdf

(78) Herrera, N. N.; Letoffe, J. M.; Reymond, J. P.; Bourgeat-Lami, E. *J. Mater. Chem.* **2005**, *15*, 863.

(79) Wheeler, P. A.; Wang, J. Z.; Baker, J.; Mathias, L. J. *Chem. Mater.* **2005**, *17*, 3012.

(80) Wheeler, P. A.; Wang, J. Z.; Baker, J.; Mathias, L. J. *Chem. Mater.* **2006**, *18*, 3937.

(81) Whilton, N. T.; Burkett, S. I.; Mann, S. *J. Mater. Chem.* **1998**, *8*, 1927.

(82) da Fonseca, M. G.; Airoldi, C.; *J. Mater. Chem.* **2000,** *10*, 1457.

(83) Carrado, K. A.; Xu, L.; Csencsits, R.; Muntean, J. V. *Chem. Mater.* **2001**, *13*, 3766.

(84) Fujii, K.; Hayashi, S.; Kodama, H. *Chem Mater* **2003**, *15*, 1189.

(85) Kresge, C. T.; Leonowicz, M. E.; Roth, W. J.; Vartuli, J. C.; Beck, J. S. *Nature* **1992**, *359*, 710.

(86) Beck, J. S.; Vartuli, J. C.; Roth, W. J.; Leonowicz, M. E.; Kresge, C. T.; Schmitt, K. D.; Chu, C. T. W.; Olson, D. H.; Sheppard, E. W.; McCullen, S. B.; Higgins, J. B.; Schlenker, J. L. *J. Am. Chem. Soc.* **1992**, *114*, 10834.

(87) Yanagisawa, T.; Shimizu, T.; Kuroda, K.; Kato, C. *Bull. Chem. Soc. Jpn.* **1990**, *63*, 988.

(88) Wan, Y.; Zhao, D. Y. *Chem. Rev*. **2007**, *107*, 2821.

(89) Huo, Q. S.; Margolese, D. I.; Ciesla, U.; Feng, P. Y.; Gier, T. E.; Sieger, P.; Leon, R.; Petroff, P. M.; Schuth, F.; Stucky, G. D. *Nature* **1994**, *368*, 317.

(90) Sun, T.; Ying, J. Y. *Nature* **1997**, *389*, 704.

(91) Tian, Z. R.; Tong, W.; Wang, J. Y.; Duan, N. G.; Krishnan, V. V.; Suib, S. L. *Science* **1997**, *276*, 926.

(92) Yang, P. D.; Zhao, D. Y.; Margolese, D. I.; Chmelka, B. F.; Stucky, G. D. *Nature* **1998**, *396*, 152.

(93) Zou, X. D.; Conradsson, T.; Klingstedt, M.; Dadachov, M. S.; O'Keeffe, M. *Nature* **2005**, *437*, 716.

(94) Tian, B. Z.; Liu, X. Y.; Tu, B.; Yu, C. Z.; Fan, J.; Wang, L. M.; Xie, S. H.; Stucky, G. D.; Zhao, D. Y. *Nat. Mater.* **2003**, *2*, 159.

(95) Grosso, D.; Boissiere, C.; Smarsly, B.; Brezesinski, T.; Pinna, N.; Albouy, P. A.; Amenitsch, H.; Antonietti, M.; Sanchez, C. *Nat. Mater.* **2004**, *3*, 787.

(96) Corma, A.; Atienzar, P.; Garcia, H.; Chane-Ching, J. Y. *Nat. Mater*. **2004**, *3*, 394.

(97) MacLachlan, M. J.; Coombs, N.; Ozin, G. A. *Nature* **1999**, *397*, 681.

(98) Braun, P. V.; Osenar, P.; Stupp, S. I. *Nature* **1996**, *380*, 325.

(99) Trikalitis, P. N.; Rangan, K. K.; Bakas, T.; Kanatzidis, M. G. *Nature* **2001**, *410*, 671.

(100) Attard, G. S.; Bartlett, P. N.; Coleman, N. R. B.; Elliott, J. M.; Owen, J. R.; Wang, J. H. *Science* **1997**, *278*, 838.

(101) Armatas, G. S.; Kanatzidis, M. G. *Nature* **2006**, *441*, 1122.

(102) Sun, D.; Riley, A. E.; Cadby, A. J.; Richman, E. K.; Korlann, S. D.; Tolbert, S. H. *Nature* **2006**, *441*, 1126.

(103) Landskron, K.; Ozin, G. A. *Science* **2004**, *306*, 1529.

(104) Meng, Y.; Gu, D.; Zhang, F. Q.; Shi, Y. F.; Yang, H. F.; Li, Z.; Yu, C. Z.; Tu, B.; Zhao, D. Y. *Angew. Chem., Int. Ed.* **2005**, *44*, 7053.

(105) Huo, Q. S.; Margolese, D. I.; Ciesla, U.; Demuth, D. G.; Feng, P. Y.; Gier, T. E.; Sieger, P.; Firouzi, A.; Chmelka, B. F.; Schuth, F.; Stucky, G. D. *Chem. Mater.* **1994**, *6*, 1176.

(106) Hoffmann, F.; Cornelius, M.; Morell, J.; Fröba, M. *Angew. Chem. Int. Ed.* **2006**, *45*, 3216.

(107) Corma, A. *Chem. Re*v. **1997**, *97*, 2373.

(108) Schuth, F.; Schmidt, W. *Ad*v. *Mater.* **2002**, *14*, 629.

(109) Ying, J. Y.; Mehnert, C. P.; Wong, M. S. *Angew. Chem., Int. Ed.* **1999**, *38*, 56.

(110) Schuth, F. *Chem. Mater.* **2001**, *13*, 3184.

(111) Attard, G. S.; Glyde, J. C.; Goltner, C. G. *Nature* **1995**, *378*, 366.

(112) Szwarc, M. *Nature* **1956**, *178*, 1168.

(113) Szwarc, M.; Levy, M.; Milkovich, R. *J. Am. Chem. Soc.* **1956**, *78*, 2657.

(114) Webster, O. W. *Science* **1991**, *251*, 887.

(115) Matyjaszewski, K., Xia. J. H., *Chem. Rev.* **2001,** *101,* 2921.

(116) Fischer, H. J. *Polym. Sci., Part A: Polym. Chem.* **1999**, *37*, 1885.

(117) Patten, T. E.; Matyjaszewski, K. *Adv. Mater.* **1998**, *10*, 901.

(118) Matyjaszewski, K. *Chem. Eur. J.* **1999**, *5*, 3095.

(119) Min, K.; Gao, H.; Matyjaszewski, K. *J. Am. Chem. Soc.* **2005**, *127*, 3825.

(120) Matyjaszewski, K.; Coessens, V.; Nakagawa, Y.; Xia, J.; Qiu, J.; Gaynor, S.; Coca, S.; Jasieczek, C. *ACS Symp. Ser.* **1998**, *704*,16.

(121) Zhang, X.; Matyjaszewski, K. *Macromolecules* **1999**, *32*, 7349.

(122) Haddleton, D. M.; Waterson, C.; Derrick, P. J. *Chem. Commun.* **1997**, 683.

(123) Patten, T. E.; Matyjaszewski, K. *Acc. Chem. Res.* **1999**, *32*, 895.

(124) Xia, J.; Zhang, X.; Matyjaszewski, K. *ACS Symp. Ser.* **2000**, *760*, 207.

(125) Matyjaszewski, K.; Wei, M.; Xia, J.; McDermott, N. E. *Macromolecules* **1997**, *30*, 8161.

(126) Matyjaszewski, K.; Davis, K.; Patten, T.; Wei, M. *Tetrahedron* **1997**, *53*, 15321.

(127) Matyjaszewski, K. *Macromol. Symp.* **1998**, *134*, 105.

(128) Percec, V.; Barboiu, B.; Neumann, A.; Ronda *Macromolecules* **1996**, *29*, 3665.

(129) Uegaki, H.; Kotani, Y.; Kamigato, M.; Sawamoto, M. *Macromolecules* **1997**, *30*, 2249.

(130) Matyjaszewski, K. *ACS Symp. Ser.* **2000**, *768*, 2.

(131) Matyjaszewski, K. *Macromol. Symp* **1996**, *111*, 47.

(132) Jakubowski, W.; Matyjaszewski, K. *Macromolecules* **2005**, *38*, 4139.

(133) Min, K.; Gao, H.; Matyjaszewski, K. *Macromolecules* **2007**, *40*, 1789.

(134) Matyjaszewski, K.; Dong, H.; Jakubowski, W.; Pietrasik, J.; Kusumo, A. *Langmuir* **2007**, *23*, 4528.

(135) Jakubowski, W.; Min, K.; Matyjaszewski, K. *Macromolecules* **2006**, *39*, 39.

(136) Pietrasik, J.; Dong, H.; Matyjaszewski, K. *Macromolecules* **2006**, *39*, 6384.

(137) Dong, H.; Tang, W.; Matyjaszewski, K. *Macromolecules* **2007**, *40*, 2974.

(138) Drummy, L. F.; Koerner, H.; Farmer, K.; Tan, A.; Farmer, B. L.; Vaia, R. A. *J. Phys. Chem. B.* **2005**, 109, 17868.

(139) Li, C. P.; Huang, C. M.; Hsieh, M. T.; Wei, K. H. *J. Polym. Sci., Part A: Polym. Chem*. **2005**, *43*, 534.

(140) Ryoo, R., Joo, S. H., Kim, J. M., *J. Phys. Chem. B.* **1999**, *103*, 7435.

(141) Ryoo, R.; Kim, J. M. *J. Chem. Soc., Chem. Commun.* **1995**, 711.

(142) Kim, J. M.; Sakamoto, Y.; Hwang, Y. K.; Kwon, Y.-U.; Terasaki, O.; Park, S.-E.; Stucky, G. D. *J. Phys. Chem. B*., **2002**, *106*, 2552.

(143) Kruk, M.; Dufour, B.; Celer, E. B.; Kowalewski, T.; Jaroniec, M.; Matyjaszewski, K. *Macromolecules* **2008**, *41*, 8584.

(144) (a) Antochshuk, V.; Jaroniec, M. *Chem. Commun.* **1999**, *23*, 2373; (b) Antochshuk, V.; Jaroniec, M. *Chem. Mater.* **2000**, *12*, 2496.

(145) (a) Ogawa, M.; Okutomo, S.; Kuroda, K. *J. Am. Chem. Soc.* **1998**, *120*, 7361; (b) Ogawa, M.; Masanori, M.; Kuroda, K. *Chem. Mater.* **1998**, *10*, 3787; (c) Isoda, K.; Kuroda, K.; Ogawa, M. *Chem. Mater.* **2000**, *12*, 1702; (d) Shimojima, A.; Mochizuki, D.; Kuroda, K. *Chem. Mater.* **2001**, *13*, 3603; (e) Henrist, C.; Vogels, C.; Rulmont, A.; Cloots, R. *New J. Chem.* **2005**, *29*, 2017; (f) Henrist, C.; Rulmont, A.; Cloots, R. *J. Eur. Ceram. Soc.* **2007**, *27*, 1023; (g) Toussaint, G.; Brisbois, M.; Grandjean, J.; Cloots, R.; Henrist, C. *J. Colloid Interface Sci.* **2009**, *329*, 120; (h) Toussaint, G.; Rodriguez, M. A.; Cloots, R.; Rubio, J.; Rubio, F.; Vertruyen, B.; Henrist, C. *J. Non-cryst. Solids* **2011**, *357*, 951.

(146) M. Kruk, B. Dufour, E. B. Celer, T. Kowalewski, M. Jaroniec and K. Matyjaszewski, *J. Phys. Chem. B*, **2005**, *109*, 9216.

(147) (a) Ding, P.; Zhang, M.; Gai, J.; Qu, B. J. *J. Mater. Chem.* **2007**, *17*, 1117; (b) Chastek, T. T.; Que, E. L.; Shore, J. S.; Lowy III, R. J.; Macosko, C.; Stein, A. *Polymer* **2005**, *46*, 4421.

(148) (a) Hadata, K; Kitayama, T. *In Macromolecular Design of Polymeric Materials*; Hadata, K.; Vogl, O., Eds.; Marcel Dekker Inc: New York, **1997**; p 147; (b) Matyjaszewski, K. *Macromolecules* **2012**, *45*, 4015.

(149) (a) Takahashi, H.; Ando, T.; Kamigaito, M.; Sawamoto, M. *Macromolecules* **1999**, *32*, 6461. (b) Wang, J.-S.; Matyjaszewski, K. *Macromolecules* **1995**, *28*, 7901.

(150) Brandrip, J.; Immergnt, E. H. *Polymer Handbook, 3rd ed.*; Wiley: New York, **1989**.

(151) Feng, L. B.; He, L.; Ma, Y. X.; Wang, Y. L. *Mater. Chem. Phys.* **2009**, *116*, 158.

(152) Wallace, W. E.; Van Zanten, J. H.; Wu, W. L. *Phys. Rev. E* **1995**, *52*, R3329.

(153) Van Zanten, J. H.; Wallace, W. E.; Wu, W. L. *Phys. Rev. E* **1996**, *3*, R2053.

(154) Keddie, J. L.; Jones R. A. L.; Cory R. A. *Europhys. Lett.* **1994**, *27*, 59.

(155) Forrest, J. L.; Dalnoki-Veress, K.; Dutcher, J. R. *Phys. Rev. E* **1997**, *56*, 5705.

(156) Fukao, K.; Miyamoto, Y. *Phys. Rev. E* **2000**, *61*, 1743.

(157) Grohens, Y.; Brogly, M.; Labbe, C.; David, M. O.; Schulzt, J. *Langmuir* **1998**, *14*, 2929.

(158) Kawana, S.; Jones, R. A. L. *Phys. Rev. E* **2001**, *63*, 021501-1.

(159) Forrest, J. A.; Mattson, J. *Phys. Rev. E* **2000**, *61*, R53.

(160) Yamamoto, S.; Tsujii, Y.; Fukuda, T. *Macromolecules* **2002**, *35*, 6077.

(161) Berriot, J.; Montes, H.; Lequeux, F.; Long, D.; Sotta, P. *Macromolecules* **2002**, *35*, 9756.

(162) Wu, W. L.; van Zanten, J. H.; Orts, W. J. *Macromolecules* **1995**, *28*, 771.

(163) Keddie, J. L.; Jones, R. A. L.; Cory, R. A. *Faraday Discuss.* **1995**, *98*, 219.

(164) Seymour/Carraher's Polymer Chemistry, 7th Edition CRC Press, **2008**, p. 197.

(165) Ueberreiter, K.; Kanig, G. *J. Chem. Phys.* **1950**, *18*, 399.

(166) Cao, L.; Kruk, M. *Polym. Chem.* **2010**, *1*, 97.

(167) Cao, L.; Kruk, M. in Controlled Radical Polymerization: Materials and Applications; Matyjaszewski, K.; Sumerlin, B.; and Tsarevsky, N. V. (Editors) ACS symposium series, Vol. 1101, American Chemical Society, Washington DC, **2012**, p. 231-240.

(168) Cao, L.; Man, T.; Zhuang, J. Q.; Kruk, M. *J. Mater. Chem.* **2012**, *22*, 6939.